A thesis submitted to Durham University in accordance with the requirements for the degree of Doctor of Philosophy 2011

Histamine H_3 Receptor Heterogeneity in the Central Nervous System in Aging and Dementia.

Natasha Louise Lethbridge

School of Biological and Biomedical Sciences

Durham University

Supervisor: Dr. Paul Chazot

Abstract

The histamine H_3R is a classic G-protein coupled receptor and is a potential therapeutic target for a number of central nervous system pathologies. Major pharmacological heterogeneity between and within species has hindered the clinical development of H_3R-targeted drugs. The pharmacological heterogeneity displayed by the H_3R is thought in part to be a result of alternative splicing of the H_3R which generates a number of possible splice variants, some of which have been shown to be functional and others which appear to be non-functional in terms of ligand binding and signal transduction. mRNA encoding the different isoforms has been shown to be distributed throughout the central nervous system in a region specific manner. For the first time we have shown three of the common H_3R isoforms ($hH_{3\ 329}$, $hH_{3\ 365}$, $hH_{3\ 445}$) to be expressed in the human brain using a novel panel of immunological isoform specific probes. We provide preliminary evidence for raised levels of $H_{3\ 445}$ and $H_{3\ 329}$ isoforms in Parkinson's disease and Lewy Body Dementia cases, respectively, compared to age-matched controls. We have shown a variety of H_3R ligands display differential pharmacological properties at the three hH_3R isoforms expressed in HEK 293 cells. Most notably a 5- and 10- fold lower affinity for a highly selective clinical lead H_3R inverse antagonist, GSK189254, at the $H_3R_{\ 329}$ and $H_3R_{\ 329\ +\ 365}$ isoforms, respectively. The pharmacological differences observed indicate, together with the availability of the immunological probes, that it will be possible to dissect the physiological roles of human H_3 receptor isoforms.

The H_3R is an attractive therapeutic target for age-related dementias. H_3R antagonists have undergone a large number of pre-clinical assessments in

which they display pro-cognitive effects, particularly in drug-induced amnesias. It is important to establish whether there are any changes in H_3R expression in normal physiological aging and in age-related human dementias. Based on quantitative [^{3}H] GSK189254 autoradiography, we have shown that H_3Rs are largely preserved in key cortical and striatal brain regions in aged CD-1 and TASPM mice, as well as in aged humans. Furthermore, H_3 receptors were largely unchanged in Lewy Body Dementia and Alzheimer's disease cases, which provide further evidence validating the H_3R as a promising target for age-related cognitive disorders. Psychotic symptoms are common features in both Lewy Body Dementia and Alzheimer's disease. Interestingly, higher levels of H_3R in the globus pallidus correlated with the presence of both delusions (+ 40% and + 37%) and hallucination symptoms (+22% and +14%) within these human dementias, consistent with the recent positive clinical use of H_3R antagonists in psychotic disorders. In contrast, using a novel validated all-in-one behavioural elevated platform test in mice, evidence is provided for the lack of H_3R involvement in anxiety behaviour, suggesting the lack of utility in human anxiety disorders.

Acknowledgements

This thesis would not have been possible without the help and support of my colleagues at the University of Durham.

I am especially indebted to Dr. Paul Chazot, whose seemingly inexhaustible encouragement, guidance and long hours of supervision proved invaluable throughout the course of this research.

I would also like to express my appreciation to Dr. Abdel Ennaceur and my fellow lab members, and in particular to Dr. Stephanie Burroughs.

Finally, I wish to thank my family, and in particular my incredible partner Kenny Lowe for their enduring patience and support over the past four years.

DECLARATION

I confirm that no part of the material presented has previously been submitted for a degree in this or any other university. If material has been generated through joint work, my independent contribution has been clearly indicated. In all other cases, material from the work of others has been clearly indicated, acknowledged and quotations and paragraphs indicated.

ABBREVIATIONS

G protein coupled receptor (GPCR), Histidine decarboxylase (HDC), α-fluoromethylhistidine (α-FMH), Histamine N-methyltransferase (HNMT), Histamine H1 receptor (H_1R), Histamine H2 receptor (H_2R), Histamine H3 receptor (H_3R), Histamine H4 receptor (H_4R), Central nervous system (CNS), Tuberomammillary nucleus (TMN), Diamine oxidase (DAO), Knock out (KO), Parkinson's disease (PD), Alzheimer's disease (AD), Neurofibrillary tangles (NFTs), Dementia with Lewy bodies (DLB), *Escherichia coli* (E.coli), R-α-Methylhistamine (RαMHA), *N*-Methylhistamine (NMHA), Intraperitoneal (i.p), Spontaneously hypertensive rat (SHR), Attention deficit hyperactivity disorder (ADHD), Gamma aminobutyric acid (GABA), N-methyl-D-aspartate (NMDA), Disintegrations per minute (dpm), Counts per minute (cpm), Mitogen activated protein kinase (MAPK), Phospholipase A_2 (PLA_2), Phosphatidylinositol-3-kinase (PI3K), Extracellular signal-regulated kinases (ERK's), Protein kinase B (PKB), Glycogen synthase kinase 3β (GSK3β), Wild type (WT), Tetramethylethylenediamine (TEMED), Tris Buffered Saline (TBS), Sodium dodecyl sulphate (SDS), Room Temperature (RT), Phosphate suffered saline (PBS), Messenger RNA (mRNA), Long Term Potentiation (LTP), Horse radish peroxidise (HRP), Foetal Calf Serum (FCS), Ethyleneglycotetraacetic Acid (EGTA), Ethylenediaminetetraacetic acid (EDTA), Deoxyribonucleic Acid (DNA), Dentate gyrus (DG), Cyclic adenosine monophosphate (cAMP), Caudate Putamen (CPu), Cerebellum (Cb), cAMP response element binding protein (CREB), Brain derived neurotrophic factor (BDNF), Bovine serum albumin (BSA), Antibody (Ab), β-amyloid (Aβ), 3,3-Diaminobenzidine (DAB).

CONTENTS

Development and Characterisation of Novel Anti- Human Histamine H_3 Receptor Isoform Specific Antibodies

CHAPTER 1

Introduction

1. Histamine and the histaminergic system

Histamine is an endogenous, biogenic amine ubiquitously expressed in the body, present at high concentrations in the lungs, skin and gastrointestinal tract. Over 90% is stored in granules in basophils and mast cells, where it is associated with heparin, whilst non-mast cell histamine occurs in histaminocytes in the stomach and in varicosities of the histaminergic neurons in the brain. Histamine acts as a transmitter in the nervous system and as a signalling molecule in the gut, skin and immune system. Histamine brings about complex physiological changes including neurotransmission, inflammation, smooth muscle contraction, dilation of capillaries, chemotaxis, cytokine production and gastric acid secretion. These biological changes occur via four G protein coupled receptor (GPCR) subtypes: histamine H_1, H_2, H_3 and H_4 (Parsons and Ganellin, 2006).

Histamine is a modified amino acid that is synthesized from the oxidative decarboxylation of the amino acid histidine, a reaction that is catalyzed by histidine decarboxylase (HDC) (Fig 1.1). HDC is highly conserved throughout the animal kingdom (Haas et al., 2008). Histamine synthesis is limited by its precursor histidine which is taken up by amino acid transporters into the cerebral spinal fluid and neurons. The formation of histamine from histidine can be blocked by α-fluoromethylhistidine (α-FMH), a highly selective HDC inhibitor. Once formed, histamine is either stored or rapidly metabolized by either methylation or oxidation (Fig 1.1). Methylation of histamine results in the

formation of N-methylhistamine (NMHA) which is catalyzed by Histamine N-methyltransferase (HNMT), while oxidation of histamine results in the formation of imidazole acetic acid by the enzyme diamine oxidase (DAO). CNS deactivation of histamine occurs mainly via HNMT while peripheral histamine is deactivated via DAO (Haas et al., 2008).

Formation and metabolism of histamine:

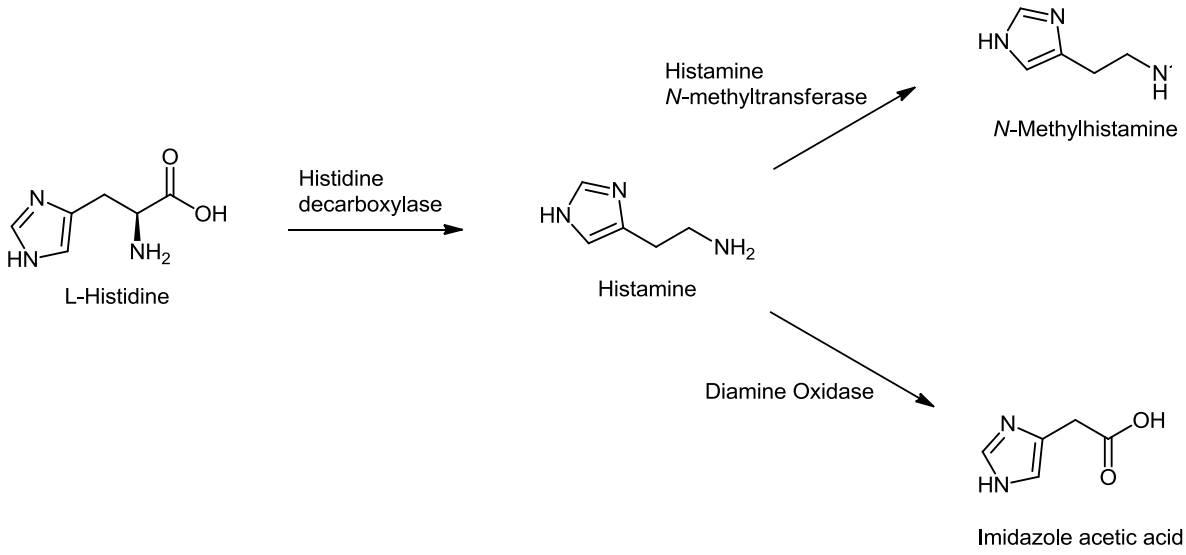

Figure 1.1 shows the formation of histamine from histidine and the metabolism of histamine to either imidazole acetic acid or N-methylhistamine.

Histamine has long been known to be an important mediator in different (patho) physiological processes. It was first synthesised by the decarboxylation of histidine in 1907 (Windaus and Vogt, 1907). Subsequently, histamine in the periphery was shown to have a stimulant effect on smooth muscle from the gut and respiratory tract, depression of cardiac contractility, vasodilation and induced anaphylaxis when injected into animals (Dale & Laidlaw, 1910 & 1919). Histamine was also discovered to have a stimulant effect on acid secretion from the stomach of dogs, which was later shown to

be brought about by the activation of the H_2 receptor (H_2R) (Black et al., 1972). In 1924, Lewis described the classic ‘triple response' to histamine consisting of a red spot due to vasodilatation, a wheal which was the consequence of increased permeability and flare due to an axon reflex (Lewis et al., 1924); this response was later shown to occur due to activation of the H_1 receptor (H_1R) (Ash et al., 1966). Histamine was found to be a natural constituent of the body in 1927, when it was first isolated from liver and lung samples (Best et al*.,* (1927). The association between histamine and anaphylactic shock was soon demonstrated by showing the variation between histamine content of the lung before and after shock as well as the increase in histamine content of the blood after anaphylaxis. In 1937, Ungar et al., reported the first anti-histamine compound (H_1R antagonist), adrenolytic benzodioxan, piperoxan (933F), which blocked the effects of histamine on the guinea-pig ileum. This was then followed by a series of structurally related aryl ethers, thymol ether 929F, which were shown to protect the guinea-pig from the lethal effects of histamine-induced anaphylaxis (Bouvet et al., 1937). Classical anti-histamines were soon developed as successful therapies and were widely used to treat allergic and inflammatory conditions, however, sedation and drowsiness was a major issue. This then lead to the idea that histamine was able to act upon the central nervous system (CNS). In 1943, Kwiatkowski identified histamine within mixed cortical nerves in the brain and he found that the histamine content of nerves varied. Later studies demonstrated the formation and catabolism of histamine in the brain.

In the early 1970s, there emerged an understanding that histamine was a neurotransmitter and/or neuromodulator and it was then hypothesized that

blockade of brain histamine transmission could be the reason for the drowsiness associated with anti-histamines. Following this discovery, second generation anti-histamines that did not cross the blood brain barrier were designed to treat allergy and inflammation (Schwartz et al., 1970).

Lesion studies carried out by Garbarg et al. (1974) identified the tuberomammillary nucleus (TMN) as the origin of brain histamine. In the early 1980s two groups documented the histochemical localisation of the histaminergic neurons in the CNS (Watanabe et al., 1984 and Panula et al., 1989). Brain histamine is classified as either neuronal or non-neuronal histamine. Neuronal histamine originates from histaminergic neurons while non-neuronal histamine originates from neuroepithelial and haematopoietic cells, mainly mast cells (Garbarg et al., 1976). Mast cells in the brain contribute a significant amount to the production of brain histamine. Mast cells are present in the circumventricular organs; the meninges, hypophysis, pineal gland, area postrema, the median eminence, thalamus, hypothalamus and along the blood vessels in the gray matter. In other brain regions, it is assumed that the action of histamine is mediated by release from neurons (Hough, 1988). Non-neuronal histamine displays a much slower turnover rate than neuronal histamine (Haas et al., 2008). Compound 48/80 is a basic polymer that causes exocytosis of the granular content within mast cells, however it does not cause histamine to be released from the varicosities in axons, allowing neuronal and non-neuronal histamine release to be differentiated. Non-neuronal mast cells are involved in gastric acid secretion, immunomodulation, bronchial smooth muscle contraction, vascular vasodilatation and epi/endothelial barrier control (Haas et al., 2008).

The basic organization and functional disposition of the histaminergic system is highly conserved in the vertebrate brain (Fig 1.2).

Histaminergic innervation in the human CNS:

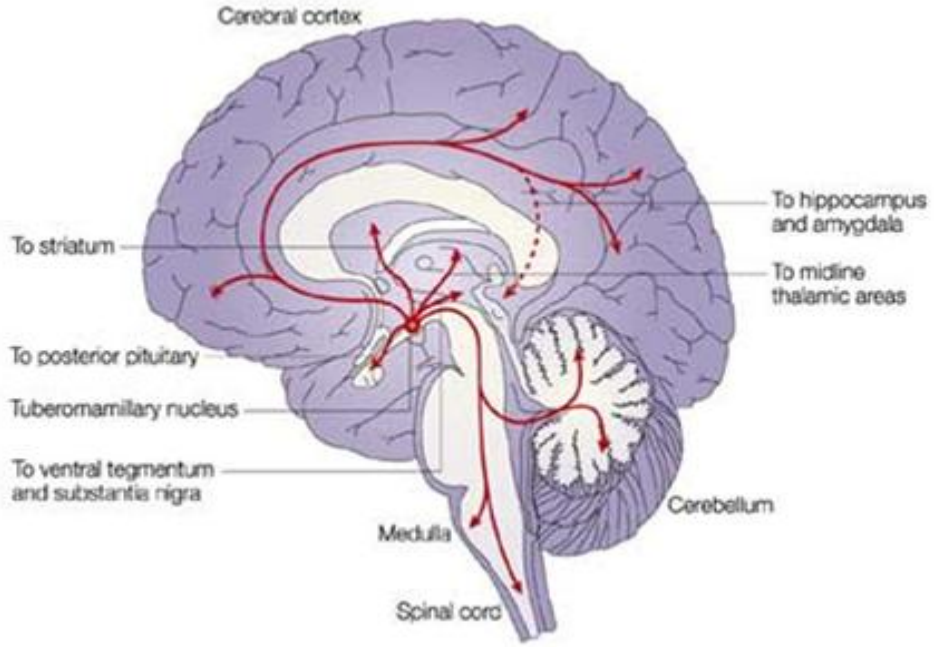

(Haas et al., 2003)
Figure 1.2 shows histaminergic innervation in the human CNS. Arrows represent histaminergic innervation emanating from the TMN to a variety of brain regions including the cortex, striatum and cerebellum.

In the mammalian brain, histamine is synthesized and stored in the cell somata and axon varicosities in restricted populations of neurons that originate from the TMN located in the posterior hypothalamus. Neuronal histamine is transported into vesicles by a vesicular monoamine transporter (VMAT-2) in exchange for 2 protons, and in the presence of an action potential is released from the vesicle (Ericson et al., 1991). The TMN is the only source of histamine, however other transmitters or their synthetic enzymes have been found within the TMN neurons; GAD 65/67, galanin,

enkephalins, thyrotrophin releasing hormone and substance P (Haas et al., 2008).

The TMN in the rat has been subdivided into five groups; a ventral group around the mammillary bodies, which is subdivided into a rostral and caudal part, a medial group around the mammillary recess, which is subdivided into a dorsal and ventral part, and a diffuse part (Wada et al., 1991). The five histaminergic cell groups are bridged by scattered neurons and are considered to be one functional group (Watanabe et al., 1984). Similarly, in human the TMN has been subdivided into four groups; a ventral group corresponding to the classical TMN, a medial group which includes the supramammillary nucleus, a caudal paramammillary section and a minor lateral area (Airaksinen et al., 1991). The TMN is innervated by two ascending pathways (ventral and dorsal) and one descending pathway (Panula et al., 1989). Histaminergic neurons projecting from the ventral ascending pathway have strong innervation at the hypothalamus, diagonal band, septum and olfactory bulb whilst the dorsal pathway has lower density fibres which innervate the thalamus, hippocampus, amygdala and rostral forebrain structures. The descending pathway in rats is associated with the medial longitudinal fasciculus and provides input to the brain stem and spinal cord. The cerebral cortex has a moderate density of fibres in all areas and layers with a slightly increased density in the outer layers. Innervation of the thalamus is concentrated at the periventricular nuclei. The subiculum and dentate gyrus have the strongest innervation in the hippocampal formation, with lower innervation at the CA1 and CA3 of the hippocampus. Low to moderate innervation is also present at the striatum and nucleus accumbens.

The descending pathway has lower innervation than the ascending pathways. The substantia nigra, ventral tegmental area, inferior and superior colliculi, pariaqueductal gray, trigeminal nerve and nucleus tractus solitarius receive prominent projections (Wada et al., 1991). Schwartz et al., (1991), showed using electrophysiological techniques that histamine still affected regions with low density histaminergic innervation indicating considerable mismatch between histaminergic fibre density and the density of histamine receptors in different brain regions. Areas with high density of fibres are likely to be affected tonically during waking, while areas with lower fibre densities may only be affected under particular behavioural situations when histamine neurons fire more rapidly (Schwartz et al, 1991). The lack of histamine in some brain areas where there is high histamine receptor expression may suggest that there are still unknown functional aspects within the system. Since histamine receptor expression is not limited to neurons but can also be found on endothelial cells, ependymal cells and astrocytes, this may indicate diurnal regulation of brain histamine is also important for several non-neuronal functions (Haas et al., 2003).

Histamine forms part of the brain aminergic system in the CNS along with the serotonergic, dopaminergic and noradrenergic systems (Baudry et al., 1975). The histaminergic system consists of small bundles of neurons that have wide spread projection networks to most brain areas and the spinal cord. Histamine at the beginning of this project was believed to bind to three of the four known histamine receptors as well as to the polyamine site on N-methyl-D-aspartate (NMDA) receptors to control excitability and plasticity within the CNS.

Specificity of action is likely achieved through the organisation of the TMN histaminergic neurons into functionally distinct circuits projecting to different output regions, under presynaptic control (Giannoni et al., 2009). The major afferent inputs into the TMN are the infralimbic cortex, lateral septum and preoptic nucleus (Ericson et al., 1991). This helps to establish the broad modulatory effect that is tightly regulated by higher brain functions to maintain a constant homeostatic balance through its interaction with the aminergic and peptidergic systems.

Brain histamine levels are lower than other biogenic amines, however its turnover is much quicker (Dismukes and Snyder, 1974). Histaminergic neurons are pacemakers that fire at a slow regular rate of less than 3Hz, depending on the behavioural state (Brown et al., 2001). Histamine release shows a clear circadian rhythm, which parallels the change in the firing rate of histamine neurons over the sleep-wake cycle (Mochizuki et al., 1992). Histamine release from the posterior hypothalamus has a faster rhythm which correlates with delta and theta bands in electroencephalographic recordings (Philippu et al., 1991). The synthesis and release of histamine is controlled by negative feedback through the H_3R.

Central histamine is an important neuromodulatory neurotransmitter that plays an important role in the regulation of several (patho)physiological processes such as arousal, activation of the sympathetic nervous system, stress related release of hormones from the pituitary and of central aminergic neurotransmitters, nociception, addiction, memory, anaesthesia, water retention and appetite suppression.

1.2 Histamine receptors

Four receptors to date have been defined H_1R, H_2R, H_3R and H_4R; all have been defined at the pharmacological and molecular levels (Morse et al., 2001). Histamine receptors span the membrane seven times and are associated with a variety of different internal signalling G proteins. Histamine receptors belong to the class A family of rhodopsin-like G protein coupled receptors (GPCRs) Fig 1.3 and Fig 1.4.

Schematic showing a typical G Protein Coupled Receptor (GPCR):

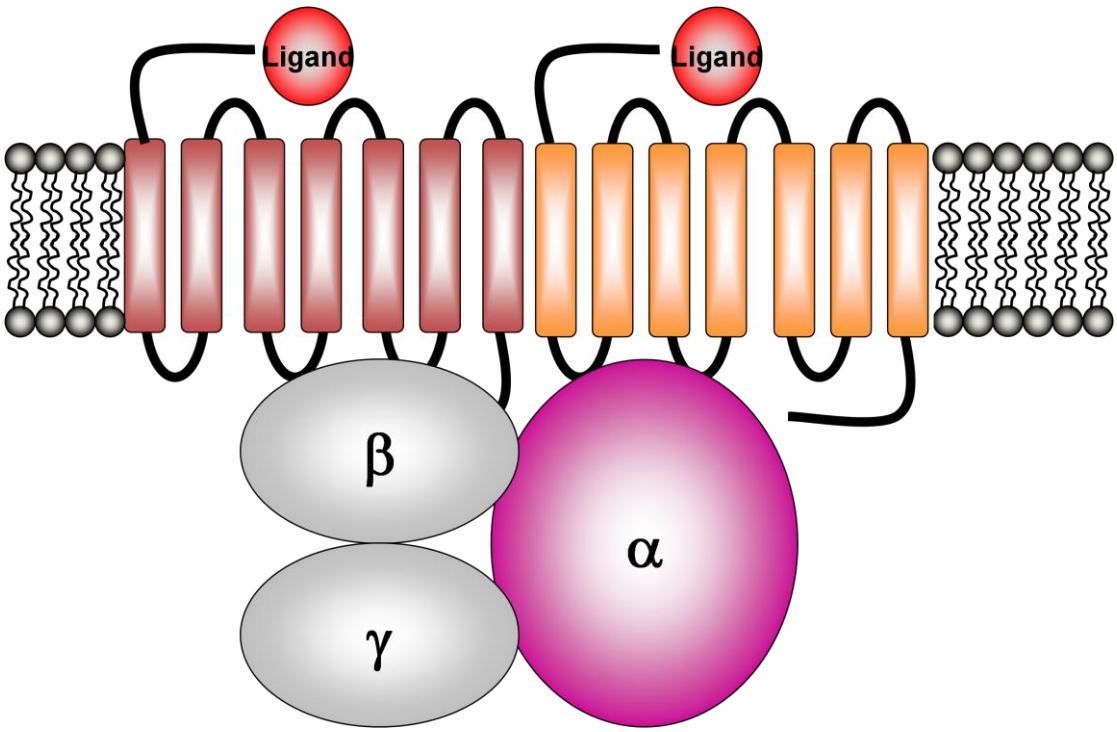

Figure 1.3 shows the typical structure of a dimeric GPCR.

All amine receptors belong to this family of GPCR and share the same features:

1) Conserved aspartate residues at position 80 in transmembrane region 1 (TM1) and position 114 TM3

2) DRY (DRF for the H_3R) or ERW motif at the interface of the TM3 and intercellular loop

3) Disulphide bridge between the first and second cysteine residues (C107 and C188 on extracellular loops 1 and 2, respectively)

4) Conserved tryptophan residues at position 174 and 371 in TM4 and TM6, respectively

5) Conserved proline residues at position 210, 373 and 409 in TM5, TM6 and TM7, respectively

6) NP*XX*Y motif in TM7, (NPVLY for the H_3R)

7) Potential palmitoylation site at C428 near the C-terminal tail

8) Conserved asparagine residue at position 404 in TM7

9) N-linked glycosylation (N11)

10) Sites for putative phosphorylation by protein kinases in all three intracellular loop at positions: 1^{st} intracellular loop – Serine 63 or serine 64, 2^{nd} intracellular loop – serine 141 and threonine 149, 3^{rd} intracellular loop – Serines 310, 319, 341, 343 or threonines 314 and 345 (Leurs et al., 2000).

This subset of GPCRs includes receptors that are activated by small ligands, such as biogenic amines; larger peptide ligands and glycoprotein hormones.

Crystal structure of a class A GPCR - human adenosine A_{2A} receptor:

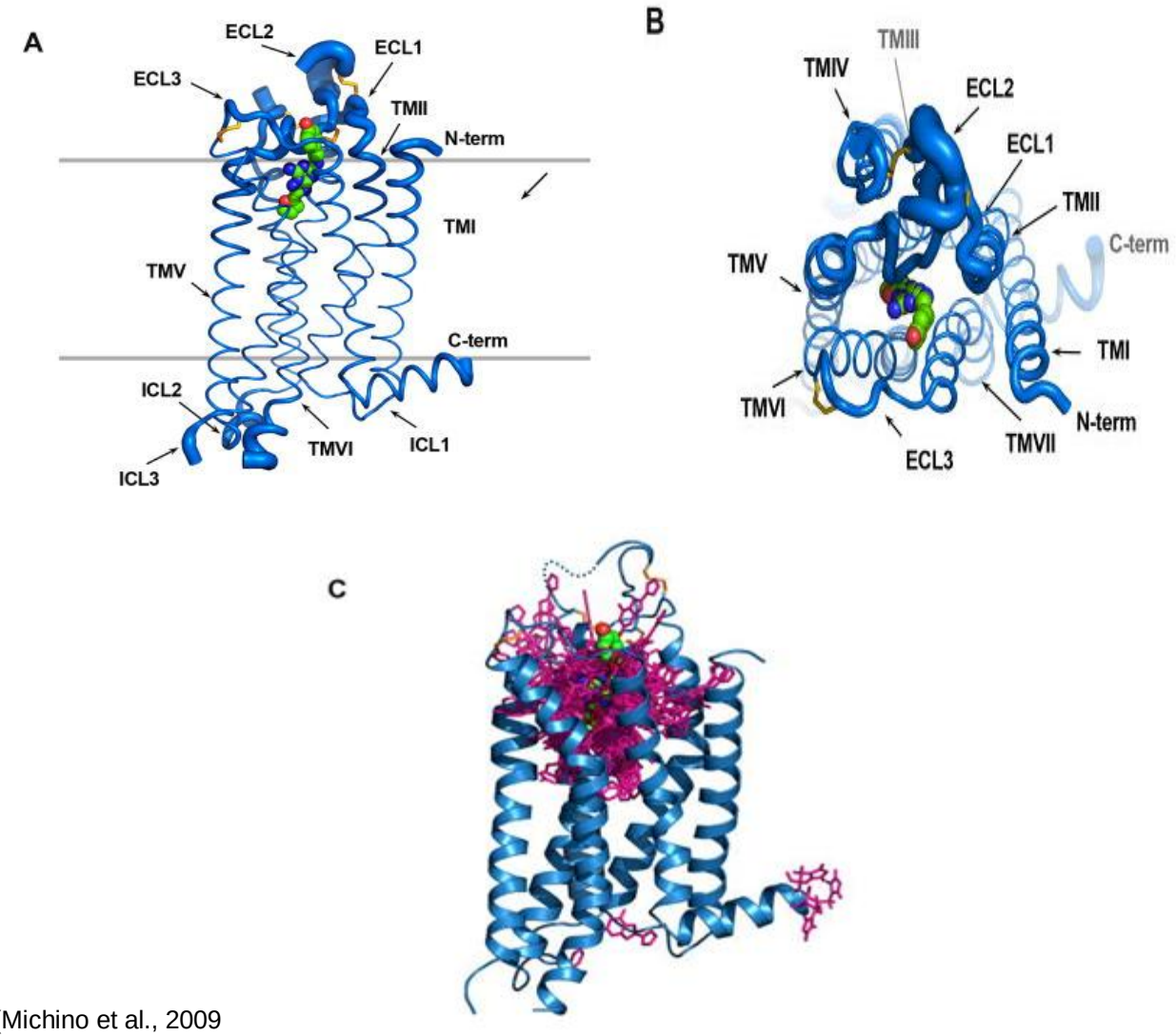

(Michino et al., 2009

Figure 1.4 Crystal structure of a class A GPCR - human adenosine A_{2A} receptor. Superposition of all 206 submitted models to the crystal structure of the human adenosine A_{2A} receptor (PDB ID: 3EML without the T4-lysozyme). Protein Cα atom superposition between model and crystal structure was performed using the align command in PyMOL. The receptor is shown as two orthogonal views of Cα traces (A, B) with tube thickness being proportional to the RMSD about each Cα position clearly showing how well the TM regions were modelled and how much uncertainty are in the loop regions. (C) A superposition of stick diagrams of the ligand (ZM241385) from 169 models, a CPK model is used to delineate the observed position in the crystal structure. The C-terminus (residue numbers >306) is removed from all models.

1.2.1 Histamine H_1R and H_2R

Central histamine H_1R's are the main site responsible for the sedative effects of classical anti-histamines. The H_1R was first cloned in 1991 by Yamishita et al., (1991). The human H_1R has been mapped to chromosome 3p25 (Le

Coniat et al., 1994) and it has shown to be expressed in the brain, on immune cells, endothelial cells, smooth muscle cells, endothelial cells, as well as in the gastrointestinal tract, genitourinary system, adrenal medulla and the heart (Hill et al., 1990). [^{3}H] mepyramine, a H_1R antagonist, was used in autoradiography studies to determine H_1R expression in the human brain. High levels were shown to be present in the thalamus, cortex, mesopontine tegmentum, basal forebrain, locus coeruleus and raphe nuclei, primary areas involved in arousal. High H_1R levels are also present in many nuclei of the hypothalamus, septal nuclei, medial amygdala and hippocampal subfields, all parts of the limbic region. High densities are also present in the nucleus accumbens, molecular layer of the cerebellum, nuclei of the cranial nerves, area postrema and nucleus tractus solitarius, while relatively low densities are present in the cerebellum and basal ganglia (Martinez-Mir et al., 1990, Villemange et al., 1991 and Yanai et al., 1992). H_1Rs in the brain play an important role in eating, drinking, thermoregulation and memory (Brown et al., 2001, Knoche et al., 2003 and Dia et al., 2007). Binding of histamine to the H_1R results in modulation of the $G\alpha_{q/11}$ family of GPCRs, resulting in activation of phospholipase C-β (PLC), phospholipase A_2 (PLA_2) and phospholipase D (PLD) (Leurs et al., 1994). Activation of PLC hydrolyses phosphatidylinositol-4, 5-bisphosphate (PIP_2) into diacylglycerol (DAG) and inositol-1,4,5-trisphosphate (IP_3). DAG activates protein kinase C (PKC), whilst IP_3 binds to the IP_3 receptor on the endoplasmic reticulum, resulting in the release of stored calcium into the cytoplasm. Activation of PLA_2 elicits the formation of arachidonic acid (Leurs et al., 1994) and cyclic guanosine 3′, 5′ monophosphate (cGMP) (Richelson, 1978). cGMP formation is thought to be

the result of increased intracellular calcium leading to the activation of nitric oxide and hence the stimulation of guanylate cyclase. Activation of H_1Rs in the brain results in excitation of neurons or potentiation of excitatory inputs. Activation of the H_1R in the periphery activates a series of biochemical pathways, bringing about physiological changes including smooth muscle contraction, stimulation of nitric oxide formation, endothelial cell contraction and an increase in vascular permeability. These physiological changes have a close relationship with allergic conditions, and therefore therapeutic agents have been developed to block the activation of peripheral H_1Rs to reduce allergic reactions. The H_1R also plays an important role in wakefulness as previously discussed (Hill et al., 1997).

Histamine research focused solely on the role of histamine in allergic diseases up until the 1970's when potent anti-histamines which had been developed were useful in inhibiting certain symptoms of allergic conditions but did not antagonise all histamine induced effects particularly in the stomach, uterus and heart. This led to the hypothesis that there were two different types of histamine receptor subtypes (Ash et al., 1966). This hypothesis was accepted when Sir James Black succeeded in the synthesis of a series of new compounds (e.g. burimamide, cimetidine), which were capable of blocking the effects of histamine on the stomach and the heart. These H_2R antagonists were fundamental in the development of the first therapy for gastric ulcers. The H_2R was first cloned in 1991 and shares 28% homology with the H_1R (Gantz et al., 1991). The human H_2R has been mapped to chromosome 5q35.2 and has been shown to be expressed in gastric cells, cardiac tissues

and smooth muscle cells (Black et al., 1972). H_2Rs have also been identified on immune cells where it negatively controls histamine release, as well as on B cells where it affects antibody synthesis and on T cells where it is involved in T cell proliferation (Hill et al., 1990). [^{125}I]- iodoaminopotentidine, a H_2R antagonist, was used in autoradiography studies to determine H_2R expression in the human brain. High levels were observed in the basal ganglia, hippocampal formation and amygdala, while low levels were present in septal areas, hypothalamic and thalamic nuclei. Layers I-III of the cerebral cortex displayed the densest H_2R labelling, located on the dendrites of pyramidal cells. H_2R expression has been shown to be present on the dendrites of principal cells in the hippocampal formation, including the dentate gyrus, as well as on purkinje and granule cells in the cerebellar cortex. H_1 and H_2 receptors have also been shown to be co-localised in several areas of the brain including pyramidal and granule cells in the hippocampal formation and on other aminergic cell groups (locus coeruleus, raphe nuclei, substantia nigra, ventral tegmental area) where the receptors can act synergistically.

Activation of the H_2R stimulates $G\alpha_s$, resulting in the production of cyclic adenosine 3′, 5′ monophosphate (cAMP) through the activation of adenylyl cyclase (Baudry, 1975). cAMP targets protein kinase A (PKA), which then is capable of phosphorylating target proteins in the cytosol, cell membrane or translocate to the nucleus where it activates cAMP responsive element binding protein (CREB). Activation of H_2Rs in the brain results in excitation of neurons or potentiation of excitatory inputs. Activation of H_2Rs in the periphery

results in gastric acid secretion in the stomach (Hill et al., 1997 and Oda et al., 2000).

The development of highly specific antagonists which target the H_1R and H_2R has resulted in drugs which have attained 'block-buster' status.

1.2.2 Histamine H_3R

The histamine H_3R was first described in 1983 as a novel auto-receptor regulating the synthesis and release of histamine (Arrang et al., 1983). It was not until 1999 that the receptor was cloned (Lovenberg et al., 1999), mainly because of its low overall homology with the H_1R and the H_2R. The H_3R pharmacology is also distinct from either H_1R or the H_2R. The H_3R is primarily expressed in the CNS were it acts as both an auto- and hetero-receptor controlling the release of histamine itself and other neurotransmitters, respectively. The H_3R has led to vast interest from many pharmaceutical companies because of its capability to increase the level of neurotransmitters involved in learning and memory, in particular acetylcholine in the nucleus basilis magnocellularis (NBM) and pre-frontal cortex.

1.2.2.1 Anatomical distribution

The H_3R has been detected in human, rat and non-primate brain as well as in the spinal cord of humans and on peripheral ganglia. Detection has been based upon ligand autoradiography*, in situ* hybridisation and immunological techniques with H_3R specific antibodies.

Specific [^{3}H] RαMH autoradiography binding studies have shown the presence of the H_3R in the rat brain (Pollard et al., 1993). A recent study using

a novel highly specific H_3R antagonist [^3H] GSK189254 have also confirmed the presence and expression pattern of the H_3R in the CNS (Medhurst et al., 2007). H_3R Binding sites were present in the nucleus accumbens, cerebral cortex, corpus striatum, Islands of Calleja, olfactory tubercle, hippocampus, hypothalamus, and substantia nigra, and layers IV – VI in the cerebral cortex. [^3H] GSK189254 has also been used to map H_3R binding sites at the level of the human spinal cord; intense binding was detected in the dorsal horn at both the cervical and lumbar levels as well as on dorsal root ganglia (Medhurst et al., 2007).

Immunological identification of the H_3R in the mouse brain was first achieved by our group in 2001, and on the whole is very similar to the ligand autoradiography data described above (Chazot et al., 2001). The distribution of H_3R differs to both the H_1R and H_2R, however there are some areas where a combination of the receptors are co-expressed. Both H_3R and H_1R are expressed at high levels in the deep layers of the cortex (Pollard et al., 1992), unlike H_2R which are highly expressed in the superficial layers (Martinez-Mir et al., 1990). In the basal ganglia H_3R distribution parallels that of the H_2R (Pollard et al., 1992), whereas H_1R expression is low. H_3R and H_1R are both expressed in the nucleus accumbens where they have been shown to be involved in locomotor hyper- and hypoactivity, respectively in rats (Bristow et al., 1988).

H_3R mRNA and protein expression studies in rodents have shown that the H_3R is not limited to the CNS; it is also found by our group in the skin, dorsal root ganglia, sensory neurons (Cannon et al., 2007), stomach, intestine

(Grandi et al., 2008) and others on brown adipose tissue (Karlstedt et al., 2003).

1.2.2.2 Auto- and hetero-receptors: matching anatomy and functional data

Initially the synthesis and release of histamine was thought to be under tonic inhibitory control from the release of local histamine acting on H_3 auto-receptors located on the somata and axon terminals of histamine neurons (Arrang et al., 1983). It was subsequently discovered that the H_3R also acted as a hetero-receptor by controlling the release of other neurotransmitters such as glutamate, GABA, noradrenalin, dopamine, acetylcholine, serotonin and neuropeptides (reviewed by Brown et al., 2001). The H_3R controls the release of neurotransmitters by inhibiting the calcium current which reduces the size and frequency of the spontaneous calcium-dependent pre-potentials leading to the depression of the firing rate and hence neurotransmitter release (Takeshita et al., 1998). To help maintain specificity of action, histamine release in target regions is under the control of inhibitory M_1 muscarinic, α_2-adrenoreceptors, 5-HT_{1A}, opioid κ-receptors, galanin receptors as well as facilitatory μ-opioid receptors (reviewed by Brown et al., 2001 and Haas et al., 2008). Histamine levels are very low in the brain (0.1-0.2 nmols/g) due to tight regulation via the histaminergic system working closely with other neuronal transmitter systems.

The differential responses to $GABA_A$ or H_3R antagonists, suggests the existence of distinct subpopulations among histaminergic neurons (Giannoni

et al., 2009). By using a dual probe microdialysis, one electrode placed in the TMN and the other placed at varying histaminergic projections sites, the effect of either $GABA_AR$ or H_3R antagonists could be analysed. Both GABA and histamine tonically modulates histaminergic neuronal activity. The differential histamine response generated from the distinct projections projecting from the TMN following administration of two different antagonists suggested the presence of functionally distinct histamine neuronal populations. The TMN in the rat has been shown to be heterogenous through the use of our antibodies reactive to either H_3R or GABA, some are GABA positive (anti-GAD_{67} antibody) neurons expressing the H_3R, while others are H_3R positive and GABA negative, or GABA positive and H_3R negative. (Giannoni et al., 2007). Combinations of both physiological and pharmacological tools have also demonstrated heterogeneity among histaminergic neuron populations, showing distinct control of dopamine release in the substantia nigra and pre frontal cortex; both regions differ in their dopaminergic innervation (Garduno-Torres et al., 2006). In superfused rat substantia nigra slices depolarisation-evoked [^{3}H]-dopamine release was diminished by a H_3R agonist immepip. However, immepip was unable to affect [^{3}H]-dopamine release in the pre-frontal cortex synaptosomes. This same group showed the presence of H_3R coupled to $G_{\alpha i/o}$ proteins on thalamic nerve terminals, activation of these H_3Rs modulated glutamatergic, but not GABAergic transmission.

1.2.2.3 H_3R structure and signalling

The histamine H_3R was first described in 1983 (Arrang et al., 1983), however it was not until 1999 that the receptor was cloned (Lovenberg et al., 1999).

The H_3R was not cloned by similarity screening to either of the H_1R and H_2R due to its low overall homology with either of the other two receptors. Lovenberg and colleagues used a partial clone (GPCR97) derived from an EST database that had been shown to display significant homology to biogenic amine receptors and also shared homology with the α_2 adrenergic receptors. The GPCR97 clone was used to probe a human thalamus cDNA library, which resulted in the isolation of a full-length clone encoding the H_3R, with an open reading frame encoding 445 amino acids. The human H_3R was subsequently mapped to chromosome 20q13.33 and shown to be highly expressed in the human CNS (Tardivel-Lacombe et al., 2001 and Cogé et al., 2001).

After the cloning of the human H_3R, the H_3R was cloned in the rat in 2000 (Lovenberg et al., 2000) followed by guinea pig (Tardival-Lacombe et al., 2000) and then monkey (Yoa et al., 2003). The H_3R is approximately 92% conserved between the different species (Hancock et al., 2003).

a) Splice variants generate receptor isoforms

The H_3R gene is rare among typical GPCR due to the fact that it has multiple introns. The H_3R gene has been shown to consist of four exons and three introns (Fig 1.5) (Cogé et al., 2001).

Organisation of the human H_3R gene and cDNA:

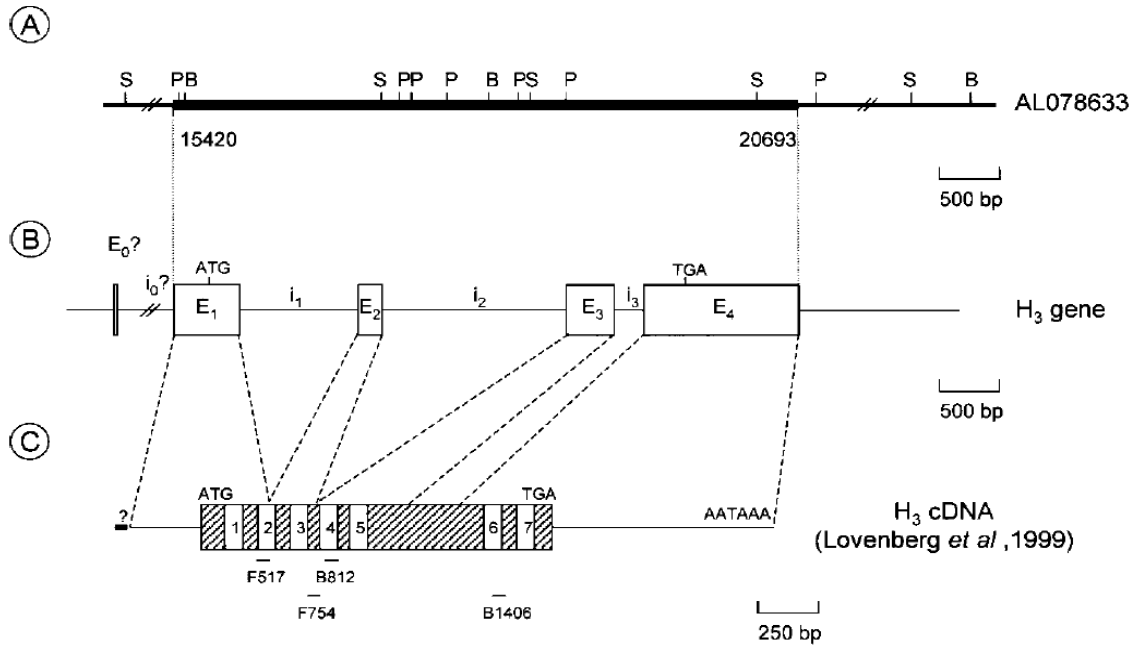

Figure 1.5 Schematic organisation of the human H_3R gene and cDNA**.** (*A*) Restriction map of the genomic DNA fragment from human chromosome 20 (accession number AL078633). B, *Bam*HI ; P, *Pst* I ; S, *Sa* cI. (*B*) Schematic structure of the H_3 gene with the location of exons (E_{1-4}) shown by boxes and the location of introns (I_{1-3}) shown by horizontal lines. The exons are numbered from the 5' end of the gene with exon E_1 containing the first ATG codon. The initiation (ATG) and termination (TGA) codons are indicated. Exon E_0 and intron i_0 were deduced from the H_3R cDNA described by Lovenberg et al, 1999, but are not confirmed. (*C*) Structure of the human H_3R cDNA. The coding region is shown by boxes and the 5'- and 3'-UTRs are shown by horizontal lines. The putative TMs (1-7) are mentioned in the coding region. The translation initiation site (ATG), the termination site (TGA) and the polyadenylation signal sequence (AATAAA) are indicated. The forward (F) and reverse (B) primers used for RT-PCR analysis are shown under the cDNA structure.

The result of the diverse exon/intron junctions results in alternative splice sites with the potential to generate a large number of distinct receptor isoforms (Fig 1.6).

Figure 1.6: Generation of the major histamine H_3R splice isoforms:

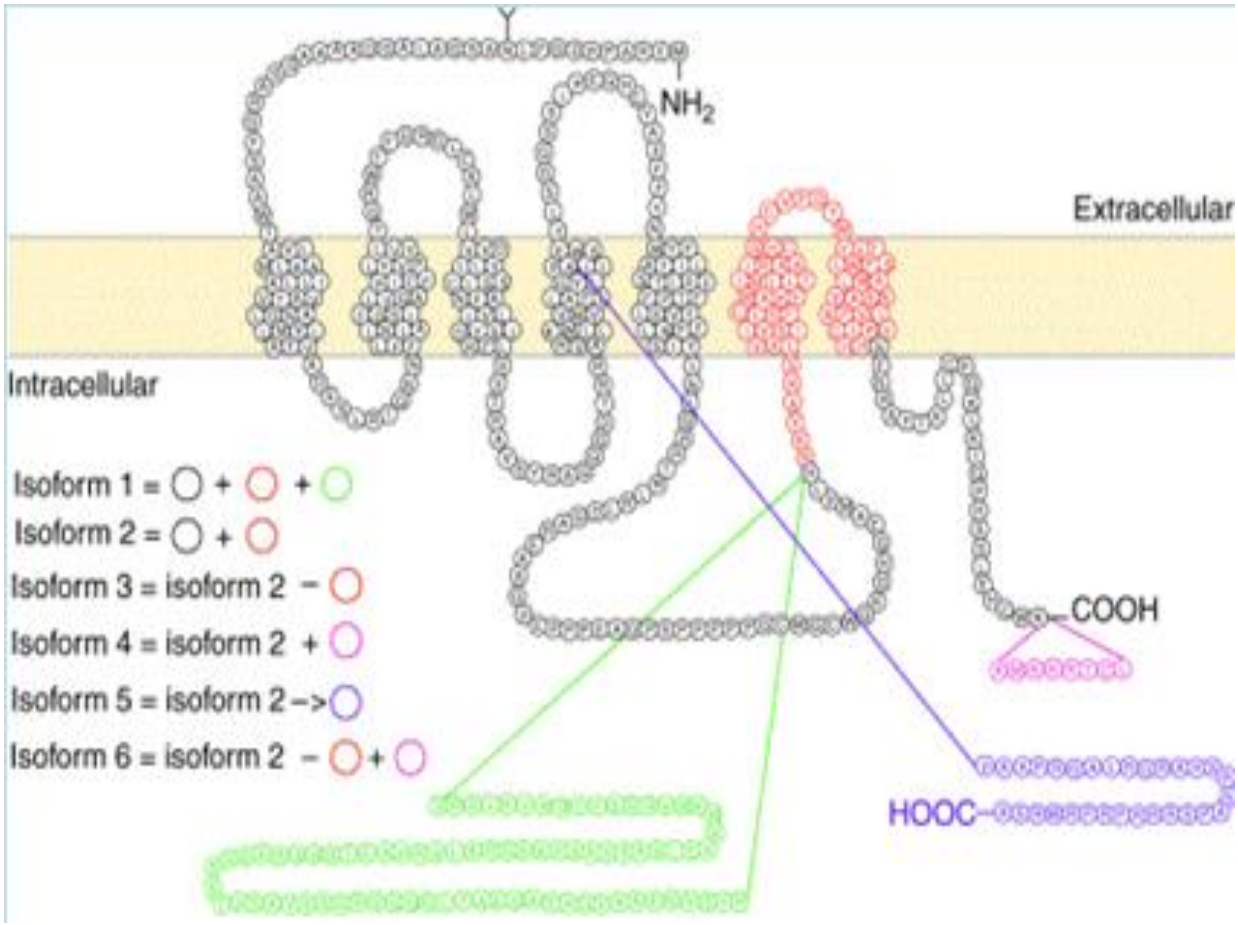

Reproduced with kind permission of Rob Leurs Vrije Universiteit, The Netherlands

Figure1.6 Reported human histamine H_3R isoforms. Isoforms 1 (H_3R_{445}) is similar to that previously reported by Lovenberg et al., 1999, whereas isoform 2 (H_3R_{365}) has an 80 amino acid deletion in the third intracellular loop. Isoform 4 (H_3R_{373}) has the same deletion as isoform 2 combined with an 8 amino acid longer C terminal. Isoform 3 (H_3R_{301}) contains a 144 amino acid deletion, which includes the same deletion as isoform 2 but also eliminates transmembrane domain (TM) 6 and TM7. This deletion is also found in combination with the additional eight amino acids at the C terminus, producing isoform 6 (H_3R_{309}). Isoform 5 (H_3R_{200}) is generated as a 409 nucleotide deletion and a frame shift, resulting in a protein with a deleted TM4 and TM5, and a new 30 amino acid C terminal.

The existence of multiple human H_3R isoform mRNAs has opened up possibilities to account for the pharmacological heterogeneity reported for many years for the H_3R, within and across species. The reasons for this heterogeneity are complex and not fully understood. In all species tested so far, the full length H_3R encodes a polypeptide of 445 amino acids. Approximately 20 shorter human isoforms have been identified to date with

deletions in the N terminus, second TM domain and first extracellular loop, intracellular loops or at the C terminus. The majority of isoform receptors are produced through deletions predominately in the third intracellular loop domain (usually beginning at amino acid residues 274 or 275) resulting in loss of TM 5/6 and/or 7. Isoforms that have deletions in their third intracellular loop have attracted a lot of interest because of the coupling of the third intracellular loop with different G proteins (Drutel et al., 2001). These isoforms show variation in their pharmacological profile (Hancock et al., 2003) such as agonist potencies (Wellendorf et al., 2002), signalling properties (Drutel et al., 2001) and constitutive activity (Morisset et al., 2001 and Leurs et al., 2008).

H_3R isoforms have also been identified in the rat (Drutel et al., 2001 and Morisset et al., 2001), mouse (Rouleau et al., 2004) and guinea pig (Tardival-Lacombe et al., 2000). The number of H_3R isoforms possible is high due to simultaneous occurrence of multiple splicing events in the same H_3R mRNA. The mechanisms regulating alternative splicing of the H_3R gene remains to be investigated.

Reverse Transcriptase-PCR was used to detect the presence of human H_3R isoforms in the CNS (Cogé et al., 2001). The data generated highlighted regional variation in the distribution of the different isoform mRNAs, however expression patterns of the isoform proteins have not been investigated and will investigated in this project. The hH_3R_{445}, hH_3R_{365} and hH_3R_{329} isoforms will be the focus of the thesis, as their respective mRNAs have been shown to be highly expressed in regions involved in motor, anxiety behaviours and learning and memory. Moreover these isoforms have also been shown to display a high degree of overlap in these brain areas (Cogé et al., 2001) indicating the

possibility of H_3R isoform hetero-oligomers. Regional variation has given rise to speculation that H_3R heterogeneity could underlie different functions of the H_3R in specific brain regions. Furthermore, there is growing evidence that homo- and hetero-oligomerisation of H_3 isoforms may occur and yield a novel regulatory mechanism (Shenton et al., 2004 and Bakker et al., 2006). Oligomerisation occurs in most GPCRs however, it is not clear whether this occurs *in vivo* and what the functional significance of this might be.

Not all of the isoforms are likely to be expressed at the cell surface; rat isoforms D, E and F have been shown to act as dominant negatives *in vitro* to either directly or indirectly control surface expression of the rat isoforms A, B and C (Bakker et al., 2006). Furthermore, receptors with deletions in regions thought to be important in ligand binding, and/ or signal transduction may not be functional. Previously, Cogé et al., (2001) has shown two of the H_3R isoforms varied from the full length in terms of binding and signal transduction. The pharmacological properties of the hH_3R_{431} and the hH_3R_{365} were compared to the full length hH_3R_{445}. The hH_3R_{431} was unable to bind [^{125}I]-iodoproxyfan, a H_3R antagonist, due to the deletion in the second TM domain while the hH_3R_{365} displayed the same pharmacological profile as the full length, however the hH_3R_{365} was unable to transduce a signal in the recombinant cell lines. Recently Leurs et al., (2008) reported differential expression of the hH_3R_{365} and the $hH_3R_{445,}$ with the hH_3R_{365} displaying higher expression levels than the hH_3R_{445} in many brain structures. The hH_3R_{365} also displayed higher affinity and potency for H_3R agonists and conversely a lower potency and affinity for H_3R inverse agonists. The hH_3R_{365} also displayed

higher constitutive signalling compared to the hH_3R_{445} in both [^{35}S] GTPγS binding and cAMP assays. Lower expression patterns were observed for the $hH_3R_{415,}$ hH_3R_{413} and hH_3R_{329} which were also capable of binding H_3R ligands and exhibited subtle difference in coupling to signalling mechanisms. H_3R isoforms activate different G proteins resulting in differential signalling, function and potency. Due to differential G protein coupling, H_3R ligands may behave variably at the individual isoforms *in vivo*. These differences observed in the H_3R pharmacology and signalling of the H_3R isoforms are likely to be important for obtaining a detailed understanding of the physiological and potential therapeutic roles of the H_3Rs. Part of this thesis will involve determining the pharmacological profile of an array of H_3R ligands at three of the major human H_3R isoforms.

b) Genetic Polymorphism

Genetic polymorphisms have also been identified within the human H_3R gene which contributes to the wide diversity of the H_3R pharmacology. Independent publications and GenBank submissions of the human H_3R sequences have identified either a glutamic acid (Accession nos. XM009561, AB019000 and AB045369) or aspartic acid (AF363791) at position 19 (Hancock et al., 2003). A polymorphism was identified at position 280, an alanine to valine substitution. The polymorphism was discovered in a patient suffering with Shy-Drager syndrome which is also known as neurological orthostatic hypotension, a disease characterised by neuronal degeneration and autonomic failure. Abbott Laboratories confirmed this finding as well as a polymorphism at position 197, a tyrosine to a cysteine substitution (Hancock

et al., 2003). Several single amino acid polymorphisms have also been identified in the third intracellular loop in the rat H_3R (Cogé et al., 2001).

c) Signalling pathways

Before the cloning of the H_3R it was already shown to be coupled to the inhibitory class of GPCR's, $G\alpha_{i/o}$. This discovery was shown by pertussis-toxin (PTX) sensitivity of the H_3R agonist-dependant [^{35}S]GTPγS binding in the rat brain (Clark et al., 1996). This was later confirmed once the H_3R had been cloned, by the transfection of the H_3R in various recombinant cell lines (Lovenberg et al., 1999). Our laboratory provided the first evidence for the interaction of native the H_3R in rat striatum with the $G\alpha_{i/3}$ protein (Victoria Hann PhD Thesis 2003). Activation of the H_3R in recombinant cells results in the activation of the pertussis-toxin sensitive $G\alpha_{i/\ olf}$ family of G proteins (Clark et al., 1996), resulting in the inhibition of adenylyl cyclase. Decreased adenylyl cyclase activation lowers the level of cAMP which in turn inhibits activation of downstream events such as the activation PKA and hence CREB dependant gene transcription. Activation of H_3R also leads to activation of other effector molecules such as mitogen activated protein kinase (MAPK), phospholipase A_2 (PLA_2) and phosphatidylinositol-3-kinase (PI3K). Activation of PLA_2 results in the release of arachidonic acid, inhibition of Na^+/K^+ anti-porter and K^+ induced reduction of intracellular Ca^{2+} and hence reduced neurotransmitter release. Activation of MAPK and PI3K results in phosphorylation of extracellular signal-regulated kinases (ERKs) and protein kinase B (PKB). The MAPK pathway is thought to be important in memory consolidation and neuronal plasticity (reviewed by Leurs et al., 2005). The activation of

PKB/GSK3β pathway is important in neuronal development and function, regulating synaptic strength and memory consolidation and retrieval. Furthermore, deregulation of GSK3β is linked to disease such as diabetes, insulin resistance and Alzhiemer's Disease. Activation of some of the rat isoforms that have deletions in the third intracellular loop vary in their effectiveness in activating cAMP responsive element independent transcription or MAPK activation (Drutel et al., 2001).

d) Effector mechanisms

The H_3R has been shown to be coupled with voltage activated calcium Ca^{2+} channels. Activation of the H_3R controls the release of neurotransmitters by inhibiting the calcium current crucial for neurotransmitter release. Reduction of the current reduces the size and frequency of the spontaneous calcium-dependent pre-potentials to depress the firing rate and hence neurotransmitter release. H_3R activation was shown to suppress N- and P- type calcium channels in a pertussis toxin-sensitive G protein-sensitive manner (Takeshita et al., 1998). H_3R agonists have also been shown to reduce noradrenalin (Levi et al., 2000) during myocardial ischemia via reducing intracellular Ca^{2+} (Silver et al., 2001).

e) Constitutive activity

H_3Rs can be activated in an agonist-independent manner as well as in the presence of an agonist, indicating the receptor has constitutive activity (Morisset et al., 2000). Typically GPCRs do not show constitutive activity because they lack the 8 amino acid sequence at the C terminal of the third

intracellular loop that confers constitutive activity. A mutation in the β adrenergic receptor in the last 8 amino acids at the C terminal domain of the third intracellular loop conferred constitutive activity. The H_3R also has the same sequence as the mutated the β adrenergic receptor resulting in the receptor having constitutive activity. The H_3Rs has been shown both *in vitro* and in native tissue to have high constitutive activity (Morisset et al., 2000). This may have significant effects on how the receptor is regulated *in vivo*, although this still remains controversial. Antagonists that reduce the receptors tonic activity are known as inverse agonists, whilst a neutral antagonist will simply return the receptor activity back down to its normal tonic activity.

1.2.2.4 Histamine H_3R pharmacology

a) Agonists

All histamine agonists show a similar structure to the endogenous agonist histamine (Fig 1.7), which binds to the H_3R with high affinity.

H_3R agonists:

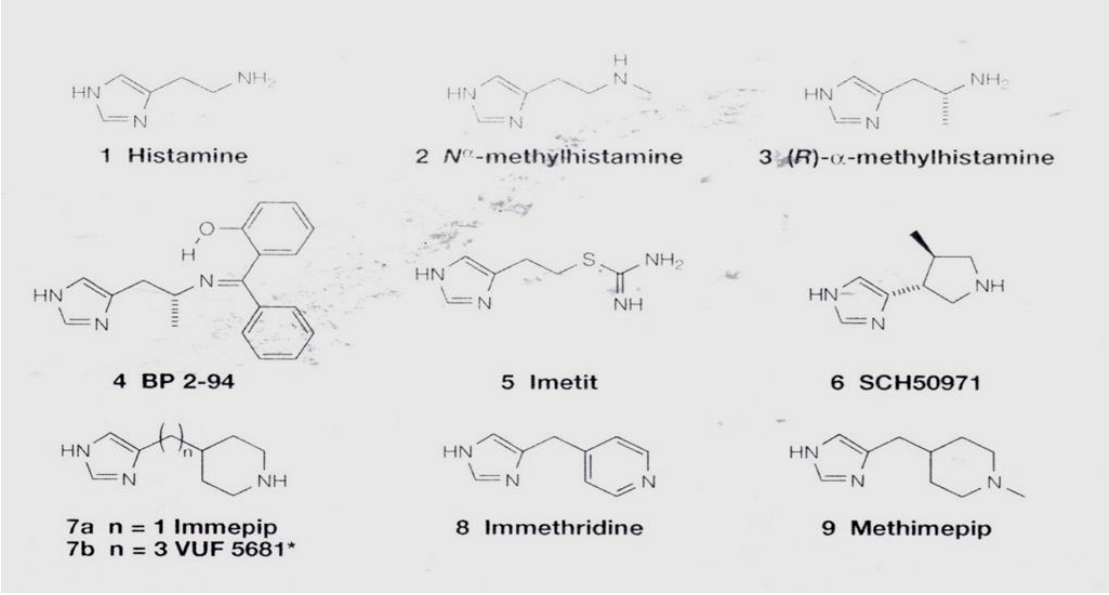

(Leurs et al, 2005)

Fig. 1.7 shows a variety of imidazole-containing histamine H_3R agonists all displaying varying degrees of affinity and potency at the H_3R. * Compound 7b is not an agonist but a neutral antagonist.

H_3R agonists contain a 4(5)-substituted imidazole moiety which is essential for H_3R activity. Additional attachments to the 4(5)-substituted imidazole moiety eliminate H_3R activity (Leurs et al., 2005). Potency and selectivity of H_3R agonist can be increased by small structural modifications to the imidazole side chain. Compound 2 – N-α-methylhistamine is three times more potent than histamine and is formed from methylation of the basic amine group. Methylation of the imidazole side groups results in compound 3 – RαMHA. RαMHA is considered to be the standard H_3R agonist and has been extensively used in pharmacological studies, however it is not used *in vivo* because it is hydrophilic, extensively metabolized and has low oral bioavailability (Leurs et al., 2005). These problems were overcome by the use of pharmacologically inactive pro-drug compounds that are converted to an active form of the drug by endogenous enzymes or metabolism. Pro-drugs overcome problems associated with stability, toxicity, lack of specificity or limited oral bioavailability. Novel azomethane pro-drugs of RαMHA include BP 2-94, compound 4. Replacement of the amine group with an isothiourea moiety results in compound 5 – imetit (Lovenberg et al., 1999 and van der Goot et al., 2000). SCH50971, compound 6 and immepip, compound 7 are formed by incorporation of a flexible side chain of RαMHA into a pyrrolidine ring or piperidine ring, respectively. The reduced flexibility of the side chain increases the H_3R affinity (Leurs et al., 2005).

RαMH and imetit have limited use *in vivo* because of selectivity issues with the cardiovascular system, mediated through the α_2 receptors or 5-HT_3

receptors. Note, RαMH and immepip show limited selectivity for the H_3R over the recently discovered H_4R. Modification of immepip by reducing the basicity of the pyridine ring results in immethridine, a slightly less active compound, but with a 300-fold selectivity for the H_3R versus the H_4R (Kitbunnadaj et al., 2004). N-methylation of the piperidine ring on immepip produces compound 9 – methimepip. Methimepip shows high affinity for the H_3R as well as 2000-fold selectivity for the H_3R over the H_4R and is capable of penetrating the blood brain barrier (Kitbunnadaj et al., 2004 and Leurs et al., 2005). Impentamine, compound 10 has antagonist properties in the guinea pig jejunum, whereas in recombinant human H_3Rs it displays agonistic properties (reviewed Leurs et al., 2005).

b) Antagonist

There are two major classifications of H_3R antagonists imidazole-containing or non-imidazole containing antagonists (Fig 1.8).

H_3R antagonists:

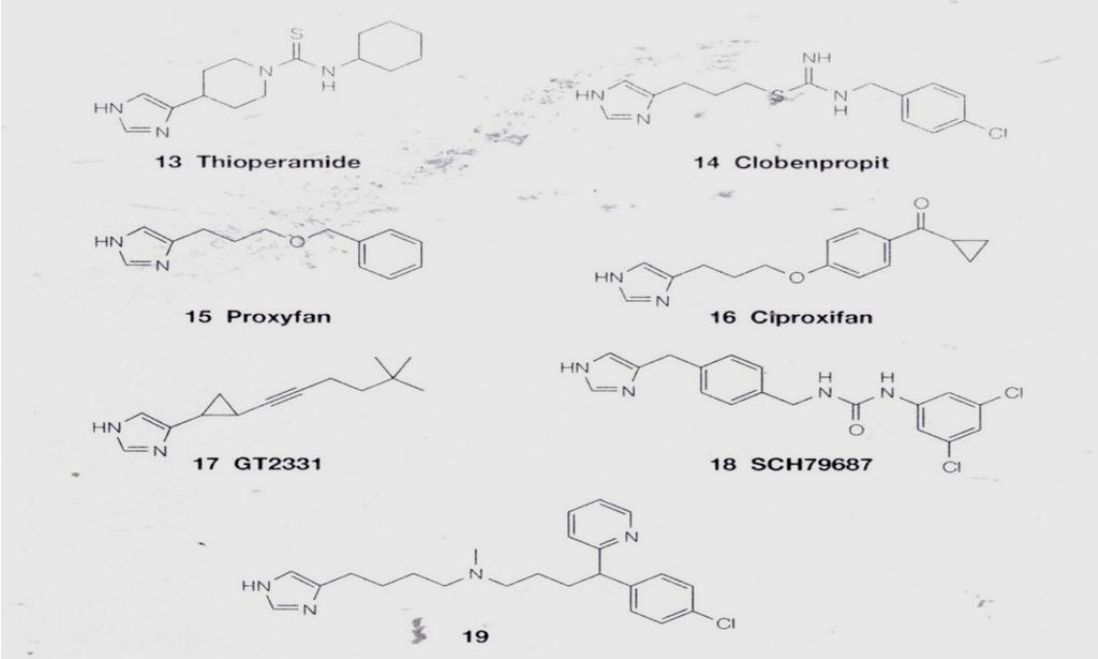

(Leurs et al, 2005)
Fig. 1.8 shows a variety of imidazole-containing histamine H_3R antagonist**s** all displaying varying degrees of affinity and potency at the H_3R.

i) Imidazole-containing antagonists

First generation imidazole-based H_3R antagonists, such as thioperamide, clobenpropit, and ciproxifan, were discovered several years ago before the molecular characterization of the H_3R. Thioperamide, compound 13 was the first H_3R antagonist to be developed that lacked both H_1R and H_2R activity (Arrang et al., 1987). After the discovery of constitutive activity of the H_3R all antagonists that reduced the tonic activity of the receptor were re- classified as inverse agonists. Thioperamide has been used as the gold standard for over two decades. However, it displays higher affinity for the rat H_3R than the human H_3R (Lovenberg et al., 2000), it also has high affinity for the H_4R, rat 5-HT_3 receptor, α_{2A} receptor and the human α_{2C} receptor (Esbenshade et al., 2003).

Potent H_3R antagonists can be produced by increasing the distance between the basic moieties of agonists and/or the attachment of larger lipophilic moieties in the side chain, such as clobenpropit an imetit analogue (compound 14), (van der Goot et al., 2000). Proxyfan, compound 15 (Morrisset et al., 2000) is known as a protean agonist because it shows an array of pharmacological profiles dependant on the signalling assay used, however it is generally classed as a neutral antagonist at the H_3R (Gbahou et al., 2006). Proxyfan is produced by removing the basic moieties in the imidazole side chain. Relatively small structural changes to proxyfan can change its mode of action e.g. ciproxifan, compound 16 is a potent inverse agonist (Hancock et al., 2003 & 2006). Ciproxifan has limited *in vivo* use

because of its moderate affinity to the human H_3R, rat 5-HT_3 receptor, α_{2A} receptor and the human α_{2C} receptor (Esbenshade et al., 2003).

However, these compounds proved to be undevelopable as therapeutic agents for humans due to a number of liabilities, including cytochrome P450 inhibition, low affinity for human compared with rat H_3 R, lack of selectivity and/or suboptimal brain penetration (LaBella et al., 1992 and Yang et al., 2002), leading to the development of non-imidazole containing compounds (reviewed by Leurs et al., 2005).

ii) Non-imidazole containing antagonist

Non-imidazole containing antagonists show the most promise as future drugs for the treatment of cognitive impairment, attention deficit hyperactivity disorder (ADHD), schizophrenia, narcolepsy, seizure and obesity. To date the following compounds are in clinical trials: BP2.649, GSK-189254, JNJ-17216498 with others in line, GSK-239512, CEP-16095, CEP-26401 and SAR-110894. Further properties have been engineered into the compounds depending on their therapeutic potential use, acetylcholine esterase (Petrianou et al, 2006), serotonin re-uptake (Keith et al, 2007) or on their use as pharmacological tools (fluorescent, radioactivity), maintaining or increasing their H_3R affinity.

1.2.2.5 Pharmacological heterogeneity

Pharmacological heterogeneity of H_3Rs both within and between species has long been recognised and has in part resulted in the delay of H_3R ligands entering the clinic. Cloning of the H_3R has led to better understanding of the

structure of the H_3R and the occurrence of alternative splicing. Receptor polymorphism, receptor isoforms and differential distribution profiles are likely to underlie some of this diversity (Coge et al., 2001, Drutel et al., 2001, Wellendorf et al., 2002, Hancock et al., 2003 and Rouleau et al., 2004).

a) Inter-species and intra-species isoform heterogeneity

Radioligand binding along with functional assays have shown the different pharmacological profiles of various H_3R ligands across the species. Numerous H_3R ligands display variable affinities across the species (Leurs et al., 2005 and Medhurst et al., 2007). Isoforms of the H_3R have also been shown to vary in their affinities for different H_3R ligands. The hH_3R_{365} has been shown to display higher affinity and potency for H_3R agonists and conversely a lower potency and affinity for H_3R inverse agonists when compared with the hH_3R_{445} isoform. The hH_3R_{365} also displayed higher constitutive signalling compared to the hH_3R_{445} in both [^{35}S] GTPγS binding and cAMP assays (Leurs et al., 2008).

b) Evidence for key amino acid residues being responsible for inter-species difference

Comparison of H_3Rs between species; human, canine, rat and guinea pig identified key amino acids involved in the distinct inter-species heterogeneity. For example, A-304121 was shown to display varying affinities at rat 30-fold > guinea pig 300 fold > human (Hancock et al., 2003). Two key amino acids were found to explain the variation seen; mutation of the rat full length receptor at a single site V122A or at two sites V122A and A119T, resulted in

H_3R ligands displaying a pharmacological profile which matched that of the human H_3R. The single mutation resulted in ciproxifan, a H_3R inverse agonist/ antagonist displaying a 5-fold lower affinity at the rat H_3R whilst the double mutation resulted in an 18-fold lower affinity resulting in the rat H_3R displaying an identical pharmacological profile to the human H_3R (Ligneau et al., 2000). Amino acids at position 119 and 122 in TM3 have been shown to be critical for determining the affinity for a number of non-imidazole antagonists.

c) Heterogeneity within species

Pharmacological data since the 1990s has pointed to H_3R heterogeneity and the possibility of receptor subtypes. To date there has been 20 different putative human H_3R isoforms described, some of which have been shown to be pharmacologically functional whilst others are non-functional (Coge et al., 2001 and Wellendorf et al., 2002). In rat cortical membranes it has been shown that there are different classes of H_3R binding site, having either a slow or fast off rate in the presence of [^{3}H]-RαMHA (West et al., 1990). Thioperamide and burimamide were then used to show that the rat H_3R has two types of receptor a high affinity (H_3R_A) and a low affinity (H_3R_B).

d) Evidence for different splice variants exhibiting distinct pharmacologies

The existence of splice variants of the H_3R opens up the possibility that the heterogeneity seen within species may be the result of H_3R ligands displaying variable affinities at the splice isoforms. Thioperamide, a H_3R antagonist has been shown by one group to display a higher affinity at the full length receptor

when compared with H_3R_{365} isoform (Wellendorf et al., 2002). However, other studies failed to show any variation in affinity at the two isoforms with ciproxifan, thioperamide or clobenpropit (Coge et al., 2001 and Hancock et al., 2003). On the other hand, thioperamide was shown to be more potent at shorter isoforms of the rat H_3R (Morisset et al., 2001), also seen with clobenpropit and ciproxifan (Drutel et al., 2001). Part of this present project is designed to determine the pharmacological profile of a number of H_3R ligands at three of the major human histamine H_3R isoforms, $H_3R_{445,}$ H_3R_{365} and $H_3R_{329.}$

Co-expression of isoforms may also account for some of the pharmacological heterogeneity seen with H_3R ligands. Co-expression of the full length rat H_3R_A with the shorter rat H_3R_D isoform has been shown to reduce the expression of the full length receptor in a dominant negative manner. Part of this present project is designed to determine whether co-expression of three of the human isoforms has any effect the pharmacological profile of a number of H_3R ligands.

1.2.2.6 *In vivo* role of histamine H_3R

Histamine and the histaminergic system both play a vital role in nervous system regulation and behaviour. The role of histamine in arousal, attention and homeostatic mechanisms has been well documented (reviewed by Brown et al, 2001). Selective H_3R antagonists have been shown to improve performance in a diverse range of rodent cognition paradigms, including object recognition, olfactory recognition, water maze, radial maze, and

passive avoidance, with most pronounced effects being observed in models where a cognitive deficit is present such as in aged animals or following a pharmacological challenge, eg. scopolamine (Hancock et al., 2004 and Witkin et al., 2004). H_3R antagonists can also clearly increase wakefulness in preclinical and clinical models, consistent with the pivotal role of histamine in the sleep-wake cycle (Schwartz et al., 2010 & 2011). These studies have generated considerable interest in the development of H_3R antagonists as novel treatments for cognitive deficits in conditions such as Alzheimer's disease, other dementias, mild cognitive impairment, and schizophrenia as well as for disorders of sleep and attention such as narcolepsy and ADHD (Medhurst et al., 2007 & 2009 and reviewed in Chazot, 2010).

a) Arousal

The first evidence that the histaminergic system is involved in arousal came from one of the side effects associated with 1st generation anti-histamines, namely sedation. This was later confirmed using several techniques. Lesion studies in the TMN and the posterior hypothalamus lead to hypersomnia (Lin et al., 2008). Electrophysiology studies have shown neuronal firing to vary across the sleep/wake cycle as well as the correlation between histamine release in the pre-frontal cortex and waking (Sakai et al., 1990). Histamine release follows a circadian rhythm, with mice that lack brain histamine unable to stay awake during high vigilance (Parmentier et al., 2002). The H_3R antagonist, thioperamide, has been shown to increase brain histamine levels and wakefulness, while RαMHA, a H_3R agonist, enhanced deep slow wave sleep. Also, H_3R -/- mice have been shown to be insensitive to the wake

promoting effects of H_3R antagonists (Toyota et al., 2002). GSK189254 and pitolisant, potent H_3R antagonists are currently in phase II clinical trials for narcolepsy (reviewed in Chazot 2010, Lin et al., 2000).

c) Homeostasis

Histamine has been shown via pharmacological studies in intact animals to play a role in various homeostatic mechanisms involving the hypothalamus and including fluid balance, eating, thermoregulation and cardiovascular regulation (Hough et al., 1988 and Schwartz et al., 1991).

i) Fluid balance

Injecting histamine into the cerebral ventricles or into several hypothalamic sites elicits drinking, as well as an increase in the release of vasopressin which decreases urine output mediated by both H_1 and H_2 receptors (Brown et al., 2001). Dehydration has been shown to increase the synthesis and release of histamine in the hypothalamus. Blockade of histamine synthesis with α-FMH or activation of pre-synaptic H_3Rs or antagonism of post- synaptic receptors reduces dehydration induced vasopressin release (Kjaer et al., 1994).

ii) Food intake

Intracerebroventricular (ICV) injection of histidine or application of the H_3R antagonist thioperamide suppresses food intake through the increase in histamine acting at the H_1R, whereas application of α-FMH or an H_1R antagonists increases food intake (Brown et al., 2001). H_3R -/- mice tend to

show a mild obese phenotype with increased body weight, food intake and adiposity and decreased energy expenditure (Takahashi et al., 2002). H_3R antagonists, in obesity induced by a high fat diet in mice, have been shown to be effective in reducing food intake and weight in comparison to that of mice on a low fat diet (Hancock et al., 2006). However, H_3R antagonists do not induce an anorexigenic effect in H_3R -/- mice. *In situ* hybridisation studies have also revealed H_3R mRNA expression in rat brown adipose tissue, indicating that H_3R antagonists in the periphery may be able to regulate thermogenesis (Karistedt et al., 2003).

iii) Cardiovascular control

ICV injection of histamine increases blood pressure and decreases heart rate in conscious animals; similarly inhibiting histamine break down in the hypothalamus has similar effects (Brown et al., 2001). H_3Rs have been identified as inhibitory hetero-receptors in cardiac adrenergic sympathetic nerve endings and H_3R activation decreases carrier mediated noradrenergic release in guinea-pig and human heart. Transfection of H_3R in SKNMC neuroblastoma cells inhibited the Na+/K+ exchanger which is important in the transport of noradrenalin across the cell membrane. H_3R activation may have a cardioprotective effect by limiting the excessive release of noradrenalin during protracted myocardial ischemia (Silver et al., 2001). H_3R -/- mice have increased noradrenalin release and reperfusion–induced arrhythmias induced by ischemia (Koyama et al., 2003). The role of the H_3R on adrenergic neurons under normal physiological conditions was not explored.

d) Cognition, learning and memory

Arousal and attention play an important part in the cognitive process. Central histamine plays a key part in cognition, learning and memory. The histaminergic system innervates several structures that are known to be involved in cognition such as the basal forebrain, cerebral cortex, anterior cingulate cortex, amygdala and thalamus. Histaminergic neurons have an excitatory action on cholinergic projections to the hippocampus (Medhurst et al., 2007a & 2009). Direct and indirect activation of brain histamine has been shown to have pro-cognitive effects. Increasing brain histamine has been shown to improve social memory in rats whilst histamine reduction have detrimental effects (Prast et al., 1996).

Histamine interacts with the polyamine site on the NMDA NR2B receptor subtype (reviewed in Witkin et al., 2004 and Shenton & Chazot, 2007) as well as induced facilitation of long-term potentiation in rat hippocampal slices (Selbach et al., 1997), further supporting a role of histamine in cognition.

In neuropsychiatric disorders such as AD, ADHD and schizophrenia, cognitive deficits play a major role in the disease (Leurs et al., 2005, Chazot, 2010). Decreased levels and/ or function of acetylcholine are thought to be a major contributor to age-related cognitive decline. Increased brain histamine is also positively correlated with age which may play a role in decreased acetylcholine uptake and function (Prell et al., 1991). Therefore, it is thought that H_3R antagonists may be able to prevent the reduction in acetylcholine through its role as a hetero-receptor (Blandina et al., 1996, Orsette et al., 2002 and Bacciottini et al., 2002).

Several H_3R agonists and antagonists have been tested in different learning paradigms. Generally, H_3R antagonists improve memory either by an increase in histamine (Miyazaki et al., 1995 and Miyazaki et al., 1997) or by an increased release of other neurotransmitters such as acetylcholine, noradrenaline and dopamine (Blandina et al., 1996). In contrast, H_3R agonists were shown to reverse the effects of H_3R antagonists. The H_3R antagonist, thioperamide has been shown to increase acetylcholine in the rat hippocampus (Mochizuki et al., 1994), and enhances recall of a passive avoidance response in rats and senescence-accelerated rats. H_3R antagonists also show promise in short term memory novel object recognition test (Giovannini et al., 1999) and social recognition tests (Prast et al., 1996), while immepip, a H_3R agonist produces cognitive deficits in tests of olfactory and social memory (Prast et al., 1996). Abbott laboratories reported that A-317920, a highly potent H_3 antagonist, was as effective as methylphenidate (Ritalin) and ABT-418 (a nicotinic receptor ligand), both of which are clinically effective drugs in AD (Hancock et al., 2006). ABT-239, a H_3R antagonist entered clinical development after displaying promising results in preclinical trials in models of ADHD and AD. ABT-239 also increased acetylcholine in the prefrontal cortex and hippocampus (Cowart et al., 2005), improved learning in a five trail inhibitory avoidance using rat pups, improved recall in a social memory test, and improved spatial working and reference memory in a water maze (Fox et al., 2005 and Esbenshade et al., 2005). An ABT-239 congener, A-304121, also shows promising pro-cognitive effects in rodent models (Fox et al., 2005, Esbenshade et al., 2005 and reviewed by Chazot 2010).

GSK189254 is derived from a novel benzazepine series of H_3R antagonists (Medhurst et al., 2007a) that are structurally distinct from other recently described non-imidazole H_3R antagonists (Fig 1.9).

Structure of GSK189254:

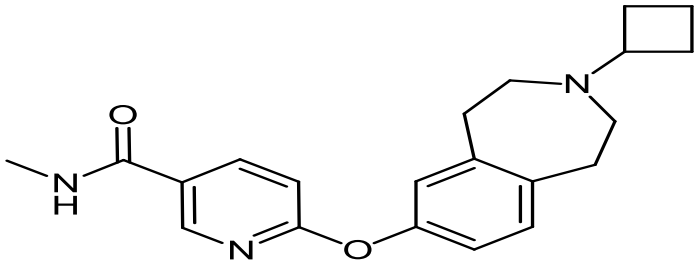

GSK189254

Figure 1.9 Shows the structure of the H_3R ligand GSK189254.

GSK189254 shows sub-nanomolar affinity for the human H_3R, and a 6-10 fold lower affinity for the rat H_3R. These pharmacological differences have been attributed to two amino acid differences in the third transmembrane domain where threonine 119 and alanine 122 of the human H_3R are replaced with alanine 119 and valine 122 in the rat (Ligneau et al., 2000). GSK189254 has been shown to significantly improve performance of rats in diverse cognition paradigms, including passive avoidance (1 and 3 mg/kg p.o.), water maze (1 and 3 mg/kg p.o.), object recognition (0.3 and 1 mg/kg p.o.), and attentional set shift (1 mg/kg p.o.) (Medhurst et al., 2007a and reviewed by Chazot 2010).

The data so far for H_3R antagonists points to a possible therapeutic potential for diseases where cognitive deficits occur such as AD, other dementias, and schizophrenia.

Part of this thesis will determine whether H_3R expression is preserved in aging and dementia in both human (AD and dementia with Lewy bodies (DLB)) and rodent ageing and dementia models (CD-1 and TASTPM), refer to chapter 5 for details on models.

d) Pain and stress

A number of studies have examined the role of the central histamine system in modulating nociception. Peripheral histamine plays a role in the stimulation of nociceptive fibres, while central histamine plays an important role in anti-nociception (Chazot et al., 2004 and Hough et al., 2011). Administration of histamine into the cerebral ventricles or periaqueductal gray, has been shown to have an analgesic effect in several paradigms including the tail-flick and hot-plate tests (Thoburn et al., 1994). The anti-nociceptive effect of histamine varies depending on the site of administration. Increasing brain histamine by administration of histidine, as well as using a catabolism inhibitor metoprine or a H_3R antagonists thioperamide have all displayed an anti-nociceptive action (Malmberg et al., 1997). On the hand a reduction in brain histamine by administration of either α-FMH or H_3R agonists have a pro-nociceptive action (Malmberg et al., 1997). The anti-nociceptive effect seen with histamine is the result of blocking the enhanced firing of nociceptive neurons located in the nucleus lateralis and ventrobasalis of the thalamus following noxious test stimuli via a H_1R mediated inhibition of afferent pathways (Brown et al., 2001). H_1 and H_2 receptor antagonists applied ICV or into the periaqueductal gray have been shown to block histamine-induced anti-nociception, confirming the role of the H_1R and the H_2R in pain perception. H_1R -/- and H_2R -/- mice show

fewer nociceptive responses in a wide range of pain models (Brown et al., 2001).

The potential involvement of H_3R in pain processing has been suggested by previous studies using H_3R agonists and antagonists in preclinical pain models. H_3R agonists have been shown to either cause allodynia, or attenuate hyperalgesia, depending on the model used (Cannon et al., 2005 and Medhurst et al., 2007b). Secondly, the H_3R antagonist thioperamide can produce anti-nociceptive effects in a number of acute pain models (Medhurst et al., 2007b), but can also block morphine-induced analgesia (Owen et al., 1994). One study adopting a chronic constriction injury (CCI) model showed that the effects of acute thioperamide administration were opposing, depending on whether the compound was administered centrally or peripherally (Huang et al., 2007). The interpretation of thioperamide data is complicated by the recent discovery of its potent H_4R activity (Gbahou et al., 2006). H_3R antagonists were shown to be effective in a capsaicin-induced secondary hyperalgesia model (Medhurst et al., 2007b) suggesting an involvement of H_3R in pain processing, including central sensitisation. The chronic oral administration of the H_3R antagonists GSK189254 and GSK334429 were shown to display anti-nociceptive effects in two models of chronic pain, CCI model, and the varicella-zoster virus (VZV)-induced allodynia model (Medhurst et al., 2007b) . Furthermore, the H_3R has been shown to be expressed on the dorsal horn, suggesting a possible site of action for these analgesic effects. H_3R are also expressed in brain areas associated with pain processing such as thalamus and periaqueductal gray (Pollard et al., 1993). Our studies using H_3 specific antibodies (validated

using H_3 (-/-) mice, have also demonstrated H_3 expression not only in rat spinal cord, but in the skin (Cannon et al., 2007), on a subset of A-delta fibres. Furthermore, H_3R antagonists such as GSK189254 and GSK334429 may be useful for the treatment of neuropathic pain (Medhurst et al., 2007b).

1.2.2.7 Potential H_3R targeted therapies

Histamine acts as a powerful stimulant of gastric acid secretion, immune modulation, bronchoconstriction, vasodilation and neurotransmission. The hypothalamic histamine neurons are involved in the basic brain and body functions linking both behavioural state and biological rhythms with vegetative and endocrine control of body weight and temperature. Histamine maintains CNS readiness to react and keeps the organism alert.

Among the many roles of histamine in homeostatic and higher integrative brain functions, novelty-induced attention and arousal are of major importance for adaptation to the changing environments by comparing news with the remembrance of things past. This is important for brain development, physiology and pathophysiology, danger recognition, and survival.

Current areas of therapeutic interest lie in cognitive deficits (Leurs et al., 2005 and Hancock et al., 2006), dementias (Medhurst et al., 2007a & 2009), psychoses (Akhtar et al., 2006), movement disorders (Gomez-Ramirez et al., 2006), sleep disorders (Leurs et al., 2005), obesity (Hancock et al., 2006), migraine (Millan-Guerrero et al., 2003), cerebral ischemia (Lozada et al., 2005), cardiac arrhythmias (Levi and Smith, 2000), epilepsy (Chazot and Hann, 2001) and neuropathic pain (Medhurst et al., 2007b).

Histamine acting on the hypothalamus modulates the release of many hormones from the pituitary gland. The hypothalamic-pituitary-adrenal axis constitutes a major part of the neuroendocrine system that controls reactions to stress and regulates various body processes. The hypothalamic-pituitary-adrenal axis has similar features among different species. It is the mechanism for a set of interactions among glands, hormones and parts of the mid brain that mediate a general adaptation response. Histamine plays a key role in learning and memory as well as homeostasis during times of stress or threat, it seems that histamine and the histaminergic system have a physiological role to play in the danger response system. This thesis will address whether the H_3R has a specific role in anxiety behaviour rather than fear-induced avoidance behaviour, using a novel validated all-in-one elevated platform behavioural test.

1.3 Histamine H_4 receptor

The human histamine H_4 receptor (H_4R) was the latest histamine receptor to be identified (Oda et al., 2000, Nguyen et al., 2001 and Liu et al., 2001). As with the other histamine receptors, the H_4R belongs to the class A rhodopsin-like GPCRs. The amino acid sequence of the novel hH_4R protein was compared to known GPCRs, and was shown to have low homology with other histamine receptors. The closest resemblance is with the hH_3R in which the hH_4R shares 37.4% amino acid homology (Oda et al., 2000), and 58% homology in the transmembrane region (Hofstra et al., 2003). The H_3R gene structure is similar to that of the H_3R. The H_4R also undergoes alternative

splicing to generate isoforms, to date there are two validated splice variants, namely H_4R_{302} and H_4R_{67} (Van Rijn et al., 2008).

Similarly to the H_3R, the H_4R couples to the $G\alpha_{i/olf}$ family of heterotrimeric GPCRs, resulting in pertussis toxin sensitive (PTX) decrease in the forskolin-induced production of cAMP, which modulates the activity of PKA resulting in the inhibition of downstream events such CREB dependant gene transcription (Oda et al., 2000, Hofstra et al., 2003 and Liu et al., 2001).

The hH_4R has a distinct tissue distribution and is predominantly expressed on haematopoietic cells, especially peripheral eosinophils, mast cells, dendritic cells with low levels in tissues such as the small intestine, colon and trachea. The receptor is predominately expressed on tissues and cells implicated in inflammatory response, suggesting a role for the receptor in chronic inflammation (de Esch et al., 2005).

The H_4R has also been shown to be transcribed and expressed in the CNS. The first indications of the presence of the H_4R in the CNS were mRNA levels identified in the human cerebellum and hippocampus (Coge et al., 2001). Recently, H_4R transcripts have also been shown to be present in the human CNS, including spinal cord, hippocampus, cortex, thalamus and amygdala, with the highest levels of H_4 mRNA detected in the spinal cord. In rat, H_4 mRNA was detected in cortex, cerebellum, brainstem, amygdala, thalamus and striatum with low levels detected in the hypothalamus, and no signal obtained in the hippocampus. H_4R mRNA was also detected in the rat dorsal root ganglia and spinal cord. The H_4R for the first time was shown to not only be transcribed but also to be expressed on neurons in the rat lumbar DRG and in the lumbar spinal cord (Strakhova et al., 2009 and Connolly et al.,

2010). The H_4R has been shown in our own laboratory to be expressed in specific areas of the mouse brain; layer IV of the cerebral cortex, CA3 of the hippocampus and dense expression on the thalamus (Connolly et al., 2010). The expression of the H_4R in the DRG and spinal cord may suggest the presence of the receptor on peripheral neurons and may provide a link to the anti-pruritic and anti-nociceptive properties of selective H_4R antagonists (Strakhova et al., 2009). Our laboratory provided the first evidence for the functional expression if the H_4R on central neurons (Connolly et al., 2010).

The similarities between the H_3R and H_4R and the presence of both the receptors within the CNS has resulted in re-evaluations of compounds aimed at targeting either receptor due to their lack of selectivity and potential for cross reactivity. NMHA was shown to have modest affinity for the human H_4R and low affinity for the rat and mouse H_4Rs, whilst also displaying agonism at the human H_2R. Burimamide and imetit have been shown to display affinity for the H_4R, thioperamide, a H_3R antagonist was shown to have equal affinity for all three H_4R species orthologs. VUF8430 is a high affinity agonist for the human H_4R but also displays agonist activity at the human H_3R. RαMHA a known H_3R agonist, used in many autoradiographical studies to study the anatomical expression of the H_3R, has also been recently shown also to bind to the hH_4R. Clobenpropit acts as an antagonist at the H_3R whereas at the H_4R it acts as a partial agonist (Oda et al., 2000). Drug development for targeting the human H_4R is very complex not only because of the close homology the receptor shares with the human H_3R, but also the pharmacological variation displayed between species (de Esch et al., 2005).

1.4 Conclusions and Aims

The biology of histamine and its receptors are complex. Histamine is present in many parts of the body and receptor distribution is wide spread. Histamine plays a crucial role in many homeostatic and higher integrative brain functions. This is important for brain development, physiology and pathophysiology, danger recognition, and survival. Histamine interacts both directly and indirectly with a variety of receptors and chemical messengers to allow the body to respond to different situations allowing an integrated response to multiple influences.

The existence of multiple human H_3R isoform mRNAs has opened up possibilities to account for the heterogeneity seen with the H_3R. Regional variation in the distribution of the different isoform mRNAs could underlie the different activities and functions of the H_3R in specific brain regions and it is therefore important to establish the protein expression profiles of these isoforms in the CNS. Furthermore, there is growing evidence that homo- and hetero-oligomerisation of H_3R isoforms may occur and yield a novel regulatory mechanism (Shenton et al, 2005 and Bakker et al., 2006). Not all of the isoforms are likely to be expressed at the cell surface and may therefore modulate activity, expression and or function of other H_3R isoforms. Isoforms with deletions in their third intracellular loop show variation in their pharmacological profile (Hancock et al., 2003). The third intracellular loop is important in agonist/inverse agonist ligand binding, and/ or signal transduction and deletions within this region may result in non-functional isoforms. Due to differential G protein coupling, H_3R ligands may behave variably at the individual isoforms. It is therefore important to establish if expression of these

isoforms occur in vivo. The differences observed in the H_3R pharmacology and signalling of the H_3R isoforms are likely to be important for obtaining a complete understanding of the physiological and potential therapeutic roles of the H_3Rs.

Hypotheses to address relating to rodent and human H_3 receptors;

1. H_3R are preserved in murine and human aging and age-related dementias
2. Human H_3R homomeric isoforms and heteromeric subtypes display differential pharmacological properties
3. H_3R are involved in anxiety and memory behaviours

To test the hypotheses firstly, a panel of anti-human H_3R isoform specific antibodies require development and validation to identify and map the expression topography of central H_3R isoforms and to determine if there are any changes in isoform expression with aging and in age-related diseases. The next step is to determine whether there are any pharmacological differences between human H_3R isoforms using a novel, highly potent selective H_3R ligand GSK189254 to determine whether the human H_3R is preserved in murine and human aging and dementia. The final step is to determine the role of the H_3R in anxiety, motor and memory behaviours using a novel recently patented all-in-one open space behavioural test.

CHAPTER 2

Materials and general methods

2.1 Source of materials

2.1.1 Amersham International (Aylesbury, Bucks, UK)

Binding filters, Blotting paper, HRP linked secondary antibody – mouse, HRP linked secondary antibody – rabbit, Hyperfilm^{TM}, Nitrocellulose

2.1.2 BDH laboratory supplies (Leicestershire, UK)

Acetic acid, Ammonium persulphate, Chloroform, Citric acid, Diethylamine, Dimethyl sulphoxide (DMSO), DPX mountant, Ethanol, Glycerol, Hydrochloric acid, Isopropanol, Methanol, N,N,N',N'-tetramethylethylenediamine (TEMED), Potassium chloride, Potassium phosphate, Sodium chloride, Sodium hydrogen carbonate.

2.1.3 Calbiochem (Nottingham, UK)

Protease inhibitor cocktail set III

2.1.4 Cambrex Bio Science (Verviers, Belgium)

Foetal calf serum

2.1.5 Cambridge Research Biochemicals (Billingham, UK)

Peptides generated for anti-peptide antibody development

Name	Peptide Sequence	Position	Site of action
H_3RPAN peptide	RLSRDRKVAK- Cys	349 – 358	sequence common across species
human $H_{3(365)}$ peptide 1	EAMPLHRKVAKSLA-Cys	268 – 281	Intracellular loop 3, before TM6
human $H_{3(365)}$ peptide 2	Cys-EAMPLHRKVAKS	268 – 278	Intracellular loop 3, before TM6
human $H_{3(329)}$	Cys-YLNIQSFTQR	222 – 231	Intracellular loop 3
human $H_{3(200)}$	Cys-RRPRPRWRSA	190 – 200	C-terminal
Chazot 3 human H_4	Cys-IKKQPLPSQHSRSVSS	374 – 390	C-terminal
Chazot 4 human H_4	Cys-ERRRRKSSLMFSSRTK	251 – 266	Intracellular loop 3
Mouse H_4	Cys-VTKQPALSQNQSVSS	376 – 391	C-terminal

2.1.6 Immune systems (Bristol, UK)

Rodent/human Histamine H_3R peptide

Name	Peptide Sequence	Position	Site of action
ratH_3R_{AC} & human$H_3R_{453/445}$ peptide	EAMPLHRGSK-Cys.	268 – 277	Intracellular loop 3

2.1.7 Pierce (Rockford, UK)

Sulpho-NHS-SS-Biotin

2.1.8 Promega Ltd (South Hampton, UK)

VECTASTAIN® ABC kit, XL-1 Blue Competent *Escherichia coli* cells

2.1.9 Sigma-Aldridge chemical company (Poole, Dorset, UK)

3-maleimidobenzoic acid N-hydroxysuccinimide ester (MBS), Acrylamide/bis-acrylamide 30%, Agar, Agarose, Albumin bovine fraction V powder, Ampicillin, Anti-Flag M2 monoclonal antibody (Product code F3165), Anti-β-actin, Bis

(sulfosuccinimidyl) suberate, Bromophenol blue, CH-sepharose beads, Dialysis tubing (visking size 11/4''), Diaminobenzidine tablets, Dithiothreitol (DTT), Dulbecco's modified eagle medium/F12 (DMEM), Ethylene glycol tetraacetic acid (EGTA), Ethylenediaminetetraacetic acid (EDTA), Folin-ciolcalteau phenol reagent, Freund's adjuvant complete, Freund's adjuvant incomplete, Glutaraldehyde, Hydrogen peroxide (30% v/v), Kodak D- 19 developer, Kodak fixer, Luminol, Metyrapone, N-2-Hydroxyethylpiperazine-N'-2-ethane sulphonic acid (HEPES), P-coumaric acid, Penicillin (500µg /ml)/ streptomycin (500µg/ml) solution, Poly(ethyleneimine) solution, Pre-stained molecular weight markers (molecular weight range 200-2.5kDa), Sodium azide, Sodium bicarbonate 7.5% (w/v), Sodium dodecyl sulphate (SDS), Sodium Hydroxide, Sodium phosphate, Streptavidin beads., Terrific broth, Thyroglobulin, Tris (hydroxymethyl) methylamine, Triton X-100, Trypsin 0.5g, EDTA 0.2g per litre of Hanks, Tween-20, β-mercaptoethanol.

2.1.10 Tocris (Bristol, UK)

Immepip, Iodophenpropit, Proxyfan, R-α-Methylhistamine dihydrobromide, Thioperamide.

2.1.11 QIAGEN Ltd (Dorking, Surrey, UK)

QIAGEN plasmid maxi kit.

2.1.12 Miscellaneous

[^{3}H]-GSK189254, 81Ci/mmol, 99% purity was a gift from Dr Andrew Medhurst, GlaxoSmithKline, Harlow.

GSK334429B, molecular weight 434.94, 90% purity was a gift from Dr Andrew Medhurst, GlaxoSmithKline, Harlow.

H_3R -/- mouse material a gift from Prof. Tim Lovenberg, Johnsons & Johnson, USA.

Human putamen samples gift from Dr Margaret Piggott, Newcastle University.

Human embryonic kidney (HEK) 293 cells from the European collection of cell cultures, Salisbury, Wilts.

Human and mouse H_4R cDNA a gift from Prof. Rob Leurs, Vrije Universiteit, The Netherlands

Human H_3R cDNA C-terminally labelled with FLAG a gift from Prof. Francis Cogé, Institut de Recherches Servier, France

Vector	**Insert**	**N terminal Tag**
pc DNA 3.1 (-)	Human $hH_{3\ 445}$	Flagged tagged DYKDDDDK
pc DNA 3.1 (-)	Human $hH_{3\ 365}$	Flagged tagged DYKDDDDK
pc DNA 3.1 (-) D-V5-His-TOPO	Human $hH_{3\ 329}$	Flagged tagged DYKDDDDK
pCINEO	Human $hH_{3\ 453}$	
pc DNA PCR2.1 TOPO	Human $hH_{3\ 200}$	

2.2 Instruments and Equipment

Spectrophotometry: Jenway Genova spectrophotometer

Centrifuges: A sorval RC5C centrifuge was used with a GS-3 fixed angle rotor (for large volumes > 400ml). A Biofuge fresco Heraeus (Kendro Laboratory Products) was used for all volumes less than 1.5ml.

Incubators: shaking incubator, cell incubator Shel Lab (Sheldon Manufacturing Inc.).

Orbital shaker: Stuart Scientific 505.

Water bath: Nüve bath

Heating block: QBT2 heating block (Grant)

Hot plate: FALC

Stirrer: Bibby Sterilin

Rocker: Grant-Bio PMR-30

Balances: Milligram amounts were weighed using a Mettler Toledo classic. All other amounts were weighed using a Scouts Pro balance

Electrophoresis: Polyacrylamide gels were cast in a Hoefer SE 245 dual gel caster using gel plates of 10x8cm, electrophoresis was performed using a Hoefer mini-vertical gel electrophoresis unit SE260 and transferred using a Hoefer TE 22 tank transfer unit, electrical supply was from an Electrophoresis Power Supply EPS 301, all supplied by Amersham Biosciences.

Radioligand binding equipment: Bound radioactivity was collected using a Brandel cell harvester. Radioactivity was counted using a TriCarb 1600TR Liquid Scintillation Analyser (Packard).

Microscopes: Nikon Eclipse E400 used for Immunohistochemistry and cells

Photography: Nikon digital camera Coolpix E950 used for Immunohistochemistry

Other equipment: Immunoblotting cassette, pH meter was a Mettler Toledo MP220, automatic pipetteman

Glassware, plastics and disposables: Hamilton syringe. Dounce glass/ glass homogeniser. Cell scrapers, 250ml sterile cell culture flasks, petri dishes and sterile pipettes from Greiner. Sterile filters: 0.2µm Sartorius Sartolab. V150 filter unit, microtitre plates, cryogenic vials, sterile pipettes and 250ml sterile filter lid cell culture flasks from Bibby sterilin. Falcon tubes, columns, Whatman GF/B filters, radioligand binding tubes, eppendorf tubes, pipette tips, syringes from SLS, UK.

2.3 Preparation of standard solutions

2.3.1 Lowry reagent A:

2% (w/v) sodium carbonate, 0.1M sodium hydroxide and 5% (w/v) SDS.

2.3.2 Lowry reagent B:

2% (w/v) sodium potassium tartrate.

2.3.3 Lowry reagent C:

1% (w/v) copper sulphate.

2.3.4 Stacking gel buffer:

0.5 M Tris-glycine, pH 6.8, containing 8 mM EDTA and 0.4% (w/v) SDS.

2.3.5 Resolving gel buffer:

50 mM Tris, 384 mM glycine, 1.8 mM EDTA and 0.1% (w/v) SDS pH 8.8.

2.3.6 Stock acrylamide:

30% (v/v) acrylamide and N,N'-methylenebisacrylamide.

2.3.7 Electrode buffer:

50 mM Tris, 384 mM glycine, 1.8 mM EDTA and 0.1% (w/v) SDS pH 8.8.

2.3.8 Sample buffer:

30 mM sodium hydrogen phosphate, pH 7.0, 30% (v/v) glycerol, 0.05% (v/v) bromophenol blue and 7.5% (w/v) SDS.

2.3.9 Pre-stained molecular weight markers:

Stored in sample buffer, section 2.3.8.

2.3.10 Transfer buffer:

25 mM Tris, pH 8.4, 192 mM glycine and 20% (v/v) methanol.

2.3.11 TEE buffer:

50 mM Tris-citrate pH 7.1, containing 5mM EDTA and 5mM EGTA.

2.3.12 Phosphate buffered saline (PBS):

0.01 M sodium hydrogen phosphate, 1.7 mM potassium hydrogen phosphate, pH 7.4, 137 mM sodium chloride, 107 mM potassium chloride.

2.3.13 Tris buffered saline (TBS):

50 mM Tris-HCl, pH 7.4.

2.3.14 HEPES buffered saline (HBS):

280 mM sodium chloride and 1 M sodium hydrogen phosphate pH 7.12.

2.3.15 Tris/EDTA buffer (TE):

10 mM Tris, 1 mM EDTA, pH 8.0.

2.3.16 Homogenisation buffer:

50 mM Tris-HCl pH 7.4, containing 5 mM EDTA and 5 mM EGTA

2.4 General methods

2.4.1 Membrane Preparation for Immunoblotting

Adult male CD-1 or TASTPM mice were sacrificed by schedule 1 methods, either stunned or placed in a CO_2 chamber and 100% CO_2 was added at a

flow rate of 20% of the chamber volume per minute, the mice were then decapitated. The brain tissue was dissected and kept cool on ice. The tissue was then homogenised in ice-cold homogenisation buffer (section 2.3.17) supplemented with 320mM sucrose using a dounce glass/ glass homogeniser. Membrane debris was pelleted by centrifugation of the homogenate at 1,200 x g, 4^{o}C for 10 minutes.

The supernatant was transferred to a clean JA20 centrifugation tube, the volume was made up to 10ml with homogenisation buffer + sucrose and was spun at 20,000 x g, 4^{o}C for 30 minutes. The supernatant was discarded and the pellet was re-suspended in 5 ml of homogenisation buffer (without sucrose), for every gram of starting material. The homogenate was stored in 100 µl aliquots at -20^{o}C.

2.4.2 Determination of Protein Concentration

The protein concentration was determined using the method of Lowry et al., (1951), bovine serum albumin (BSA) was used as the standard protein. All samples were carried out in triplicate. A stock solution of 1mg/ml of BSA was serially diluted in distilled water to give a range of standard BSA concentrations from 0 to 100 µg/ml. Lowry reagent A (section 2.3.1), Lowry reagent B (section 2.3.2) and Lowry reagent C (section 2.3.3) were mixed in a volume ratio of A (50): B (1): C (1). To both the BSA standards and the unknown protein concentration samples 0.5 ml of the mixture of reagent A, B and C was added, each sample was vortex mixed and incubated at room temperature for 10 minutes. After the incubation 50 µl of a 1:1 ratio of Folin-Ciocalteu phenol reagent and water was added to the samples, which were

then vortex mixed and incubated at room temperature for 30 minutes. The reaction was terminated by the addition of 500 µl of water. The O.D. at λ = 750 nm was determined for each sample using a Jenway Genova spectrophotometer.

A calibration curve was constructed of O.D. at λ = 750 nm for the BSA samples. This was then used to determine the unknown protein concentration.

2.4.3 Chloroform/methanol method for protein precipitation and preparation of protein samples

Protein samples for SDS-PAGE were precipitated using the chloroform/ methanol precipitation, detailed as follows. To the protein sample (25-50 µg), 4 x volumes of ice-cold methanol was added and samples were vortex mixed and centrifuged at room temperature at 18,000 x g for 1 minute. 1 x volume of ice-cold chloroform was added to the samples, which were vortex mixed and centrifuged at room temperature at 18,000 x g for 1 minute. 3 x volumes of ice-cold water were added to the samples which were vortex mixed and centrifuged at room temperature at 18,000 x g for 1 minute. The upper layer was carefully discarded and 1x volume ice-cold methanol was added to the samples, which were vortex mixed and centrifuged at room temperature at 18,000 x g for 4 minute. The supernatant was discarded and the pellet air dried. The dried protein pellet was re-suspended by vortex mixing in 5 µl of sample buffer (section 2.3.8), 2 µl of 200mM DTT and 8 µl of water to a final volume of 15 µl. The samples were boiled at 95^{o}C in the heat block for 5 minutes and then centrifuged at 18,000 x g for 30 seconds at room temperature before analysis by SDS-PAGE.

2.4.4 Preparation of competent *Escherichia coli* cells

The standard $CaCl_2$ method described by (Cohen et al., 1972) was used to prepare the *Escherichia coli* (E. coli) XL-1 Blue Competent (Stratagene) cells used in all plasmid transformations. 2ml of an overnight XL-1 Blue culture (5ml Terrific broth, 12.5µg/ml tetracycline and 0.8% glycerol) was used to inoculate 200ml Terrific broth medium (47.7g Terrific broth and 0.8% glycerol in 1 litre ddH_2O). Cells were grown at 37^oC on an orbital shaker at 250xg to logarithmic (log) phase (OD_{550} = 0.5). The cells were collected by centrifugation at 7,000 x g for 5 minutes at 4^oC. The pellet was then gently re-suspended in 100ml of freshly made ice-cold 50mM $CaCl_2$, centrifuged at 7,000 x g for 5 minutes at 4^oC. The pellet was then gentle re-suspended in 10ml ice-cold 50mM $CaCl_2$. The cells were kept on ice for 1h before sterile 15% (v/v) glycerol was added and the cells frozen away at -80^oC.

2.4.5 Transformation of competent cells

Transformation of competent cells was performed as described by Dagert and Ehrlich (1979). 100µl aliquot of competent cells was thawed on ice for 5 minutes before 20 ng/µl of the appropriate plasmid DNA was added and mixed gently. The cell mixture was allowed to absorb for 30 min on ice and then subjected to a 90 second heat shock at 42^oC. The mixture was then left to cool on ice for 2 min. 900 µl Terrific broth medium was added, followed by an incubation period at 37^oC on an orbital shaker at 250 x g. Aliquots of 100 µl were then plated out on Terrific broth agar plates (1.2% agar in Terrific broth

medium) containing 12.5 µg/ml tetracycline hydrochloride and 50 µg/ml ampicillin. Plates were inverted and then incubated overnight at 37^{o}C.

2.4.6 Amplification and preparation of plasmid DNA

2.4.6.1 Preparation of small scale culture of plasmid DNA

Selected colonies from the agar plates were inoculated into 10 ml of Terrific broth medium, (containing 12.5 µg/ml tetracycline hydrochloride and 50 µg/ml ampicillin), and grown for 16 h at 37^{o}C on an orbital shaker at 250 x g.

2.4.6.2 Preparation of large scale culture of plasmid DNA

500 ml Terrific broth medium containing appropriate antibiotics (as above), was inoculated with 3 ml of the small overnight culture, and grown for 16 h at 37^{o}C on an orbital shaker at 250 x g.

2.4.6.3 Harvesting the large scale culture and purification of plasmid DNA using QIAGEN^{TM} Plasmid Maxi-Kit

E. coli cells were harvested from the large overnight culture by centrifugation at 6,500 x g for 10 min at 4^{o}C. The pellet was re-suspended in 10 ml ice-cold P1 Buffer. Bacteria cells were lysed by the addition of 10 ml ice-cold P2 Buffer, mixed by gentle inversion and incubated at room temperature for 5 min. The mixture was then neutralised by the addition of 10 ml ice-cold P3 Buffer, mixed by gentle inversion and incubated on ice for 20 min. The solution was then centrifuged at 14,000 x g for 30 min at 4^{o}C, and the clear lysate was removed into a fresh tube. A QIAGEN^{TM} 500 tip was equilibrated with 10 ml QBT buffer. The lysate was then added to the column and allowed

to pass through the column under gravity flow. The column was then washed twice with 30 ml QC Buffer and then the plasmid DNA eluted with 15 ml QF Buffer. 0.7% vol (10.5 ml) ice-cold isopropanol was added to the eluted plasmid DNA and the solution was centrifuged at 14,000 x g for 30 min at 4^{o}C. The pellet was carefully washed with 1 ml ice-cold ethanol and allowed to air dry for 30 min. The purified DNA was then dissolved in 500 µl TE Buffer and stored at 4^{o}C until the purity and yield of DNA was calculated.

2.4.6.4 Quantification and determination of purity of the DNA yield

The purity of the plasmid DNA was determined by reading the OD at λ = 260nm and λ = 280nm. For pure plasmid DNA the ratio of the optical densities (OD_{λ} = 260nm / OD_{λ} = 280nm) should be within the range 1.8 – 2.0. Plasmid DNA concentration was determined by measuring the OD at λ = 260nm (OD = 1 corresponds to ~ 50µg/µl double stranded DNA (dsDNA)).

The DNA was diluted to a final concentration of 1 µg/ml in TE buffer and stored in 100 µl aliquots at -20^{o}C. Once thawed the cDNA was stored at 4^{o}C.

CHAPTER 3

Development and Characterisation of the first panel of Anti-Human Histamine H_3 Receptor Isoform Specific Antibodies

3.1 Objectives

To develop and characterise a panel of novel anti-human H_3R isoform specific antibodies and to determine whether expression of these isoforms are altered in aging and in CNS diseases in which dementia is a common feature.

3.2 Introduction

Alternative splicing is a common feature of the H_3R gene that occurs not only in humans but also in mouse and rat, yielding potentially different protein sequences. In order to define the importance of H_3R heterogeneity, specific immunological probes are required. Our laboratory has developed the first anti-hH_3R antibodies (Chazot et al., 2001, Cannon et al., 2007, Victoria Hann PhD thesis 2004 and Fiona Shenton PhD thesis 2007). The first two antibodies were raised against H_3R sequences common to most human and rodent isoforms: anti-H_3R (346-358) and anti-H_3R (175-187) sequence specific antibodies. Probing immunoblots with rodent brain samples, the antibodies detect two specific immunoreactive bands migrating at approximately Mr 68,000 and Mr- 93,000, which on incubation with the respective peptide antigen were greatly suppressed. These species are likely to be glycosylated dimeric forms of the rodent H_3R receptor (Shenton et al., 2006). In an attempt to generate an antibody specific to the rat H_3R_{397} isoform a sequence was chosen that flanked the splice site within the third intracellular

loop (Fig 3.1). In theory, the antibody would only pick up the 397 sequence as the peptide would hopefully be short enough to be specific for that local sequence, as the unspliced isoform and alternatively spliced forms would produce distinct epitopes.

Schematic showing the rationale behind selecting the peptide sequence for immunisation:

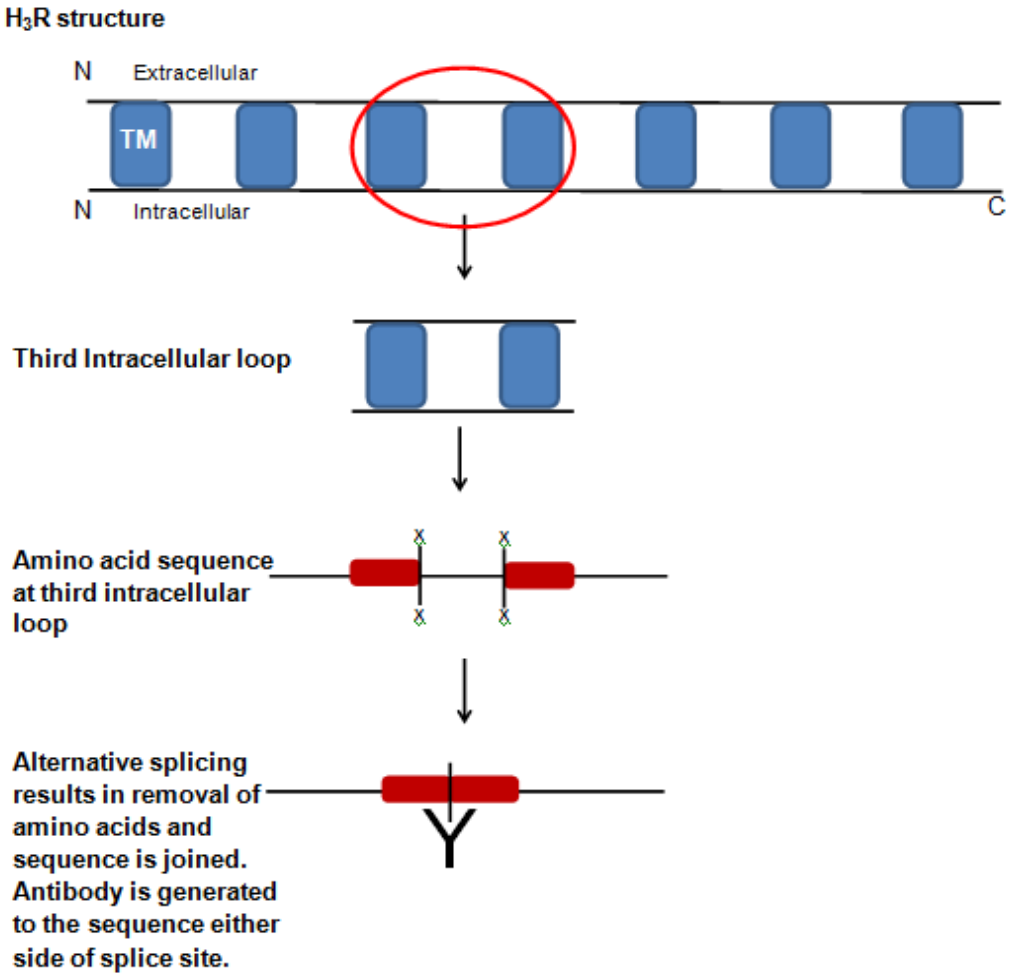

Figure 3.1 Schematic showing how peptide sequences were generated to produce isoform specific antibodies against the third intracellular loop of the human H_3R. Amino acid sequences were chosen that spanned either side of the splicing event so once the sequence was removed and the sequence at either side joined, the antibody generated would hopefully detect the sequence. The sequence selected was long enough so that the antibody was specific but not too long that the antibody would detect other isoforms.

When the antibody was tested on HEK 293 cells transfected with the different isoforms (hH_3R_{445}, hH_3R_{365}, hH_3R_{329}, $rH_3R_{A/\ 445}$, $rH_3R_{B/\ 413}$ and $rH_3R_{C/\ 397}$), the antibody was found to detect both the full length rat $rH_{3A}R_{445}$ and full length human isoforms $hH_{3\ (445)}$, as well as the expected $rH_{3C}R_{397}$. The antibody did not detect any of the other rat or human isoforms tested. The antibody also detected protein species in both human and rodent native tissue. Therefore, the antibody generated is useful for the detection of the full length rat and human H_3R isoform as well as the shorter rat $H_3R_{C/\ 397}$ isoform.

Antibodies specific for three other highly expressed human isoforms (Coge et al., 2001) were developed using peptide sequences unique to each of the H_3R isoforms: 445, 365, 329 and 200 (see Fig 3.2). Antibodies were generated to particular sequences within the third intracellular loop flanking the splicing site for the human H_3R isoforms, 445, 365 and 329. The hH_3R_{200} has a deletion at 170-306 resulting in a frame shift and a novel stop codon, so that the last 10 amino acids of the C-terminus is novel to this isoform; these last 10 amino acids were selected as immunogen to raise an anti-hH_3R_{200} antibody.

Herein, the methods for preparing peptides for immunisation, the immunisation procedure, antibody purification and the experiments performed to check the individual antibody specificity are described.

Peptide sequence chosen for each isoform:

(A) Full length human H_3R sequence. (Peptide sequence used to generate anti-pan H_3R antibody, blue)

1 merappdgpl nasgalagea aaaggargfs aawtavlaal mallivatvl gnalvmlafv
61 adsslrtqnn ffllnlaisd flvgafcipl yvpyvltgrw tfgrglcklw lvvdyllcts
121 safnivlisy drflsvtrav syraqqgdtr ravrkmllvw vlafllygpa ilsweylsgg
181 ssipeghcya effynwyfli tastlefftp flsvtffnls iylniqrrtr lrldgareaa
241 gpepppeaqp sppppgcwg cwqkghgeam plhrygvgea avgaeageat lgggggggsv
301 asptsssgss srgterprsl krgskpsass aslekrmkmv sqsftqrfrl srdrkvaksl
361 avivsifglc wapytllmii raachghcvp dywyetsfwl lwansavnpv lyplchhsfr
421 raftkllcpq klkiqphssl ehcwk

(B) Full length human H_3R_{445} sequence. (Peptide sequence used to generate anti-$rH_3R_{A/C}$ and $hH_3R_{453/445}$ antibody, blue)

1 merappdgpl nasgalagea aaaggargfs aawtavlaal mallivatvl gnalvmlafv
61 adsslrtqnn ffllnlaisd flvgafcipl yvpyvltgrw tfgrglcklw lvvdyllcts
121 safnivlisy drflsvtrav syraqqgdtr ravrkmllvw vlafllygpa ilsweylsgg
181 ssipeghcya effynwyfli tastlefftp flsvtffnls iylniqrrtr lrldgareaa
241 gpepppeaqp sppppgcwg cwqkghgeam plhrygvgea avgaeageat lgggggggsv
301 asptsssgss srgterprsl krgskpsass aslekrmkmv sqsftqrfrl srdrkvaksl
361 avivsifglc wapytllmii raachghcvp dywyetsfwl lwansavnpv lyplchhsfr
421 raftkllcpq klkiqphssl ehcwk

(C) Human sequence showing the H_3R_{453} isoform (**Addition of 8 amino acids in green**). (Peptide sequence used to generate: anti-human $H_3R_{445/453}$ antibody, blue)

1 merappdgpl nasgalagea aaaggargfs aawtavlaal mallivatvl gnalvmlafv
61 adsslrtqnn ffllnlaisd flvgafcipl yvpyvltgrw tfgrglcklw lvvdyllcts
121 safnivlisy drflsvtrav syraqqgdtr ravrkmllvw vlafllygpa ilsweylsgg
181 ssipeghcya effynwyfli tastlefftp flsvtffnls iylniqrrtr lrldgareaa
241 gpepppeaqp sppppgcwg cwqkghgeam plhrygvgea avgaeageat lgggggggsv
301 asptsssgss srgterprsl krgskpsass aslekrmkmv sqsftqrfrl srdrkvaksl

361 avivsifglc wapytllmii raachghcvp dywyetsfwl lwansavnpv lyplchhsfr

421 raftkllcpq klkiqphssl ehcwk **rrprprwrsa**

(D) Human sequence showing the H_3R_{365} deletion / isoform 2 **(deletion in red and bold)**. (Peptide sequence used to generate: anti-human H_3R_{365} peptide 1 antibody, blue)

1 merappdgpl nasgalagea aaaggargfs aawtavlaal mallivatvl gnalvmlafv

61 adsslrtqnn ffllnlaisd flvgafcipl yvpyvltgrw tfgrglcklw lvvdyllcts

121 safnivlisy drflsvtrav syraqqgdtr ravrkmllvw vlafllygpa ilsweylsgg

181 ssipeghcya effynwyfli tastlefftp flsvtffnls iylniqrrtr lrldgareaa

241 gpepppeaqp sppppgcwg cwqkghgeam plhr**ygvgea avgaeageat lgggggggsv**

301 **asptsssgss srgterprsl krgskpsass aslekrmkmv sqsftqrfrl srdr**kvaksl

361 avivsifglc wapytllmii raachghcvp dywyetsfwl lwansavnpv lyplchhsfr

421 raftkllcpq klkiqphssl ehcwk

(E) Human sequence showing the H_3R_{365} deletion / isoform 2 **(deletion in red and bold)**. (Peptide sequence used generate: anti-human H_3R_{365} peptide 2 antibody, blue)

1 merappdgpl nasgalagea aaaggargfs aawtavlaal mallivatvl gnalvmlafv

61 adsslrtqnn ffllnlaisd flvgafcipl yvpyvltgrw tfgrglcklw lvvdyllcts

121 safnivlisy drflsvtrav syraqqgdtr ravrkmllvw vlafllygpa ilsweylsgg

181 ssipeghcya effynwyfli tastlefftp flsvtffnls iylniqrrtr lrldgareaa

241 gpepppeaqp sppppgcwg cwqkghgeam plhr**ygvgea avgaeageat lgggggggsv**

301 **asptsssgss srgterprsl krgskpsass aslekrmkmv sqsftqrfrl srdr**kvaksl

361 avivsifglc wapytllmii raachghcvp dywyetsfwl lwansavnpv lyplchhsfr

421 raftkllcpq klkiqphssl ehcwk

(F) Human sequence showing the H_3R_{329} deletion / isoform 2 **(deletion in red and bold)**. Peptide generated to the sequence at position 222-231 (anti-

hH_3R_{329} antibody). (Peptide sequence used to generate: anti-human H_3R_{329} antibody, blue

1 merappdgpl nasgalagea aaaggargfs aawtavlaal mallivatvl gnalvmlafv
61 adsslrtqnn ffllnlaisd flvgafcipl yvpyvltgrw tfgrglcklw lvvdyllcts
121 safnivlisy drflsvtrav syraqqgdtr ravrkmllvw vlafllygpa ilsweylsgg
181 ssipeghcya effynwyfli tastlefftp flsvtffnls iylniq**rrtr lrldgareaa**
241 **gpepppeaqp sppppgcwg cwqkghgeam plhrygvgea avgaeageat lgggggggsv**
301 **asptsssgss srgterprsl krgskpsass aslekrmkmv sq**sftqrfrl srdrkvaksl
361 avivsifglc wapytllmii raachghcvp dywyetsfwl lwansavnpv lyplchhsfr
421 raftkllcpq klkiqphssl ehcwk

(G) Human sequence showing the H_3R_{200} deletion / isoform 5 **(deletion in red and bold)**. (Peptide sequence used to generate: anti-human H_3R_{200} antibody, blue

1 merappdgpl nasgalagea aaaggargfs aawtavlaal mallivatvl gnalvmlafv
61 adsslrtqnn ffllnlaisd flvgafcipl yvpyvltgrw tfgrglcklw lvvdyllcts
121 safnivlisy drflsvtrav syraqqgdtr ravrkmllvw vlafllygpa **ilsweylsgg**
181 **ssipeghcya effynwyfli tastlefftp flsvtffnls iylniqrrtr lrldgareaa**
241 **gpepppeaqp sppppgcwg cwqkghgeam plhrygvgea avgaeageat lgggggggsv**
301 **asptsssgss srgterprsl krgskpsass aslekrmkmv sqsftqrfrl srdrkvaksl**
361 **avivsifglc wapytllmii raachghcvp dywyetsfwl lwansavnpv lyplchhsfr**
421 **raftkllcpq klkiqphssl ehcwk paaprgalrg rahsrgapsr** rrprprwrsa

Figure 3.2 The amino acid sequences of the full length human H_3R and its respective isoforms and the peptide sequences used to generate specific antibodies to those isoforms. (A) H_3R amino acid coding sequence, (B) H_3R_{445} amino acid sequence and selected immunogen sequence. (C) H_3R_{365} amino acid sequence with the area spliced out highlighted in red and selected immunogen sequence in blue. (D) H_3R_{365} amino acid sequence with the area spliced out highlighted in red and selected immunogen sequence in blue. H_3R_{329} amino acid sequence with the area spliced out highlighted in red and selected immunogen sequence in blue. H_3R_{200} amino acid sequence with the area spliced out highlighted in red and sequence highlighted to raise an antibody against selected immunogen sequence in blue.

3.3 Methods

3.3.1 Choice of Peptide Sequences

Specific peptide sequences were chosen to immunize rabbits to produce anti-peptide antibodies (Fig 3.2). The peptide was chosen based on the peptide specificity being unique to the particular isoform and its likely immunogenicity. A cysteine residue was added to one end of each sequence so that the peptide could be directionally coupled to a carrier protein keyhole limpet hemocyanin (KLH):

Human/ rodent antibodies:

- Rodent/ human histamine $H_3R_{AC/\ 445/453}$ (268 - 277) EAMPLHRGSK-C.
- H_3R PAN (349 - 358) RLSRDRKVAK-C

Human specific antibodies:

- Human $H_3R_{(365)}$ peptide 1 (268 – 281) EAMPLHRKVAKSLA-C
- Human $H_3R_{(365)}$ peptide 2 (268 – 278) C-EAMPLHRKVAK
- Human $H_3R_{(329)\ \Delta I3}$ (222 – 231) C-YLNIQSFTQR
- human $H_3R_{(200)}$ (191 – 200) C-RRPRPRWRSA

3.3.2 Antibody Production

The peptide alone is too small to stimulate an immune response and is therefore conjugated to a large immunogenic carrier protein before being injected into the rabbit. The peptide was conjugated using Imject® Maleimide activated mcKLH kit to illicit a humoral immune response. The rabbit serum was collected and purified using peptide affinity chromatography.

3.3.3 The Imject Maleimide activated mcKLH method of coupling peptides to carrier proteins

The method was used to conjugate the peptide to the carrier protein KLH through its carboxyl-terminal cysteine residue. One vial of maleimide-activated mcKLH was dissolved by adding 200 µl of distilled water, making a 10 mg/ml solution. 200 µl of conjugation buffer was added to 5 mg peptide. The peptide solution was then immediately added to the reconstituted mcKLH. The carrier protein and peptide mixture were incubated for a further 2 hours at room temperature with gentle agitation. The conjugated peptide was then separated from EDTA in the mixture by desalting. One bottle of purification buffer salts was dissolved in 60 ml of distilled water. The top and bottom caps were removed from a desalting column and washed 3 times with 15 ml of purification buffer salts. The hapten-carrier mixture was then added to the centre of the column disc. 10 lots of 0.5 ml aliquots were added to the column and each of the fractions collected. The absorbency of each fraction was read at 280 nm to detect the fractions containing the conjugate (Fig 3.3). The peak fractions were pooled, and the absorbency read. The peptide protein conjugate was diluted with PBS to a final concentration of 1 mg/ml and stored in 100 µl aliquots at -20^{o}C.

Representative graph showing the OD values from a typical antibody elution:

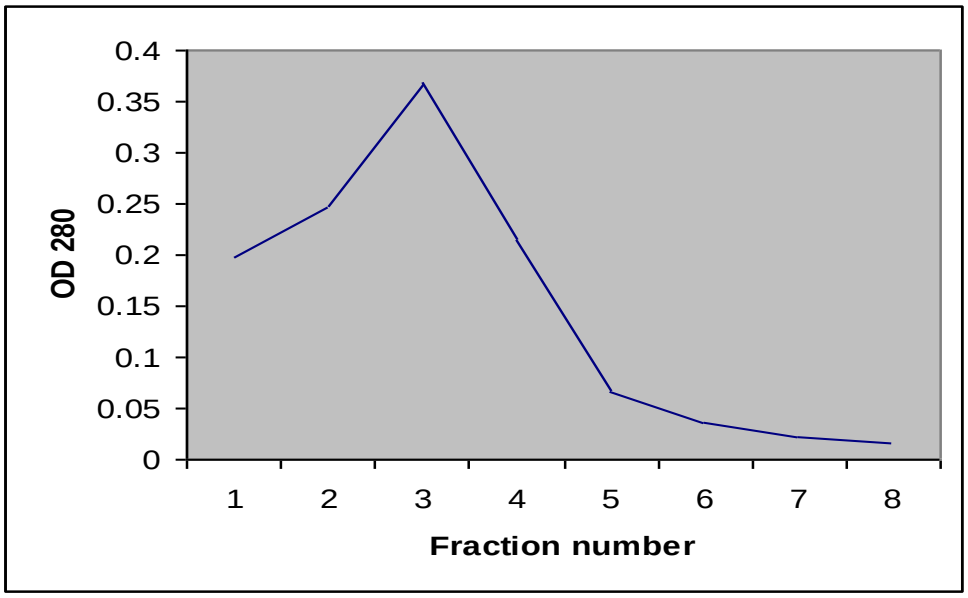

Figure 3.3: A representative elution profile**.** Column fractions 2-4 were chosen on this occasion as these are the fractions with the peak absorbence values. The absorbence readings were zeroed accordingly and fraction 1 corresponds to the first elution containing antibody.

3.3.4 Inoculation Procedure

200 µl of sterile PBS was mixed with 100 µg of freshly thawed peptide-carrier protein conjugate, and emulsified with an equal volume of Freund's adjuvant. This preparation was then injected intramuscularly into both hind legs of a Dutch rabbit. The primary immunisation was performed using complete Freund's adjuvant, while subsequent immunisations (at 1 month intervals), used Freund's incomplete adjuvant. Rabbits were bled from the marginal ear vein 7 – 10 days following the booster injections, 10 – 15 ml of blood were collected. Blood was allowed to stand at room temperature for 2 hours, and then clot contraction was allowed to occur over 16 hours at 4^{o}C. Cellular material was removed by centrifugation at 12000 x g for 10 minutes at 4^{o}C, and the serum was stored in 1 ml aliquots at -20^{o}C. All procedures were

performed in accordance with the Animals Scientific Procedures Act 1986, project license number **(PPL602/657)**

3.3.5 Affinity Purification

3.3.5.1 Coupling of Peptides to Sepharose Beads

The method was carried out as described by (Duggan et al., 1991) and was used to couple the peptide to activated thiol-sepharose beads via its C-terminal cysteine residue. 0.35g of activated thiol-sepharose were allowed to swell in 100 ml distilled water for 15 minutes at room temperature. The swollen sepharose beads were placed in a 25 ml column containing a filter and washed with 100 ml of 0.1 M Tris-HCL pH 8.0, containing 0.3 M NaCl and 1mM EDTA. The column was then drained until 0.7 ml of buffer remained. 1 ml of 5 mg/ml peptide dissolved in the same buffer was added to the sepharose beads and incubated for 2 hours at room temperature with gentle agitation. The reaction was terminated by draining the column and washing the sepharose beads with 25 ml of Tris pH 8.0 followed by 10 ml of 0.1 M citric acid pH 4.5. All remaining un-reacted thiol groups on the sepharose beads were blocked by incubation with 3 ml of 1 mM β-mercaptoethanol in 0.1 M citric acid pH 4.5 for 1 hour at room temperature with gentle agitation. The blocking reaction was terminated by washing the sepharose beads with 25 ml of 0.1 M citric acid pH 4.5. Finally the sepharose column was equilibrated with 25 ml PBS and stored in 10 ml PBS containing 0.02% (w/v) sodium azide, at 4^{o}C until required.

3.3.5.2 Peptide Affinity Purification of Antibodies

Purification of the anti-peptide polyclonal antibody requires the use of a 1 ml sepharose column linked to the appropriate peptide (5 mg). The column was equilibrated with 100 ml of TBS, and then 4 ml of the immune serum was applied to the column followed by either a 2 hour incubation period at room temperature or overnight at 4^{o}C with gentle agitation. Unbound immune serum was drained from the column, and then the column washed with 100 ml of TBS. The bound antibody was eluted from the column with 8 ml of 50 mM glycine/HCL pH 2.3. The elute was collected in 8 X 1 ml fractions, containing 15 µl of 1 M Tris to neutralise the contents to a final pH of 7.4. For each fraction the O.D. at λ = 280 nm was determined and the protein concentration calculated using the Beer Lambert law,

$$\mathbf{C = A / \epsilon L}$$

Where,

C, is the protein concentration of the antibody

A, is the absorbance at λ = 280 nm

L, is the sample path length = 1 cm.

Є, is the molar absorptivity or extinction coefficient of the chromophore at wavelength λ (the optical density of a 1 cm thick sample of a 1 M solution). Є is a property of the material and the solvent = 1.35

The fractions containing the highest protein concentrations were pooled and dialysed against 500 ml TBS, overnight at 4^{o}C. The affinity column was regenerated with 100 ml of TBS and stored in 10 mls TBS containing 0.02% (w/v) sodium azide at 4^{o}C.

3.3.6 Cell culture and transfection of Human Embryonic Kidney (HEK) 293 cells

3.3.6.1 Preparation of DMEM/F12 media

All procedures were performed under sterile conditions. Powdered Dulbecco's Modified Eagle Medium/F12 (DMEM/F12 1:1 ratio) (15g/L) and 15mM N-2-hydroxyethylpoiperazine-N'-2-ethane sulphonic acid (HEPES) were mixed with 800 ml of sterile water. The media was supplemented with 40 ml of 10% (v/v) foetal calf serum (FCS), 7.5 % (w/v) $NaHCO_3$ giving a final concentration 3.0g/L, and 20 ml of penicillin (500 µg/ml)/ streptomycin (500 µg/ml) solution. The pH of the media was adjusted to pH 7.6 using 10M NaOH and the final volume made up to 1 L using sterile ddH_2O. The media was filter sterilised using a 0.2 µm Sartorius Satolab-V150 filter unit, and then stored at 4^{o}C.

3.3.6.2 Sub-culturing of HEK 293 Cells

All procedures were performed under sterile conditions. HEK 293 cells were grown in 250 ml Greiner flasks containing DMEM/F12 (as described above). The flasks were incubated in a Sanyo incubator at 37^{o}C humidified in 5% CO_2. Every seven days the cells were sub-cultured. 30 minutes before sterile PBS, DMEM/F12 media and trypsin-EDTA were pre-warmed to 37^{o}C. The old medium was removed from the cells and the cells were washed in 10 ml of pre-warmed PBS. The PBS was then removed and the cells were incubated for 2 min in 2ml of trypsin-EDTA, at 37^{o}C. The cells were re-suspended in 10 ml of fresh pre-warmed DMEM/F12 media by gentle pipetting up and down. 2 ml of the cell suspension was added to a fresh sterile flask with a further 10 ml of fresh media and returned back to the incubator.

3.3.6.3 Preparation of new stocks of HEK 293 cells

The old media was removed from a flask of HEK 293 cells and the cells were washed with 10 ml of PBS. The PBS was then removed and the cells were incubated for two minute in 4 ml of trypsin-EDTA, at 37^{o}C. The cells were re-suspended in 20 ml of fresh pre-warmed DMEM/F12 media. The cells were pelleted by centrifugation at 200 x g for 5 minutes at 4^{o}C. The pellet was re-suspended in 4.8 ml of fresh media supplemented with 0.6 ml of FCS and 0.6 ml of dimethylsuphoxide (DMSO). The cell suspension was immediately divided into 3 cryogenic vials and stored at -80^{o}C for 24 hours before being transferred to liquid nitrogen.

Preparation of a new culture of HEK 293 cells, a single cryogenic vial was thawed at 37^{o}C for 5 minutes. The cells were then added to 50ml of pre-warmed DMEM/F12 media and pelleted by centrifugation at 200 x g for 5 minutes at 4^{o}C and then re-suspended in 15 ml of fresh media. The cells were then added to a tissue culture flask for culture at 37^{o}C in 5% CO_2.

3.3.6.4 Polyethyleneimine (PEI) transfection method

HEK 293 cells were transfected using polyethyleneimine (PEI) transfection method adapted from van Rijn R et al., 2008. Briefly, 1 µg DNA was diluted in 100 µl 0.9% NaCl, then 2 µl of 1 mg/ml PEI (linear MW ~ 25,000) was added to the eppendorf. The DNA/PEI mixture was incubated for 10 minutes at room temperature. During the incubation period the old media was removed from the HEK 293 cells and 2 ml of fresh pre-warmed media added. Following the incubation period 1 ug of DNA/PEI mixture was added to the HEK 293 cells. The cells were incubated at 37^{o}C and harvested 48 hours post-transfection.

3.3.6.5 Harvesting and membrane preparation of HEK 293 cells

HEK 293 cells were harvested 48 hours post transfection. The culture media was removed and replaced with 1 ml of homogenisation buffer (section 2.3.17). Cells were scraped from the bottom of the petri dish using Greiner cell scrapers. The re-suspended cells were homogenised using a douce glass/ glass homogeniser, kept ice cold. The homogenate was pelleted by centrifugation at 18000 x g at 4^{o}C for 5 minutes. The supernatant was discarded and the pellet was re-suspended in 1 ml of ice cold homogenisation buffer. The cells were re-homogenised and separated in 100 µl aliquots and stored at -20^{o}C.

3.3.7 Immunoblots

Sodium dodecyl sulphate polyacrylamide gel electrophoresis (SDS-PAGE) was carried out using either 7.5 (v/v) or 10% (v/v) polyacrylamide slab gels under reducing conditions. Immunoblots were probed either with anti-FLAG antibody in the case of the FLAG tagged human H_3R clones, or with the appropriate rabbit anti-H_3R antibody.

3.3.7.1 Preparation of resolving gel

The resolving gel was prepared by mixing 6 ml of distilled water with 3 ml of resolving gel buffer (section 2.3.5), 6 µl of TEMED, 3 ml of stock acrylamide (section 2.3.6), and 60 µl 10% (w/v) ammonium persulphate (APS). The polyacrylamide solution was immediately poured into a Hoefer SE 245 dual gel caster, using two gel plates of 10 x 8cm and spacers of 1 mm width. 100

µl of saturated water/ butanol solution was added over the top of each gel. The gels were covered with parafilm and were allowed to polymerise for 40 - 60 minutes at room temperature. The gels were individually wrapped in tissue paper and stored in electrode buffer (section 2.3.7) at 4^{o}C until required.

3.3.7.2 Preparation of protein samples for SDS-PAGE

Protein samples for SDS-PAGE were precipitated using the chloroform/ methanol precipitation, detailed in chapter 2.

3.3.7.3 SDS-PAGE

The resolving mini-slab acrylamide gel was clamped into a Hoefer mini-vertical gel electrophoresis unit SE260. The stacking gel was prepared by mixing 2.3 ml of water with 1 ml of stacking gel buffer (section 2.3.4), 650 µl of stock acrylamide (section 2.3.6), 5 µl of TEMED and 80 µl of 10% (w/v) ammonium persulphate. The stacking gel buffer was then immediately poured into the mini-slab gel on top of the resolving gel and a welled comb inserted into the stacking gel. After the stacking gel had polymerised, the comb was carefully removed and the wells washed with water. Approximately 300 ml of electrode buffer (section 2.3.7) was poured into and behind the wells and into the base of the electrophoresis unit. 15 µl of Protein samples and pre-stained standards (protein molecular weight range of 200 – 6.5 kDa) were loaded into the wells of the stacking gel using a Hamilton syringe. Electrophoresis was carried out at 180 V, 10 mA (per gel) which was increased by 5 mA (per gel) once the samples reached the resolving gel. The gel was run for

approximately 2 hours until the appropriate pre-stained molecular weight marker (25 kDa) were at the bottom of the gel.

3.3.7.4 Immunoblotting

After SDS-PAGE (section 2.4.3.3), the proteins from the gels were transferred to a nitrocellulose membrane. A transfer cassette was constructed in the following order of components each of which had been pre-equilibrated in transfer buffer (section 2.3.10) sponge, two sheets of blotting paper, nitrocellulose membrane, SDS-PAGE, two sheets of blotting paper and a piece of sponge. On the addition of each component to the transfer cassette air bubbles were carefully removed. Proteins were transferred at a constant voltage of 50 V for 2 hours using a Hoefer TE 22 tank transfer unit containing transfer buffer kept cool with ice and ice packs.

Following the transfer of the proteins, the nitrocellulose membrane was briefly rinsed with TBS (section 2.3.13) and incubated with 15 ml of blocking buffer, which comprised of TBS, containing 5% (w/v) dried milk and 0.02% (v/v) Tween-20, for 1 hour at room temperature with gentle agitation. After blocking of the non-specific antibody sites the nitrocellulose membrane was washed with 10 ml of TBS. The appropriate affinity-purified primary antibodies was diluted in incubation buffer, which comprised of TBS, containing 2.5% (w/v) dried milk to working concentrations of (0.25 – 5 µg/ml). The nitrocellulose membranes were incubated with 10 ml of the diluted primary antibody solution for 1 hour at room temperature, or overnight at 4^{o}C with gentle agitation.

After incubation with the primary antibody the nitrocellulose membranes were washed four times in 10 ml of wash buffer, consisting of TBS, containing 2.5%

(w/v) dried milk and 0.2% (v/v) Tween-20, at 10 minute intervals with gentle agitation at room temperature. Nitrocellulose membranes were then incubated for 1 hour with gentle agitation with horseradish peroxidise (HRP) labelled secondary antibody, either anti rabbit or anti mouse depending on the what the primary antibody was raised in, at a dilution of 1/2000 in 10 ml of incubation buffer. The unbound secondary antibody was removed by washing the membrane as detailed above. The nitrocellulose was then drained and briefly rinsed with TBS.

Immunoreactive bands on the nitrocellulose membrane were developed by processing in a solution containing, 100 µl of 68mM p-coumaric acid, 10 ml of 1.25 mM luminal and 6 µl of 30% (v/v) H_2O_2, for 1 minute at room temperature. After incubation the immunoblot was wrapped in cling film, and placed in a film cassette. The immunoblots were exposed to Hyperfilm^{TM} for various times between 1-5 minutes. The film was then developed in Kodak D-19 Developer until the immunoreactive bands were visible and fixed in Kodak Unifix for 5 minutes at room temperature.

3.3.8 Immunohistochemical analysis

Immunohistochemical analysis was carried out as described previously by Chazot et al., (2001). Adult mouse brains (perfusion-fixed with 4% (w/v) paraformaldehyde (0.05% (v/v) glutaraldehyde in 0.1M phosphate buffer, pH 7.4). Brains were removed, post-fixed overnight and then cryoprotected by incubation in 30% (w/v) sucrose in 0.01 M phosphate buffer, pH 7.4 at 4^{o}C for 48 hours. The tissue was then frozen at -80^{o}C in isopentane for 1.5 minutes, and horizontal sections (25 µm thick) were cut on a cryostat. Free floating

sections were initially treated with 10% (v/v) methanol and 3% (v/v) hydrogen peroxide in 50 mM TBS, pH7.4, for 10 minutes to quench endogenous peroxidise activity. Sections were incubated in TBS, 0.2% (w/v) glycine and 0.2% (v/v) Tween-20, for 15 minutes to mop up residual un-reacted aldehyde groups from the fixative. Non-specific antibody binding sites on the tissue were blocked by incubating with 2% (v/v) foetal calf serum in TBS, 0.02% (v/v) Tween-20 for 1 hour. Sections where then incubated overnight at 4^{o}C in the primary antibody at a range of concentrations (0 – 5 µg/ml) in 1% (v/v) foetal calf serum/ TBS. After washing the sections three times in TBS/ 0.1% (v/v) Triton X 100, antibody binding was detected using the Vectastain ABC Elite kit. The sections were incubated in a biotin linked, anti-rabbit secondary antibody for 2 hours followed by incubation for 1 hour with streptavidin-horse radish peroxidase (HRP) complex. The immune reaction visualised using 3,3'-diaminobenzidine tetrahydrochloride as the HRP substrate. Antibody specificity was confirmed by a peptide block test (section 3.3.8.1). In addition a control was carried out where the primary antibody and the secondary antibody were individually left out to rule out any non-specific binding.

3.3.8.1 Peptide block to confirm antibody specificity

In order to confirm that immunoreactivity detected either in the immunoblots or in immunohistochemical analysis was specific to the amino acid sequence of the immunizing peptide, a peptide block was carried out in which the antibody was pre-incubated overnight at 4^{o}C with an equal volume of the relevant peptide. The peptide concentration during the incubation was 500 µg/ml, excess peptide was used to completely block the antibody and therefore

prevent it from binding to equivalent binding sites on the immunoblot or on slices in the IHC analysis. During incubation of the immunoblot with the peptide/antibody solution, the antibody dilution was adjusted to take into account the initial 1:2 dilution with the peptide. Any immunoreactive bands or staining which persisted after the antibody block were considered to be non-specific antibody binding.

Results

3.4.1 Final antibody concentrations for all bleeds purified

The table below shows the final concentrations obtained for the different antibodies and different bleeds taken:

Antibody	Bleed 1	Bleed 2	Bleed 3	Bleed 4	Bleed 5
$rH_3R_{A/C}$ $hH_3R_{445/453}$	137 µg/ml	151 µg/ml	150 µg/ml	148 µg/ml	
H_3R pan	43 µg/ml	37 µg/ml	74 µg/ml	150 µg/ml	216 µg/ml
hH_3R_{365} P1	1629 µg/ml	1025 µg/ml	1629 µg/ml		
hH_3R_{365} P2	419 µg/ml	154 µg/ml	359 µg/ml		
hH_3R_{329}	354 µg/ml	215 µg/ml	348 µg/ml	548 µg/ml	
hH_3R_{200}	341 µg/ml	345 µg/ml			

Table 3.1 shows the final concentrations of the pooled antibodies purified from different bleeds obtained from rabbits immunized with a particular peptide;
$hH_3R_{(445/453)}$ / rH_{3AC} (268-277) (Fiona Shenton PhD Thesis 2007)
H_3R pan (346-358) (Batch 2) (Chazot et al., 2001, Victoria Hann PhD Thesis 2004)
$hH_3R_{(365)}$ Peptide 1 (268-281)
$hH_3R_{(365)}$ Peptide 2 (268-278)
$hH_3R_{(329)}$ (222-231)
$hH_3R_{(200)}$ (191-200)

Once the antibody concentration was determined, the antibodies were then validated against HEK 293 cells transfected with the respective H_3R isoform cDNA. The next set of results looks at the validation of each of the antibodies generated.

3.4.2 Antibody validation of the anti-H_3R antibodies generated

3.4.2.1 Isoform specificity of the anti-$rH_{3A/C}$/ $hH_3R_{445/453}$ (268-277) antibody

The sequence chosen is specific to third intracellular loop region of the rat H_3R_C isoform. The antibody has previously been shown to be selective for the rat H_3R_A, rat H_3R_C and the human H_3R_{445} isoform (Fiona Shenton PhD Thesis 2007 and Cannon et al., 2007). Herein, it was shown that the antibody also detects the human H_3R_{453} isoform (Fig 3.4A and 3.B). The H_3R_{453} isoform is the result of an additional exon utilised resulting in an additional 8 amino acids added at the C-terminus (Wellendorph et al., 2002). The significance of this very rare isoform is yet to be determined.

Immunoblot showing labelling of the human $H_3R_{445/453}$ isoforms using the anti-rH_3R_{AC} / $hH_3R_{445/453}$ antibody:

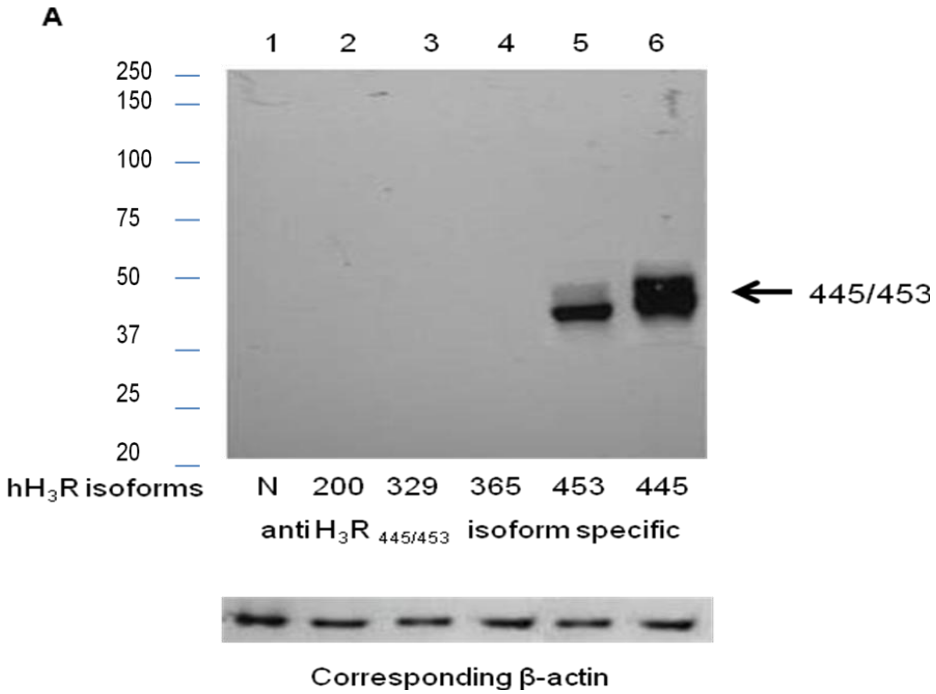

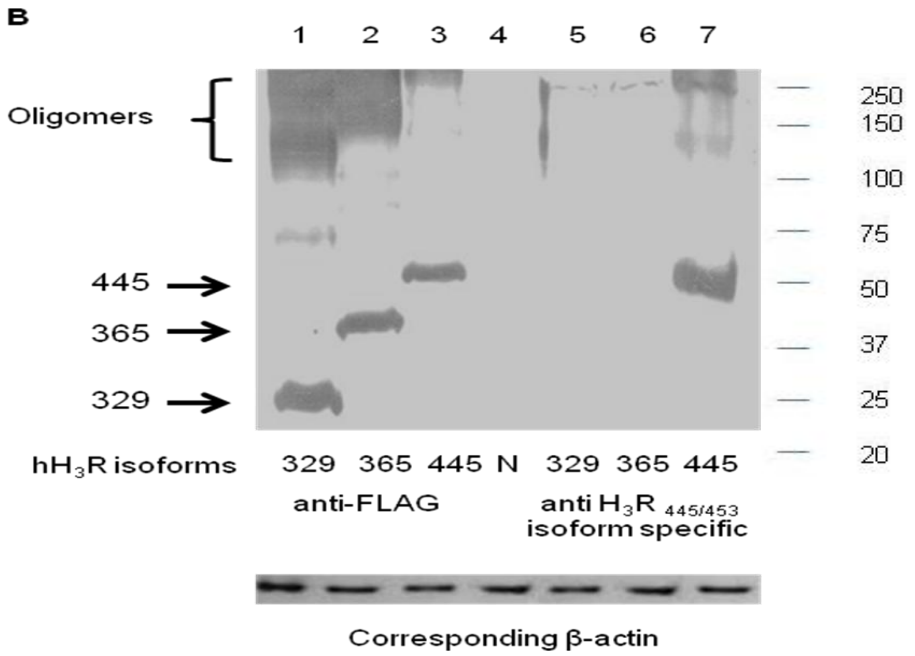

Figure 3.4 (A) Immunoblot of five different human H_3R isoforms probed with anti-rH_{3AC}/ $hH_3R_{445/453}$ specific antibody.
Approximately 25 µg of protein/ well were loaded onto a 7.5% PAGE gel. Once transferred the membrane was probed with affinity purified anti-rH_{3AC}/ $hH_3R_{445/453}$ antibody (1 µg/ml concentration). The antibody detects only the full length hH_3R 445 and 453 isoforms with no cross reactivity with the shorter isoforms. The lower panel shows the corresponding β-actin, probed with monoclonal mouse anti β-actin antibody (1:5000).
Lane 1, HEK 293 cells untransfected but still contain PEI; Lane 2, HEK 293 cells expressing hH_3R_{200}; Lane 3, HEK 293 cells expressing hH_3R_{329}; Lane 4, HEK 293 cells expressing hH_3R_{365}; Lane 5, HEK 293 cells expressing hH_3R_{453}; Lane 6, HEK 293 cells expressing hH_3R_{445}.

Figure 3.4 (B) Immunoblot of three different FLAG tagged human H_3R isoforms probed with anti-FLAG (lanes 1-3) and the anti-rH_{3AC}/ $hH_3R_{445/453}$ specific antibody (lanes 4-7).
Homogenates of HEK 293 cells transfected with three different human H_3R isoforms (329, 365 and 445), all epitope tagged with FLAG were prepared. Approximately 25 µg of protein/ well were loaded onto a 7.5% PAGE gel. Identical sample were run on both left and right hand sides of the gel. Once transferred onto a nitrocellulose membrane, the left side panel was probed with a monoclonal mouse anti-FLAG antibody (1:5000 dilution) while the right side panel probed with affinity purified anti-rH_{3AC}/ $hH_3R_{445/453}$ antibody (1 µg/ml concentration). The FLAG antibody reacts with all three isoforms with monomeric species migrating at approximately Mr 33, 36, 44 kDa. The anti-rH_{3AC}/ $hH_3R_{445/453}$ antibody detects only the full length 445 isoform with no cross reactivity with the two shorter isoforms. Lower panel shows corresponding β-actin signal, probed with monoclonal mouse anti β-actin antibody (1:5000).
Lanes 1 and 5, HEK 293 cells expressing hH_3R_{329}; Lanes 2 and 6, HEK 293 cells expressing hH_3R_{365}; Lanes 3 and 7, HEK 293 cells expressing hH_3R_{445}; Lanes 4, HEK 293 cells untransfected but still contain PEI. All blots shown are representative blots from at least 8 similar experiments.

Once the reactivity of antibody against the human H_3R isoform transfected cells was determined, the selectivity of the antibody was determined (Fig 3.4C).

Selectivity of the anti-rH_{3AC}/ h$H_3R_{445/453}$ antibody using the corresponding peptide sequence:

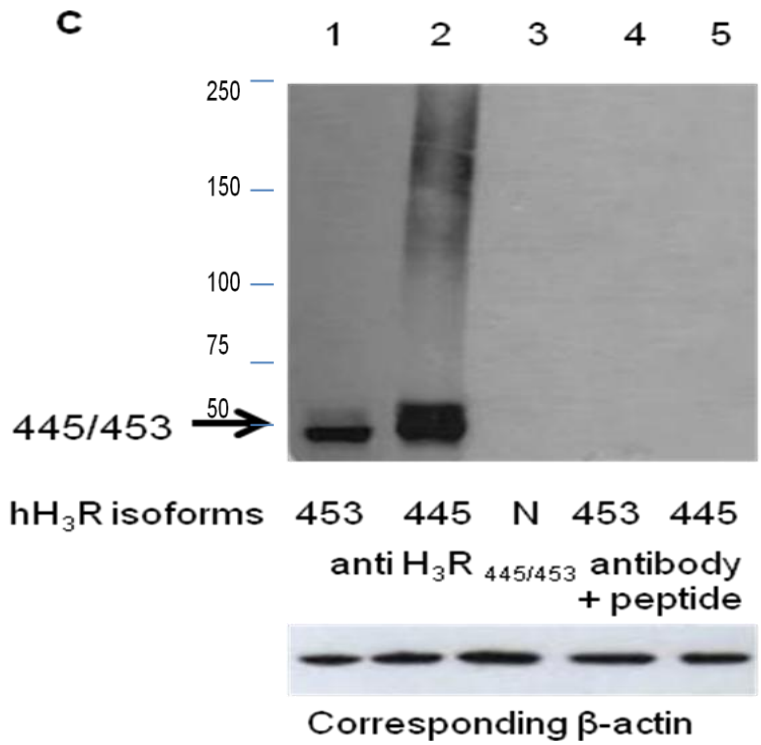

Figure 3.4 (C) Immunoblot confirming the selectivity of the anti-rH_{3AC} / h$H_3R_{445/453}$ antibody. Approximately 25 µg of protein/ well were loaded onto a 7.5% PAGE gel. Identical samples were run on both left and right hand sides of the gel. Once transferred onto a nitrocellulose membrane, the left side was probed with the affinity purified anti-rH_{3AC}/ h$H_3R_{445/453}$ antibody (1µg/ml concentration) while the right side was probed with affinity purified anti-rH_{3AC}/ h$H_3R_{445/453}$ antibody pre-incubated with the antigen peptide (1 µg/ml concentration). The major immunoreactive bands labelled in HEK 293 expressing the hH_3R_{453} or hH_3R_{445} (lanes 1 and 2, respectively) were greatly suppressed by pre-incubation with the antigen peptide (lanes 4 and 5), demonstrating the sequence selectivity of the antibody. Lane 3, HEK 293 cells mock transfected. Lower panel shows corresponding β-actin, probed with monoclonal mouse anti β-actin antibody (1:5000).

The anti-rH_3R_{AC}/ h$H_3R_{445/453}$ antibody has been shown to detect the full length human and rat isoforms as well as a truncated rH_3R_C isoform. This antibody is useful for looking at the full length H_3R in both rodent and human tissue.

3.4.2.2 Isoform specificity of the anti-H_3R Pan (349-358) antibody

The sequence is common to both human and rodent H_3R sequences as well as a number of isoforms. Previously the antibody has been shown to detect

major species in human putamen and rodent brain (Figure 3.5), (Victoria Hann PhD Thesis 2004 and Chazot et al., 2001). Immunohistochemical analysis on mouse brain using the affinity-purified anti-H_3R (349-358) antibody yielded a high degree of coincidence with ligand-autoradiographical information, with high levels detected in the CA3 and dentate gyrus of the hippocampus, laminae V of the cerebral cortex, the olfactory tubercle, Purkinje cell layer of the cerebellum, substantia nigra, globus pallidus, thalamus and striatum (Martinez et al., 1990, Goodchild et al., 1999 and Drutel et al., 2001).

Immunoblot showing labelling of the human, mouse and rat brain homogenates using the anti-H_3R Pan antibody:

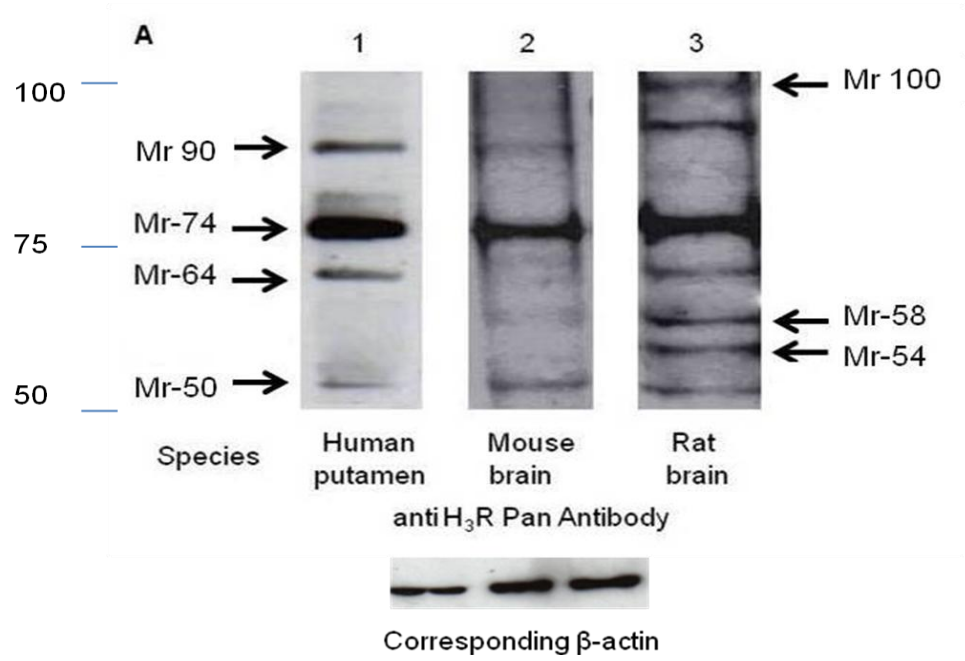

Figure 3.5 Immunoblot showing H_3R pan (346-358) antibody reactivity against native tissue, rat, mouse and human.
Approximately 25 µg of protein/ well were loaded onto a 7.5% PAGE gel. Once transferred the membrane was probed with affinity purified anti-H_3R pan antibody (1 µg/ml concentration). The anti-H_3R pan antibody detects a variety of different molecular weight species in human, mouse and rat brain likely representing monomeric, dimeric, glycosylated isoforms. Panel below shows the corresponding β-actin, probed with monoclonal mouse anti β-actin antibody (1:5000).
Lane 1, Human putamen; Lanes 2, Mouse forebrain; Lanes 3, Rat forebrain.

Previous data has shown that the anti-pan H_3R antibody detects a variety of different molecular weight species in both human and rodent brain homogenates. The array of molecular weight species detected is likely to represent monomeric, dimeric, and glycosylated H_3R isoforms since the sequence is common to a number of isoforms.

3.4.2.3 Isoform specificity of the anti-hH_3R_{365} peptide 1 (268-281) antibody

The sequence chosen is specific to the third intracellular loop region in the human H_3R_{365} isoform. This antibody was shown to be selective for the human H_3R_{365} and H_3R_{445} isoforms (Figure 3.6).

Immunoblot showing labelling of the human $H_3R_{445/\ 365}$ isoforms using the anti-hH_3R_{365} peptide 1 antibody:

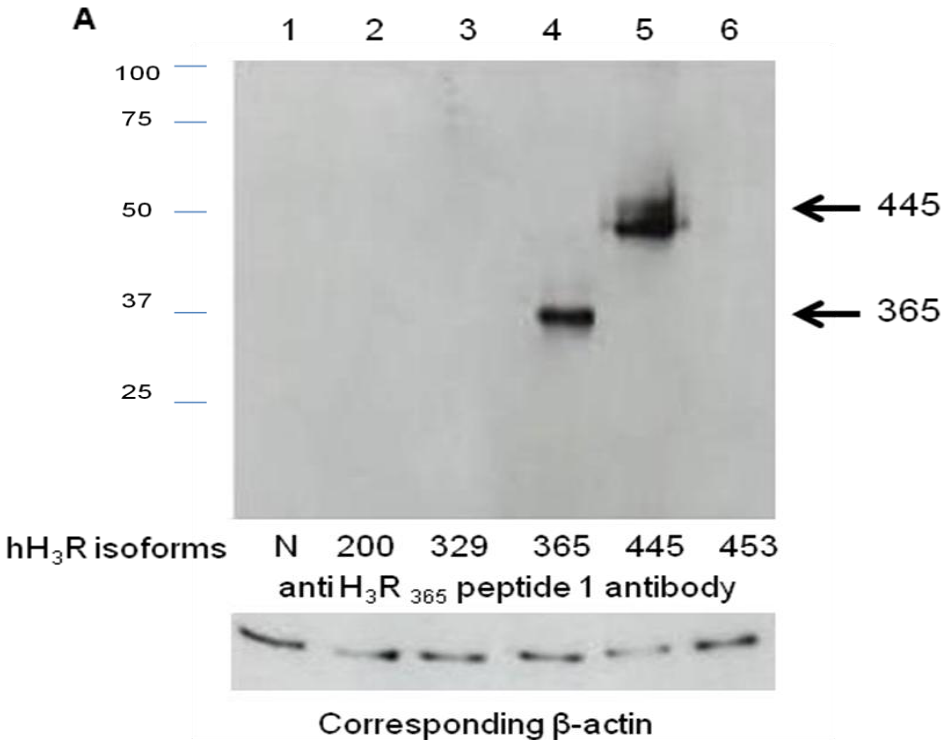

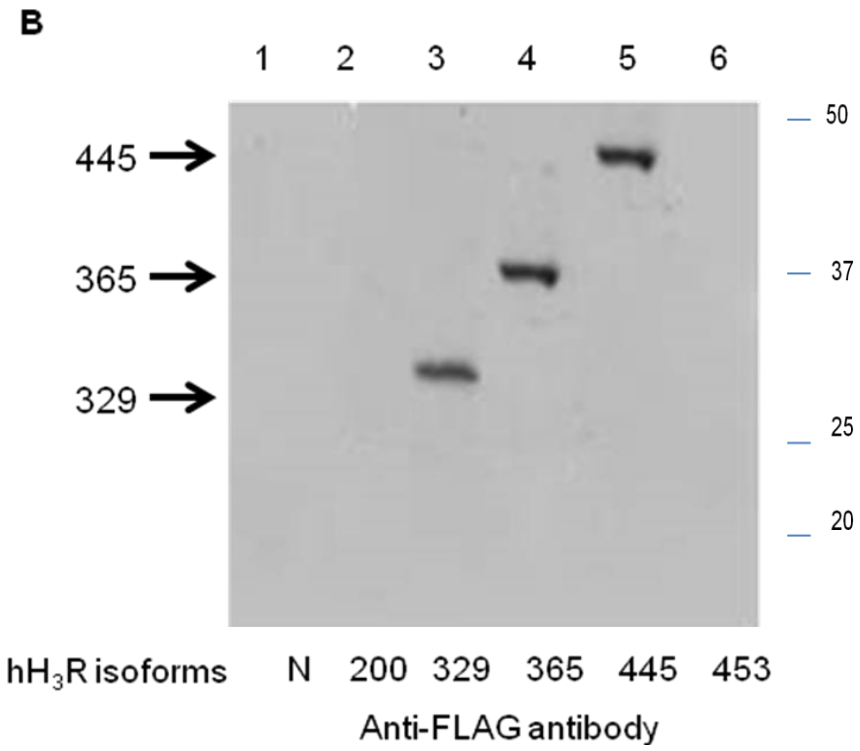

Figure 3.6 (A) Immunoblot of five different human H_3R isoforms probed with anti-hH_3R_{365} peptide 1 specific antibody.
Approximately 25 µg of protein/ well were loaded onto a 7.5% PAGE gel. Once transferred the membrane was probed with affinity purified anti-hH_3R_{365} peptide 1 antibody (1 µg/ml concentration). The anti-hH_3R_{365} peptide 1 antibody detects the H_3R 365 isoform, but also the full length H_3R 445 isoform. There was no cross reactivity with the other shorter or longer isoforms. Lower panel shows the corresponding β-actin, probed with monoclonal mouse anti β-actin antibody (1:5000).
Lane 1, HEK 293 cells mock transfected; Lane 2, HEK 293 cells expressing hH_3R_{200}; Lane 3, HEK 293 cells expressing hH_3R_{329}; Lane 4, HEK 293 cells expressing hH_3R_{365}; Lane 5, HEK 293 cells expressing hH_3R_{445}; Lane 6, HEK 293 cells expressing hH_3R_{453}.

Figure 3.6 (B) Immunoblot confirming the expression of FLAG tagged cDNA transfected into HEK 293 cells. Blot probed with anti-FLAG specific antibody (1:5000).

The anti-hH_3R_{365} peptide 1 antibody has been shown to detect the full length human H_3R and the shorter H_3R_{365} isoform. This antibody can be used to look at the expression of the human H_3R_{445} and the H_3R_{365} isoforms.

3.4.2.4 Isoform specificity of the anti-hH_3R_{365} peptide 2 (268-278) antibody

The sequence chosen is specific to the third intracellular region in the human H_3R_{365} isoform. This antibody was shown to be selective for the human H_3R_{445} isoform only (Figure 3.7).

Immunoblot showing labelling of the human H_3R_{445} isoform using the anti-hH_3R_{365} peptide 2 antibody:

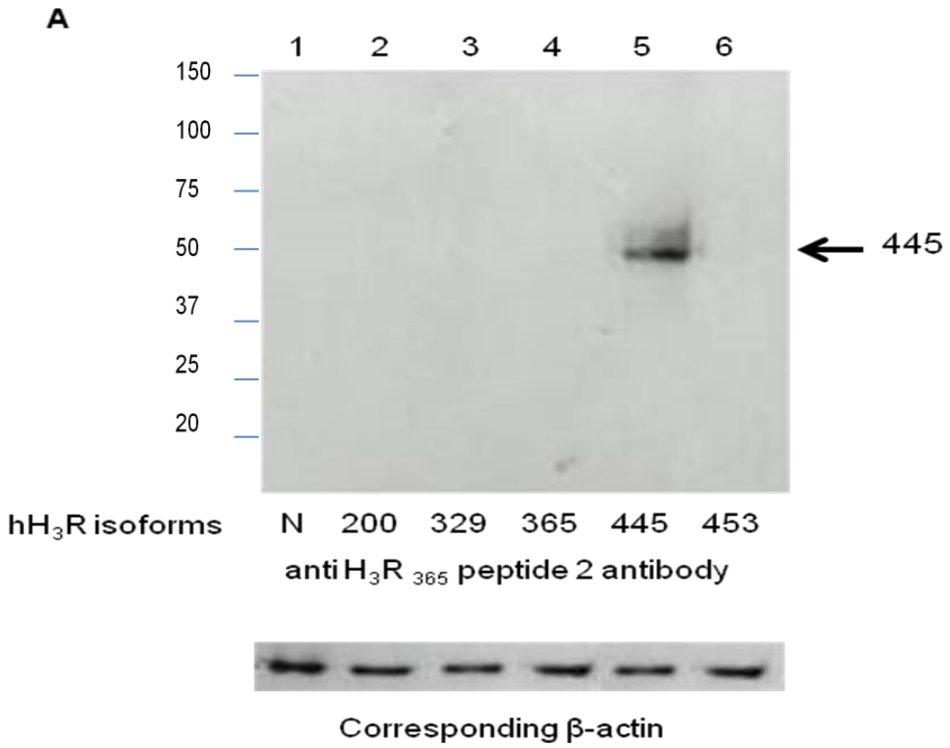

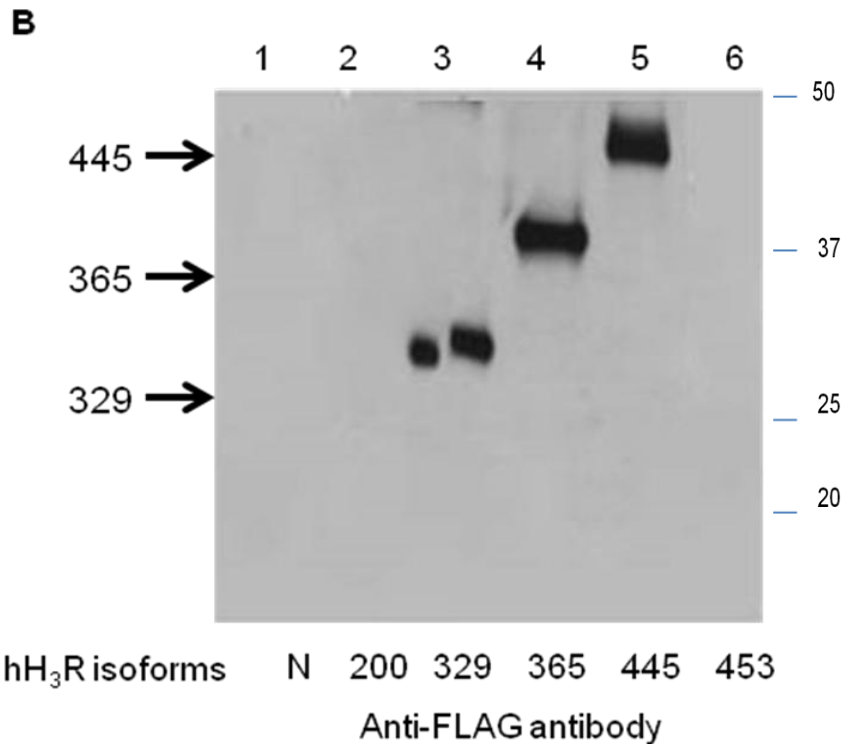

Figure 3.7 (A) Immunoblot of five different human H_3R isoforms probed with anti-hH_3R_{365} peptide 2 specific antibody.
Approximately 25 µg of protein/ well were loaded onto a 7.5% PAGE gel. Once transferred the membrane was probed with affinity purified anti-hH_3R_{365} peptide 2 antibody (1 µg/ml concentration). The anti-hH_3R_{365} peptide 2 antibody detects only the full length H_3R 445, but not the H_3R 365 isoform. No cross reactivity with the other shorter or longer isoforms. Lower panel shows the corresponding β-actin, probed with monoclonal mouse anti β-actin antibody (1:5000).
Lane 1, HEK 293 cells mock transfected; Lane 2, HEK 293 cells expressing hH_3R_{200}; Lane 3, HEK 293 cells expressing hH_3R_{329}; Lane 4, HEK 293 cells expressing hH_3R_{365}; Lane 5, HEK 293 cells expressing hH_3R_{445}; Lane 6, HEK 293 cells expressing hH_3R_{453}.

Figure 3.7 (B) Immunoblot confirming the expression of FLAG tagged cDNA transfected into HEK 293 cells. Blot probed with anti-FLAG specific antibody (1:5000).

The anti-hH_3R_{365} peptide 2 antibody was shown to detect the full length human H_3R_{445} isoform.

3.4.2.5 Isoform specificity of the anti-hH_3R_{329} (222-231) antibody

The sequence selected is specific to the third intracellular loop region in the human H_3R_{329} isoform. This antibody was shown to be selective for the human H_3R_{329} isoform (Figure 3.8).

Immunoblot showing labelling of the human H_3R_{329} isoform using the anti-hH_3R_{329} antibody:

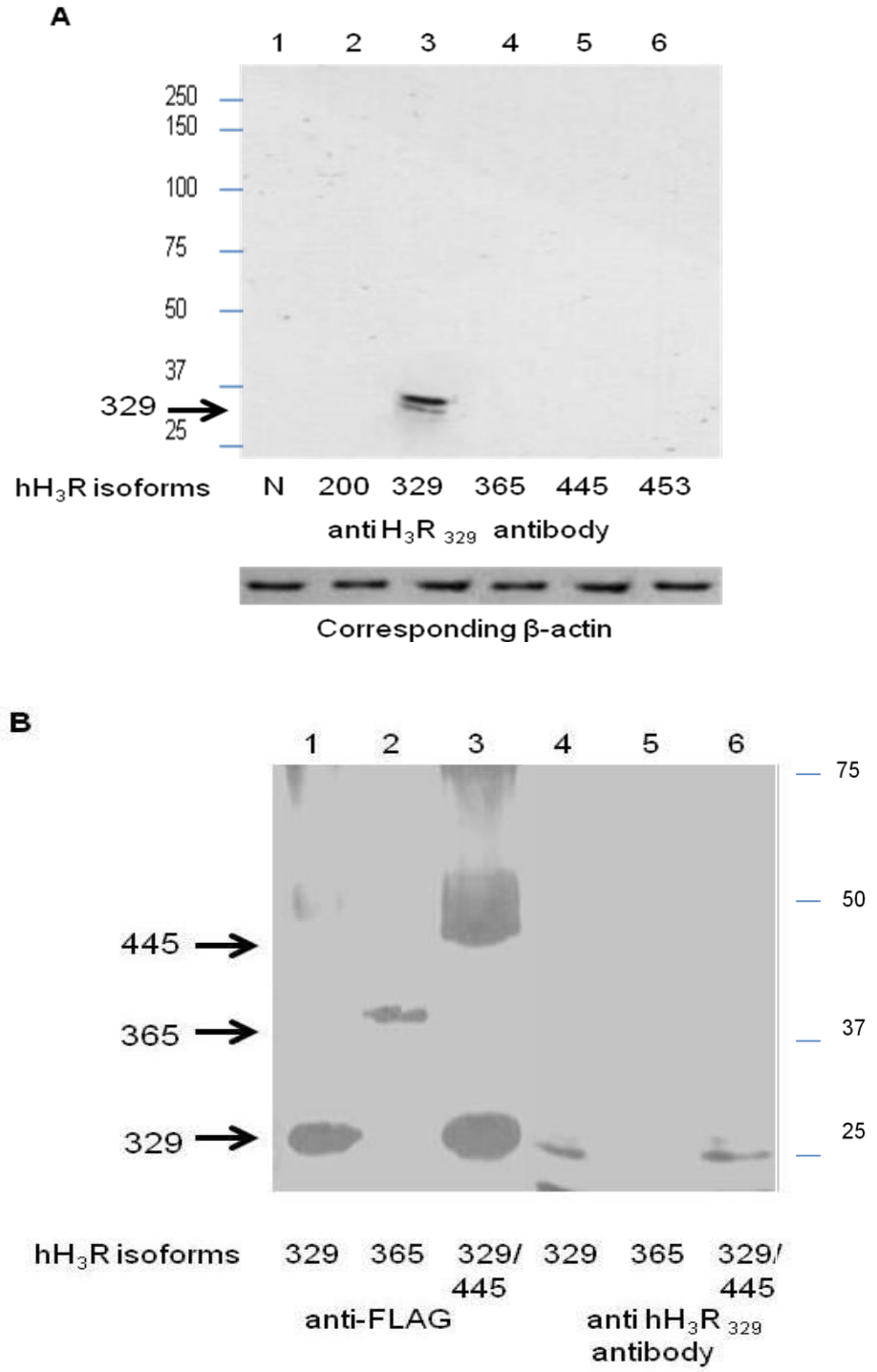

Figure 3.8 (A) Immunoblot of five different human H_3R isoforms probed with anti-hH_3R_{329} specific antibody.
Approximately 25 µg of protein/ well were loaded onto a 7.5% PAGE gel. Once transferred the membrane was probed with affinity purified anti-hH_3R_{329} antibody (3 µg/ml concentration). The anti-hH_3R_{329} antibody detects only the H_3R 329 isoform. No cross reactivity with the other

shorter or longer isoforms was detected. Lower panel shows the corresponding β-actin, probed with monoclonal mouse anti β-actin antibody (1:5000).
Lane 1, HEK 293 cells mock transfected; Lane 2, HEK 293 cells expressing hH_3R_{200}; Lane 3, HEK 293 cells expressing hH_3R_{329}; Lane 4, HEK 293 cells expressing hH_3R_{365}; Lane 5, HEK 293 cells expressing hH_3R_{445}; Lane 6,HEK 293 cells expressing hH_3R_{453}.

Figure 3.8 (B) Immunoblot of three different FLAG tagged human H_3R isoforms probed with anti-FLAG (lanes 1-3) and the anti-hH_3R_{329} specific antibody (lanes 4-6).
Homogenates of HEK 293 cells transfected with three different human H_3R isoforms (329, 365 alone OR 329 + 445), all epitope tagged with FLAG. Approximately 25 µg of protein/ well were loaded onto a 7.5% PAGE gel. Identical samples were run on both left and right hand sides of the gel. Once transferred onto a nitrocellulose membrane, the left side was probed with a monoclonal mouse anti-FLAG antibody (1:5000 dilution) while the right probed with affinity purified anti-hH_3R_{329} antibody (3 µg/ml concentration). The anti-hH_3R_{329} antibody detects only the 329 isoform with no cross reactivity with the other longer isoforms.
Lanes 1 and 4, HEK 293 cells expressing hH_3R_{329}; Lanes 2 and 5, HEK 293 cells expressing hH_3R_{365}; Lanes 3 and 6, HEK 293 cells co-expressing hH_3R_{445} and hH_3R_{329}.

The anti-hH_3R_{329} antibody was shown to be selective for the hH_3R_{329} isoform.

3.4.2.6 Isoform specificity of the H_3R_{200}/ isoform 5 (191-200) antibody

The sequence was generated to the C terminus of the human H_3R_{200} because of its unique C terminal sequence. The antibody was shown to detect immunoreactivity in both human putamen (not shown) and recombinant HEK 293 cells expressing the H_3R_{200} cDNA (Fig 3.9).

Immunoblot showing labelling of the human H_3R_{200} isoform using the anti-hH_3R_{200} antibody:

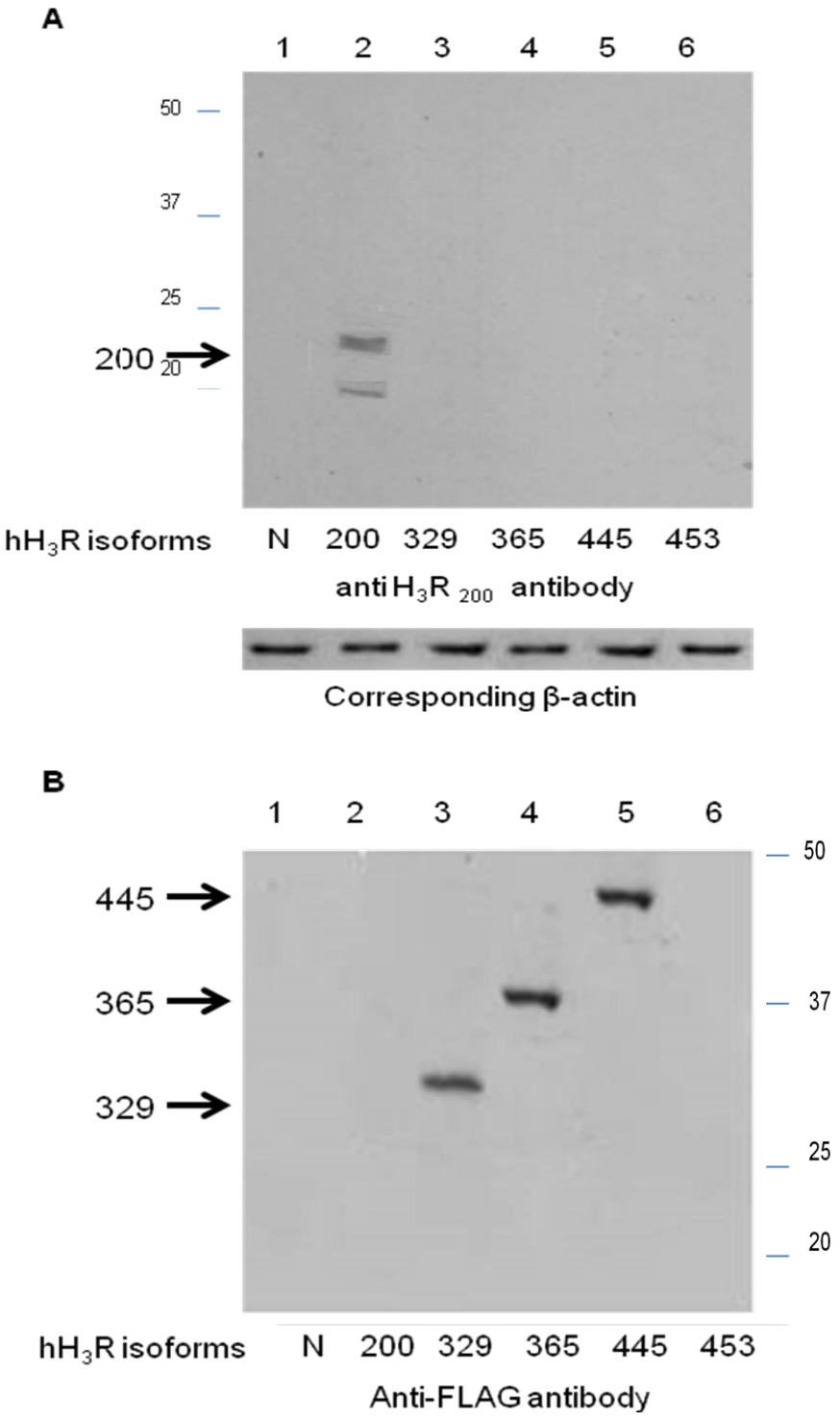

Figure 3.9 Immunoblot of five different human H_3R isoforms probed with anti-hH_3R_{200} specific antibody.
Approximately 25 µg of protein/ well were loaded onto a 10% PAGE gel. Once transferred the membrane was probed with affinity purified anti-hH_3R_{200} antibody (3 µg/ml concentration). The anti-hH_3R_{200} antibody detects only the 200 isoform. No cross reactivity with the longer

isoforms was detected. Lower panel shows the corresponding β-actin, probed with monoclonal mouse anti β-actin antibody (1:5000).
Lane 1, HEK 293 cells mock transfected; Lane 2, HEK 293 cells expressing hH_3R_{200}; Lane 3, HEK 293 cells expressing hH_3R_{329}; Lane 4, HEK 293 cells expressing hH_3R_{365}; Lane 5, HEK 293 cells expressing hH_3R_{445}; Lane 6, HEK 293 cells expressing hH_3R_{453}.

Figure 3.9 (B) Immunoblot confirming the expression of FLAG tagged cDNA transfected into HEK 293 cells. Probed with anti-FLAG specific antibody (1:5000).

The anti-hH_3R_{200} antibody was shown to be selective for the hH_3R_{200} isoform

The antibodies generated have been validated against recombinantly expressed cDNA and specific immunoreactivity demonstrated by competition binding with the respective peptide. The antibodies was then used to look at the expression of the H_3R in both rodent and human CNS. Initially, the anti-pan H_3R antibody and the anti-rH_{3AC}/ $hH_3R_{445/453}$ antibody that have been shown to detect rodent H_3R isoforms were used to look at the expression profile of the H_3R in two mouse strains (CD-1 and TASTPM). These antibodies were then used to determine whether the H_3R is preserved with age and in age related dementias in two mouse strains, CD-1 mice, previously shown to have premature learning deficits, and TASTPM mice, a mouse model of AD.

3.4.3 Immunoblotting and immunohistochemical analysis using two rodent specific antibodies to compare the immunoreactivity in TASTPM and CD-1 mice with age.

The anti-H_3R pan and anti-H_{3C}/ $hH_3R_{445/453}$ antibodies were used to determine whether H_3R expression was altered in two mouse models. CD-1 mice, known to have premature age-related learning deficits in first 12 months of age (in house published behavioural data), and TASTPM mice, a mouse model of AD

(age-dependent learning deficits within 7 months confirmed in house). These mice strains were selected to look at H_3R expression because of their premature learning phenotype. Pre-clinical and clinical studies have elucidated the use of H_3R antagonists in learning and memory. The rationale for looking at H_3R expression is to determine whether expression is changed with aging or with disease. If expression is unaltered it would indicate that the H_3R is a valid available therapeutic target for the treatment of cognitive deficits in dementia related diseases.

Brain tissue samples from 18 mice: 9 CD-1 and 9 TASTPM were used; left hemisphere subjected to semi-quantitative immunohistochemistry and the right hemisphere to quantitative immunoblotting.

Immunoblot showing CD-1 mouse timeline labelled using the anti-pan H_3R antibody:

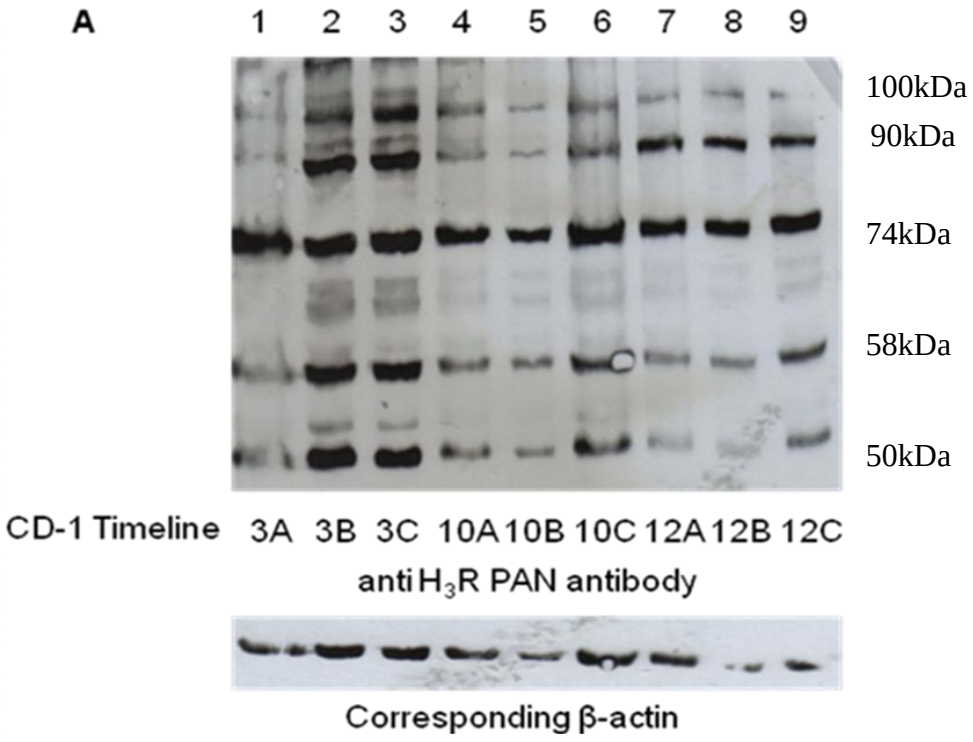

Figure 3.10 (A) Immunoblot of CD-1 mice at three age points 3, 10 and 12 months probed with anti-H_3R PAN antibody. Immunoreactive bands detected with the anti-H_3R antibodies were normalized to β-actin.
Approximately 50 µg of protein/ well were loaded onto a 7.5% PAGE gel. Once transferred the membrane was probed with affinity purified anti-H_3R PAN antibody (1 µg/ml concentration). The anti-H_3R pan antibody detected a variety of different molecular weight species in mouse brain, five major bands (M_r 100,000, 90,000, 74,000 58,000 and 50,000) were detected. Lower panel shows the corresponding β-actin, probed with monoclonal mouse anti β-actin antibody (1:5000).
Lane 1, 2, 3, CD-1 mouse forebrain from 3 separate mice at 3 months.
Lane 4, 5, 6, CD-1 mouse forebrain from 3 separate mice at 10 months.
Lane 7, 8, 9, CD-1 mouse forebrain from 3 separate mice at 12 months.
All blots shown are representative blots from at least 5 similar experiments.

The molecular weight species detected are likely to represent homo- and hetero-dimers, glycosylation, proteolytic fragments of the H_3R and its respective isoforms. The bands at 50kDa and 90kDa represent the monomeric and dimeric versions of the full length rat H_3R receptor.

3.4.3.1 Mean immunoreactive intensity of each of the protein species detected using the anti-pan H_3R antibody in CD-1 timeline

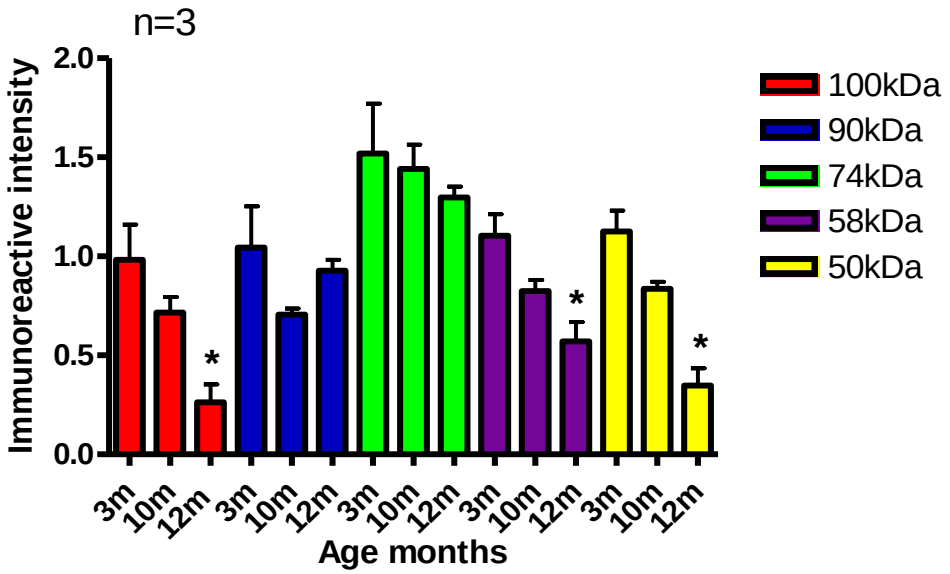

Figure 3.11 Comparing the immunoreactivity of CD-1 mice at three age points 3, 10 and 12 months probed with anti-H_3R PAN antibody. Immunoreactive bands detected with the anti-H_3R antibodies were normalized to β-actin. Data show the mean immunoreactive intensity $\pm$ SEM for n = 3 determinations. Statistical significance was determined from the generated p value, where $p \leq 0.05$ was considered to show significance.

Figure 3.11 shows there were significant decreases in the immunoreactive banding intensity with the anti-H_3R PAN antibody at 12 months compared to 3 months, for the molecular weight species migrating at 100kDa ($p<0.01$). The immunoreactivity for the 50kDa band was significantly lower in the 12 month CD-1 mice compared with both the 3 and 10 month time point ($p<0.01$). There appears to be a general trend for a decrease in immunoreactivity with increasing age between 10 and 12 month. A similar result was obtained for the corresponding immunohistochemistry (IHC), see below.

Immunoblotting would suggest that there appears to be a general decrease in some of the immunoreactive species detected with anti-pan H_3R antibody between the 10 - 12 month age points in CD-1 mouse forebrain.

The anti-pan H_3R antibody was then used to determine whether the H_3R was preserved in the brain of CD-1 mice over 3, 10, 12 & 19 months, using IHC.

IHC showing H_3R labelling in the cortex of CD-1 mice timeline at 3, 10, 12 & 19 months:

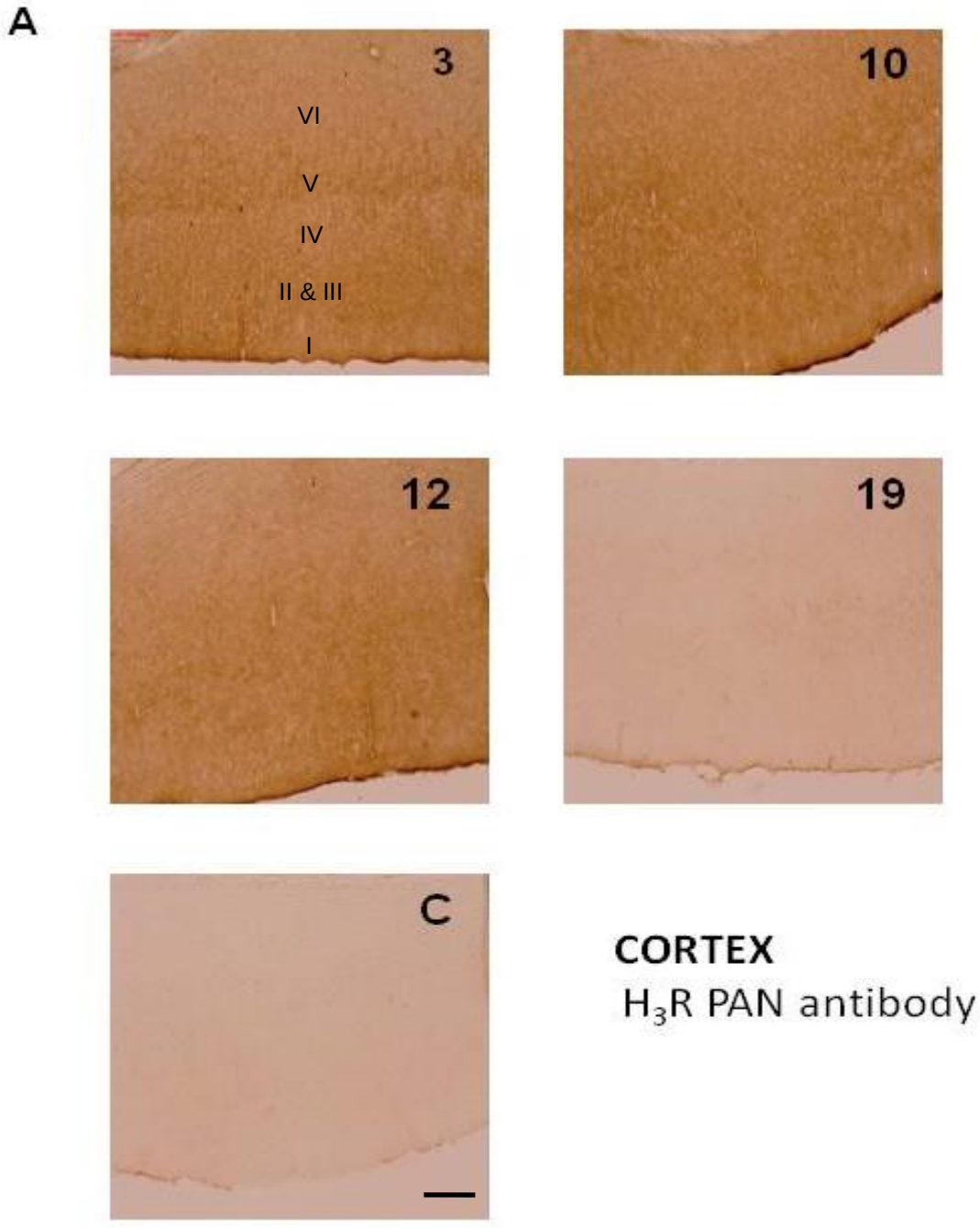

Figure 3.12 (A) Immunohistochemistry of CD-1 mice cortex at four age points 3, 10, 12 and 19 months probed with anti-H_3R PAN antibody. C represents control experiment incubated without either the primary antibody or secondary antibody. H_3R immunoreactivity was detected in layers I-VI of the cortex, with intense labelling detected in layer V. Immunostaining of mouse 20µm sagittal brain slice (X20). Scale bar = 200 µm and represents all images shown. All immunohistochemistry data shown are representative images from at least 3 repeats for each time point.

IHC showing H_3R labelling in the CA1 of CD-1 mice timeline at 3, 10, 12 & 19 months:

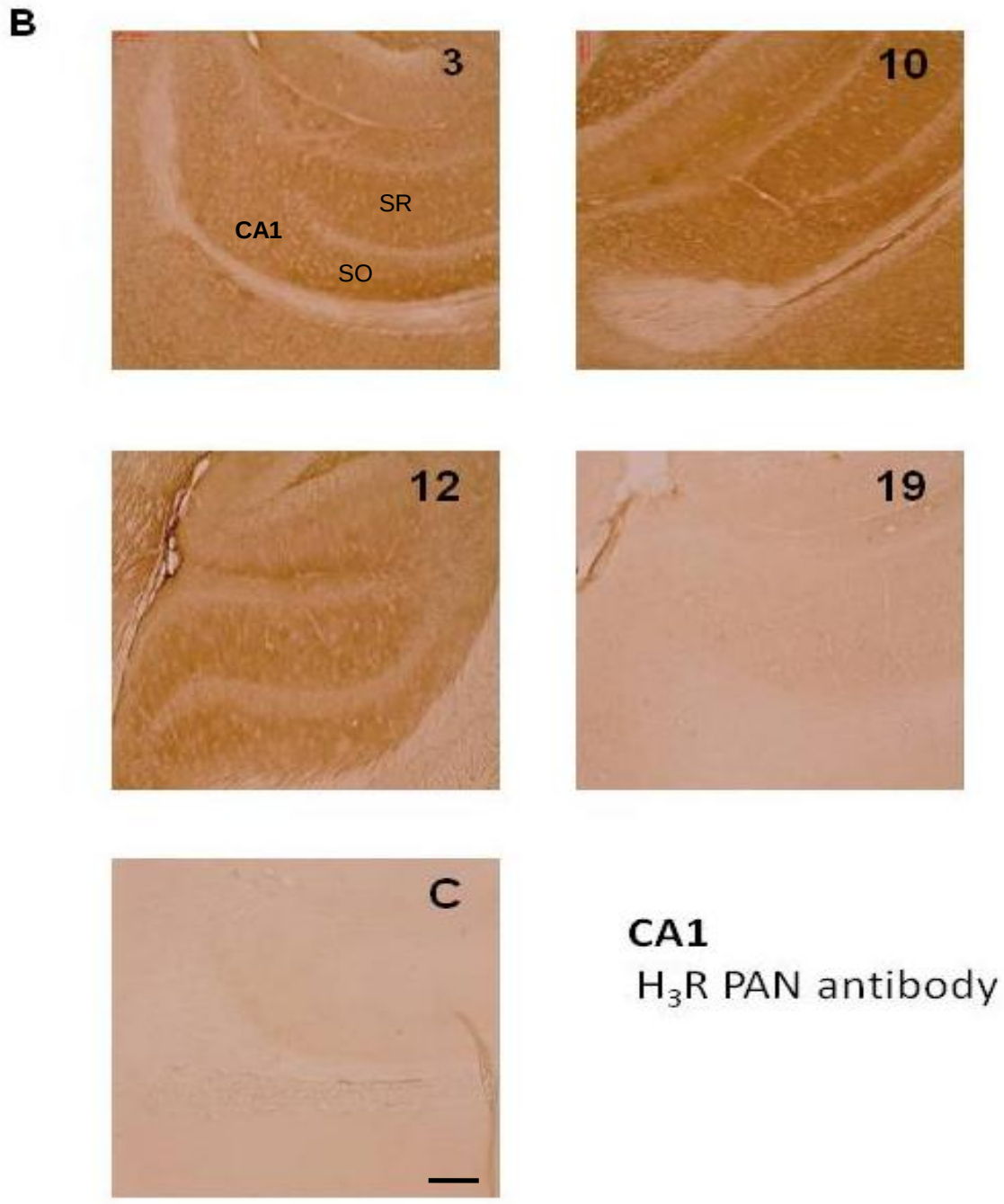

Figure 3.12 (B) Immunohistochemistry of CD-1 mice CA1 at four age points 3, 10, 12 and 19 months probed with anti-H_3R PAN antibody. C represents control experiment incubated without either the primary antibody or secondary antibody. H_3R immunoreactivity was intense on the dendrites in the stratum radiatum (SR) and stratum oriens (SO). Immunostaining of mouse 20 µm sagittal brain slice (X20). Scale bar = 200 µm and represents all images shown. All immunohistochemistry data shown are representative images from at least 3 repeats for each time point.

IHC showing H_3R labelling in the CA2/3 of CD-1 mice timeline at 3, 10, 12 & 19 months:

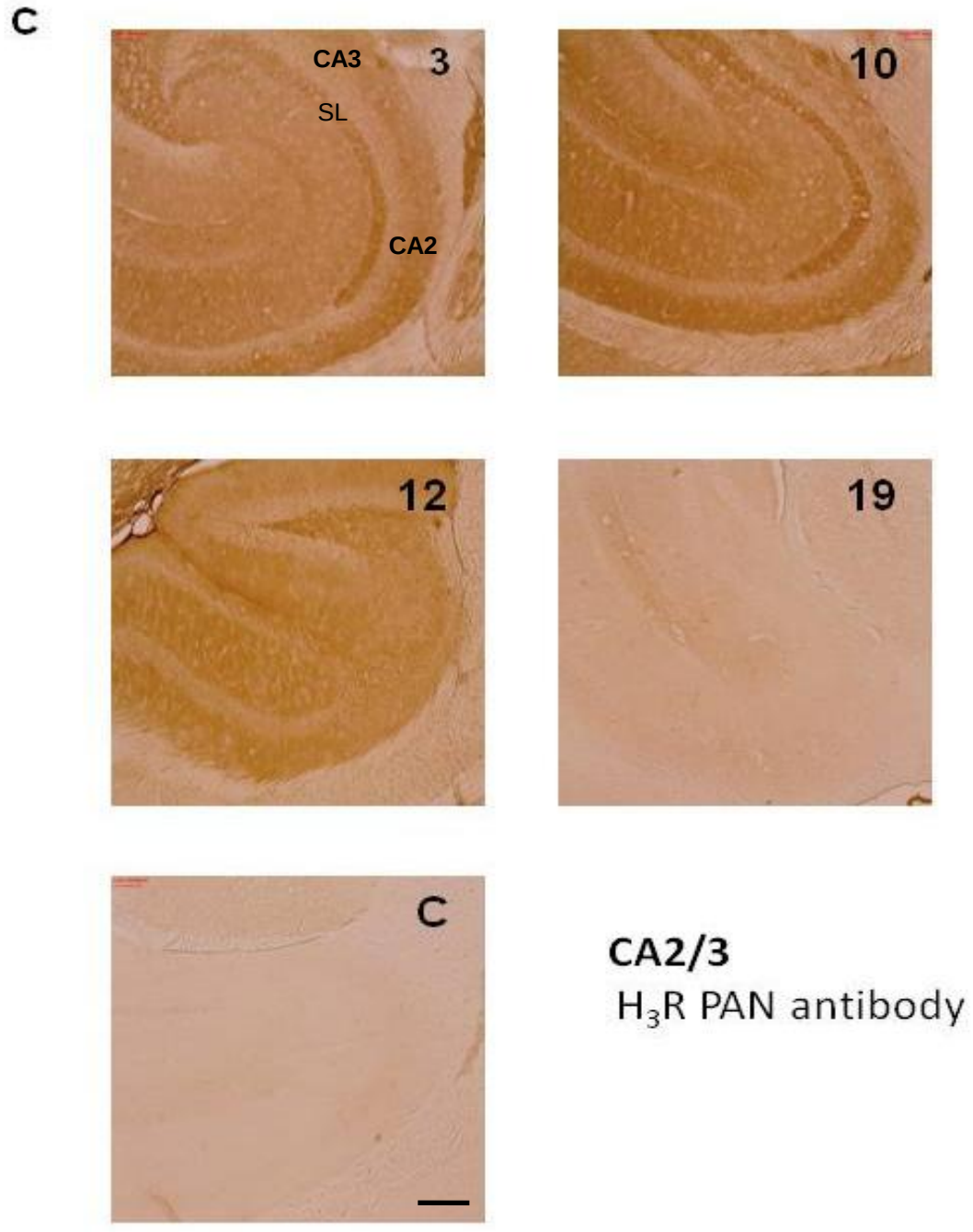

Figure 3.12 (C) Immunohistochemistry of CD-1 mice CA2/CA3 at four age points 3, 10, 12 and 19 months probed with anti-H_3R PAN antibody. C represents control experiment incubated without either the primary antibody or secondary antibody. H_3R immunoreactivity was intense on the dendrites in the stratum lucidum (SL). Scale bar = 200 µm and represents all images shown. Immunostaining of mouse 20 µm sagittal brain slice (X20). All immunohistochemistry data shown are representative images from at least 3 repeats for each time point.

IHC showing H_3R labelling in the dentate gyrus of CD-1 mice timeline at 3, 10, 12 & 19 month:

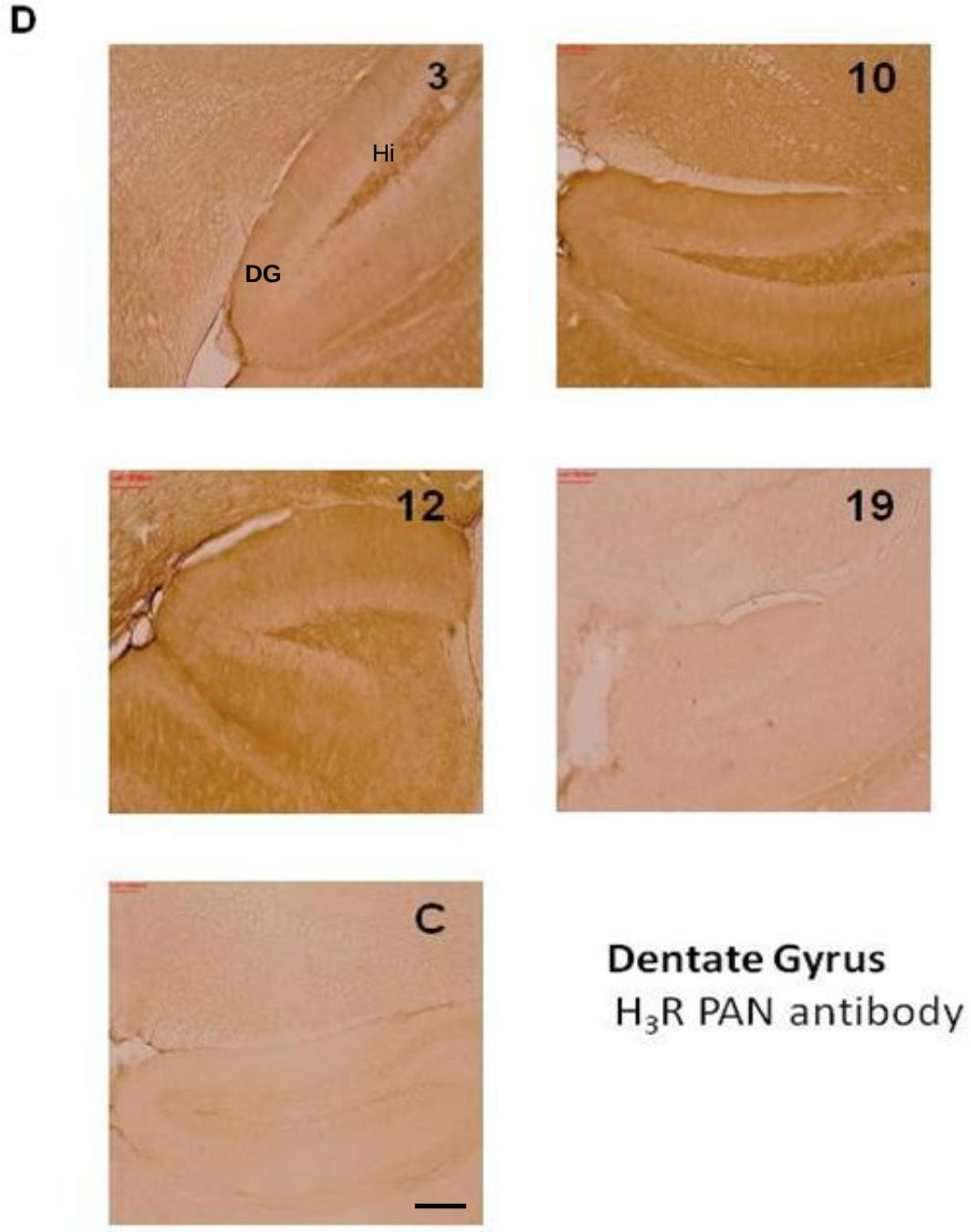

Figure 3.12 (D) Immunohistochemistry of CD-1 mice dentate gyrus at four age points 3, 10, 12 and 19 months probed with anti-H_3R PAN antibody. C represents control experiment incubated without either the primary antibody or secondary antibody. DG represents dentate gyrus. H_3R immunoreactivity was intense in the hilus region (Hi) of the dentate gyrus. Immunostaining of mouse 20 µm sagittal brain slice (X20). Scale bar = 200 µm and represents all images shown. All immunohistochemistry data shown are representative images from at least 3 repeats for each time point.

IHC showing H_3R labelling in the cerebellum of CD-1 mice timeline at 3, 10, 12 & 19 months:

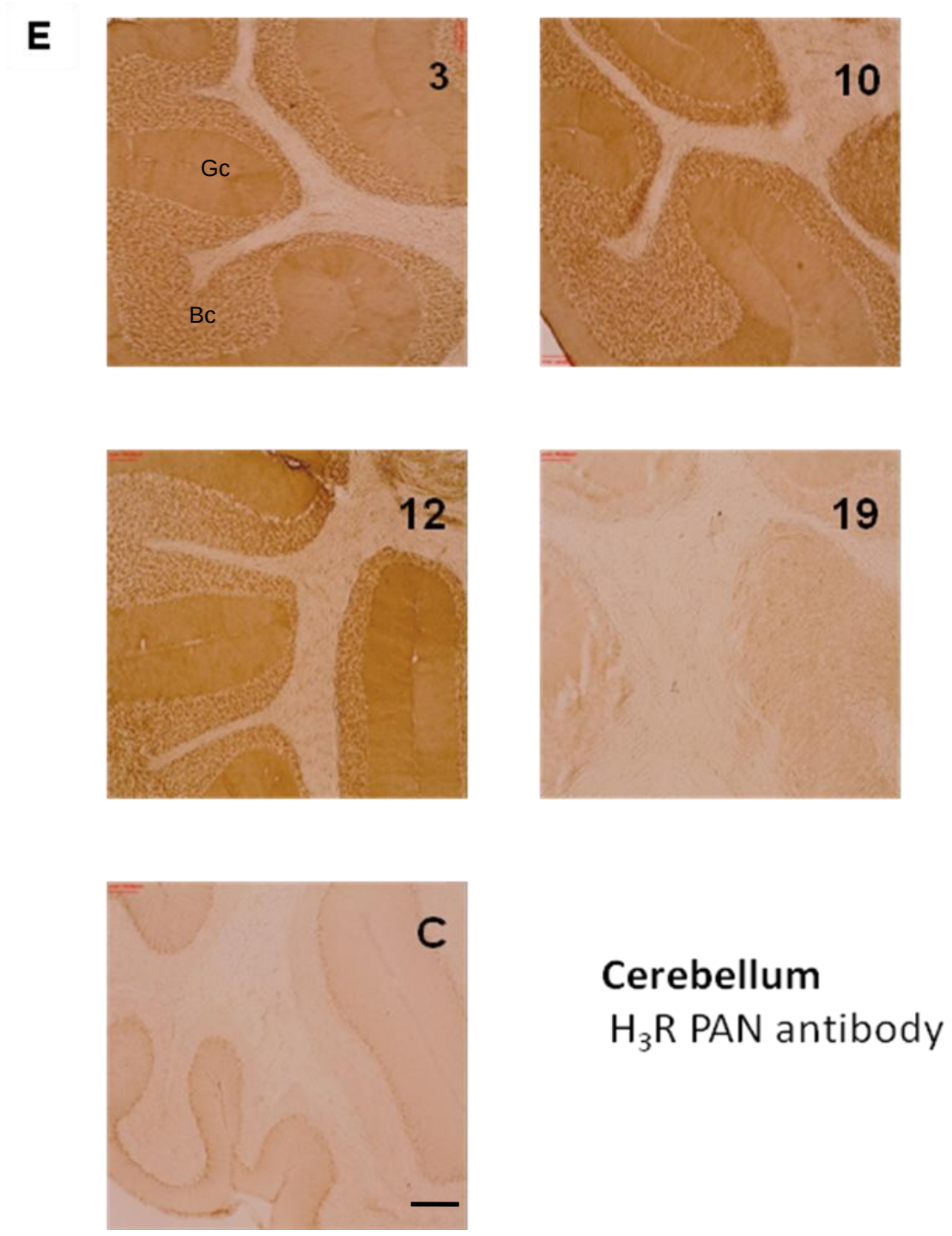

Figure 3.12 (E) Immunohistochemistry of CD-1 mice cerebellum at four age points 3, 10, 12 and 19 months probed with anti-H_3R PAN antibody. C represents control experiment incubated without either the primary antibody or secondary antibody. H_3R immunoreactivity was associated with the cerebellar granule cells (Gc) and basket cells (Bc) of the cerebellum. Immunostaining of mouse 20 µm sagittal brain slice (X20). Scale bar = 200 µm and represents all images shown. All immunohistochemistry data shown are representative images from at least 3 repeats for each time point.

IHC data would suggest that immunostaining detected using the anti-pan H_3R antibody is preserved between 3-10 months in the cortex, CA1, 2 & 3, dentate gyrus and cerebellum of CD-1 brain. However, at 19 months a dramatic decrease in immunostaining was observed in all areas of the CD-1 brain.

The anti-pan H_3R antibody was then used to determine whether the H_3R was preserved in dementia related diseases, in TASTPM mice, a model of AD.

Immunoblot showing TASTPM mouse timeline labelled using the anti-pan H_3R antibody:

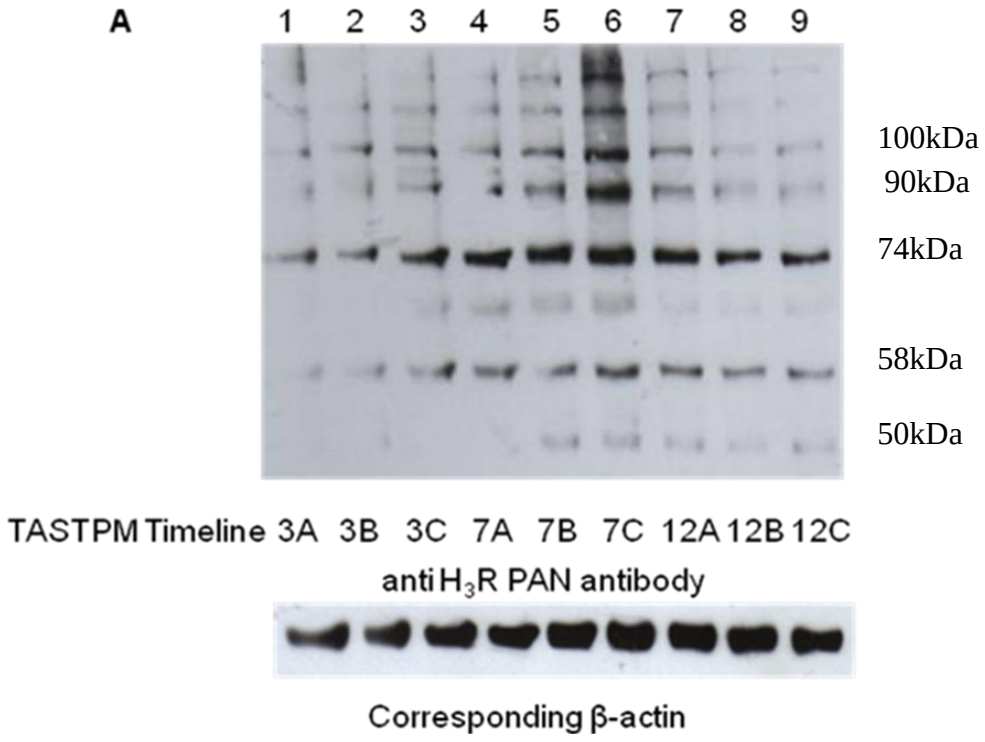

Figure 3.13 (A) Immunoblot of TASTPM mice at three age points 3, 7 and 12 months probed with anti-H_3R PAN antibody. Immunoreactive bands detected with the anti-H_3R antibodies were normalized to β-actin.
Approximately 50 µg of protein/ well were loaded onto a 7.5% PAGE gel. Once transferred the membrane was probed with affinity purified anti-H_3R PAN antibody (1 µg/ml concentration). The anti-H_3R pan antibody detects a variety of different molecular weight species in mouse brain, five major bands (M_r 100,000, 90,000, 74,000, 60,000 and 50,000) were detected. Lower panel shows the corresponding β-actin, probed with monoclonal mouse anti β-actin antibody (1:5000).
Lane 1, 2, 3, TASTPM mouse forebrain from 3 separate mice at 3 months.
Lane 4, 5, 6, TASTPM mouse forebrain from 3 separate mice at 7 months.
Lane 7, 8, 9, TASTPM mouse forebrain from 3 separate mice at 12 months.

The molecular weight protein species detected are likely to represent homo- and hetero-dimers, glycosylation, proteolytic fragments of the H_3R and its respective isoforms. The bands at 50kDa and 90kDa represent monomeric and dimeric versions of the full length receptor.

3.4.3.2 Mean immunoreactive intensity of each of the molecular weight protein species detected using the anti-pan H_3R antibody in TASTPM timeline

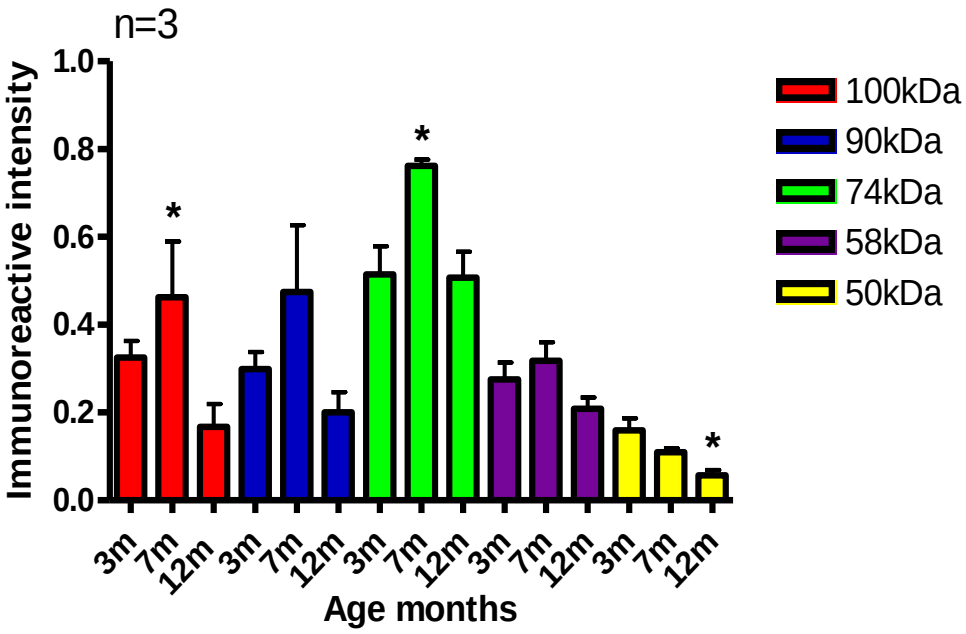

Figure 3.14 Comparing the immunoreactivity of TASTPM mice at three age points 3, 7 and 12 months probed with anti-H_3R PAN antibody. Immunoreactive bands detected with the anti-H_3R antibodies were normalized to β-actin. Mean immunoreactive intensity $\pm$ SEM for n = 3 determinations. Statistical significance was determined from the generated p value, where $p \leq 0.05$ was considered to show significance.

Figure 3.14 shows there were significant differences in the immunoreactivity of the banding detected with the anti-H_3R PAN antibody between the 3 age time points. Molecular weight species 100kDa and 74kDa had significantly higher immunoreactivity in the 7 month TASTPM mice compared with the 12

months ($p<0.001$ and $p<0.05$). Molecular weight species migrating at 74kDa had significantly higher immunoreactivity in the 7 month TASTPM mice compared with the 3 months ($p<0.05$). The band migrating at 100kDa had significantly higher immunoreactivity in the 3 month TASTPM mice compared with the 12 months ($p<0.05$). Generally more intense banding was detected at age 7 months in TASTPM mice brain compared with 3 and 12 months, a similar result was also obtained for the IHC, below and by autoradiography (chapter 5).

Immunoblotting would suggest that there appears to be a general increase in H_3R expression at 7 months in TASTPM mice, which decreases by 12 months back to similar levels detected in the 3 month old TATSPM mice.

The anti-pan H_3R antibody was then used to determine whether the H_3R was preserved in the brain of TASTPM mice over 3, 7, & 12 months, using IHC.

IHC showing H_3R labelling in the cortex of TASTPM mice timeline at 3, 7 & 12 months:

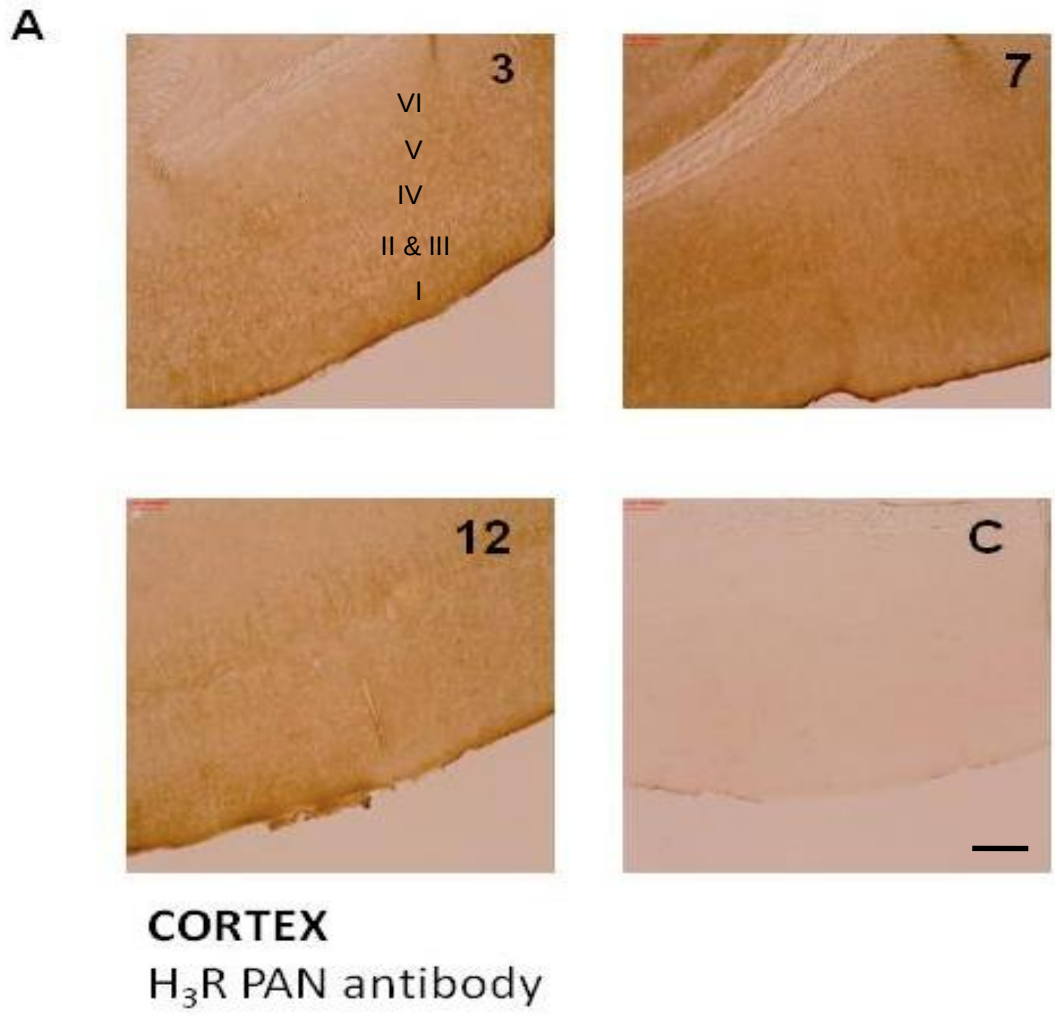

Figure 3.15 (A) Immunohistochemistry of TASTPM mice cortex at three age points 3, 7 and 12 months probed with anti-H_3R PAN antibody. C represents control experiment incubated without either the primary antibody or secondary antibody. H_3R immunoreactivity was detected in layers I-VI of the cortex. Scale bar = 200 µm and represents all images shown. Immunostaining of mouse 20 µm brain slice (X20). All immunohistochemistry data shown are representative images from at least 3 repeats for each time point.

IHC showing H_3R labelling in the CA1 of TASTPM mice timeline at 3, 7 & 12 months:

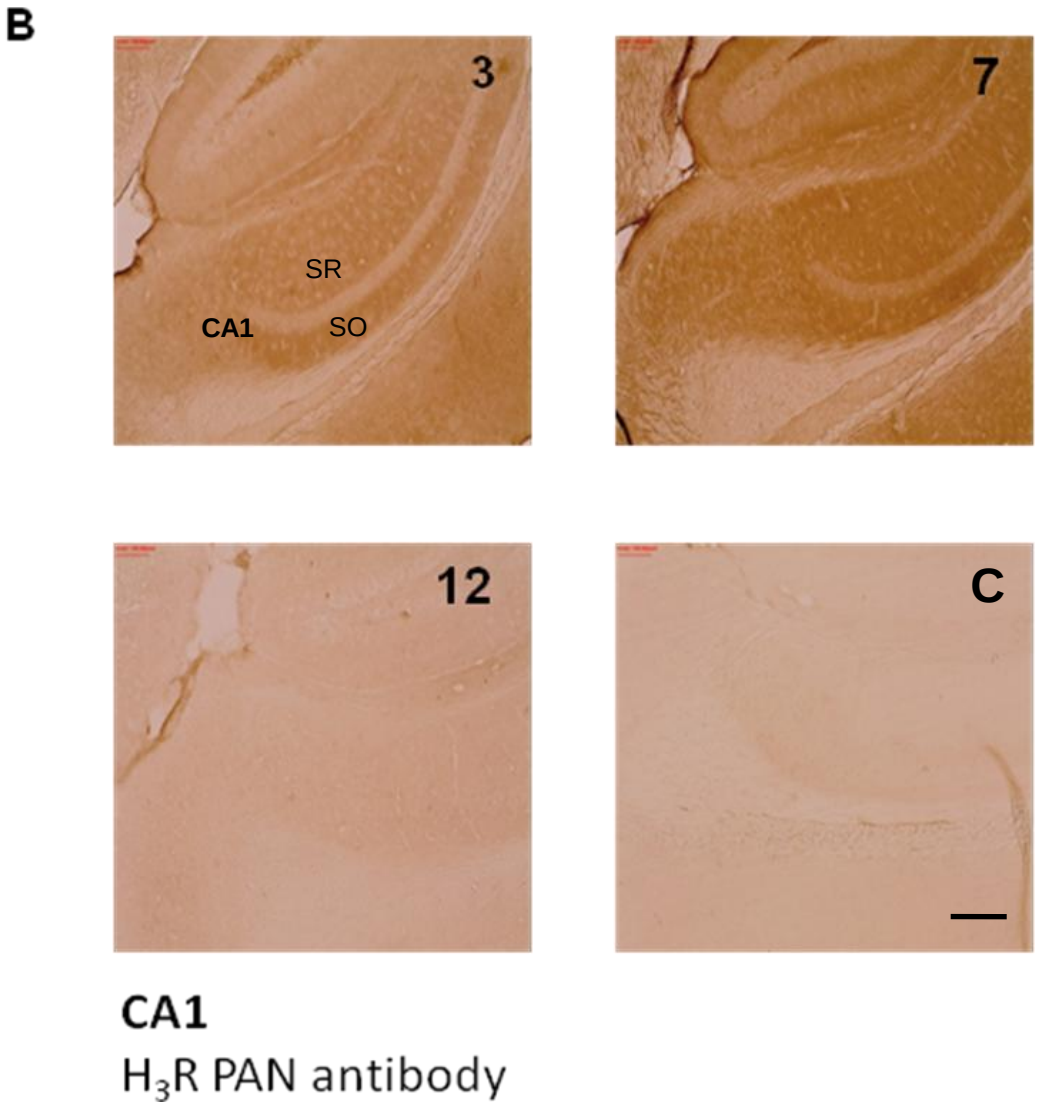

Figure 3.15 (B) Immunohistochemistry of TASTPM mice CA1 at three age points 3, 7 and 12 months probed with anti-H_3R PAN antibody. C represents control experiment incubated without either the primary antibody or secondary antibody. H_3R immunoreactivity was intense on the dendrites in the stratum radiatum (SR) and stratum oriens (SO). Scale bar = 200 µm and represents all images shown. Immunostaining of mouse 20 µm brain slice (X20). All immunohistochemistry data shown are representative images from at least 3 repeats for each time point.

IHC showing H_3R labelling in the CA2/3 of TASTPM mice timeline at 3, 7 & 12 months:

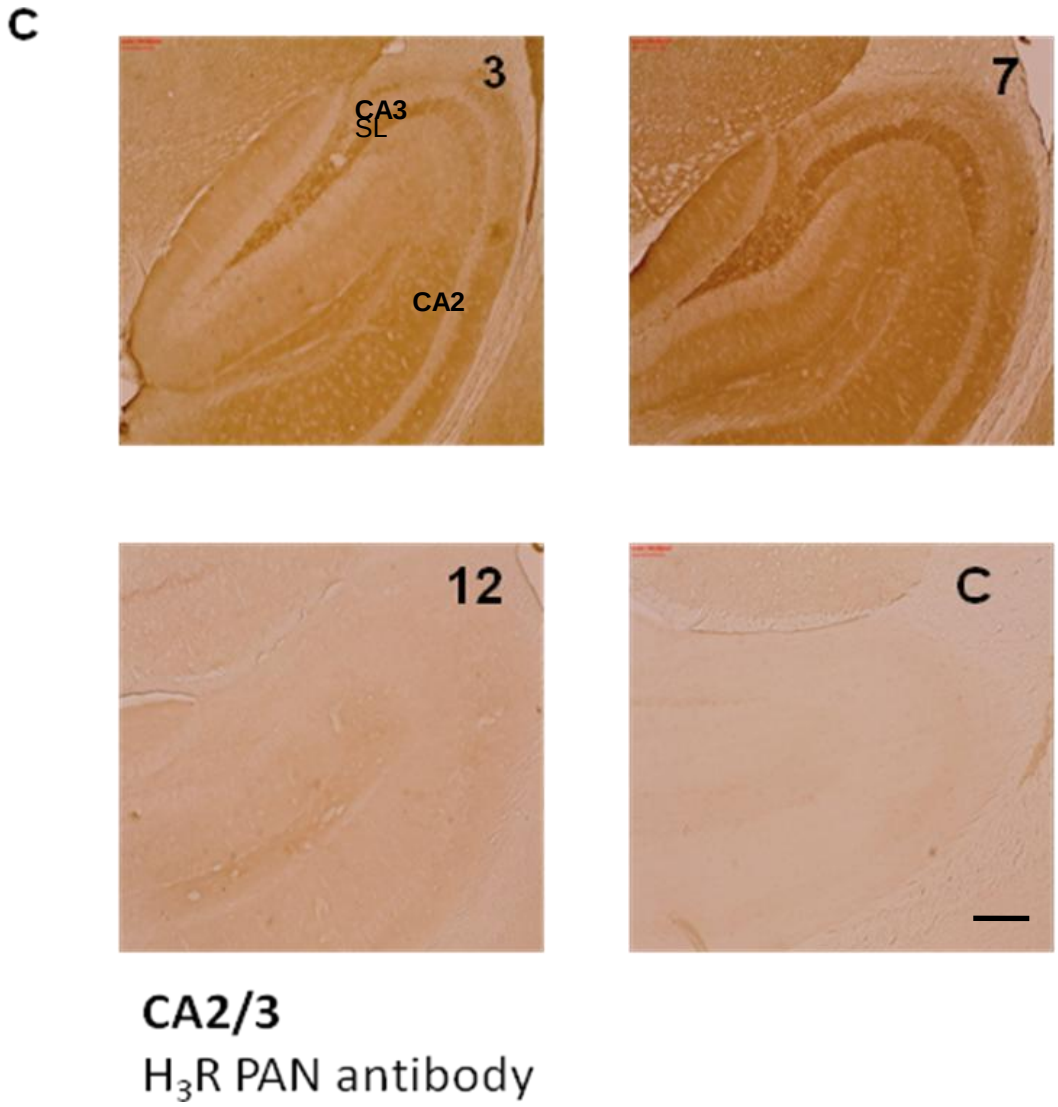

Figure 3.15 (C) Immunohistochemistry of TASTPM mice CA2/ CA3 at three age points 3, 7 and 12 months probed with anti-H_3R PAN antibody. C represents control experiment incubated without either the primary antibody or secondary antibody. H_3R immunoreactivity was intense on the dendrites in the stratum lucidum (SL). Scale bar = 200 µm and represents all images shown. Immunostaining of mouse 20 µm brain slice (X20). All immunohistochemistry data shown are representative images from at least 3 repeats for each time point.

IHC showing H_3R labelling in the dentate gyrus of TASTPM mice timeline at 3, 7 & 12 months;

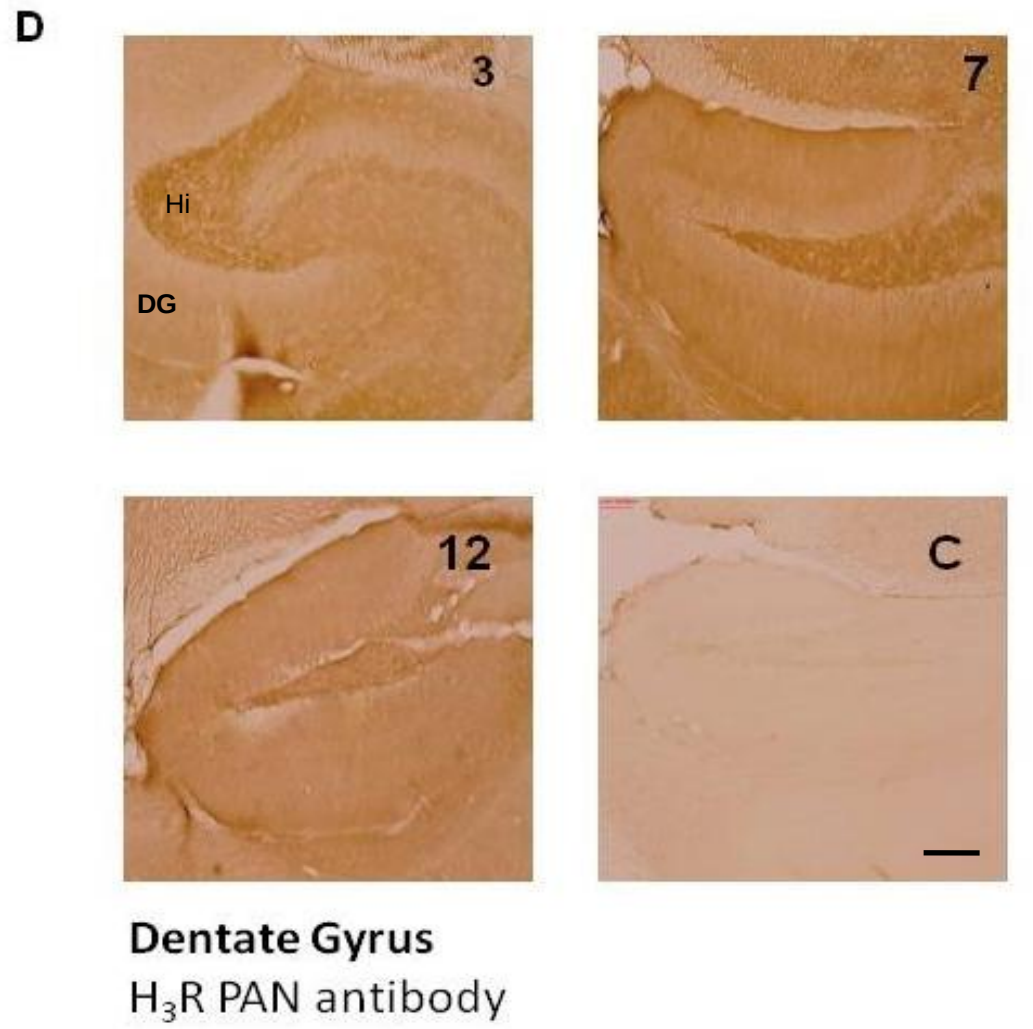

Figure 3.15 (D) Immunohistochemistry of TASTPM mice dentate gyrus at three age points 3, 7 and 12 months probed with anti-H_3R PAN antibody. C represents control experiment incubated without either the primary antibody or secondary antibody. DG represents dentate gyrus. H_3R immunoreactivity was intense in the hilus region (Hi) of the dentate gyrus. Scale bar = 200 µm and represents all images shown. Immunostaining of mouse 20 µm brain slice (X20). All immunohistochemistry data shown are representative images from at least 3 repeats for each time point.

IHC showing H_3R labelling in the cerebellum of TASTPM mice timeline at 3, 7 & 12 months;

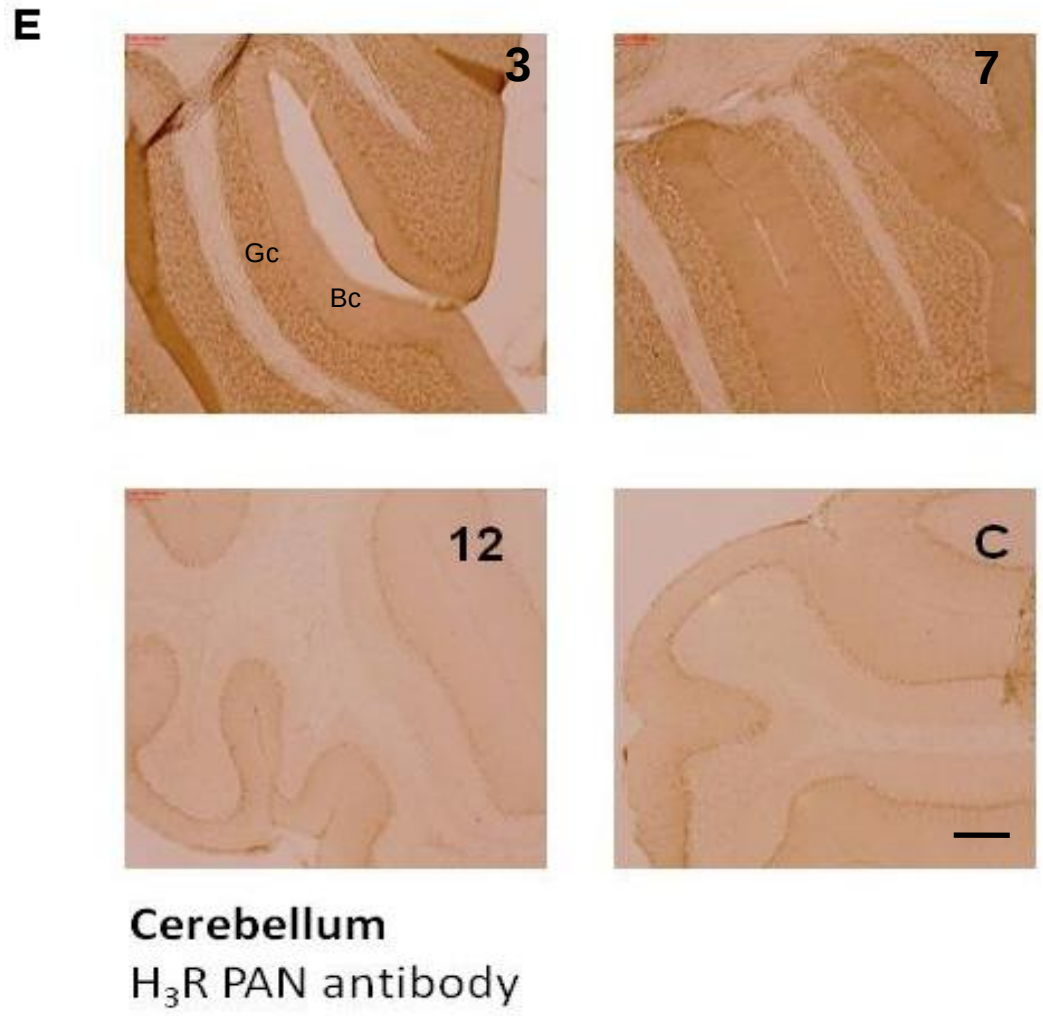

Figure 3.15 (E) Immunohistochemistry of TASTPM mice cerebellum at three age points 3, 7 and 12 months probed with anti-H_3R PAN antibody. C represents control experiment incubated without either the primary antibody or secondary antibody. H_3R immunoreactivity was associated with the cerebellar granule cells (Gc) and basket cells (Bc) of the cerebellum. Scale bar = 200 µm and represents all images shown. Immunostaining of mouse 20µm sagittal brain slice (X20). All immunohistochemistry data shown are representative images from at least 3 repeats for each time point.

IHC data would suggest that immunostaining detected using the anti-pan H_3R antibody is preserved between 3-12 months in the cortex, CA1, 2 & 3, dentate gyrus and cerebellum of CD-1 brain. However, at 7 months there was an apparent increase in immunostaining in all areas of the TASTPM brain.

The anti-pan H_3R antibody was used to confirm the preservation of the H_3R as a general population in both CD-1 (up to 10 months) and TASTPM mice brain (up to 7 months). Now the anti-rH_{3AC}/ $hH_3R_{445/453}$ antibody will be used to determine whether two of the mouse isoforms the $H_3R_{A/\ 445}$ and $H_3R_{C/\ 397}$ are preserved in aging and age-related dementias.

Immunoblot showing CD-1 mouse timeline labelled using the anti-rH_{3AC}/ $hH_3R_{445/453}$ antibody:

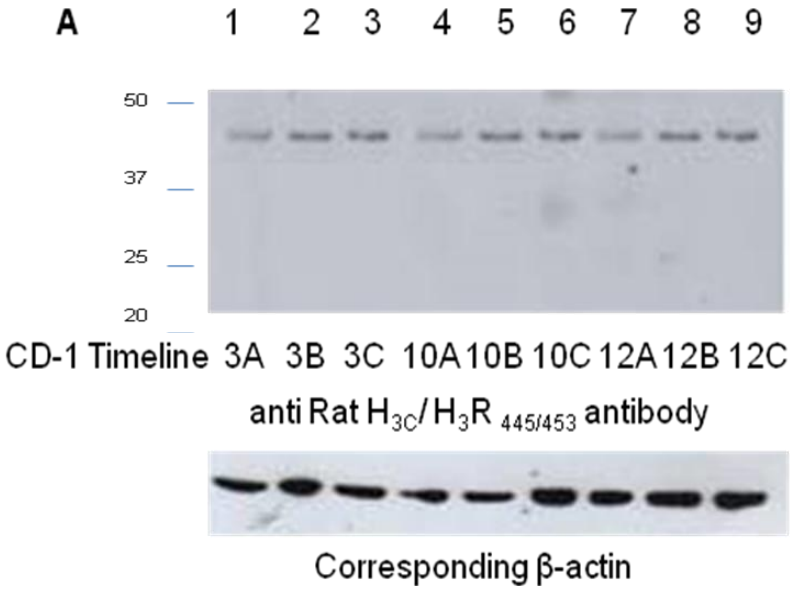

Figure 3.16 (A) Immunoblot of CD-1 mice at three age points 3, 10 and 12 months probed with anti-rH_{3AC}/ $hH_3R_{445/453}$ antibody. Immunoreactive bands detected with the anti-rH_{3AC}/ $hH_3R_{445/453}$ antibody were normalized to β-actin.
Approximately 50 µg of protein/ well were loaded onto a 7.5% PAGE gel. Once transferred the membrane was probed with affinity purified anti-rH_{3AC}/ $hH_3R_{445/453}$ antibody (1 µg/ml concentration). The antibody detects a single band in mouse brain migrating at approximately M_r 45 kDa. Lower panel shows the corresponding β-actin, probed with monoclonal mouse anti β-actin antibody (1:5000).
Lane 1, 2, 3, CD-1 mouse forebrain from 3 separate mice at 3 months.
Lane 4, 5, 6, CD-1 mouse forebrain from 3 separate mice at 10 months.
Lane 7, 8, 9, CD-1 mouse forebrain from 3 separate mice at 12 months.
All blots shown are representative blots from at least 5 similar experiments.

The single band detected represents the full length mouse H_3R_A monomer migrating at approximately 45kDa.

3.4.2.3 Mean immunoreactive intensity of the single band detected using the anti-rH_{3AC}/ h$H_3R_{445/453}$ antibody in CD-1 timeline

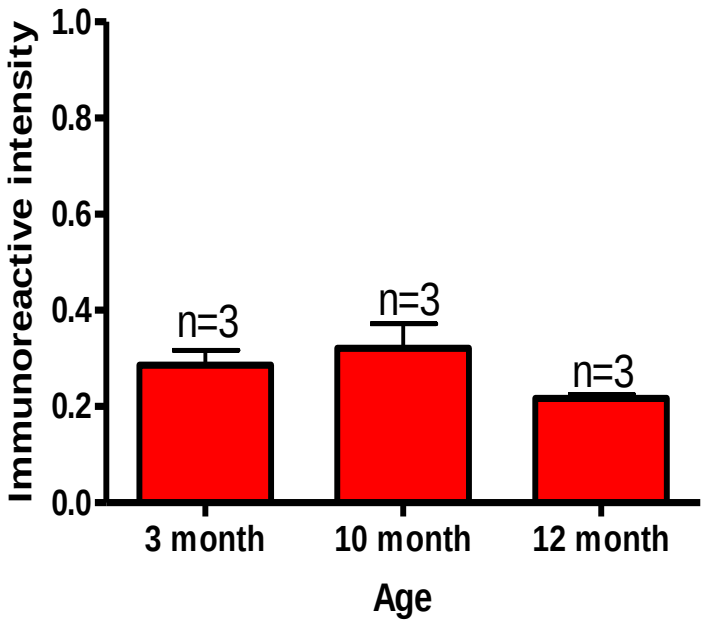

Figure 3.17 Comparing the immunoreactivity of CD-1 mice at three age points 3, 10 and 12 months probed with anti-rH_{3AC}/ h$H_3R_{445/453}$ antibody. Immunoreactive bands detected with the anti-H_3R antibodies were normalized to β-actin. Data show the mean immunoreactive intensity ± SEM for n determinations. Statistical significance was determined from the generated p value, where $p \leq 0.05$ was considered to show significance.

Figure 3.17 shows there were no significant differences in the immunoreactive banding detected with the anti-rH_{3AC}/ h$H_3R_{445/453}$ antibody over the 3 age time points, (3 - 12 months). A similar result was obtained with the IHC, shown below.

The anti-rH_{3AC}/ h$H_3R_{445/453}$ antibody was then used to determine whether the mouse H_3R_{445} isoform was preserved in the brain of CD-1 mouse over 3, 10, 12 & 19 months.

IHC showing H_3R labelling in the cortex of CD-1 mice timeline at 3, 10, 12 & 19 months:

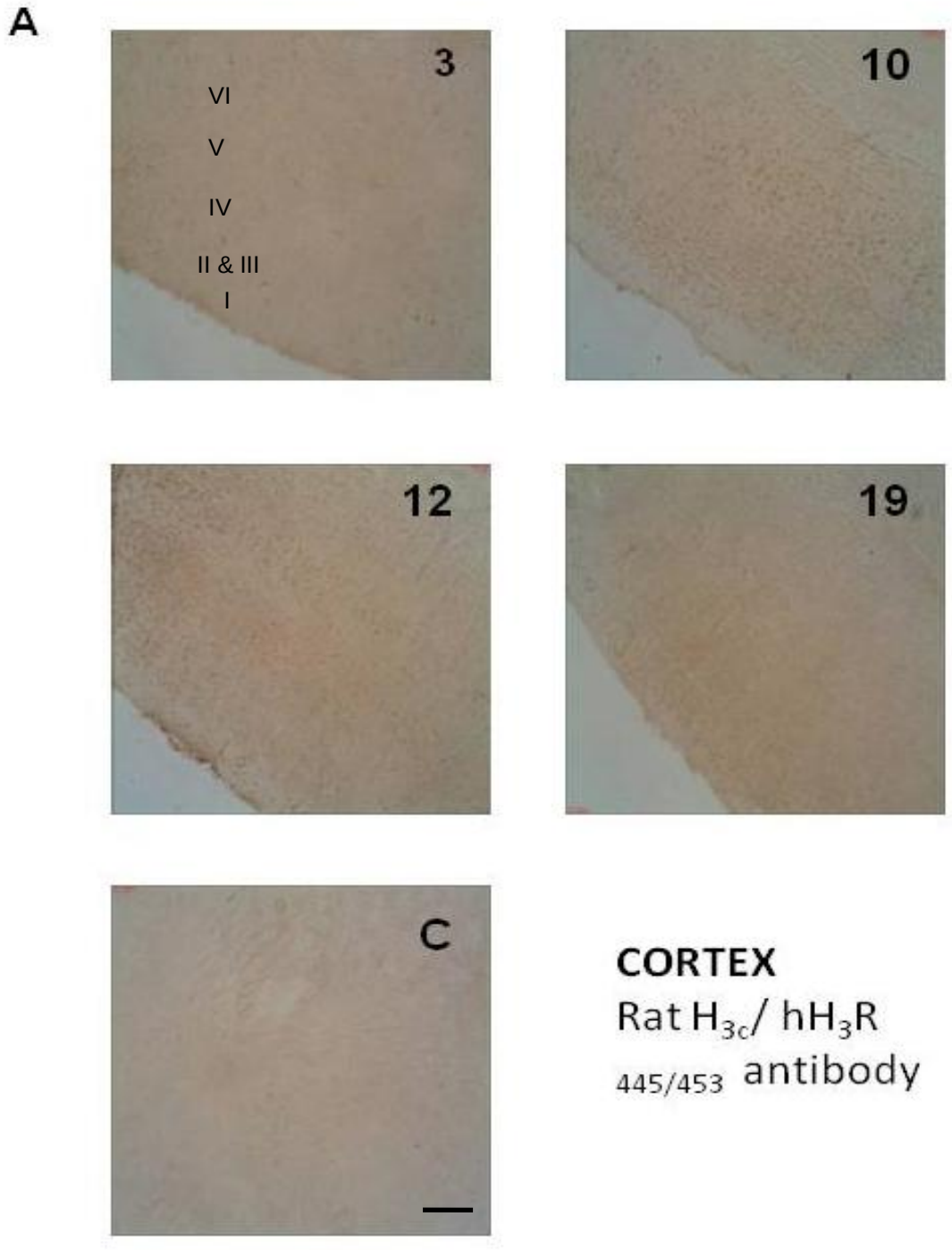

Figure 3.18 (A) Immunohistochemistry of CD-1 mice cortex at four age points 3, 10, 12 and 19 months probed with anti-rH_{3AC}/ $hH_3R_{445/453}$ antibody. C represents control experiment incubated without either the primary antibody or secondary antibody. H_3R immunoreactivity was detected in layers I-VI of the cortex. Scale bar = 200 µm and represents all images shown. Immunostaining of mouse 20 µm brain slice (X20). All immunohistochemistry data shown are representative images from at least 3 repeats for each time point.

IHC showing H_3R labelling in the CA1 of CD-1 mice timeline at 3, 10, 12 & 19 months:

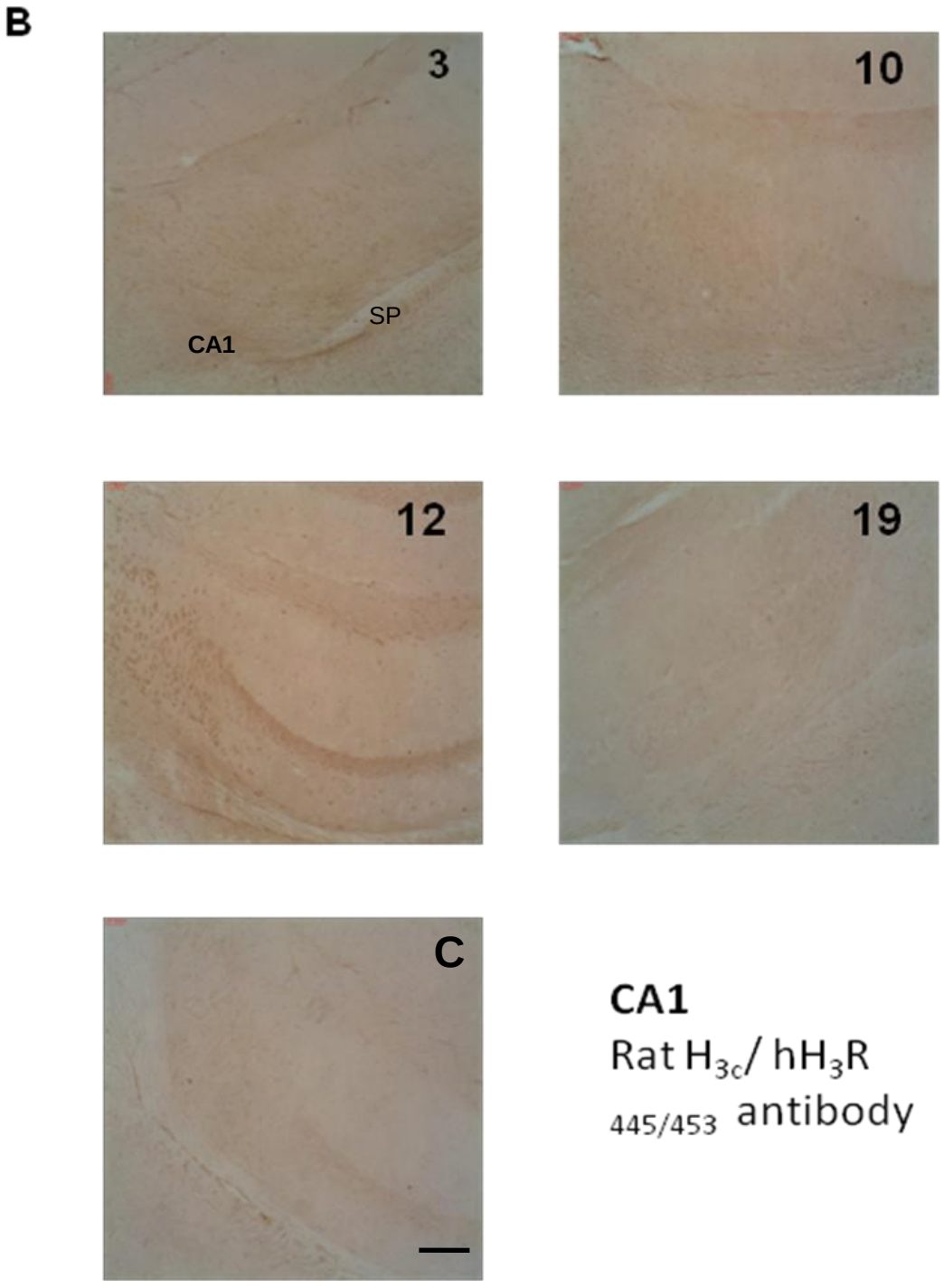

Figure 3.18 (B) Immunohistochemistry of CD-1 mice CA1 at four age points 3, 10, 12 and 19 months probed with anti-rH_{3AC}/ $hH_3R_{445/453}$ antibody. C represents control experiment incubated without either the primary antibody or secondary antibody. H_3R immunoreactivity was present in the cell somata of the stratum pyramidale (SP). H_3R immunoreactivity was intense on the dendrites in the stratum radiatum (SR) and stratum oriens (SO). Scale bar = 200 µm and represents all images shown. Immunostaining of mouse 20 µm brain slice (X20).

All immunohistochemistry data shown are representative images from at least 3 repeats for each time point.

IHC showing H_3R labelling in the CA2/3 of CD-1 mice timeline at 3, 10, 12 & 19 months:

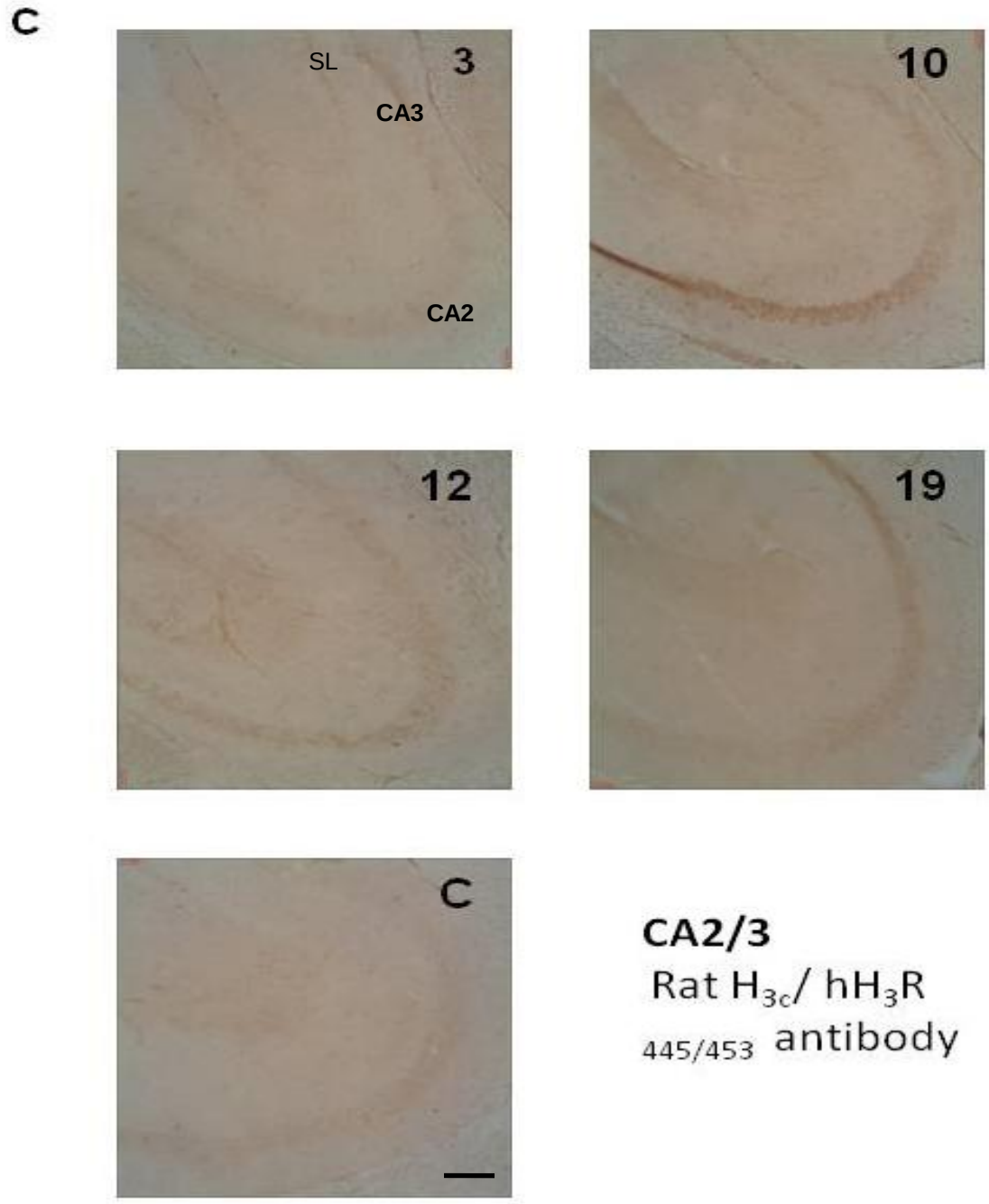

Figure 3.18 (C) Immunohistochemistry of CD-1 mice CA2/ CA3 at four age points 3, 10, 12 and 19 months probed with anti-rH_{3AC}/ $hH_3R_{445/453}$ antibody. C represents control experiment incubated without either the primary antibody or secondary antibody. H_3R immunoreactivity was intense on the dendrites in the stratum lucidum (SL). Immunostaining of mouse 20 µm

brain slice (X20). Scale bar = 200 µm and represents all images shown. All immunohistochemistry data shown are representative images from at least 3 repeats for each time point.

IHC showing H_3R labelling in the dentate gyrus of CD-1 mice timeline at 3, 10, 12 & 19 months:

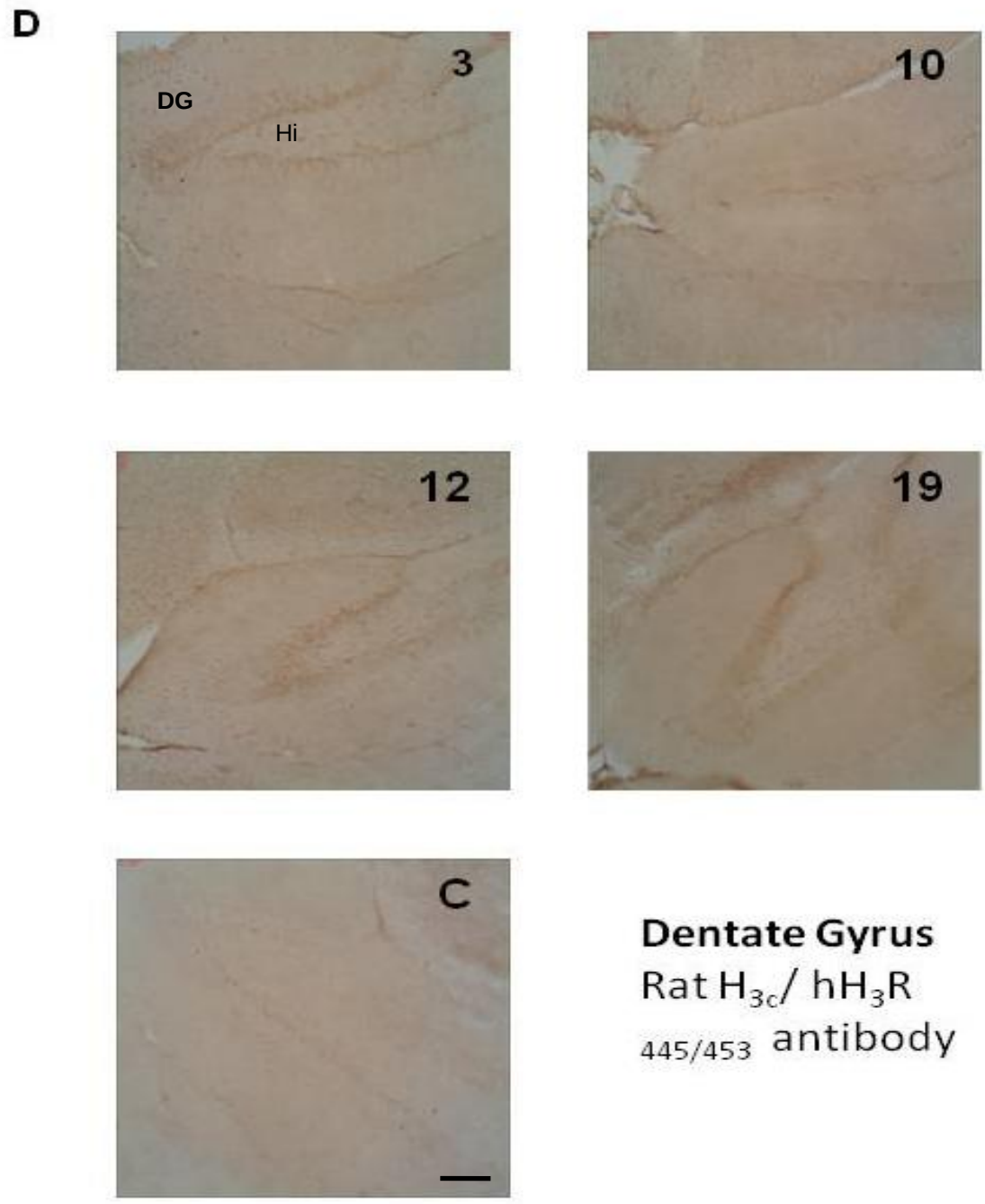

Figure 3.18 (D) Immunohistochemistry of CD-1 mice dentate gyrus at four age points 3, 10, 12 and 19 months probed with anti-rH_{3AC} /$hH_3R_{445/453}$ antibody. C represents control experiment incubated without either the primary antibody or secondary antibody. DG represents dentate gyrus. H_3R immunoreactivity was intense in the hilus region (Hi) of the

dentate gyrus. Immunostaining of mouse 20 µm sagittal brain slice (X20). Scale bar = 200 µm and represents all images shown. All immunohistochemistry data shown are representative images from at least 3 repeats for each time point.
.

IHC showing H_3R labelling in the cerebellum of CD-1 mice timeline at 3, 10, 12 & 19 months:

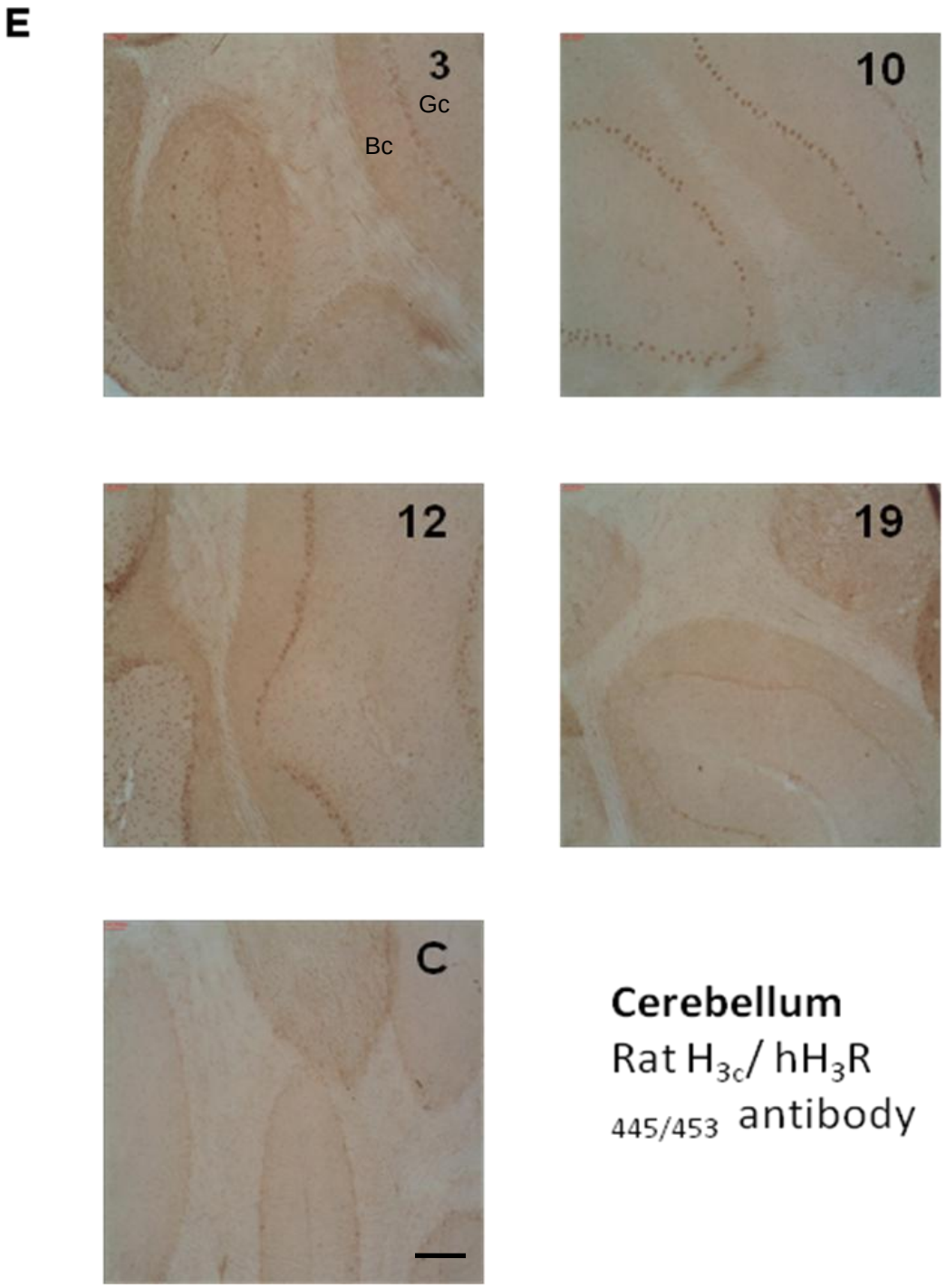

Figure 3.18 (E) Immunohistochemistry of CD-1 mice cerebellum at four age points 3, 10, 12 and 19 months probed with anti-rH_{3AC}/ $hH_3R_{445/453}$ antibody. C represents control experiment incubated without either the primary antibody or secondary antibody. H_3R immunoreactivity was associated with the cerebellar granule cells (Gc) and basket cells (Bc) of the cerebellum. Immunostaining of mouse 20 µm brain slice (X20). Scale bar = 200 µm and represents all images shown. All immunohistochemistry data shown are representative images from at least 3 repeats for each time point

IHC data would suggest that immunostaining detected using the anti-rH_{3AC}/ $hH_3R_{445/453}$ antibody is preserved between 3-19 months in the cortex, CA1, 2 & 3, dentate gyrus and cerebellum of CD-1 brain.

The anti-rH_{3AC}/ $hH_3R_{445/453}$ antibody was then used to determine whether the H_3R was preserved in dementia related diseases, in TASTPM mice, a model of AD.

Immunoblot showing TASTPM mouse timeline labelled using the anti-rH_{3AC}/ $hH_3R_{445/453}$ antibody:

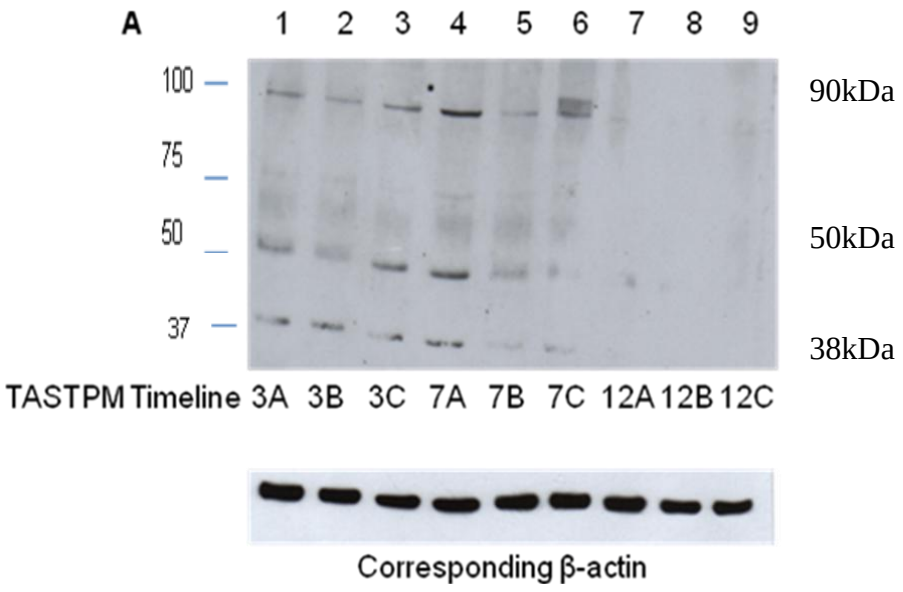

Figure 3.19 (A) Immunoblot of TASTPM mice at three age points 3, 7 and 12 months probed with anti-rH_{3AC}/ $hH_3R_{445/453}$ antibody. Immunoreactive bands detected with the anti-H_3R antibodies were normalized to β-actin.
Approximately 50µg of protein/ well were loaded onto a 7.5% separating gel. Once transferred the membrane was probed with affinity purified anti-rH_{3AC}/ $hH_3R_{445/453}$ antibody (1 µg/ml concentration). The antibody detects three major species in mouse brain, M_r 38,000, 45,000, 90,000 respectively. Lower panel shows the corresponding β-actin, probed with monoclonal mouse anti β-actin antibody (1:5000).

Lane 1, 2, 3, TASTPM mouse forebrain from 3 separate mice at 3 months.
Lane 4, 5, 6, TASTPM mouse forebrain from 3 separate mice at 7 months.
Lane 7, 8, 9, TASTPM mouse forebrain from 3 separate mice at 12 months.

The three immunoreactive bands detected in TASTPM mouse brain using the anti-rH_{3AC}/ h$H_3R_{445/453}$ antibody are likely to represents the full length H_3R migrating at approximately 50kDa and a dimeric version of the full length migrating at 90kDa. The smallest fragment migrating at approximately at 38kDa is likely to represent the mH_3R_{397} isoform.

3.4.2.4 Mean immunoreactive intensity of each of the molecular weight species detected using the anti-rH_{3AC}/ h$H_3R_{445/453}$ antibody in TASTPM timeline

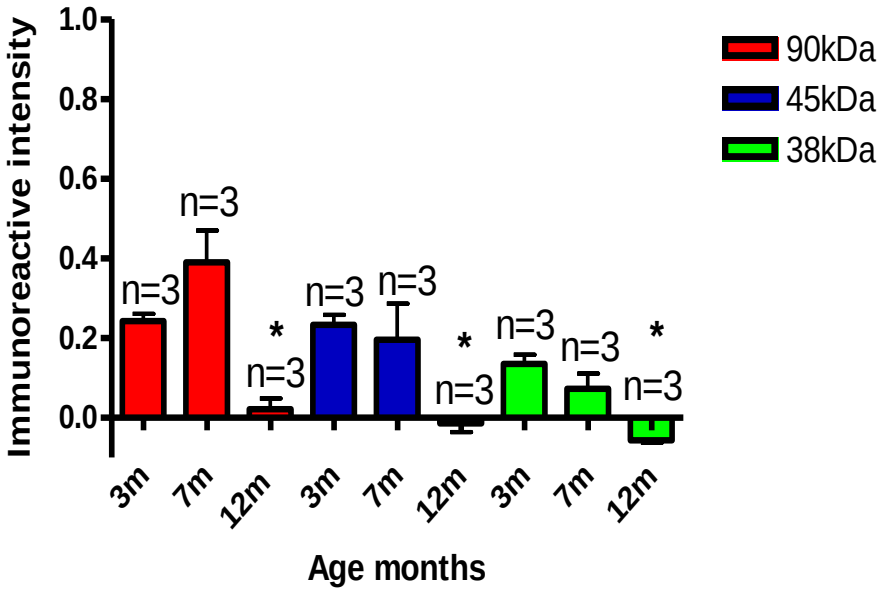

Figure 3.20 Comparing the immunoreactivity of TASTPM mice at three age points 3, 7 and 12 months probed with anti-H_{3C}/ anti-h$H_3R_{445/453}$ antibody. Immunoreactive bands detected with the anti-H_3R antibodies were normalized to β-actin. Data show the mean immunoreactive intensity ± SEM for n = 3 determinations. Statistical significance was determined from the generated p value, where $p \leq 0.05$ was considered to show significance.

Figure 3.20 shows there were significant differences in the immunoreactive banding detected with the anti-rH_{3AC}/ h$H_3R_{445/453}$ antibody between the 3 age time points. Bands migrating at 90kDa and 45kDa had significantly lower immunoreactivity in the 12 month TASTPM mice compared with the 3 ($p<0.05$ and $p<0.05$) and 7 months ($p<0.001$ and $P<0.05$), respectively, suggesting that at 12 months there is a decrease in the full length H_3R expression in the CNS of TASTPM mice.

The anti-rH_{3AC}/ h$H_3R_{445/453}$ antibody was then used to determine whether the H_3R_{445} isoform was preserved in the brain of TASTPM mouse over 3, 7, & 12 months.

IHC showing H_3R labelling in the cortex of TASTPM mice timeline at 3, 7 & 12 months:

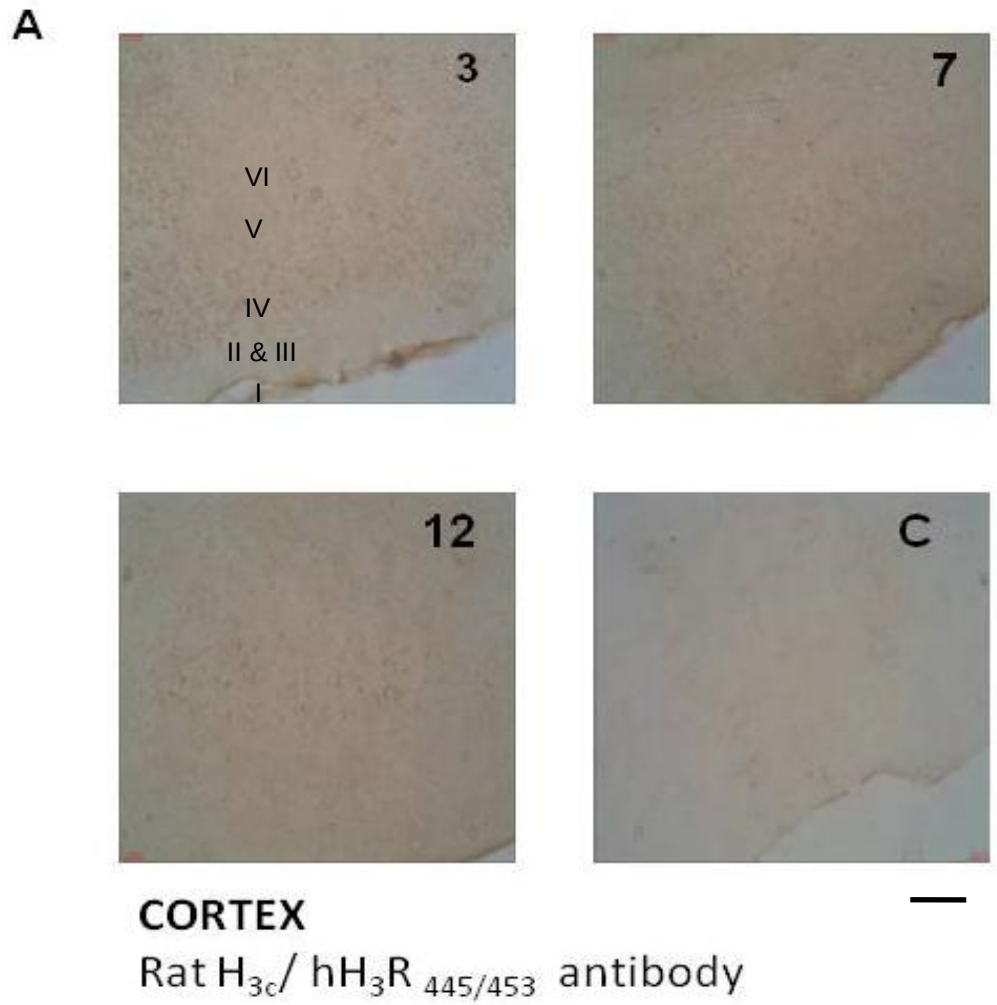

Figure 3.21 (A) Immunohistochemistry of TASTPM mice cortex at three age points 3, 7 and 12 months probed with anti-rH_{3AC}/ $hH_3R_{445/453}$ antibody. C represents control experiment incubated without either the primary antibody or secondary antibody. H_3R immunoreactivity was detected in layers I-VI of the cortex. Scale bar = 200 µm and represents all images shown. Immunostaining of mouse 20 µm brain slice (X20). All immunohistochemistry data shown are representative images from at least 3 repeats for each time point.

IHC showing H_3R labelling in the CA1 of TASTPM mice timeline at 3, 7 & 12 months:

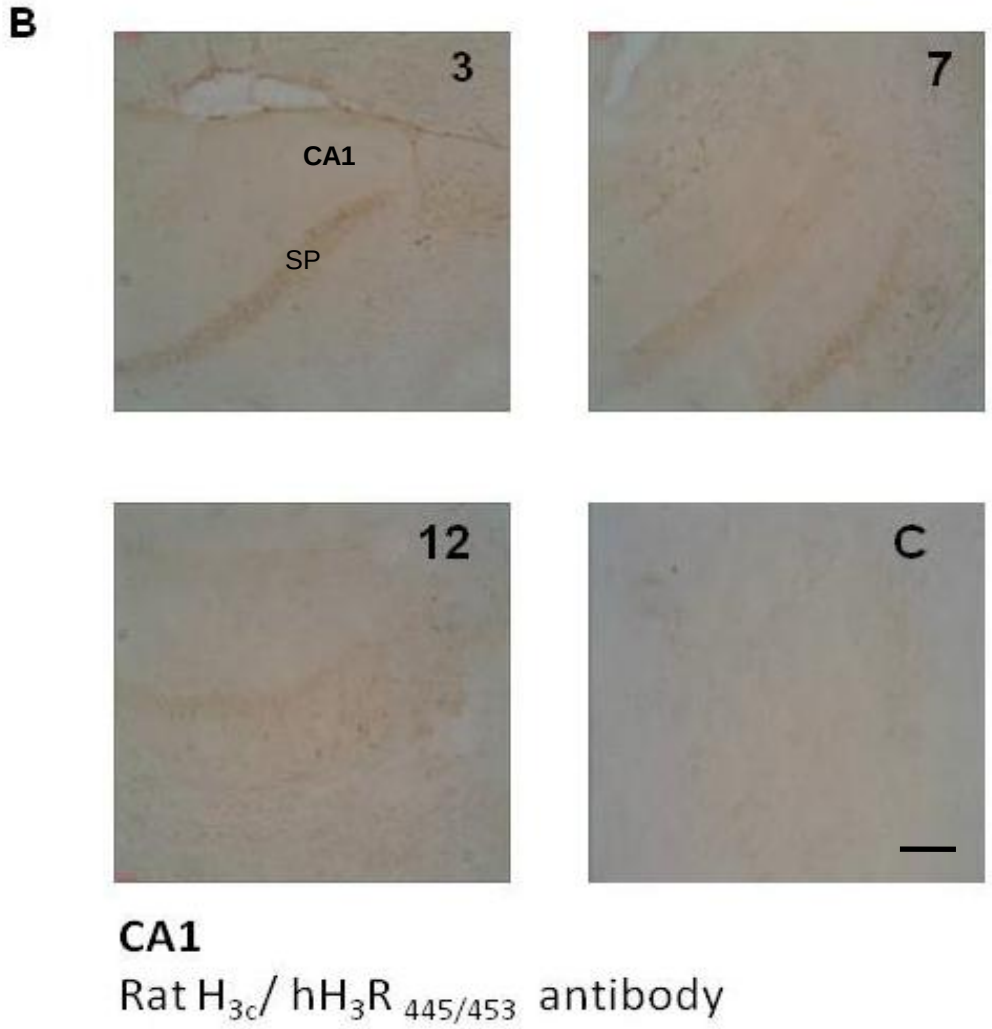

Figure 3.21 (B) Immunohistochemistry of TASTPM mice CA1 at three age points 3, 7 and 12 months probed with anti-rH_{3AC} / $hH_3R_{445/453}$ antibody. C represents control experiment incubated without either the primary antibody or secondary antibody. H_3R immunoreactivity was present in the cell somata of the stratum pyramidale (SP). Immunostaining of mouse 20 µm brain slice (X20). Scale bar = 200 µm and represents all images shown. All immunohistochemistry data shown are representative images from at least 3 repeats for each time point.

IHC showing H_3R labelling in the CA2/3 of TASTPM mice timeline at 3, 7 & 12 months:

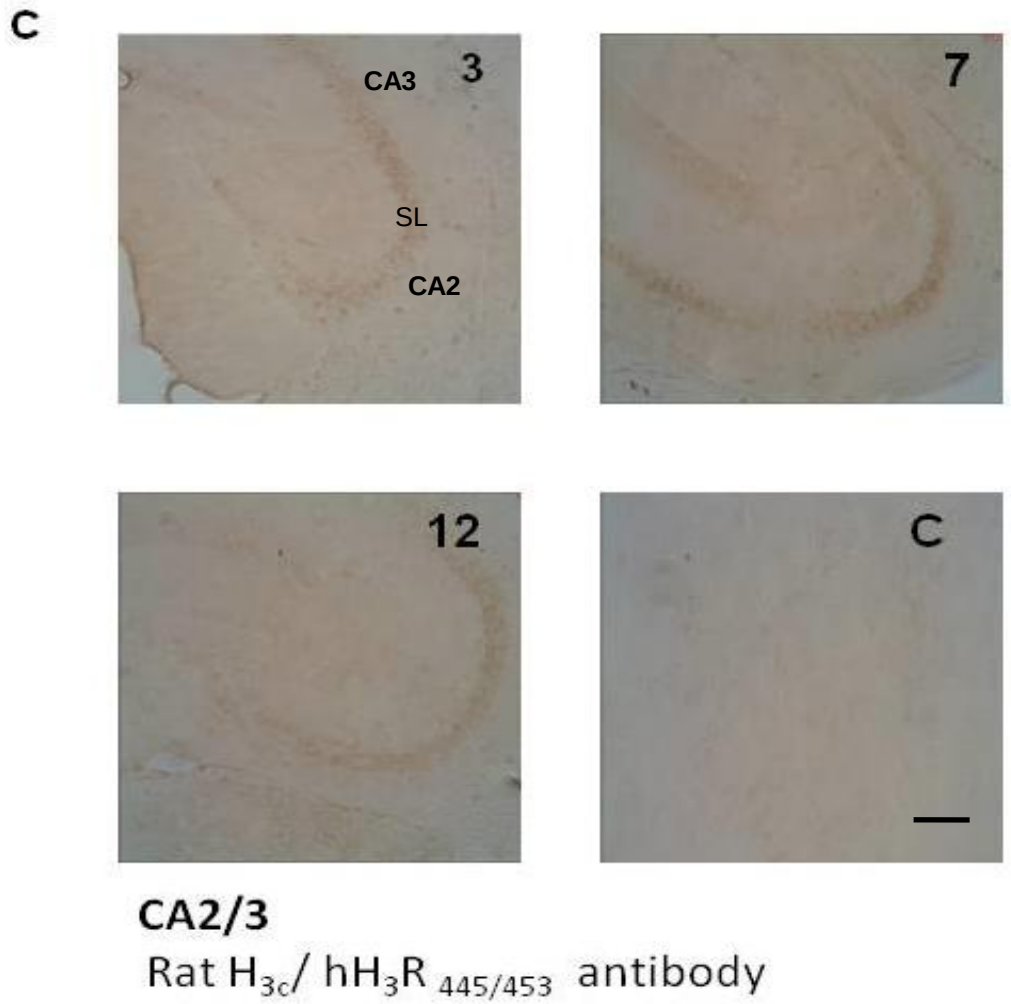

Figure 3.21 (C) Immunohistochemistry of TASTPM mice CA2/CA3 at three age points 3, 7 and 12 months probed with anti-rH_{3AC} / $hH_3R_{445/453}$ antibody. C represents control experiment incubated without either the primary antibody or secondary antibody. H_3R immunoreactivity was intense on the dendrites in the stratum lucidum (SL). Immunostaining of mouse 20 µm brain slice (X20). Scale bar = 200 µm and represents all images shown. All immunohistochemistry data shown are representative images from at least 3 repeats for each time point.

IHC showing H_3R labelling in the dentate gyrus of TASTPM mice timeline at 3, 7 & 12 months:

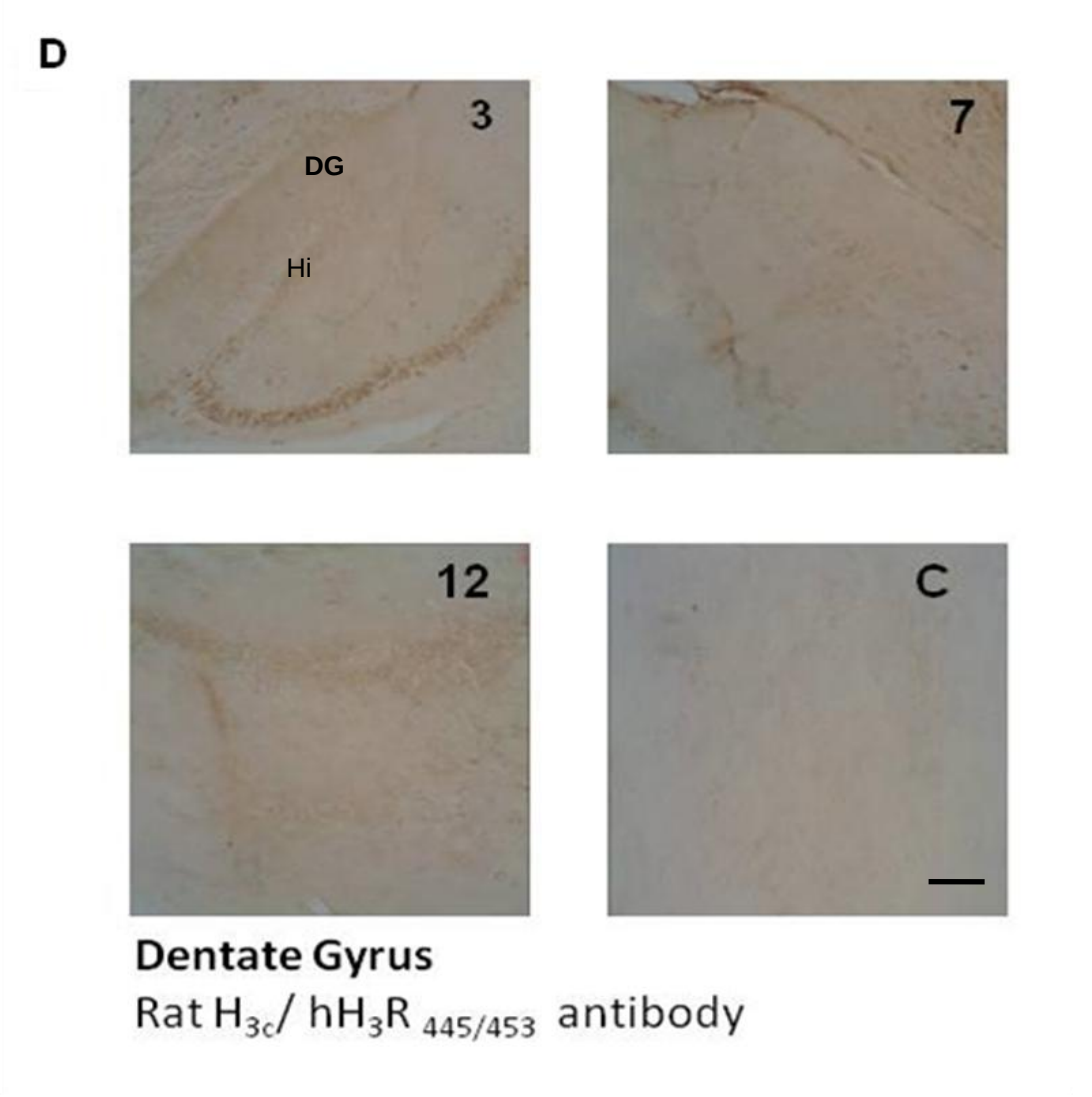

Figure 3.21 (D) Immunohistochemistry of TASTPM mice dentate gyrus at three age points 3, 7 and 12 months probed with anti-rH_{3AC} / $hH_3R_{445/453}$ antibody. C represents control experiment incubated without either the primary antibody or secondary antibody. DG represents dentate gyrus. H_3R immunoreactivity was intense in the hilus region (Hi) of the dentate gyrus. Immunostaining of mouse 20 µm brain slice (X20). Scale bar = 200 µm and represents all images shown. All immunohistochemistry data shown are representative images from at least 3 repeats for each n number.

IHC showing H_3R labelling in the cerebellum of TASTPM mice timeline at 3, 7 & 12 months:

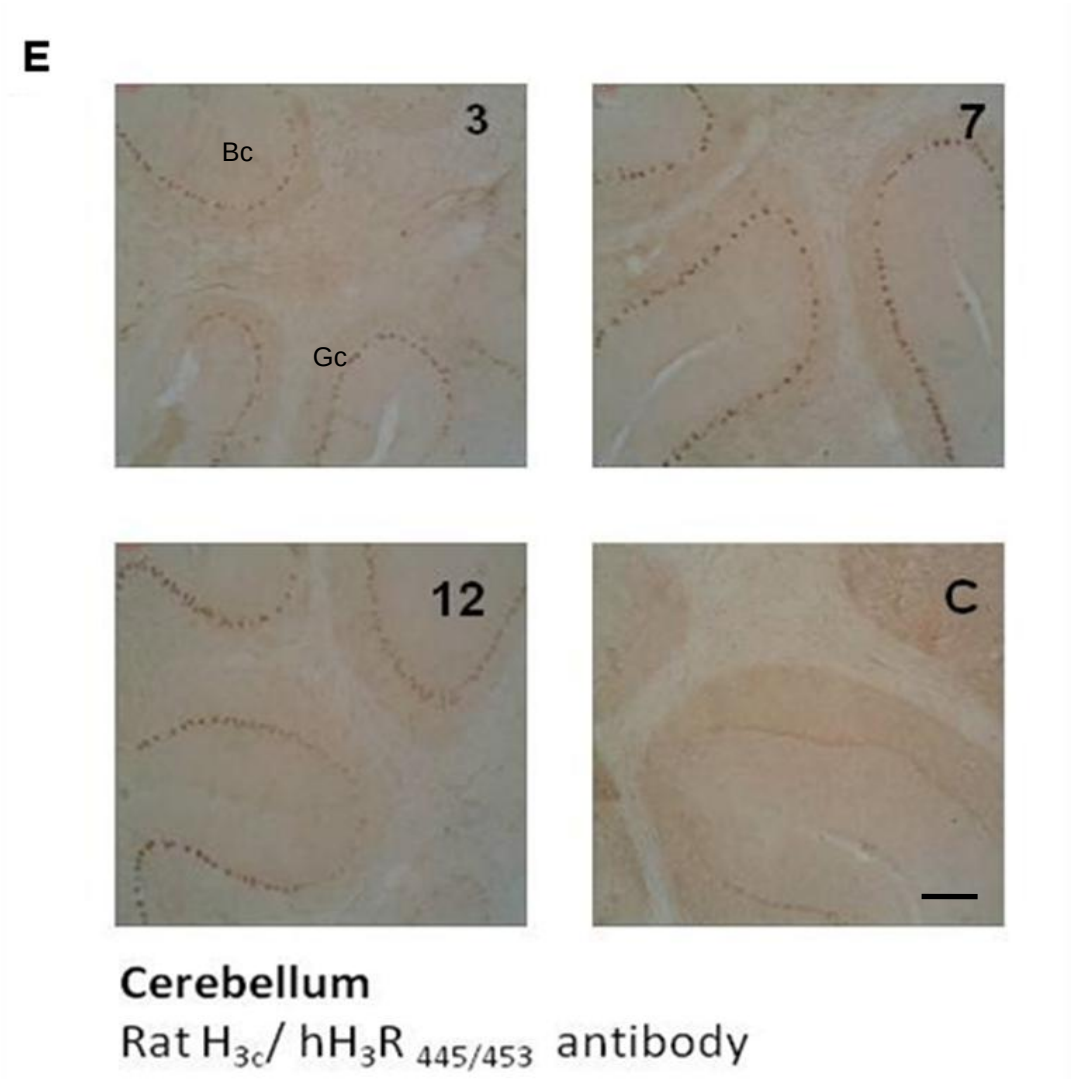

Figure 3.21 (E) Immunohistochemistry of TASTPM mice cerebellum at three age points 3, 7 and 12 months probed with anti-rH_{3AC}/ $hH_3R_{445/453}$ antibody. C represents control experiment incubated without either the primary antibody or secondary antibody. H_3R immunoreactivity was associated with the cerebellar granule cells (Gc) and basket cells (Bc) of the cerebellum. Immunostaining of mouse 20 µm brain slice (X20). Scale bar = 200 µm and represents all images shown. All immunohistochemistry data shown are representative images from at least 3 repeats for each time point.

IHC data would suggest that the mouse $H_3R_{A/C}$ isoforms detected using the anti-rH_{3AC}/ $hH_3R_{445/453}$ antibody are preserved between 3 - 12 months in the cortex, CA1, 2 & 3, dentate gyrus and cerebellum of TASTPM brain.

Two rodent specific H_3R antibodies have been used to determine H_3R expression in the CNS and to show that H_3R expression in largely preserved in cortical and striatal regions of the murine CNS. However, there was regional variation in the levels of some of the H_3R isoform.

To date only the rodent H_3R protein expression has been demonstrated using immunological probes. This next section of data will use the human isoform specific immunological probes to show for the first time that human H_3R isoforms are expressed at the protein level in the human CNS.

3.4.3 Immunobiochemical analysis of the anti-hH_3R antibodies in human central nervous disease cases.

The anti-h$H_3R_{365/445}$ and the anti-hH_3R_{329} antibodies were used to determine whether these H_3R isoforms are expressed in the human CNS and whether expression is changed in two Lewy body disease states, Parkinson's Disease (PD) and Dementia with Lewy bodies (DLB) compared with age matched control (C) cases. Brain tissue samples from 9 human brain case samples: 3 x PD, 3 x C and 3 x DLB were used.

Immunoblot showing human putamen labelled using the anti-$hH_3R_{365/445}$ antibody:

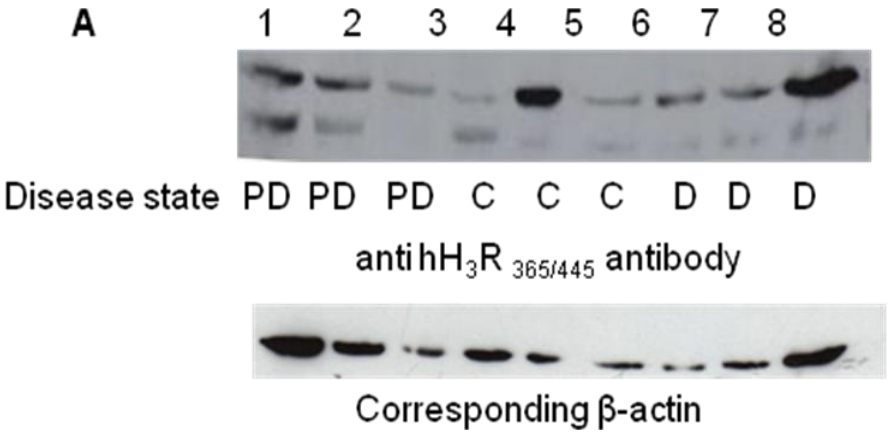

Figure 3.22 (A) Immunoblot of homogenised human brain, comparing two Lewy body disease states Parkinson's Disease (PD) and Dementia with Lewy bodies (D) with control (C) human brain probed with anti-$hH_3R_{365/445}$ antibody. Immunoreactive bands detected with the anti-H_3R antibodies were normalized to β-actin. Approximately 25 µg of protein/ well were loaded onto a 10% separating gel. Once transferred the membrane was probed with affinity purified anti-$hH_3R_{365/445}$ antibody (1 µg/ml concentration). The antibody detects two bands in human brain, M_r 45 (top band) and 38 kDa (bottom band), respectively. Lower panel shows the corresponding β-actin, probed with monoclonal mouse anti β-actin antibody (1:5000).
Lane 1, 2, 3, Human brain putamen, Parkinson's Disease, 3 individual cases
Lane 4, 5, 6, Human brain putamen, control, 3 individual cases
Lane 7, 8, 9, Human brain putamen, Dementia with Lewy bodies, 3 individual cases

3.4.3.1 Mean immunoreactive intensity of each of the protein species detected using the anti-$hH_3R_{365/445}$ antibody in human putamen

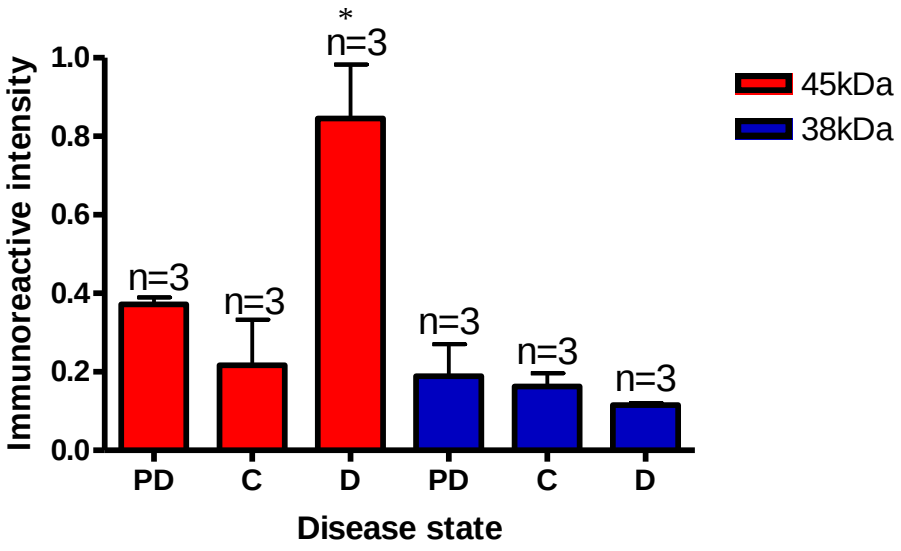

Figure 3.23 Comparing the immunoreactivity of control human brain with two Lewy body disease states Parkinson's Disease (PD) and Dementia with Lewy bodies (D) probed with anti-h$H_3R_{365/445}$ antibody. Immunoreactive bands detected with the anti-H_3R antibodies were normalized to β-actin. Data shows the mean immunoreactive intensity ± SEM for n determinations. Statistical significance was determined from the generated p value, where $p \leq 0.05$ was considered to show significance.

Figure 3.23 shows there were two bands detected, one migrating at 45kDa, representing the putative full length human H_3R_{445} and another at 38kDa, and representing the putative human H_3R_{365} isoform. No significant difference in immunoreactivity was detected for the 38kDa band between the three groups however, the immunoreactivity detected for the 45kDa band was significantly stronger in DLB cases compared to PD and C cases ($p<0.01$ and $p<0.01$), respectively. These preliminary results suggest that full length human H_3R expression maybe up-regulated in DLB.

The next set of data will determine whether the human H_3R_{329} isoform is expressed in the human brain and whether its expression is altered between the different disease states.

Immunoblot showing human putamen labelled using the anti-hH_3R_{329} antibody:

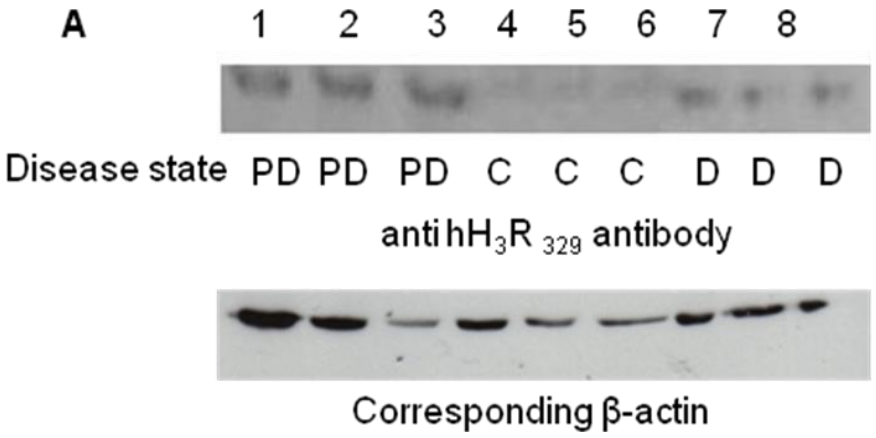

Figure 3.24 (A) Immunoblot of homogenised human brain, comparing two Lewy body disease states Parkinson's Disease (PD) and Dementia with Lewy bodies (D) with control human brain probed with anti-hH_3R_{329} antibody. Immunoreactive bands detected with the anti-H_3R antibodies were normalized to β-actin.
Approximately 25 µg of protein/ well were loaded onto a10% PAGE gel. Once transferred the membrane was probed with affinity purified anti-hH_3R_{329} antibody (3 µg/ml concentration). The antibody detects a single band in human brain, migrating at approximately M_r 30 kDa. Panel below shows the corresponding β-actin, probed with monoclonal mouse anti β-actin antibody (1:5000).
Lane 1, 2, 3, Human brain putamen, Parkinson's Disease, 3 individual cases
Lane 4, 5, 6, Human brain putamen, control, 3 individual cases
Lane 7, 8, 9, Human brain putamen, Dementia with Lewy bodies, 3 individual cases

3.4.3.2 Mean immunoreactive intensity of the single band detected using the anti-hH_3R_{329} antibody in human putamen

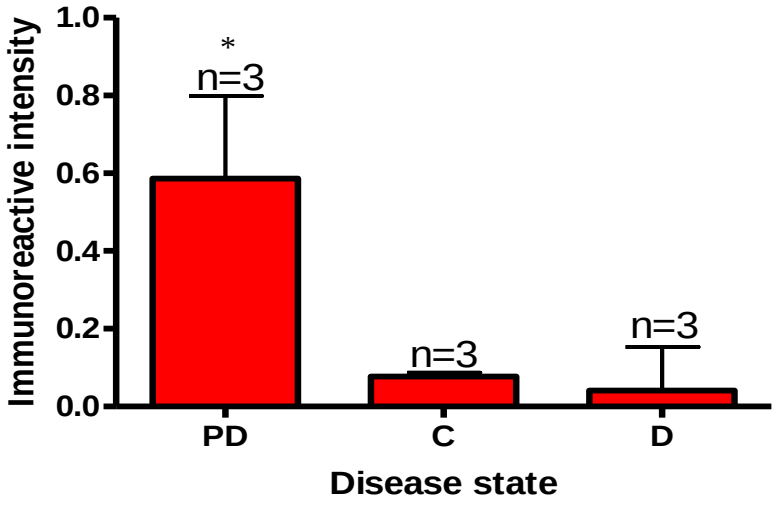

Figure 3.25 Comparing the immunoreactivity of control human brain with two dementia associated disease states Parkinson's Disease (PD) and Dementia with Lewy bodies (D) probed with anti-hH_3R_{329} antibody. Immunoreactive bands detected with the anti-H_3R antibodies were normalized to β-actin. Data shows the mean immunoreactive intensity $\pm$ SEM for n = 3 determinations. Statistical significance was determined from the generated p value, where $p \leq 0.05$ was considered to show significance.

Figure 3.25 shows there was no significant difference in immunoreactive intensity detected with the anti-hH_3R_{329} antibody between the three disease states. However, there does appear to be a profound increase in immunoreactivity in the PD cases versus control and DLB cases. There appears to be little variation in the individual control samples unlike in both

DLB and PD samples. The variation seen for the human H_3R_{329} isoform expression in disease samples maybe down to variation in disease progression and general variation in symptoms experienced by each individual. These preliminary results suggest that the human H_3R_{329} isoform expression maybe up-regulated in PD.

For the first time, the human H_3R 445, 365 and 329 isoforms have been shown to be expressed in the human brain at the protein level. The preliminary results would suggest that there are changes in isoforms expression in the different disease cases compared with age matched controls.

The $hH_3R_{445/365}$ and hH_3R_{329} antibodies were used by a group at Amsterdam Institute of Neuroscience, The Netherlands, to detect expression of the isoforms in human substantia nigra tissue.

Immunohistochemistry showing cell cytoplasm labelling of human substantia nigra tissue labelled using the anti-$hHR_3R_{445/365}$ antibody:

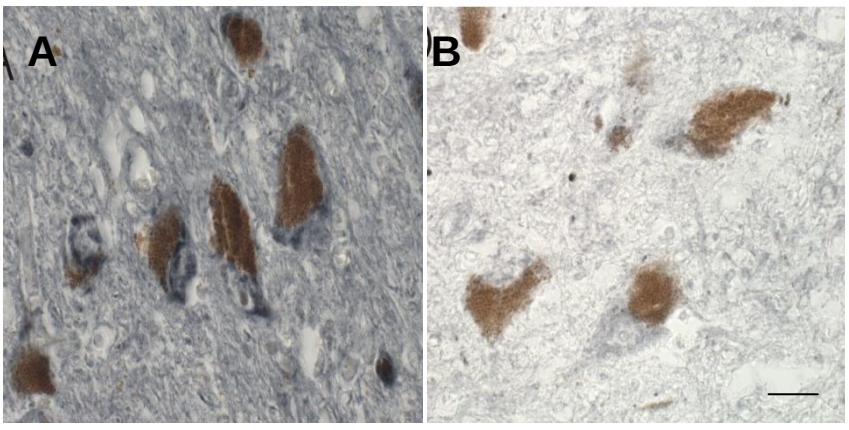

Shan et al., (2010)

Figure 3.26 Immunoreactive staining in human CNS (A) PD substantia nigra and (B) control substantia nigra, probed with anti-h$H_3R_{365/445}$ antibody (1µg/ml concentration). Scale bar = 25 µm and represents all images shown.

Figure 3.26 shows H_3R immunoreactivity in the cell cytoplasm of human substantia nigra cells when probed with anti-h$H_3R_{365/445}$ antibody.

Immunohistochemistry showing cell cytoplasm labelling of human substantia nigra tissue labelled using the anti-hH_3R_{329} antibody:

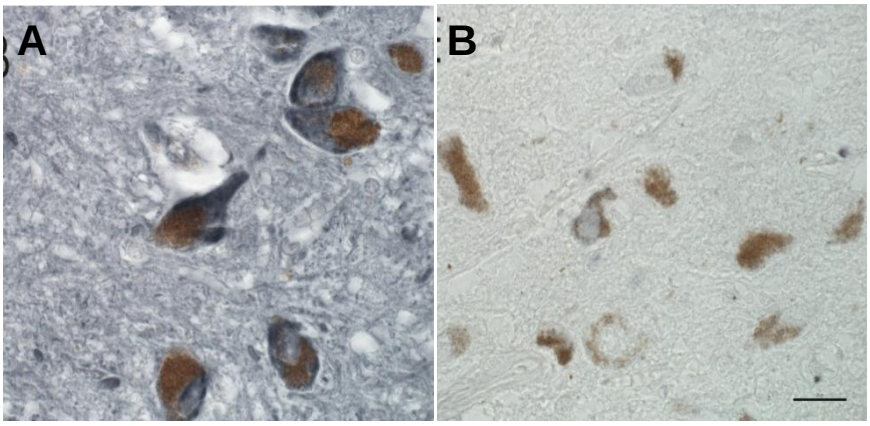

Shan et al., (2010)

Figure 3.27 Immunoreactive staining in human CNS (A) PD substantia nigra and (B) control substantia nigra, probed with anti-hH_3R_{329} antibody (1 µg/ml concentration). Scale bar = 25 µm and represents all images shown.

Figure 3.27 shows H_3R immunoreactivity in the cell cytoplasm of human substantia nigra cells when probed with anti-hH_3R_{329} antibody.

3.5 Discussion

This chapter describes the development and characterization of a selection of novel H_3R probes: anti-H_3R PAN antibody, anti-$rH_{3A/C}$/ anti-$hH_3R_{445/453}$ antibody, anti-$hH_3R_{365/445}$ antibody peptide 1, anti-hH_3R_{365} antibody peptide 2, anti-hH_3R_{329} antibody and anti-hH_3R_{200} antibody. These probes were used to investigate H_3R expression in murine brain samples, and identify expression of three of the human H_3R isoforms 445, 365 and 329 in native tissue, and determine whether there were any changes in H_3R expression in aging and in CNS diseases using murine and human brain samples.

For the anti-H_3R PAN antibody a peptide sequence common to a variety of H_3R isoforms and across the species was chosen, and for all other antibodies a peptide sequence unique to each isoform was chosen and used to immunise a rabbit for the generation of sequence specific antibodies.

3.5.1 Rodent H_3R characterization and expression in aging

The anti-H_3R PAN antibody was screened against human, mouse and rat brain samples and the antibody detected an array of bands with molecular weights ranging from 50 – 100 kDa, likely representing different isoforms/ dimers/ higher molecular weight species known to occur by homo/hetero-oligomerisation for the human H_3R and H_4R (Chazot et al., 2005, van Rijn et al., 2006). The antibody has also been previously used to map the anatomical distribution of the H_3R in mouse brain which displayed a high degree of coincidence with ligand-autoradiographical information (Martinez et al., 1990, Goodchild et al., 1999, Drutel et al., 2001 and Chazot et al., 2001). The

antibody has previously been validated against H_3R -/- tissue (Fiona Shenton PhD Thesis 2007).

In this chapter, the antibody has been used to determine whether H_3R expression is altered in aging and age-dependent dementia in two mice models; CD-1 mice, known to have premature aging, and TASTPM mice, a mouse model of AD. Previously published data in TASTPM mice suggest that H_3R expression is unaltered with age and in disease progression (Medhurst et al., 2009). In this thesis, immunoblotting would suggest that some of the H_3R isoforms would appear to be altered with aging, generally showing a decrease with age in CD-1 mouse timeline, but after 10 months of age. However, the H_3R_{445} isoform was preserved in CD-1 mouse timeline between 3-19 months. H_3R ligands show high affinity for the full length receptor and lower affinity for shorter isoforms (Chapter 4). This may be why Medhurst et al., 2009 found no alterations in H_3R expression in TASTPM mice due to lack of sensitivity of H_3R ligands to detect the various H_3R isoforms. Interestingly, both IB and IHC analysis of the H_3R receptor, expression would appear to be largely unaltered in CD-1 timeline between the ages 3-10 months where cognitive deficits have been shown to occur (Chazot et al., unpublished).

For the TASTPM mouse timeline, immunoblotting and IHC data showed generally more intense immunoreactivity at 7 months compared with 3 and 12 months. H_3R expression was increased at 7 months but by 12 months the level of expression is similar to that seen in 3 month old TASTPM mice. This increase may be the result of a compensatory mechanism occurring as a result of the changes occurring within the CNS due to disease progression/

severity. IHC data confirmed the findings seen with immunoblotting. Labelling with the anti-H_3R PAN antibody appears to increase at 7 months and decrease by 12 months to similar levels seen in 3 month TASTPM mice in the cortex and dentate gyrus however, in the CA1, 2, 3 and the cerebellum the immunoreactive staining at 12 months appears to be lower than that observed in the 3 and 7 month old TASTPM mice. This regional variation seen is likely down to the variation in isoform distribution and temporal regulation (Cogé et al., 2001). Overall, again there appears to be no major reduction over the period where cognitive deficits occur (Chazot et al., unpublished).

The anti-rH_{3AC}/ h$H_3R_{445/453,}$ antibody has previously been shown to be selective for the rodent $H_3R_{A/C}$ and the human H_3R_{445} isoform (Fiona Shenton PhD Thesis 2007 and Cannon et al., 2007). In this chapter, the antibody has been used to determine whether the H_{3A}/H_{3C} isoforms are altered in aging and dementia in the CNS of CD-1 mice and TASTPM mice.

Labelling detected with the anti-rH_{3AC}/ h$H_3R_{445/453,}$ antibody in the CD-1 timeline detected a single band migrating at 45kDa, likely to represent the full length rodent H_3R_A. Labelling detected with the anti-rH_{3AC}/ h$H_3R_{445/453,}$ antibody showed no significant differences in the immunoreactivity detected between the three time points (3- 2 months), suggesting that H_3R_A expression was unaltered with age. A similar result was obtained using immunohistochemical approaches. These findings would indicate that both the full length rodent H_3R_A is unaltered with age in the CD-1 mouse CNS.

The TASTPM mice timeline, probed with the anti-H_{3AC}/ h$H_3R_{445/453}$ antibody, detected three bands at migrating at approximately 90, 45 and 38kDa. The

90kDa and 45kDa bands represent putative dimeric and monomeric versions of the full length rodent H_3R_A. The 38kDa band is likely to represent the H_3R_{397} /H_3R_c isoform (Rouleau et al., 2004), the anti-rH_{3AC}/ $H_3R_{445/453}$ antibody is known to detect the rodent H_3R_{397} (Cannon et al., 2007). Labelling detected with the anti-rH_{3AC}/ $H_3R_{445/453,}$ antibody showed a significant decrease in H_3R immunoreactivity for all three bands detected at 12 months compared with 3 and 7 months. The full length H_3R and the shorter H_3R_{397} isoform expression appear to decrease with age in the CNS of TASTPM mice. This decrease maybe a result of the disease phenotype associated with TASTPM mice.

Overall the results for the mouse timelines would suggest that H_3R as a general population appears to be preserved from 3 – 10 months in CD-1 mice and 3-7 mice in TASTPM mice, however after 10 months and 7 months there appears to be a decrease in H_3R expression in CD-1 and TASTPM mice, respectively. In contrast, the full length receptor does not appear to be altered with age in CD-1 mice and may only modestly decrease from 12 months in TASTPM mice. The difference observed in the H_3R expression between the CD-1 mice and TASTPM mice data sets are likely to reflect the difference in pathology of the dementias seen in these different mouse models. The apparent preservation of the H_3 receptor over the period where learning deficits occur in the two mice models indicate that the deficits are independent of the H_3 receptor.

3.5.2 Human H_3R characterization and expression in two human Lewy body diseases

PD is characterized by a strong degeneration of the neuromelanin containing dopaminergic neurons in the substantia nigra (SN) (Braak and Del Tredici, 2009). The SN receives a strong histaminergic innervation from the TMN that contains the only histaminergic neurons in the brain (Watanabe et al., 1984, Panula et al., 1989 and Lee et al., 2008). It has been hypothesized that the histaminergic system is involved in the pathogenesis of PD, since animal studies showed that histamine may accelerate the degeneration of the dopaminergic neurons in the SN. Our recent collaborative study has reported a significant decrease of 40% in H_3R gene and protein expression in human PD SN samples when compared with human control cases (Shan et al., 2010).

DLB is a primary, neurodegenerative dementia sharing clinical and pathological characteristics with both PD and AD (McKeith et al., 2003). The presenting feature of DLB patients is usually cognitive decline (Barber et al., 2001), but there is often a relative preservation of short term memory (McKeith et al., 2002). One obvious clinical difference between individuals categorised as suffering from DLB, compared with “typical” AD cases, is the occurrence of fluctuations in their levels of awareness and attention (Ince 1998). Furthermore, significant motor deficits are also a feature of DLB, but to a lesser extent than that seen in PD. Thus, the clinical symptoms of DLB could reflect greater deficits in systems, such as the histaminergic system, that controls cortical activation (Pollard et al., 1993).

In this thesis the anti-$hH_3R_{365/445}$ antibody was shown to be selective for the hH_3R_{445} and hH_3R_{365} isoforms, detecting a single band migrating at 38kDa in HEK 293 cells expressing the 365 isoform and a 45kDa species in HEK 293 cells expressing the 445 isoform. The antibody was then used to confirm whether the isoforms were expressed at the protein level in human brain samples and determine whether their expression was altered in two human Lewy body diseases (PD and DLB) in putamen samples. For the first time, the hH_3R_{445} and hH_3R_{365} isoforms have been shown to be expressed in the human CNS. The hH_3R_{365} isoform showed no significant difference in immunoreactivity between the three disease states. However, the full length receptor, hH_3R_{445}, migrating at approximately Mr 45kDa displayed significantly stronger immunoreactivity in DLB cases versus control cases. These results suggest that hH_3R_{445} expression maybe up-regulated in DLB.

The anti-hH_3R_{329} antibody was shown to be selective for the hH_3R_{329} isoforms, detecting a single band migrating at 30kDa in HEK 293 cells expressing the 329 isoform. For the first time the hH_3R_{329} isoform has been shown to be expressed in the human CNS. The isoform showed no significant difference in immunoreactivity between the three disease states, although there was an apparent increase in hH_3R_{329} immunoreactivity in the PD cases compared with age matched control and DLB cases. The control group displayed little individual variation in hH_3R_{329} isoform expression unlike DLB and PD groups. The variation in H_3R expression in the disease samples maybe a result of variation in disease progression and general variation in symptoms experienced by each individual.

In conclusion, a selection of novel anti-hH_3R isoform specific probes were generated which were selective for particular human H_3R isoform targets.

Overall the data would indicate that the H_3R is largely preserved with age and in disease in cortical and striatal regions in TASTPM and CD-1 mice. Human isoforms have been shown for the first time to be expressed at the protein level in the human CNS. The data for the human disease cases would suggest that some of the isoforms appear to be altered in different disease states.

CHAPTER 4

Pharmacological Characterisation of Three Human H_3R isoforms: 329, 365 and 445 using [^{3}H] GSK189254

4.1 Objectives

To determine the pharmacological profile of a highly potent and selective H_3R antagonist [^{3}H] GSK189254 (see figure 1.9) in the presence of three of the major human H_3R isoforms: 329, 365 and 445. The first aim of this chapter was to determine the affinity of the ligand for each of the respective isoforms expressed alone and when co-expressed in HEK 293 cells. The next aim was to perform a series of competition binding assays using a variety of H_3R ligands that cover the full array of pharmacological profiles for each of the isoforms and heteromeric subtypes.

4.2 Introduction

The majority of histamine H_3R binding studies have relied on 'selective' H_3R agonists such as [^{3}H] RαMHA and [^{3}H] NMHA as radiolabels (van der Goot & Timmerman, 2000). The discovery of the H_4R in the past ten years and the recent detection of the H_4R in the CNS (Strakhova et al., 2009 and Connolly et al., 2009) has resulted in re-evaluation of the specificity of H_3R ligands. Both RαMH and NMHA along with many other H_3R ligands are known to display affinity at the H_4R resulting in limitations to their use for the detection of the H_3R. Also, agonist binding at the H_3R has been shown to be sensitive to guanine nucleotides, meaning H_3R agonists detect both high and low affinity receptor states (Arrang et al., 1990 and West et al., 1990). Witte et al. (2009)

showed the displacement of [^{3}H] A-349821, a high affinity H_3R antagonist/ inverse agonist, displayed a monophasic binding trace in the presence of H_3R antagonists/inverse agonists suggesting recognition of a single binding site, while H_3R agonists displayed a biphasic binding trace, suggesting recognition of both high- and low-affinity H_3R site. Previously, published data describe the radiolabelled binding of H_3R antagonists containing an imidazole moiety, thought to be responsible for off target binding (Esbenshade et al., 2005 and Kitbunnadaj et al., 2005).

GSK189254, 6-[(3-Cyclobutyl-2,3,4,5-tetrahydro-1*H*-3-benzazepin-7-yl)oxy]-*N*-methyl-3-pyridinecarboxamide hydrochloride, is a novel highly potent and selective histamine H_3R antagonist (structure shown in chapter 1, Fig 1.9). GSK189254 displays a 300-fold higher affinity for the human (p*K*i = 9.59–9.90) than the rat (p*K*i = 8.51–9.17) H_3R making it ideal for the detection and characterisation of the human H_3R. GSK189254 has been shown to be approximately 10,000-fold selective for human H_3R versus other targets tested, and exhibited potent functional antagonism (p*A*2 = 9.06 versus agonist-induced changes in cAMP) and inverse agonism [pIC50 = 8.20 versus basal guanosine 5-*O*-(3-[35S]thio)triphosphate binding] at the recombinant human H_3R. *In vitro* autoradiography demonstrated specific [^{3}H] GSK189254 binding in rat and human brain areas, including the cortex and hippocampus. In addition, dense H_3R binding was detected in medial temporal cortex samples from severe cases of AD, suggesting for the first time that H_3Rs are preserved in late-stage disease. Oral administration of GSK189254 inhibited cortical *ex vivo* RαMHA binding (ED_{50} 0.17 mg/kg) and increased *c-fos* immunoreactivity in prefrontal and somatosensory cortex. Microdialysis

studies demonstrated that GSK189254 increased the release of acetylcholine, noradrenalin, and dopamine in the anterior cingulate cortex and acetylcholine in the dorsal hippocampus. Functional antagonism of central H_3R was demonstrated by blockade of RαMHA induced dispogenia in rats. GSK189254 significantly improved performance of rats in diverse cognition paradigms, including passive avoidance, water maze, object recognition and attentional set shift. The data so far suggest that H_3R antagonists may have a therapeutic potential for the symptomatic treatment of dementia in AD and other cognitive disorders (Medhurst et al., 2007 and Medhurst et al., 2009).

H_3R isoforms have been shown to display variation in their expression and pharmacological profile (Hancock et al., 2003) such as agonist potencies (Wellendorf et al., 2002), signalling properties (Drutel et al., 2001) and constitutive activity (Morisset et al., 2001). Not all isoforms are likely to be expressed at the surface as a receptor, rat isoforms D, E and F have been shown to act as dominant negatives in vitro to either directly or indirectly control surface expression of the rat isoforms A, B and C (Bakker et al., 2006). Furthermore, receptors with deletions in regions thought to be important in ligand binding, and/ or signal transduction may not be functional. Recently, Leurs and colleagues (2008) reported at the European Histamine Research Society, differential expression of the hH_3R_{365} and the $hH_3R_{445,}$ with the hH_3R_{365} isoform displaying higher expression levels than the hH_3R_{445} in many brain structures. The hH_3R_{365} also displayed higher affinity and potency for H_3R agonists and conversely a lower potency and affinity for H_3R inverse agonists. The hH_3R_{365} also displayed higher constitutive signalling compared

to the hH_3R_{445} in both [^{35}S] GTPγS binding and cAMP assays (Bongers et al., 2007). Lower mRNA expression patterns were observed for the $hH_3R_{415,}$ hH_3R_{413} and hH_3R_{329} which also bind H_3R ligands and exhibit subtle difference in coupling to signalling mechanisms. Activation of the H_3R isoforms results in the activation of different G proteins resulting in differential signalling, potency and function. These differences observed in H_3R pharmacology and signalling are likely to be important for obtaining a detailed understanding of the physiological and potential therapeutic roles of the H_3R and its respective isoforms.

In this chapter, the pharmacological profile of the hH_3R_{445}, hH_3R_{365} and hH_3R_{329} isoforms were analysed. Previously, mRNA levels showed the hH_3R_{445}, hH_3R_{365} and hH_3R_{329} isoform expression to have a high degree of overlap in regions of the CNS known to be involved in the aetiology of AD and DLB, indicating the potential presence of hetero-oligomer subtypes (Coge et al., 2001).

The aim of this chapter was to characterize the pharmacology of the highly potent and selective H_3R antagonist [^{3}H] GSK189254 at each of the following human isoforms, H_3R_{445}, H_3R_{365} and the $H_3R_{329.}$ The secondary aim was to determine whether co-expression of these isoforms had any influence on the binding characteristics of [^{3}H] GSK189254.

4.3 Methods

4.3.1 Polyethyleneimine (PEI) transfection method (chapter 3)

4.3.2 Harvesting and membrane preparation of HEK 293 cells

HEK 293 cells were harvested 48 hours post-transfection. The culture media was removed and cells were washed with 10 ml PBS and the solution removed. 10 ml of 50mM Tris, 5 mM EDTA, pH7.7 buffer kept at 4^{o}C was added to the cells and the cells scraped from the bottom of the flask using a Greiner cell scraper. The re-suspended cells were homogenised using a douce glass/ glass homogeniser, kept ice cold. The homogenate was pelleted by centrifugation at 18000 x g at 4^{o}C for 5 minutes. The supernatant was discarded and the pellet re-suspended in 2ml of ice cold 50 mM Tris, 5 mM EDTA, pH7.7 buffer.

4.3.3 Saturation binding of [^{3}H]-GSK189254 at recombinant human H_3R isoforms

Saturation binding assays using [^{3}H] GSK189254 were performed essentially as described previously by Medhurst et al. (2007). RαMHA is a specific H_3R agonist which was used as the radioligand displacer to determine non-specific binding. To determine total binding 100 µg of human H_3R transfected HEK 293 cell homogenates were incubated, in triplicate for 1 hour at room temperature, 80 µl 50 mM Tris-HCl, pH 7.7 containing 5 mM EDTA and 20 µl of GSK189254, at a concentration range 0.01 – 8 nM, to a final volume of 200 µl. Non-specific binding was determined by the addition of 20 µl of 100 µM

RαMHA to give a final concentration of 10 µM. The assay was terminated by rapid filtration through a Whatman GF/B filters pre-soaked in 10mM sodium phosphate dibasic pH 7.4, which were washed (3 X 3ml) using iced cold 10mM sodium phosphate dibasic pH 7.4, using a Brandell cell harvester. Filters were transferred into scintillation vials and 1ml of optiphase safe liquid scintillation cocktail was added. After 3 hours, the bound radioactivity was determined by counting for 3 minutes.

4.3.4 Competition binding of [^{3}H]-GSK189254 at recombinant human H_3R isoforms

Competition binding assays using [^{3}H] GSK189254 were performed essentially as described previously by Medhurst et al. (2007). To determine total binding 100 µg of human H_3R transfected HEK 293 cell homogenates were incubated, in triplicate for 1 hour at room temperature, 60 µl of 50 mM Tris-HCl, pH 7.7 containing 5mM EDTA, 20 µl of [^{3}H] GSK189254 (concentration 4.5nM), and 20 µl of the competitor immepip, thioperamide, iodophenpropit, proxyfan and GSK334429B, at a concentration range of 10 pM - 100µM, in a final volume of 200 µl. Non-specific binding was determined by the addition of 20 µl of 100 µM RαMHA to give a final concentration of 10 µM. The assay was terminated by rapid filtration through a Whatman GF/B filters pre-soaked in 10 mM sodium phosphate dibasic pH 7.4, which were washed (3 X 3ml) using iced cold 10 mM sodium phosphate dibasic pH 7.4, using a Brandell cell harvester. Filters were transferred into scintillation vials and 1 ml of optiphase safe liquid scintillation cocktail was added. After 3 hours the bound radioactivity was determined by counting for 3 minutes.

4.3.5 Data Analysis for saturation studies

Results from saturation studies were analysed by non-linear least square regression using GraphPad Prism. The saturation data were analysed by either the one-site or two-site binding hyperbola. The F-test was used to assess whether the one-site or the two-site model fit the data best ($p<0.05$ was deemed significant). The K_D values for saturation curves fitted a one-site hyperbola were calculated from the following equation,

$$Y = \frac{Bmax\ X}{K_D + X}$$

Where:-

Y = specific bound [^{3}H] GSK189254

X = concentration of [^{3}H] GSK189254

B_{max} = maximum number of binding sites

Saturation data was fit to the linear regression using GraphPad prism for the scatchard transformations,

F(x) = ax = b

Where:-

F(x) = specific bound [^{3}H] GSK189254/ [^{3}H] GSK189254 free

a = slope – (1/ K_D)

x = specific bound [^{3}H] GSK189254

b = X-axis intercept (Bmax/ K_D)

Specific binding was determined by subtracting the mean non-specific binding from the mean total binding for all concentration.

4.4 Results

4.4.1 Determining the selectivity of [^{3}H] GSK189254 for the human H_3R over the human H_4R expressed in a recombinant HEK 293 cells:

The initial experiments investigated the selectivity of the radioligand for the human H_3R in comparison to the closely related human H_4R.

Determining the selectivity of [^{3}H] GSK189254:

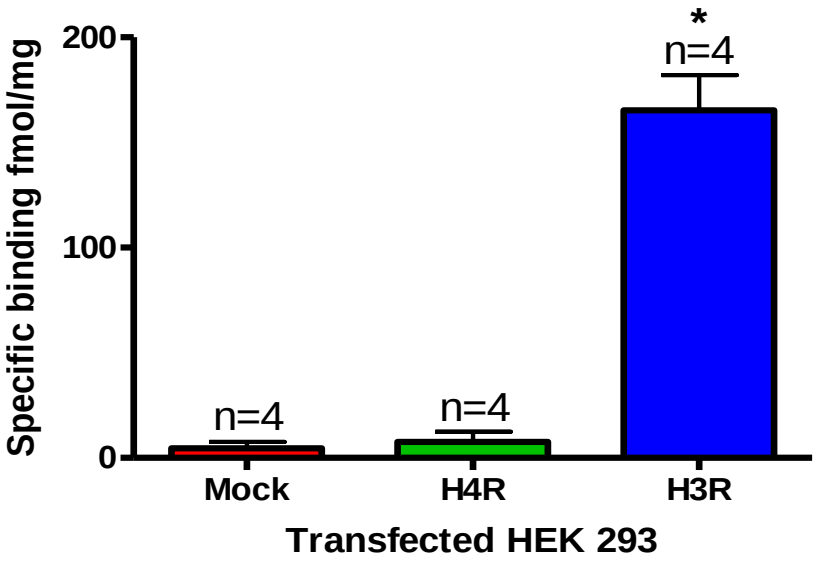

Figure 4.1: Showing the specific [^{3}H] GSK189254 binding in HEK 293 cells mock-transfected (control), hH_4R_{390} or hH_3R_{445} at 5 nM [^{3}H] GSK189254. Mean specific binding fmol/mg $\pm$ SEM for n determinations. Statistical significance was determined from the generated p value, where $p \leq 0.05$ was considered to show significance.

Figure 4.1 shows that the GSK189354 is selective for the human H_3R in comparison to the closely related human H_4R with negligible binding detected in human H_4R transfected cells or mock-transfected HEK 293 cells. All cDNA transfected into the HEK 293 cells were N-terminally FLAG tagged and expression of the receptors was confirmed by immunoblot analysis using anti-FLAG antibody, below.

Immunoblot confirming the expression of the hH_4R and the hH_3R:

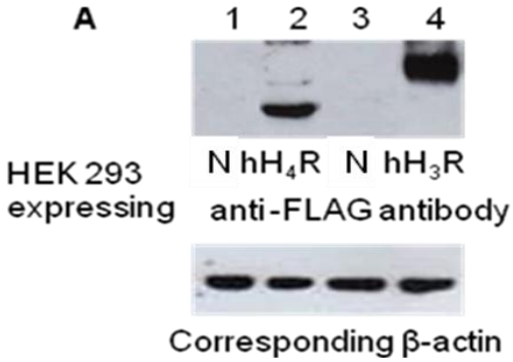

Figure 4.2: Immunoblot of mock, hH_3R_{445} and hH_4R_{390} transfected HEK 293 cells, probed with the anti-FLAG antibody.
Homogenates of HEK 293 cells transfected with either the full length human H_3R_{445} or the H_4R_{390} cDNA, all epitope tagged with FLAG were prepared. Approximately 25 µg of protein/ well were loaded onto a 7.5% PAGE gel. Once transferred the membrane was probed with affinity purified anti-FLAG antibody (1:5000). The FLAG antibody detects the two monomeric receptor species migrating at approximately M_r 37 and 45 kDa, respectively. The lower panel shows the corresponding β-actin, probed with monoclonal mouse anti β-actin antibody (1:5000).
Lane 1,HEK 293 cells mock transfected; Lane 2, HEK 293 cells expressing hH_4R_{390}; Lane 3, HEK 293 cells mock transfected; Lane 4, HEK 293 cells expressing hH_3R_{445}. All blots shown are representative blots from at least 4 separate transfection experiments.

After determining the selectivity of the radioligand for the human H_3R_{445} in comparison of the human H_4R_{390}, the next step was to determine the affinity of the ligand for each of the three human H_3R isoforms: 445, 365 and 329.

4.4.2 Saturation binding analysis of GSK189254 at the human H_3R isoforms singularly expressed in HEK 293 cells

A series of saturation binding assays were performed using [^{3}H] GSK189254 at each of the human H_3R isoforms, 445, 365 and 329 expressed alone in HEK 293 cells to determine the affinity of the compound for each of the isoforms. [^{3}H] GSK189254 was used at a concentration range of 0.01 – 8 nM, RαMHA was used to define non-specific binding at a final concentration of 10µM.

Saturation binding analysis of GSK189254 at the human H_3R_{445}

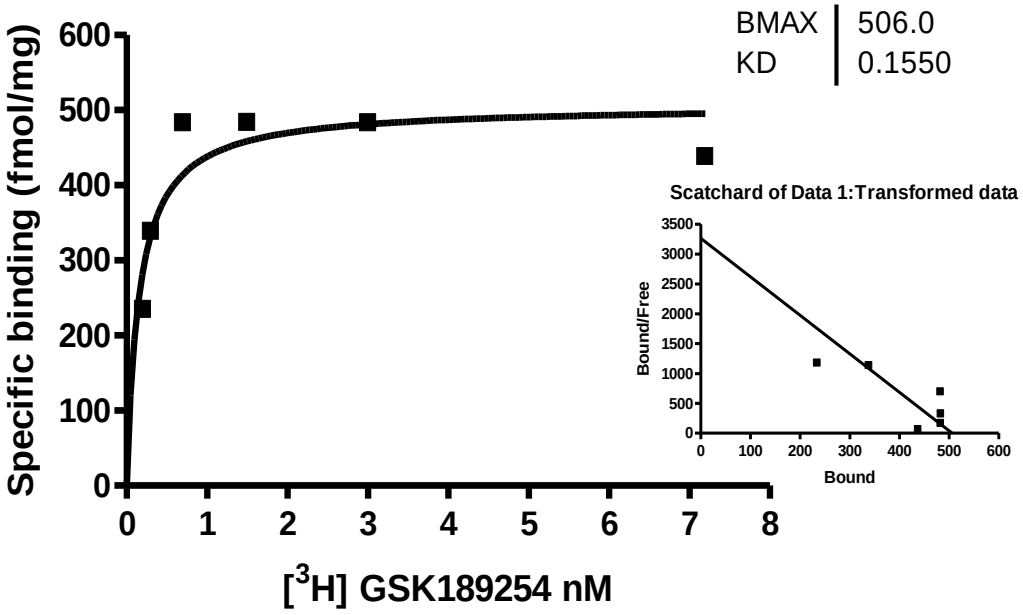

Figure 4.3: Saturation binding curve showing the specific [^{3}H] GSK189254 binding in HEK 293 cells transfected with hH_3R_{445}. Inset shows the saturation binding data transformed into a Rosenthal plot.

Figure 4.3 shows [^{3}H] GSK189254 displays high affinity for the hH_3R_{445} which reached saturation. Receptor expression was confirmed by western blot analysis shown below.

Immunoblot confirming the hH_3R_{445} expression:

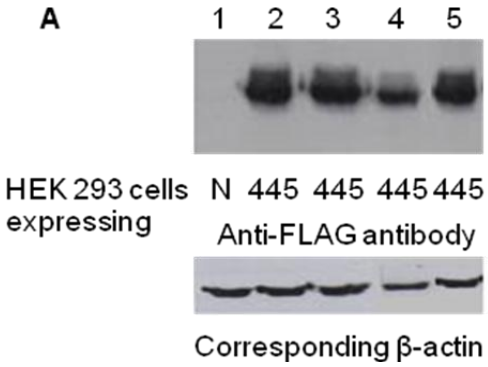

Figure 4.4: Immunoblot showing the expression of the hH_3R_{445} for 4 individual experiments probed with the anti-FLAG antibody.
Homogenates of HEK 293 cells transfected with hH_3R_{445} epitope tagged with FLAG were prepared. Approximately 25µg of protein/ well were loaded onto a 7.5% PAGE gel. Once transferred the membrane was probed with affinity purified anti-FLAG antibody (1:5000). The FLAG antibody detected a single band migrating at approximately M_r 44 kDa. Lower panel

shows the corresponding β-actin, probed with monoclonal mouse anti β-actin antibody (1:5000).
Lane 1, HEK 293 cells mock transfected; Lane 2, 3, 4, 5 HEK 293 cells expressing hH_3R_{445}. All blots shown are representative blots from at least 4 separate transfection experiments.

[^{3}H] GSK189254 shows nanomolar affinity binding at the human H_3R_{445} isoform, 0.16 ± 0.04 nM.

The affinity of GSK189254 was then determined at the human H_3R_{365} isoform.

Saturation binding analysis of GSK189254 at the human H_3R_{365}

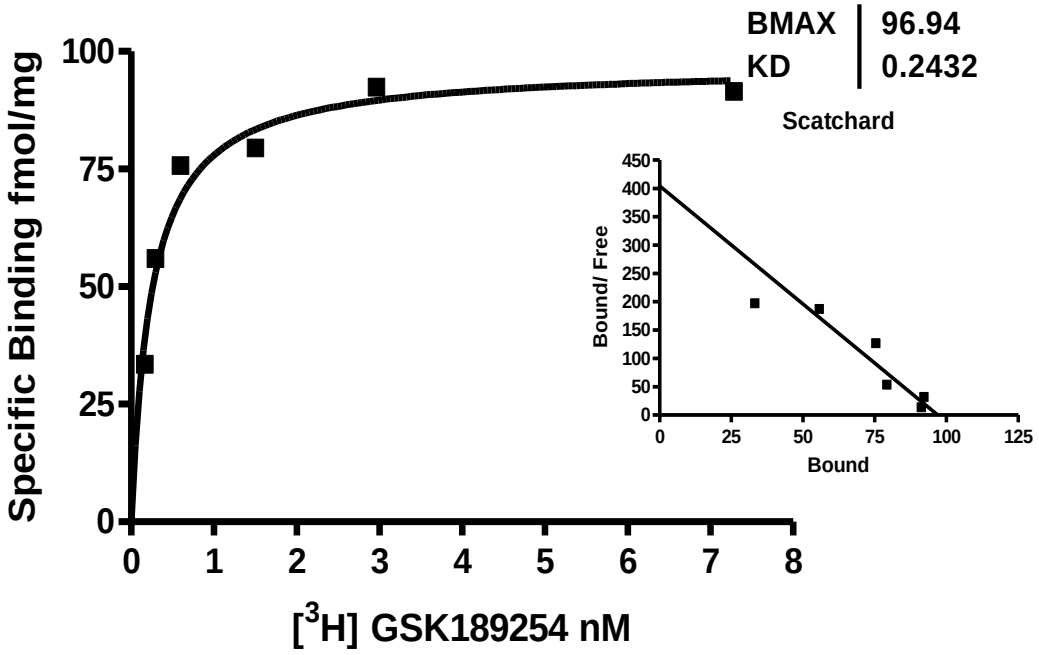

Figure 4.5: Saturation binding curve showing the specific [^{3}H] GSK189254 binding in HEK 293 cells transfected with hH_3R_{365}. Inset shows the saturation binding data transformed into Rosenthal graph.

Figure 4.5 shows GSK189254 displays high affinity binding for the hH_3R_{365} which reached saturation. Receptor expression was confirmed by western blot analysis shown below.

Immunoblot confirming the hH_3R_{365} expression:

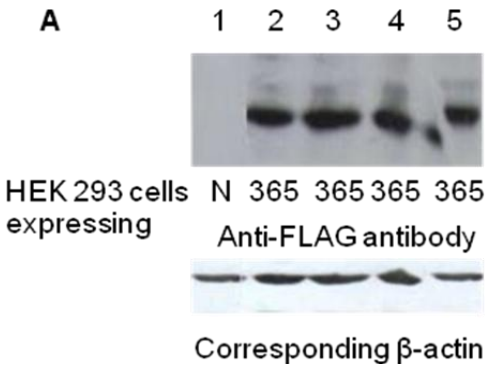

Figure 4.6: Immunoblot showing the expression of the hH_3R_{365} for 4 separate experiments probed with the anti-FLAG antibody.
Homogenates of HEK 293 cells transfected with hH_3R_{365}, epitope tagged with FLAG were prepared. Approximately 25 µg of protein/ well were loaded onto a 7.5% PAGE gel. Once transferred the membrane was probed with affinity purified anti-FLAG antibody (1:5000). The FLAG antibody detected a single band migrating at approximately M_r 36 kDa. Lower panel shows the corresponding β-actin, probed with monoclonal mouse anti β-actin antibody (1:5000).
Lane 1, HEK 293 cells mock transfected; Lane 2, 3, 4, 5 HEK 293 cells expressing hH_3R_{365}. All blots shown are representative blots from at least 4 separate transfection experiments.

[^{3}H] GSK189254 shows nanomolar affinity at the human H_3R_{365} isoform, 0.24 ± 0.07nM.

The affinity of GSK189254 was then determined at the human H_3R_{329} isoform.

Saturation binding analysis of GSK189254 at the human H_3R_{329}

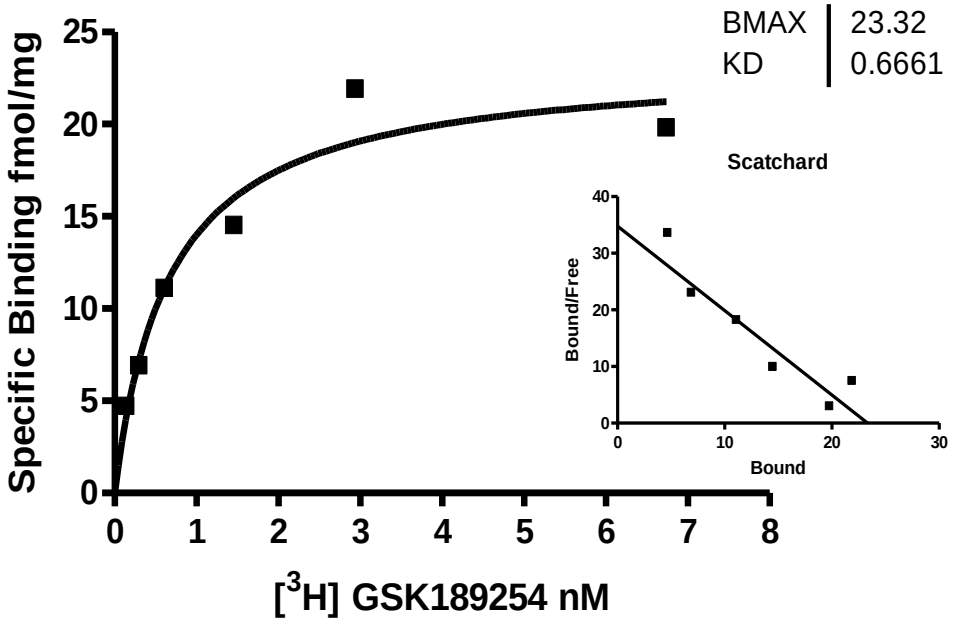

Figure 4.7: Saturation binding curve showing the specific [^{3}H] GSK189254 binding in HEK 293 cells transfected with hH_3R_{329}. Inset shows the saturation binding data transformed into Rosental graph.

Figure 4.7 shows the ligand displays high affinity binding for the hH_3R_{329} which reached saturation. Receptor expression was confirmed by western blot analysis shown below.

Immunoblot confirming the hH_3R_{329} expression:

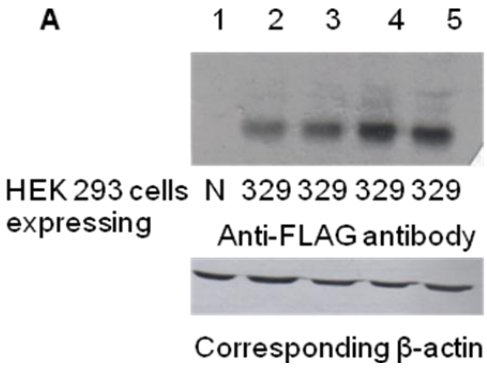

Figure 4.8: Immunoblot showing the expression of the hH_3R_{329} for 4 separate experiments probed with the anti-FLAG antibody.
Homogenates of HEK 293 cells transfected with hH_3R_{329}, epitope tagged with FLAG were prepared. Approximately 25 µg of protein/ well were loaded onto a 7.5% PAGE gel. Once transferred the membrane was probed with affinity purified anti-FLAG antibody (1:5000). The FLAG antibody detected a single band migrating at approximately M_r 33kDa. Lower panel shows the corresponding β-actin, probed with monoclonal mouse anti β-actin antibody (1:5000).
Lane 1, HEK 293 cells mock transfected; Lane 2, 3, 4, 5 HEK 293 cells expressing hH_3R_{329}. All blots shown are representative blots from at least 4 separate transfection experiments.

[^{3}H] GSK189254 shows nanomolar affinity at the human H_3R_{329} isoform, 0.98 $\pm$ 0.4nM.

The saturation binding curve data for each of the isoforms were collated and represented below in a bar chart displaying the variation in GSK189354 affinity at each of the human H_3R isoforms, 445, 365 and 329.

Mean binding affinity of [^{3}H] GSK189254 at human H_3R isoforms 445, 365 and 329 expressed in HEK 293 cells:

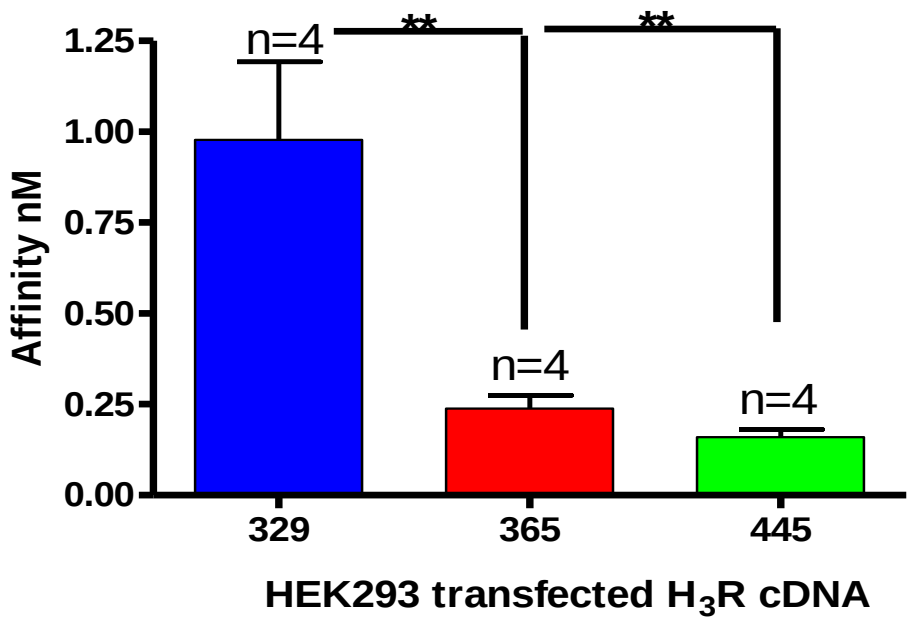

Figure 4.9: Mean affinity of [^{3}H] GSK189254 binding in HEK 293 cells expressing either $hH_3R_{445,}$ hH_3R_{365} or hH_3R_{329} isoforms. Mean affinity nM $\pm$ SEM for n determinations. Statistical significance was determined from the generated p value, where $p \leq 0.05$ was considered to show significance.

Figure 4.9 shows that [^{3}H] GSK189254 displays a significantly lower affinity of approximately 5-fold at the hH_3R_{329} isoform compared to the hH_3R_{365} or the $hH_3R_{445,}$ ($p<0.01$ and $p<0.01$, respectively). The radioligand displayed a similar binding affinity for the hH_3R_{365} and the hH_3R_{445} isoforms. The mean binding affinity of [^{3}H] GSK189254 at each of the $hH_3R_{445,}$ hH_3R_{365} and hH_3R_{329} were 0.16 $\pm$ 0.04nM, 0.24 $\pm$ 0.07nM and 0.98 $\pm$ 0.4nM, respectively.

The binding affinity of [^{3}H] GSK189254 for each of the three isoforms expressed individually has been determined so the next aim is to look whether co-expressing the isoforms has any affect the binding affinity of the ligand.

4.4.3 Saturation binding analysis of GSK189254 at the human H_3R isoforms co-expressed in HEK 293 cells

A series of saturation binding assays were performed using [^{3}H] GSK189254 at each of the human H_3R isoforms co-expressed in HEK 293 cells (445 + 365, 445 + 329 and 365 + 329). [^{3}H] GSK189254 was used at a concentration range of 0.01 – 8 nM. RαMHA was used to define non-specific binding at a final concentration of 10 µM.

Saturation binding analysis of GSK189254 at the human $H_3R_{445 + 365}$ heterodimer:

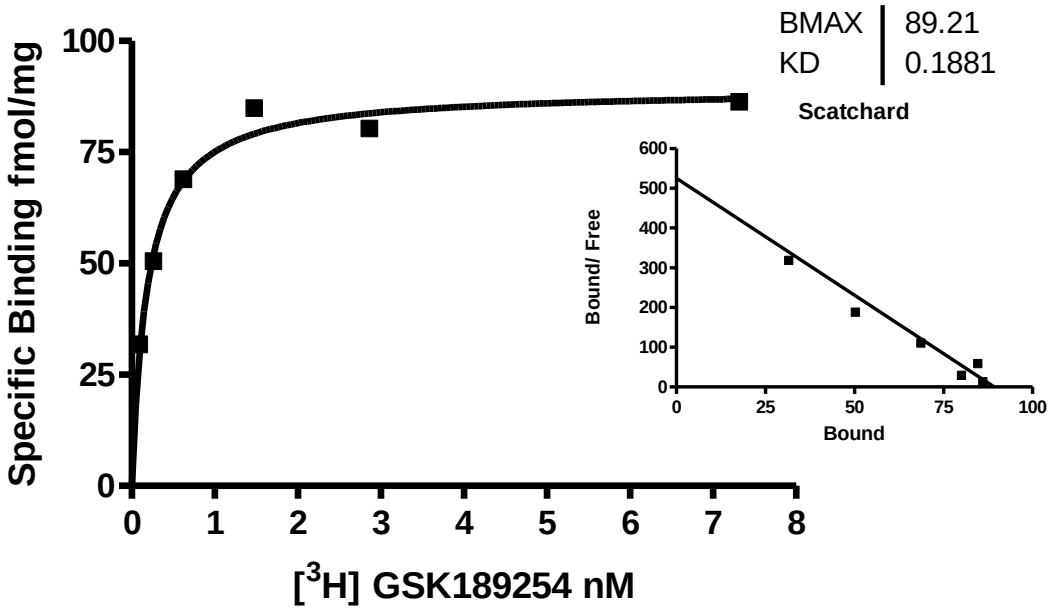

Figure 4.10: Saturation binding curve showing the specific [^{3}H] GSK189254 binding in HEK 293 cells transfected with hH_3R_{445} + hH_3R_{365}. Inset shows the saturation binding data transformed into a Rosenthal plot.

Figure 4.10 shows GSK189254 displays high affinity binding for the hH_3R_{445} + hH_3R_{365} heterodimer, which reached saturation. Receptor expression was confirmed by western blot analysis shown below.

Immunoblot confirming the $hH_3R_{445 + 365}$ expression:

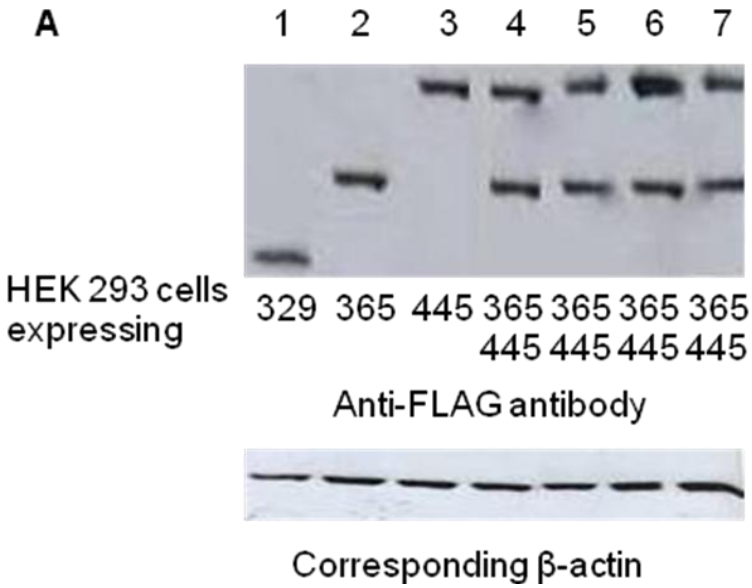

Figure 4.11: Immunoblot showing the expression of the hH_3R_{445} + hH_3R_{365} for 4 separate experiments probed with the anti-FLAG antibody.
Homogenates of HEK 293 cells transfected with a 1:1 ratio of the hH_3R_{445} + hH_3R_{365}, epitope tagged with FLAG were prepared. Approximately 25 µg of protein/ well were loaded onto a 7.5% PAGE gel. Once transferred the membrane was probed with affinity purified anti-FLAG antibody (1:5000). The FLAG antibody detects two separate bands migrating at approximately M_r 44 and 36 kDa representing the hH_3R_{445} + $hH_3R_{365,}$ respectively. Lower panel shows the corresponding β-actin, probed with monoclonal mouse anti β-actin antibody (1:5000).
Lane 1, HEK 293 cells expressing hH_3R_{329}; Lane 2: HEK 293 cells expressing hH_3R_{365}; Lane 3 HEK 293 cells expressing hH_3R_{445}; Lane 4, 5, 6, 7 HEK 293 cells expressing hH_3R_{445} + hH_3R_{365}, All blots shown are representative blots from at least 4 separate transfection experiments.

[^{3}H] GSK189254 shows a nanomolar affinity at the human $H_3R_{445 + 365}$ heterodimer, 0.18 $\pm$ 0.07nM.

The affinity of GSK189254 was then determined at the human $H_3R_{445 + 329}$ heterodimeric combination.

Saturation binding analysis of GSK189254 at the human $H_3R_{445 + 329}$ heterodimer:

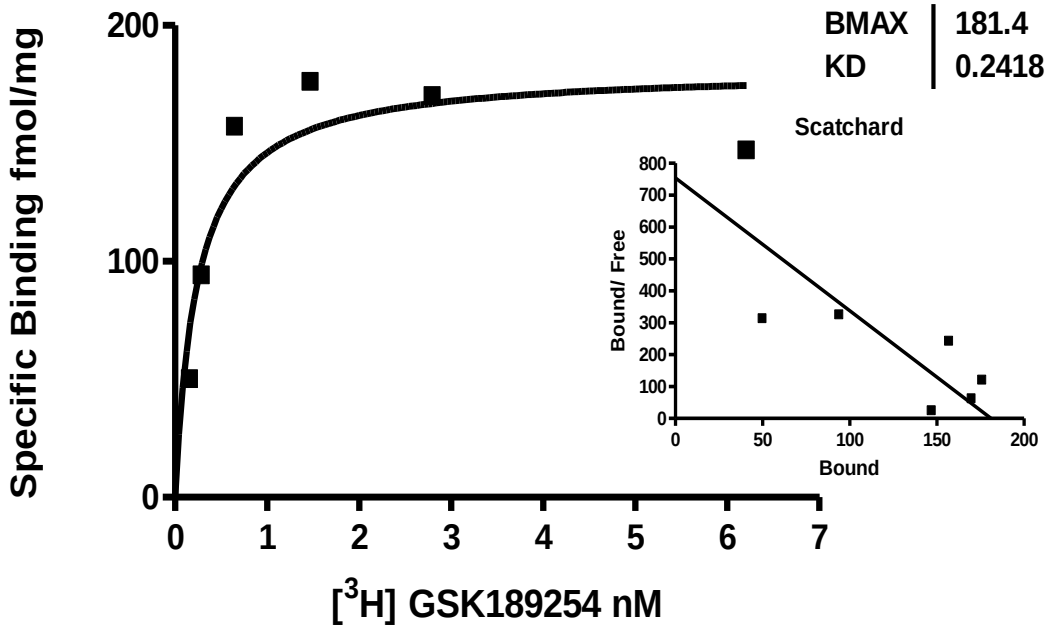

Figure 4.12: Saturation binding curve showing the specific [^{3}H] GSK189254 binding in HEK 293 cells transfected with hH_3R_{445} + hH_3R_{329}. Inset shows the saturation binding data transformed into Rosenthal plot.

Figure 4.12 shows the ligand displays high affinity binding for the hH_3R_{445} + hH_3R_{329} heterodimeric combination, which reached saturation. Receptor expression was confirmed by western blot analysis shown below.

Immunoblot confirming the $hH_3R_{445 + 329}$ expression:

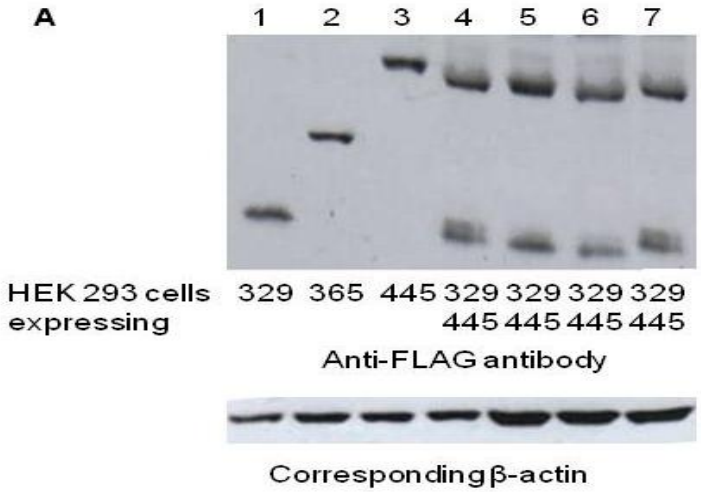

Figure 4.13: Immunoblot showing the expression of the hH_3R_{445} + hH_3R_{329} for 4 separate experiments probed with the anti-FLAG antibody.
Homogenates of HEK 293 cells transfected with a 1:1 ratio of the hH_3R_{445} + hH_3R_{329}, epitope tagged with FLAG were prepared. Approximately 25 µg of protein/ well were loaded onto a 7.5% separating gel. Once transferred the membrane was probed with affinity purified anti-FLAG antibody (1:5000). The FLAG antibody detected two single band migrating at approximately M_r 44 and 33 kDa representing the hH_3R_{445} + $hH_3R_{329,}$ respectively. Lower panel shows the corresponding β-actin, probed with monoclonal mouse anti β-actin antibody (1:5000).
Lane 1, HEK 293 cells expressing hH_3R_{329}; Lane 2: HEK 293 cells expressing hH_3R_{365}; Lane 3 HEK 293 cells expressing hH_3R_{445}; Lane 4, 5, 6, 7 HEK 293 cells expressing hH_3R_{445} + hH_3R_{329}. All blots shown are representative blots from at least 4 separate transfection experiments.

[^{3}H] GSK189254 shows a nanomolar affinity at the human $H_3R_{445 + 365}$ heterodimer, 0.27 $\pm$ 0.07nM.

The affinity of GSK189254 was then determined at the human $H_3R_{365 + 329}$ heterodimeric combination.

Saturation binding analysis of GSK189254 at the human $H_3R_{365 + 329}$ heterodimer:

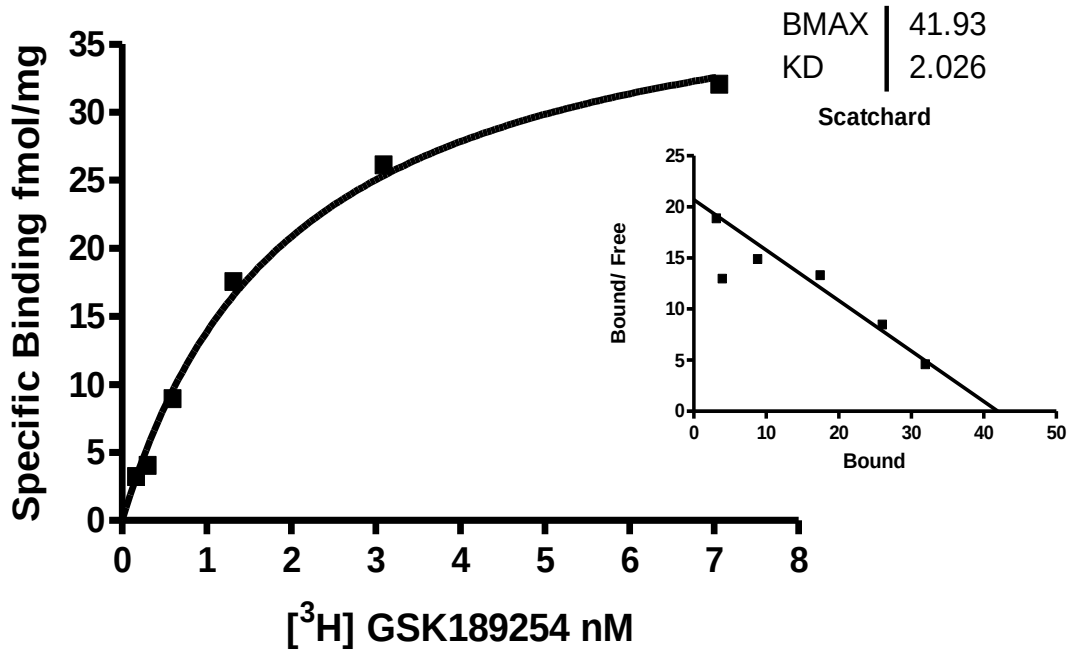

Figure 4.14: Saturation binding curve showing the specific [^{3}H] GSK189254 binding in HEK 293 cells transfected with hH_3R_{365} + hH_3R_{329}. Inset shows the saturation binding data transformed into Rosenthal graph.

Figure 4.14 shows GSK189254 displayed high affinity binding at the hH_3R_{365} + hH_3R_{329} heterodimeric combination, which reached saturation. Receptor expression was confirmed by western blot analysis shown below.

Immunoblot confirming the $hH_3R_{365 + 329}$ expression:

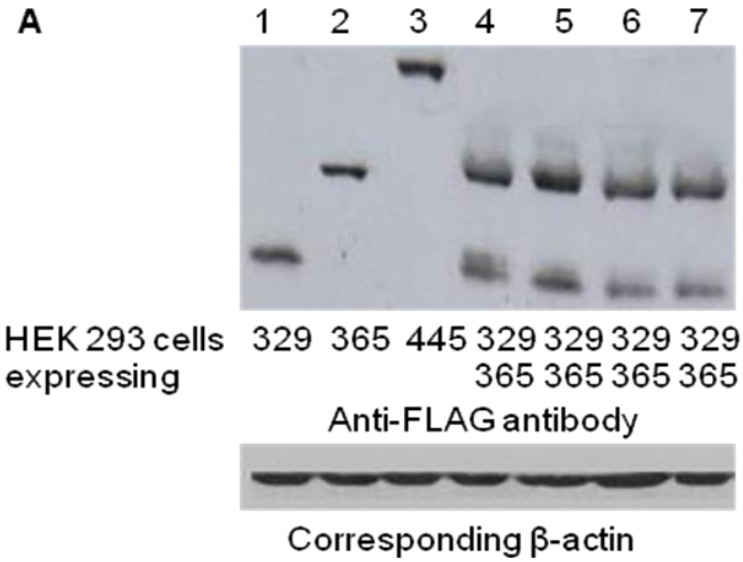

Figure 4.15: Immunoblot showing the expression of the hH_3R_{365} + hH_3R_{329} for 4 separate experiments probed with the anti-FLAG antibody.
Homogenates of HEK 293 cells transfected with a 1:1 ratio of the hH_3R_{365} + hH_3R_{29}, epitope tagged with FLAG were prepared. Approximately 25 µg of protein/ well were loaded onto a 7.5% PAGE gel. Once transferred the membrane was probed with affinity purified anti-FLAG antibody (1:5000). The FLAG antibody detected two single bands migrating at approximately M_r 36 and 33 kDa representing the hH_3R_{365} + $hH_3R_{329,}$ respectively. Lower panel shows the corresponding β-actin, probed with monoclonal mouse anti β-actin antibody (1:5000).
Lane 1, HEK 293 cells expressing hH_3R_{329}; Lane 2: HEK 293 cells expressing hH_3R_{365}; Lane 3 HEK 293 cells expressing hH_3R_{445}; Lane 4, 5, 6, 7 HEK 293 cells expressing hH_3R_{365} + hH_3R_{329}. All blots shown are representative blots from at least 4 separate transfection experiments.

[^{3}H] GSK189254 shows a nanomolar affinity at the human $H_3R_{445 + 365}$ heterodimer, 2.00 $\pm$ 1.1nM.

The saturation binding curve data for the co-expression of the isoforms has been collated and is represented below in a bar chart displaying the variation in GSK189354 affinity at each of the heterodimeric combinations.

Mean binding affinity of [^{3}H] GSK189254 at human H_3R isoforms co-expressed in HEK 293 cells:

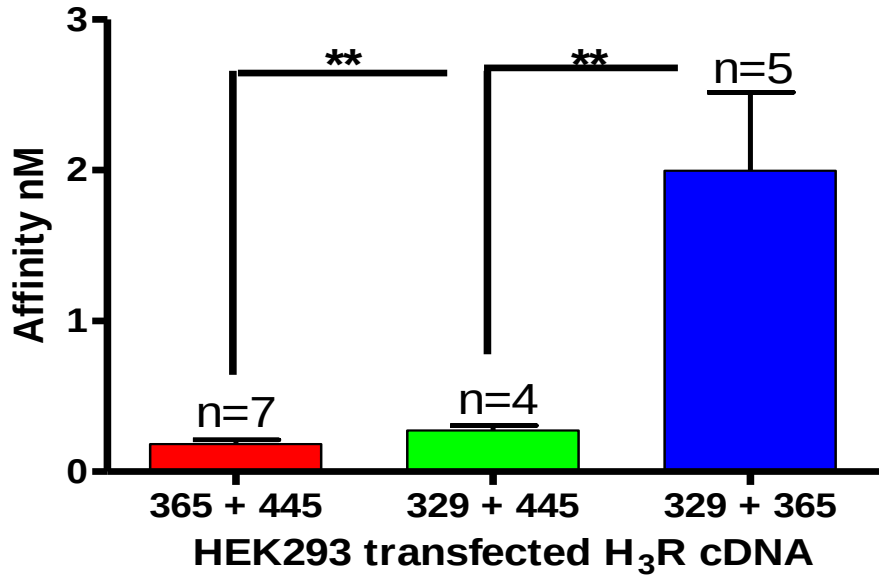

Figure 4.16: Mean affinity of [^{3}H] GSK189254 binding in HEK 293 cells co-expressing a combination of hH_3R isoforms 445 + 365, 445 + 329 and 365 + 329. Mean affinity nM ± SEM for n determinations. Statistical significance was determined from the generated p value, where $p \leq 0.05$ was considered to show significance.

Figure 4.16 shows that [^{3}H] GSK189254 displays a significantly lower affinity of approximately 10-fold at the hH_3R_{365} + hH_3R_{329} heterodimeric combination compared to other heterodimeric combinations the $hH_3R_{445,}$ + hH_3R_{365} or the hH_3R_{445} + hH_3R_{329} ($p<0.01$ and $p<0.01$, respectively). The ligand displayed a similar binding affinity at the $hH_3R_{445,}$ + hH_3R_{365} and the hH_3R_{445} + hH_3R_{329} heterodimeric combinations. The mean affinity of [^{3}H] GSK189254 for each of the heterodimeric combinations hH_3R_{445} + hH_3R_{365}, hH_3R_{445} + hH_3R_{329} and hH_3R_{365} + hH_3R_{329} were 0.18 ± 0.07nM, 0.27 ± 0.07nM and 2.00 ± 1.1nM, respectively.

The affinity of the [^{3}H] GSK189254 for the isoforms either expressed alone of co-expressed in HEK 293 cells has been determined. The next aim is to determine whether these isoforms display any binding differences in the presence of a variety of competing H_3R ligands.

4.4.4 Competition binding analysis for human H_3R isoforms individually expressed in HEK 293 cells

A series of competition binding assays were performed using [^{3}H] GSK189254 at each of the human H_3R 445, 365 and 329 isoforms expressed alone in HEK 293 cells. [^{3}H] GSK189254 was used at a concentration of 4.5 nM, RαMHA was used to define non-specific binding at a final concentration of 10 µM. The competitor drugs competing with [^{3}H] GSK189254 for the H_3R binding site were:

Immepip – A potent H_3R agonist

Thioperamide - A potent H_3R inverse agonist/ antagonist

Iodophenpropit - A H_3R neutral antagonist

Proxyfan - A high affinity H_3R ligand that acts as a protean ligand

GSK334429B - A novel, potent H_3R inverse agonist/ antagonist

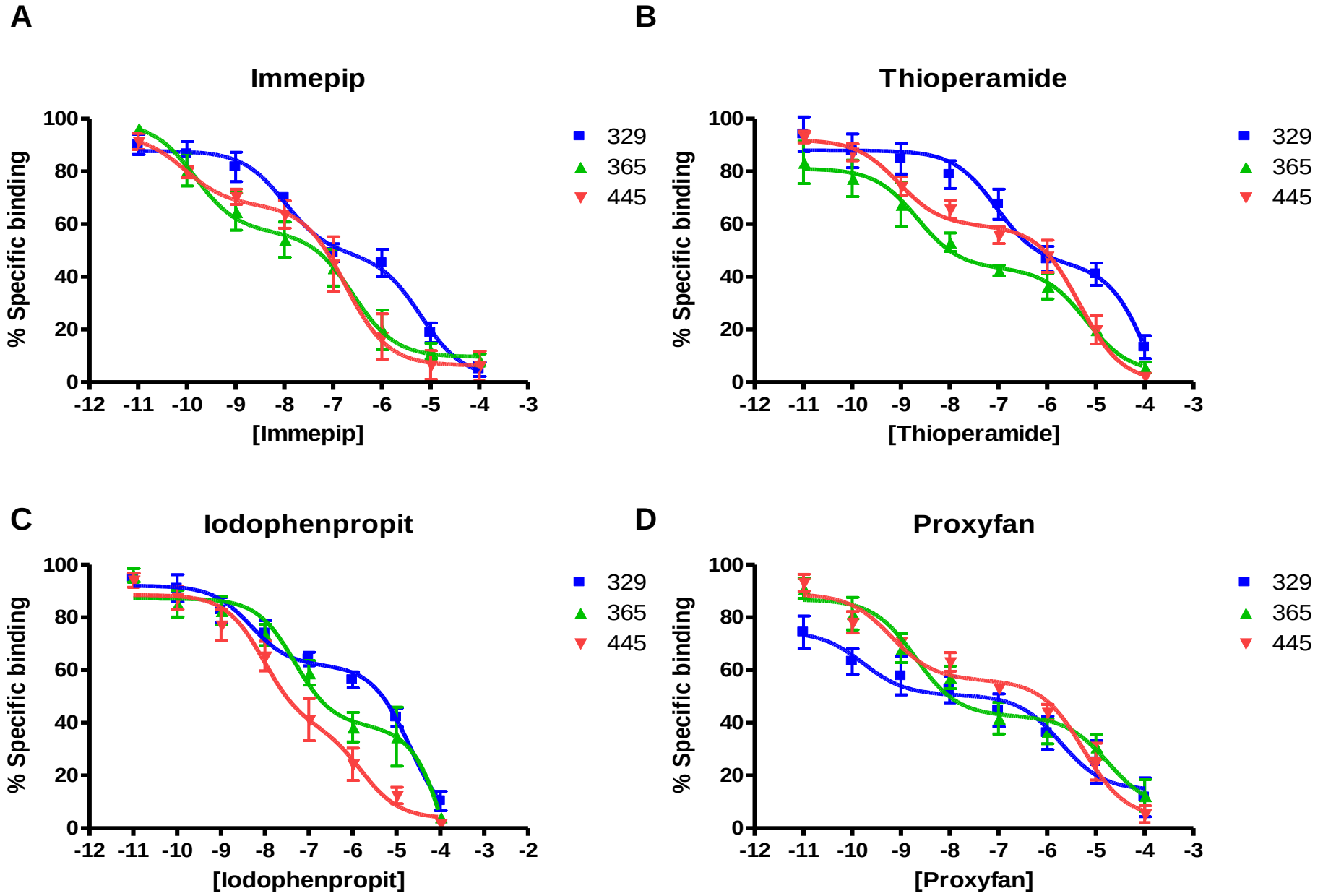
A
Immepip
% Specific binding
[Immepip]
B
Thioperamide
[Thioperamide]
C
Iodophenpropit
[Iodophenpropit]
D
Proxyfan
[Proxyfan]
329
365
445

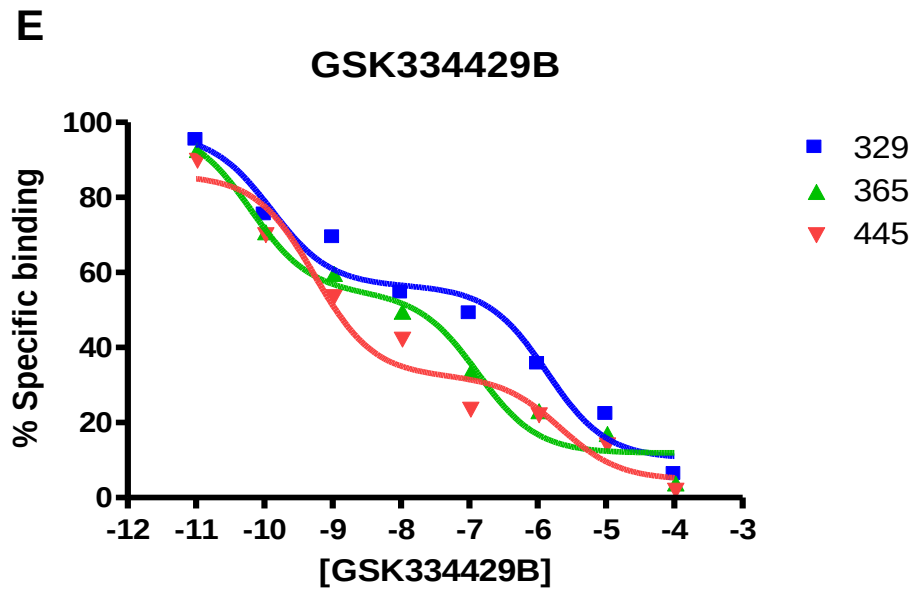

Figure 4.17: A series of competition binding curves showing specific [^{3}H] GSK189254 binding in HEK 293 cells transfected with either hH_3R_{445}, hH_3R_{365} or hH_3R_{329} plotted against the log concentration of different competing ligands (A) Immepip, (B) Thioperamide, (C) Iodophenpropit, (D) Proxyfan and (E) GSK334429B.

Figure 4.17 shows that each of the competing drugs displays differential pharmacological profiles at some of the human H_3R isoforms when expressed in HEK 293 cells.

Competition binding curve data for each of the isoforms has been collated and represented below in a bar chart displaying the differences in affinity.

Pharmacological profile for human H_3R isoforms expressed individually in HEK 293 cells

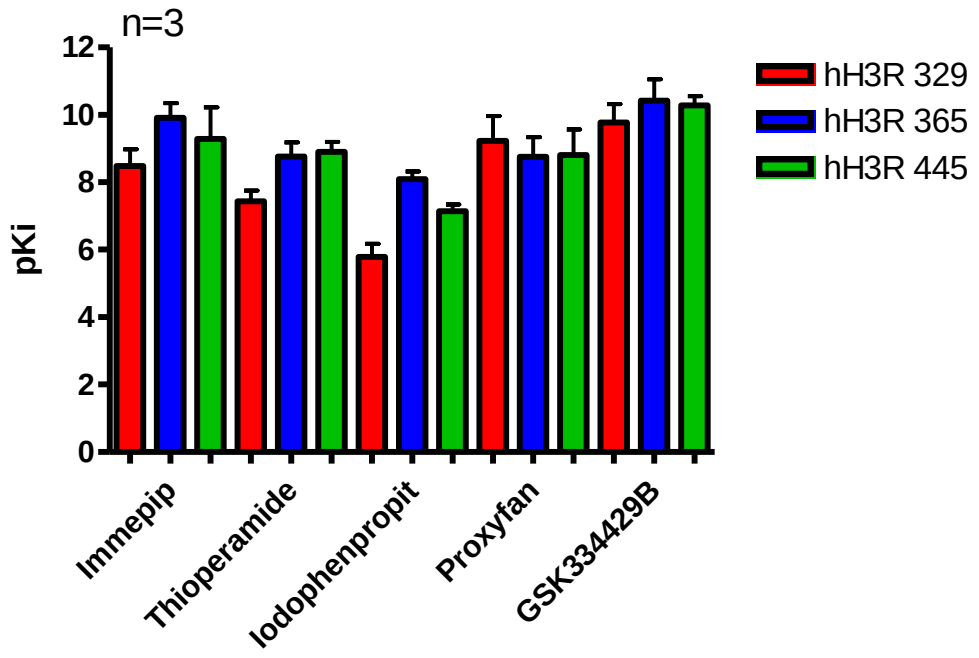

Figure 4.18: Mean high affinity site for competing compounds: Immepip, Thioperamide, Iodophenpropit, Proxyfan and GSK334429B utilising [^{3}H] GSK189254 with HEK 293 cells co-expressing either hH_3R_{445}, hH_3R_{365} or hH_3R_{329}. Mean affinity nM $\pm$ SEM for n = 3 determinations. Statistical significance was determined from the generated p value, where $p \leq 0.05$ was considered to show significance.

Figure 4.18 shows that each of the competing drugs displays differential pharmacological profiles at the human H_3R isoforms when expressed in HEK 293 cells. Iodophenpropit, thioperamide, proxyfan and GSK334429B displayed a significantly lower affinity at the hH_3R_{329} isoform than at the hH_3R_{365} and hH_3R_{445}, ($p<0.001$, $p<0.01$ and $p<0.05$, respectively). Iodophenpropit displays a significantly lower affinity than GSK334429B at the hH_3R_{445}, $p<0.05$. Iodophenpropit displays a significantly higher affinity at the hH_3R_{365} isoform than the hH_3R_{329} and hH_3R_{445}, ($p<0.01$ and $p<0.05$, respectively). Generally the hH_3R_{329} isoform displays a lower binding affinity for all the competing drugs tested except for proxyfan. The hH_3R_{365} and

hH_3R_{445} display similar affinities for all competing drugs tested, except iodophenpropit, where the hH_3R_{365} displays a higher affinity than the hH_3R_{445}.

The competition binding assay has shown that some of the H_3R competing ligands are better at competing for the H_3R binding than other ligands at particular isoforms, indicating that certain chemical properties of the compounds result in the compounds having higher affinity for different isoforms.

The next part will determine whether co-expression of the H_3R isoforms has any affect on the completion binding of different H_3R ligands.

4.4.5 Competition binding analysis for human H_3R isoforms co-expressed in HEK 293 cells

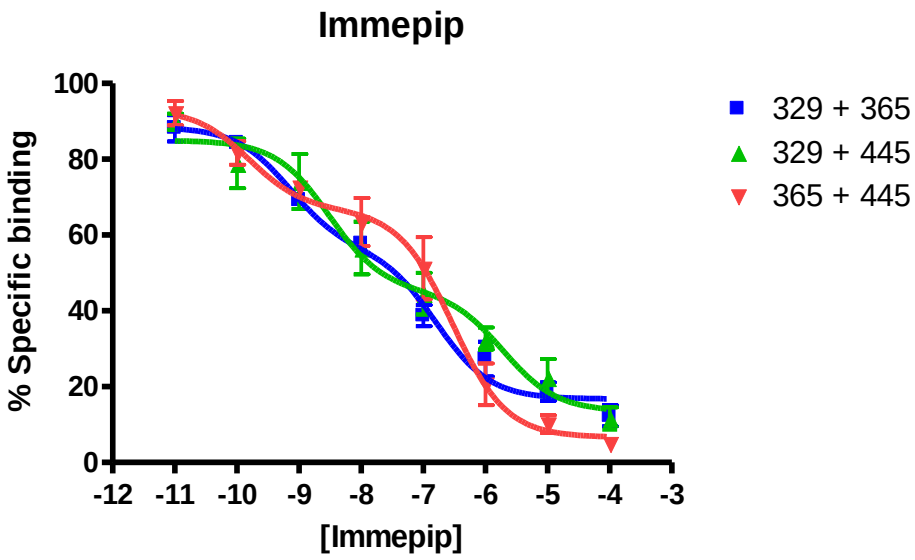
Immepip
% Specific binding
100
80
60
40
20
0
-12 -11 -10 -9 -8 -7 -6 -5 -4 -3
[Immepip]
329 + 365
329 + 445
365 + 445

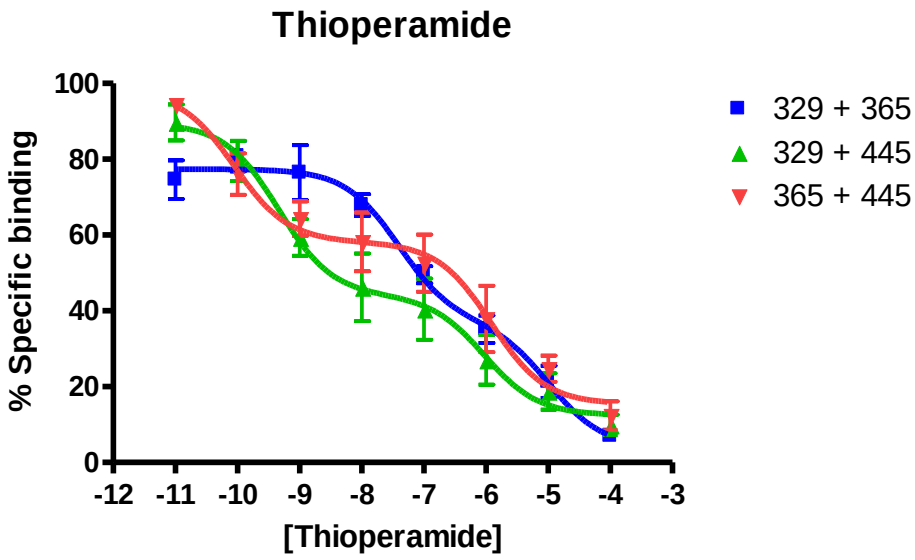
Thioperamide
% Specific binding
100
80
60
40
20
0
-12 -11 -10 -9 -8 -7 -6 -5 -4 -3
[Thioperamide]
329 + 365
329 + 445
365 + 445

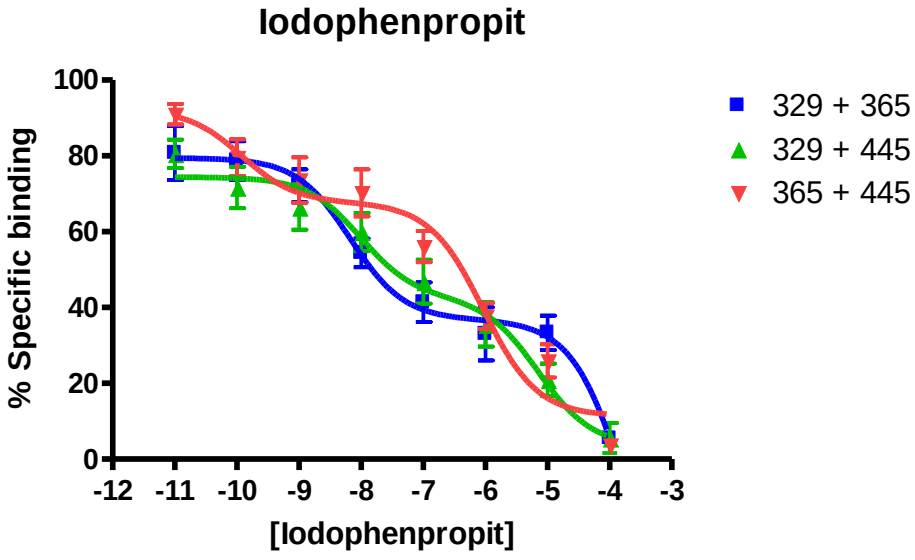
Iodophenpropit
% Specific binding
100
80
60
40
20
0
-12 -11 -10 -9 -8 -7 -6 -5 -4 -3
[Iodophenpropit]
329 + 365
329 + 445
365 + 445

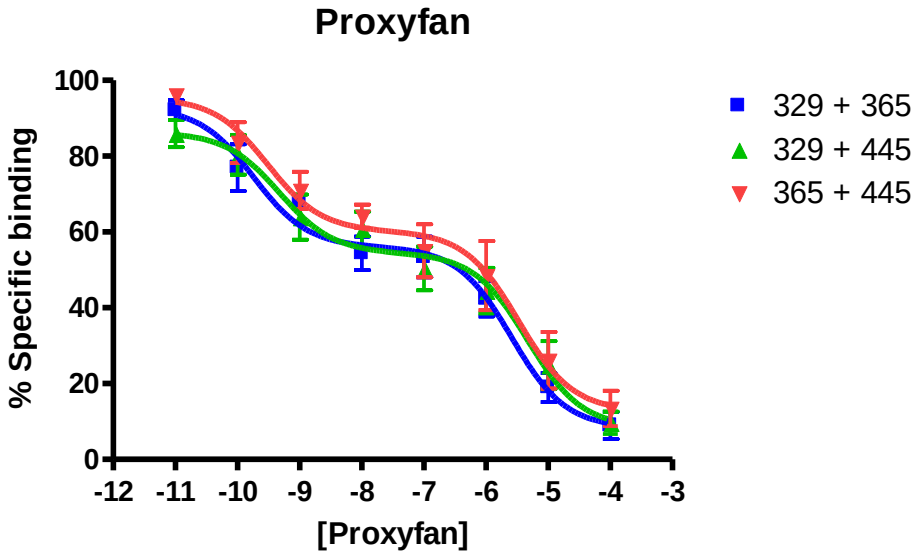
Proxyfan
% Specific binding
100
80
60
40
20
0
-12 -11 -10 -9 -8 -7 -6 -5 -4 -3
[Proxyfan]
329 + 365
329 + 445
365 + 445

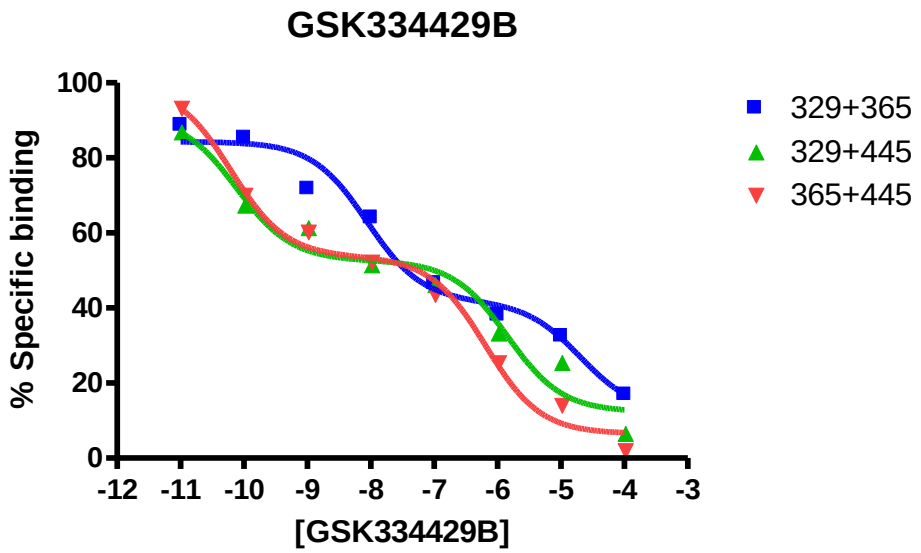

Figure 4.19: A series of competition binding curves showing specific [^{3}H] GSK189254 binding in HEK 293 cells co-transfected with either $hH_3R_{445 + 365,}$ $hH_3R_{365 + 329}$ or $hH_3R_{445 + 329}$ plotted against the log concentration of different competing ligands (A) Immepip, (B) Thioperamide, (C) Iodophenpropit, (D) Proxyfan and (E) GSK334429B. Mean affinity nM $\pm$ SEM for n = 3 determinations. Statistical significance was determined from the generated p value, where $p \leq 0.05$ was considered to show significance.

Figure 4.19 shows that each of the competing drugs displays differential pharmacological profiles at the human H_3R isoforms when co-expressed in HEK 293 cells.

Competition binding data for the isoforms co-expressed in HEK 293 cells was collated and is represented below in a bar chart displaying the difference in affinity.

Pharmacological profile for human H_3R isoforms co-expressed in HEK 293 cells

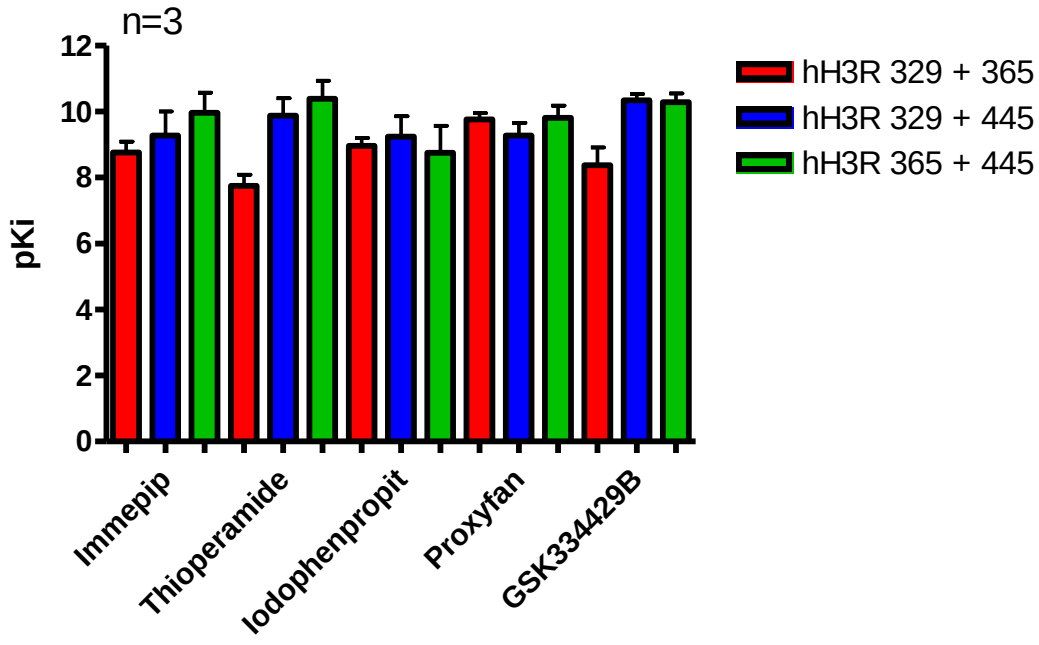

Figure 4.20: : Mean high affinity site for competing compounds: Immepip, Thioperamide, Iodophenpropit, Proxyfan and GSK334429B utilising [^{3}H] GSK189254 with HEK 293 cells co-expressing either $hH_3R_{445 + 365,}$ $hH_3R_{365 + 329}$ or $hH_3R_{445 + 329}$. Mean affinity nM $\pm$ SEM for n determinations. Statistical significance was determined from the generated p value, where $p \leq 0.05$ was considered to show significance.

Figure 4.20 shows that each of the competing drugs displays differing pharmacological profiles at the human H_3R isoforms when co-expressed in HEK 293 cells. Thioperamide and GSK334429B displays a significantly lower affinity at the $hH_3R_{329} + _{365}$ heterodimer than either the $hH_3R_{329} + _{445}$ or $hH_3R_{365} + _{445}$ combinations, ($p<0.05$ and $p<0.01$, respectively). Proxyfan displays a significantly higher affinity at the $hH_3R_{329} + _{365}$ heterodimer than thioperamide, $p<0.01$. Generally the $hH_3R_{329} + _{365}$ heterodimer displays a lower binding affinity for all the competing drugs tested except for proxyfan. The $hH_3R_{329} + _{445}$ and $hH_3R_{365} + _{445}$ combinations display similar affinities for all competing drugs tested.

Receptor expression was confirmed by western blot analysis shown below.

The competition binding assay has shown that some of the H_3R competing ligands are better at competing for the H_3R binding than other ligands at particular H_3R heterodimers, indicating that certain chemical properties of the compounds result in the compounds having higher affinity.

Immunoblot confirming the expression of all human H_3R isoforms in competition binding experiments:

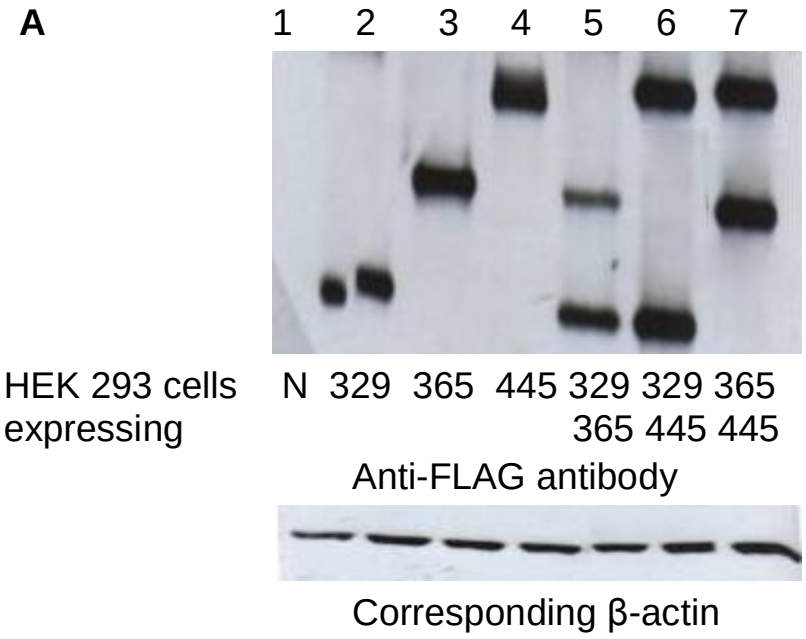

Figure 4.21: Immunoblot showing the expression of the hH_3R_{329}, hH_3R_{365}, hH_3R_{445} expressed alone and hH_3R_{329} + hH_3R_{365}, hH_3R_{329} + hH_3R_{445} and hH_3R_{365} + hH_3R_{445} co-expressed in HEK 293 cells and probed with the anti-FLAG antibody.
Homogenates of HEK 293 cells transfected with 1 ug of various human cDNA, epitope tagged with FLAG were prepared. Approximately 25 µg of protein/ well were loaded onto a 7.5% separating gel. Once transferred the membrane was probed with affinity purified anti-FLAG antibody (1:5000). The FLAG antibody shows the detection of the hH_3R_{329}, hH_3R_{365}, hH_3R_{445}, hH_3R_{329} + hH_3R_{365}, hH_3R_{329} + hH_3R_{445} and hH_3R_{365} + hH_3R_{445} isoforms (from left to right on the blot above). Lower panel shows the corresponding β-actin, probed with monoclonal mouse anti β-actin antibody (1:5000).
Lane 1, HEK 293 cells mock transfected, Lane 2, HEK 293 cells expressing hH_3R_{329}; Lane 3: HEK 293 cells expressing hH_3R_{365}; Lane 4 HEK 293 cells expressing hH_3R_{445}; Lane 5, HEK 293 cells expressing hH_3R_{329} + hH_3R_{365}; Lane 6, HEK 293 cells expressing hH_3R_{329} + hH_3R_{445} and Lane 7, HEK 293 cells expressing hH_3R_{365} + hH_3R_{445}. All blots shown are representative blots from at least 15 separate transfection experiments.

4.5 Discussion

A number of ligands that targeted the H_3R have had their specificity re-evaluated since the discovery of the H_4R, where a selection of supposedly H_3 specific ligands have shown cross reactivity to this newly discovered target. This cross reactivity is thought to occur due to ligands containing an imidazole moiety which results in off target binding not only to the H_4R but also other targets such as 5-HT_3 receptors and cytochrome P450 isoenzymes (Labella et al.,1992, Leurs et al., 1995, Alves-Rodrigues et al., 1996, Yang et al., 2002, Esbenshade et al., 2005 and Kitbunnadaj et al., 2005). The selectivity of [^{3}H] GSK189254, a H_3R antagonist/ inverse agonist for the human H_3R versus the human H_4R was confirmed initially.

The presence of numerous H_3R isoforms brings about another level of complexity in terms of ligand binding. The human H_3R has been shown to be widely distributed within the CNS with mRNA levels encoding the isoforms shown to be distributed in a region specific manner with some regions co-expressing isoforms (Cogé et al., 2001). Some of the shorter truncated isoforms have been shown to be non-functional but are expressed to similar levels of the full length receptor. These non-functional isoforms have been shown to regulate the longer functional isoforms in a dominant negative manner (Drutel et al., 2001 and van Rijn, 2008). Adding further to the diverse heterogeneity, it has been shown that the histaminergic neurons are organized into functionally distinct circuits that influence different brain regions (Giannoni et al., 2009). Very few studies have looked at the pharmacological difference between the full lengthH_3R 445 and its isoforms, and of those that

have the results are conflicting with some studies showing different pharmacological profiles (Hancock et al., 2003).

The saturation binding data confirm previous findings that H_3R isoforms display differences in pharmacological profile, with the hH_3R_{329} isoform displaying approximately a 5-fold lower binding affinity than both hH_3R_{365} and $hH_3R_{445.}$ Both the hH_3R_{365} and hH_3R_{445} isoforms display similar binding affinities. These data would suggest that the region spliced out to generate the hH_3R_{329} isoform is involved in binding affinity to certain H_3R compounds. Co-expression of the isoforms also resulted in a reduction in GSK189254 binding affinity for the hH_3R_{329} and hH_3R_{365} heterodimeric combination. The hH_3R_{329} and hH_3R_{365} heterodimer displayed approximately a 10-fold lower binding affinity than other heterodimeric combinations tested. The reduced affinity observed at the hH_3R_{329} and hH_3R_{365} heterodimer is likely the result of dimerization of the isoforms resulting in alterations in the binding pocket where [^{3}H] GSK189254 binds.

The competition binding curves show a biphasic response which would suggest that the H_3R has two binding states, a low and high affinity binding site. The high affinity site was analysed for simplicity. It would be interesting in future experiments to assess the effects of GppNHp or GTPγS (non-hydrolysable forms of GTP) upon this bi-phasic competition binding profile. Generally the hH_3R_{329} isoform displayed a lower binding affinity for all the H_3R competing drugs tested except for proxyfan. The hH_3R_{365} and hH_3R_{445} isoforms displayed similar affinities for all competing drugs tested, except iodophenpropit, where the hH_3R_{365} displays a higher affinity than the $hH_3R_{445.}$

These data support the pharmacological data produced by Leurs et al., 2008, showing the hH_3R_{365} isoform to have a higher affinity for agonists than the $hH_3R_{445,}$ however the data do not support the finding that the hH_3R_{365} isoform displays lower affinity than the hH_3R_{445} for inverse agonists/antagonists.

The competition binding assays indicate that some of the H_3R ligands display marked differences in apparent affinity for particular isoforms. Notably, the $hH_3R_{329/365}$ heterodimers have markedly reduced affinity (2-orders of magnitude) for thioperamide and GSK334429B, but not the other ligands tested.

In summary, the competition binding studies have shown significant differences exist in the binding pharmacology of human H_3R homo-oligomeric and heter-oligomeric subtypes, providing new information about the fundamental pharmacological nature of the human H_3R.

CHAPTER 5

Ligand Autoradiographical Comparison of Normal Aging with Neurodegenerative Dementia Aging using [^{3}H] GSK189254

5.1 Objectives

To determine whether the H_3R is preserved in the rodent and human CNS in aging and neurodegenerative diseases using ligand autoradiography. One aim of this chapter was to determine whether there were any changes in H_3R expression in two mice models; CD-1 mice, known to have premature learning deficits, and TASTPM mice, a transgenic mouse model of AD. Another aim was to establish whether there were any changes in human H_3R expression in normal aging and in two major types of human dementia diseases, AD and DLB. To determine if there were any H_3R changes, autoradiography was performed using a novel, high affinity, selective histamine H_3R antagonist/ inverse agonist radioligand [^{3}H] GSK189254.

5.2 Introduction

5.2.1 Human H_3R anatomical distribution in the CNS

The H_3R is expressed predominantly in the CNS and has been detected in human, rodent and non-primate brain as well as in the spinal cord of humans and on peripheral ganglia. Detection has been possible through the use of either ligand autoradiography, *in situ* hybridisation using gene transcripts or immunobiochemical techniques with anti-H_3R specific antibodies.

Previous autoradiographical studies using the H_3R agonist [^{3}H] RαMHA or antagonist [^{3}H] clobenpropit have mapped the H_3R in the rodent brain (Arrang

et al., 1987 and Pollard et al., 1993) and human brain (Martinez-Mir et al., 1990; Goodchild et al., 1999).

As observed in rat brain, H_3R sites in human brain were detected in the globus pallidus, medial and lateral segments, caudate, putamen, hippocampus, external layers of the cortex in particular the limbic and frontal cortex with lower levels in the temporal and insular cortex. Highest expression was detected in the cerebral cortex, hippocampal formation, basal ganglia and hypothalamus, areas associated with cognition, motor activity and emotional behaviours (Martinez-Mir et al., 1990 and Drutel et al., 2001). In these areas, the neurotransmitter histamine, in close association with the other biogenic amines controls numerous (patho)-physiological processes. The cortex and hippocampus are associated with cognition, the hypothalamus with sleep and homeostatic regulation and specific thalamic areas, dorsal root ganglia and spinal cord with nociception (Cannon et al., 2007).

Previous autoradiographical studies looking at H_3R expression have drawbacks due to the use of non-selective compounds such as [^{3}H] RαMHA and [^{3}H] clobenpropit. The problem associated with using radiolabelled agonists to measure receptor binding densities is G-protein coupling can cause the selective identification of only subsets of an entire receptor population since agonist binding shows increased affinity for receptors in their active state i.e. when they are bound to GTP over their inactive state. It is preferential to use radiolabelled antagonists, however first generation imidazole containing antagonists also have drawbacks such as [^{3}H]-thioperamide which displayed cross reactivity with cytochrome P_{450} isoenzymes and showed variable affinities across the species. The discovery

of the H_4R in the past 10 years has also lead to the re-evaluation of H_3R drug selectivity, since many older compounds such as RαMHA, clobenpropit, thioperamide and burimamide have also been shown to be selective for the H_4R (Leurs, 2009a,b). Re-evaluation of H_3R binding using highly selective compounds is needed to get a better understanding of H_3R expression in the CNS.

The histaminergic system plays an important role in the central nervous system regulation and behaviour through its role as an autoreceptor, regulating the synthesis and release of histamine and as a heteroreceptor, negatively regulating the release of a variety of other neurotransmitters including acetylcholine, dopamine, glutamate and gamma-aminobutyric acid (Esbenshade et al., 2006, Bonaventure et al., 2007, Esbenshade et al., 2008). Given its widespread distribution and its ability to affect multiple neurotransmitter systems, H_3R antagonists are promising clinical candidates for the treatment of excessive day time sleepiness (narcolepsy), pain disorders, obesity and cognitive disorders and ADHD (Cannon et al., 2007, Medhurst et al., 2007, Medhurst et al., 2009 and Chazot, 2010).

5.2.2 The histaminergic system in neurodegenerative dementias

There are indications that histamine deficits are present in Alzheimer's AD, however it is unknown whether these are specific for certain brain regions, including changes in histamine receptor numbers, or are specific for AD amongst other neurodegenerative disorders. The importance of the histaminergic system in AD is difficult to assess due to a number of conflicting

reports. For example, histamine levels in AD brains have been reported to be increased in temporal and frontal cortex, basal ganglia and hippocampus (Cacabelos et al., 1989). However, other studies have shown decreases in histamine content in the hypothalamus, hippocampus and temporal cortex (Mazurkiewicz-Kwilecki and Nsonwah., 1989 and Panula et al., 1998). Histaminergic cell bodies are located in the TMN, where neurofibrillary tangles (NFTs) are found. NFTs are particularly concentrated in the region containing histaminergic perikarya compared with surrounding areas (Airaksinen et al., 1991 and Nakamura et al., 1993) and together with cholinergic basal forebrain nuclei, the TMN has been described as an early affected subcortical nucleus for the presence of NFT (Braak et al., 1991). The number of histaminergic cell bodies in the TMN was shown to be similar to that of normal brains (Airaksinen et al., 1991). In contrast, another group showed a significant reduction in large-sized histamine containing neurons in the TMN where numerous NFTs were found, indicative of a central histaminergic dysfunction (Nakamura et al., 1993). HDC activity, also a marker of the histaminergic system, has been shown to be decreased in AD compared with elderly controls (Schneider et al., 1997).

Whilst there are conflicting data about the histamine content in the brain of AD patients, one recent study using a highly selective H_3R ligand had shown the level of H_3R expression to be unaltered in the late stages of human AD compared to age matched controls, as well as in TASTPM mice (a mouse model of AD) compared with wild type mice (Medhurst et al., 2007 and Medhurst et al., 2009).

The H_3R signalling cascade has also to been linked to the involvement in AD and DLB. Activation of the H_3R results in the coupling to G-protein $G_{i/o}$ (Clark and Hill 1996), which in turn leads to activation of effector molecules such as MAPK, PLA_2 and PI3K (Drutel et al., 2001 and Giovanni et al., 2003). Activation of PLA_2 results in the release of arachidonic acid, docosahexaenoic acid and lysophospholipids, which are substrates for the synthesis of potent lipid mediators, platelet activating factor, eicosanoids, and 4-hydroxynonenal. 4-hydroxynonenal is the most cytotoxic metabolite, and is associated with the apoptotic type of neural cell death and is markedly increased in neurological diseases like ischemia, AD and PD (Farooqui et al., 2006), further supporting a role for H_3R blockade with antagonist/ inverse agonist and hence a reduction in the cytotoxic 4-hydroxynonenal.

Activation of MAPK and PI3K results in the phosphorylation of ERKs and PKB. Activation of PKB phosphorylates GSK3β, a major tau kinase in the brain (Sun et al., 2002). The MAPK pathway is thought to be important in memory consolidation and neuronal plasticity (Thiel et al., 2001 and Thomas et al., 2004), and the activation of PKB/GSK3β pathway is important in neuronal migration, protection against neuronal apoptosis (Brazil et al., 2004) and is believed to be altered in AD, neurological disorders (Rickel et al., 2004 and Le et al., 2002) and schizophrenia (Emamian et al., 2004). Furthermore, loss of regulation of GSK3β is linked to disease such as diabetes, insulin resistance and AD (Jope et al., 2004).

Many neurotransmitter systems, including acetylcholine, dopamine, serotonin and glutamate contribute to specific aspects of cognition. H_3R antagonists

have been shown to increase the release of histamine, as well as noradrenalin, dopamine and acetylcholine, making H_3R antagonists an attractive drug target for cognitive disorders.

5.2.3 Therapeutic potential of H_3R ligands

A number of H_3R antagonists have been discovered and one such compound (pitolisant) has now entered advanced clinical development focussing on narcolepsy and cognitive disorders (Schwartz et al., 2010 and Schwartz et al., 2011). Understanding the molecular structure of the H_3R has increased considerably, providing a new generation of non-imidazole containing H_3R antagonists. Non-imidazole containing H_3R antagonists are currently in clinical trials for AD, ADHD, narcolepsy, pain and obesity (Leurs et al., 2005 and Chazot, 2010).

The histaminergic system has been long known to be involved in arousal since the development of 1^{st} generation anti-histamines. H_3R antagonists/ inverse agonists increase brain histamine, thence increasing wakefulness and reducing rapid eye movement (REM) and slow-wave sleep during the sleeping phase in normal animals. $H_3R^{-/-}$ mice are insensitive to the wake promoting effects of H_3R antagonists (Li et al., 2008). H_3R antagonist/ inverse agonist may be of use in diseases that display excessive daytime sleepiness (EDS) such as PD, DLB and AD. Recently Lin et al. (2008) published data on phase two clinical trials showing that the H_3R inverse agonist, pitolisant significantly improved EDS parameters in comparison to placebo in a pilot phase II study, and is currently undergoing follow-up phase III clinical trials.

Arousal and attention also play an important part in the cognitive process which H_3R antagonists have been shown to enhance. The histaminergic system innervates several structures that are known to be involved in cognition such as the basal forebrain, cerebral cortex, cingulate cortices, amygdala and thalamus (Brown et al., 2001). High levels of H_3R have been shown to be expressed in the cerebral cortex (Pollard et al., 1993), which is densely innervated by cholinergic neurons. Histamine acting on the H_3R has been shown to be involved in the inhibition of potassium evoked release of [^{3}H]-acetylcholine from rat cortical slices (Clapham et al., 1992 and Arrang et al., 1995), as well as impairing object recognition and a passive avoidance response (Blandina et al., 1996). H_3R antagonists were able to reverse this inhibition (Blandina et al., 1996). This was the first indication that the H_3R had a regulatory role in cortical acetylcholine *in vivo*, and suggested a role for histamine in learning and memory. This implied the potential of targeting the H_3R for the treatment of dementia disorders associated with impaired cholinergic function. It is thought that histamine indirectly influences the decrease in acetylcholine release through increasing the release of GABA from interneurons in the cortex which in turn inhibits acetylcholine release (Giorgetti et al., 1997). The opposite can be seen with H_3R blockade with antagonists, acetylcholine levels are enhanced in the prefrontal cortex and in the dorsal hippocampus accompanied with an improvement of cognitive functions in an array of animal cognitive function tests (Fox et al., 2005). Histamine has also been shown to interact with the polyamine site on the NMDA receptor helping facilitate long-term potentiation in rat hippocampal slices (Witkin and Nelson, 2004).

In neurophyschiatric disorders such as AD, ADHD and schizophrenia, cognitive deficits play a major role in the disease (Leurs et al., 2005). Decreased levels and/ or function of acetylcholine in the pre-frontal cortex and nucleus basalis magnocellularis are thought to be a major contributor to age related cognitive decline. Increased brain histamine is also positively correlated with age and may play a role in decreasing acetylcholine (Prell et al., 1991). It is thought that H_3R antagonists may be able to prevent the reduction in acetylcholine through its heteroreceptor characteristic (Blandina et al., 1996, Orsette et al., 2002 and Bacciottini et al., 2002). For testing the potential of compounds in ameliorating cognitive dysfunction in the clinic, a variety of rodent behavioural tasks can be used to analyse different domains of cognition that may have some relevance to the human disease. Impairments in spatial orientation and memory (observed in patients with AD) can be assessed with different paradigms such as the water maze, radial arm maze or Barnes maze. Deficits in social memory (in AD) can be measured by a social recognition task in rodents. Impulsivity, on the contrary, which seems to be a particular problem in patients with ADHD, can be studied in the five-trial inhibitory avoidance task in SHR pups, as well as in the five-choice stimulus reaction time test. Executive function is a cognitive domain impaired in schizophrenic patients and is assessed using attentional set shifting assays or models of cognitive flexibility (Gemkow et al., 2009). Generally, H_3R antagonists improve memory either by the increase in histamine (Miyazaki et al., 1995 and Miyazaki et al., 1997) or through the release of other neurotransmitters such as acetylcholine, noradrenalin and dopamine (Blandina et al., 1996), while H_3R agonists were shown to be inhibitory.

Thioperamide has been shown to increase acetylcholine in the rat hippocampus (Mochizuki et al., 1994) and enhances recall of a passive avoidance response in rats (Giovannini et al., 1999) and senescence-accelerated rats (Meguro et al., 1995). H_3R antagonists also show promise in short term memory novel object recognition test (Giovannini et al., 1999) and social recognition tests (Prast et al., 1996). While immepip, a H_3R agonist produced cognitive deficits in tests of olfactory and social memory (Prast et al., 1996). Abbott laboratories reported that A-317920, a highly potent H_3R antagonist, was as effective as methylphenidate (Ritalin) and ABT-418 (a nicotinic receptor ligand), both of which are clinically effective drugs in AD (Hancock et al., 2003). ABT-239 entered clinical trials after displaying promising results in preclinical trials in models of ADHD and AD. ABT-239, a H_3R antagonist increased acetylcholine in the prefrontal cortex and hippocampus (Cowart et al., 2004), improved learning in five trail inhibitory avoidance using rat pups, improved recall in a social memory test and improved spatial working and reference memory in a water maze (Fox et al., 2004 and Esbenshade et al., 2004). A-304121, also shows promising procognitive effects in rodent models (Fox et al., 2004 and Esbenshade et al., 2004). GSK189254 a H_3R inverse agonist has been shown to significantly improve performance of rats in diverse cognition paradigms, including passive avoidance, water maze, object recognition and attentional set shift. The data so far for H_3R antagonists point to a possible therapeutic potential for diseases where cognitive deficits are already present such as AD and other dementias.

5.2.4 Animal models: CD-1-mice and TASTPM mice.

S-1 rats tested on the radial maze behavioural test were capable of readily solving this behavioural paradigm, however CD-1 mice were not. This lead to the idea that mice generally may have limited learning capacity compared to rats, however the performance of other strains needed to be tested to distinguish if it was a result of strain difference rather than species variation (Mizumori et al., 1982). Recent data have shown CD-1 mice develop early behavioural and learning deficits in middle-aged male and female CD-1 mice (12 months) compared with young 3 month CD-1 mice (Michalikova et al., 2007 and Ennaceur et al., 2008). CD-1 mice have high mortality rates compared to other strains of mice due to their high susceptibility to immuno-pathologies and increased levels of amyloidosis with age, which is thought to be the cause of premature death (Frith and Chandra, 1991, Engelhardt et al., 1993 and Lavie and Weinreb 1996). Recent unpublished data from our laboratory has shown that CD-1 mice have sex-linked differential mitochondrial activities and deficits in heat shock protein and BDNF expression levels (Burroughs & Chazot, unpublished).

AD is characterized by deficits in a number of neurotransmitter systems which are believed to result in cognitive dysfunction as well as neuropsychiatric behaviour. Loss of cholinergic neurons in the basal forebrain is one of the most prominent and consistent events occurring in AD (Whitehouse et al., 1982). AD is characterized by the aggregation of amyloid-β (Aβ) protein accumulating into plaques (Hardy and Selkoe, 2002), as well as hyperphosphorylation of tau protein, which aggregates into NFTs (Delacourte et al., 1999). Individuals with AD show multifaceted cognitive impairments that

progressively interfere with their day-to-day functioning. Animal models of AD are a useful tool for exploring the pathological outcomes of the disease as well as preventative measures for disease acceleration, and therefore protection from irreversible neuronal loss, proposed to be caused by $A\beta_{42}$ plaques and NFTs. The TASTPM mouse model is characterised by activated microglia, reactive astrocytes, and increased expression of cytokines and complement factors surrounding amyloid deposits that develop in the cortex and hippocampus (Figure. 5.1). The Aβ plaques develop from the age of 3 months (Burroughs & Chazot, unpublished), with evidence of NFTs or neuronal loss later in the time course (Howlett et al., 2004 & 2008).

Immunohistochemistry showing labelling of Aβ plaques in TASTPM mice

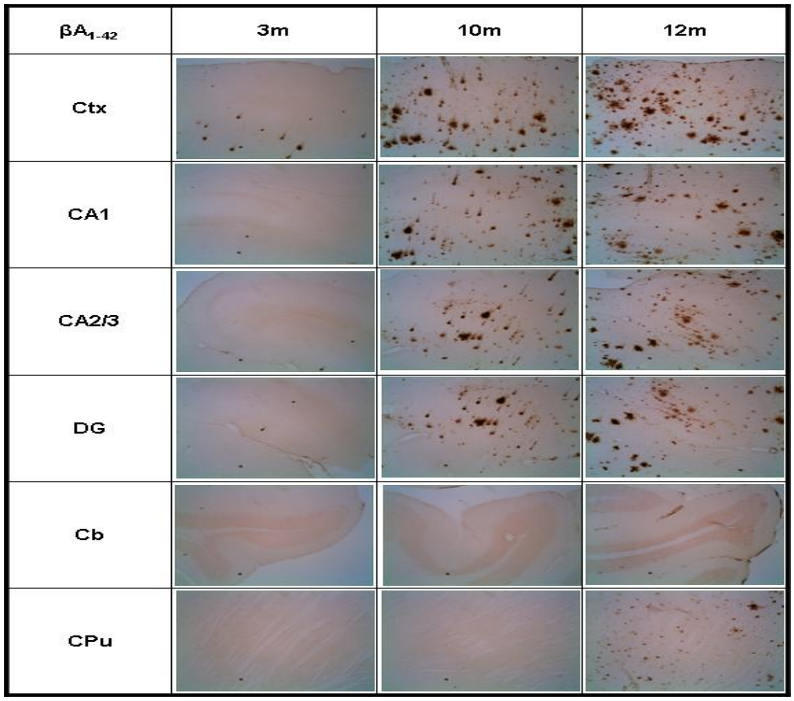

Figure 5.1 shows immunohistochemical labelling of Aβ plaques in CA1, CA2 & 3, cortex (Ctx), dentate gyrus (DG), cerebellum (Cb) and caudate putamen (CPu) in TASTPM mice at three time points 3, 10 and 12 months

In chapter 4, the pharmacology of the highly potent and selective H_3R antagonist [^{3}H] GSK189254 was investigated for each of the following major human isoforms, H_3R_{445}, H_3R_{365} and the $H_3R_{329.}$ The aim of this chapter was to investigate the abundance and distribution of the human histamine H_3R protein in DLB and AD cases and respective controls using [^{3}H] GSK189254. The secondary aim was to probe any differences in the anatomical distribution patterns between control and diseased tissue, and also any age-related changes therein. The hypothesis was that the number of H_3R is preserved in normal aging and in human dementias.

5.3 Methods

5.3.1 CD-1 and TASTPM mice tissue preparation

CD-1 or TASTPM mice were sacrificed by CO_2 narcosis and brains were rapidly dissected and dehydrated using sucrose infiltration. Brains were initially placed in 10% sucrose, followed by 20% sucrose made up with phosphate buffered saline. Once the brains had been dehydrated, they were snap frozen in iso-pentane at -40ºC for 3 minutes and stored at -80ºC. Samples were sliced horizontally using a microtone into 20 µm thick sections at -25ºC**.** Sections were collected on to poly-D-lysine coated glass slides and stored at -20ºC.

5.3.2 In vitro Autoradiography of rodent brain tissue using [^{3}H]-GSK189254

The autoradiography method used was that described by Medhurst et al., (2007). Brain sections were left to reach RT for 1 hour before the protocol commenced. The sections were incubated in (50 mM Tris, 5 mM EDTA pH 7.7) containing 2 X K_D (5 nM) [^{3}H] GSK189254 (specific activity = 81 Ci/mmol, stored at -20^{o}C from Dr Medhurst (GSK, Harlow, UK) for 1 hour at RT, until equilibrium is reached. Non-specific binding was defined using 10 µM unlabelled RαMHA. The reaction was terminated by five 3 minute washes in (50 mM Tris, 5 mM MgCl pH 7.7) at 4^{o}C and a final wash in dH_2O at 4^{o}C. Sections were left to dry in a stream of cold air for 1 – 2 hours. The sections were then transferred to X-ray cassettes, each including tritium autoradiographical microscale as calibration standards, and exposed against tritium-sensitive hyperfilm for 6 weeks at 4^{o}C. The exposed films were then

developed in D-19 developer (Kodak) for 5 minutes at RT, fixed for 6 minutes in Unifix (Kodak), washed under running water for 20 minutes and air-dried.

5.3.3 Determining the working concentration of [^{3}H] GSK189254

The radioligand concentrations used were greater than those stated by Medhurst el al. (2007). Preliminary saturation binding assays performed prior to the autoradiography showed the hH_3R 445 isoform has a K_D of 0.16$\pm$ 0.04 nM (described previously in chapter 4). The concentration of radioligand used was selected as approximately 2 x K_D (0.3 nM) to ensure that each autoradiography run detected an acceptable number of receptor binding sites. Before starting the experiment, the concentration of the radioligand was checked by taking 10 µl aliquots into a scintillation vial with 2 ml scintillation fluid (Packard Ultima Gold) and measuring the dpm (disintegrations per minute) value in a Packard tri-carb 1900CA scintillation counter. All rodent and human tissue were analysed using [^{3}H] GSK189254 ligand.

5.3.4 Image Analysis

The resulting brain images on the film were captured using a Dage 72 MTI CCD72S video camera and were quantitatively analysed by computer-assisted densitometry using Microcomputer Imaging Device (MCID Elite) version 7.0 software from imaging research Inc., Ontario, Canada. The radioactive Tritium standards were used to calculate a standard curve for each autoradiogram, which allowed the conversion from optical density values to units of concentrations (femtomoles per mg of tissue protein), for each brain region analysed. Non-specific binding was defined using 10 µM RαMHA, non-

specific binding tissue sections were present on the same film as each of the corresponding total binding tissue sections for the same case. Specific binding was determined by subtracting mean non-specific binding from mean total binding. Brain structures were identified by reference to the atlas of the Human Brain (Mai et al., 1997) and the mean and standard deviations for each brain structure in each section were calculated. Inter-assay variability was reduced by using ligand concentrations that were at least twice the ligand affinity, using ligand from the same batch for each autoradiographical run, and by standardising each film using calibration microscales.

All sections were then analysed by digital autoradiography using a Beta-Imager 2000 instrument (Biospace, Paris, France), radioactivity was measured by counting the number of β particles from delineated areas and the results expressed as mean specific binding counts per minute (cpm) per square millimetre (cpm/mm^2; *n* = 12-16 cases per group).

5.3.5 Statistical Analysis

Statistical analysis performed involved correlation analysis and students unpaired *t*-test, indicated with the use of Microsoft Excel and GraphPad Prism to analyse individual regions of the brain. Statistical significance was set at the $p<0.05$ level for the correlation analysis, with a minimum n value of 3 or more, and at $p<0.05$ level for the students *t*-tests with a minimum n value of 3 or more for each data set. Graphs were constructed using GraphPad Prism version 4. One-way Anova tests were also performed using GraphPad Prism version 4 to analyse statistical differences across data sets. Statistical significance was set at the $p<0.05$.

5.3.6 Mice used

Brains from nine CD-1 male mice and nine TASTPM male mice at three time points (3, 9 &12months and 3, 7 & 13 months, respectively, were subjected to ligand autoradiography. Figure 5.2 shows a nissl staining of a mouse brain to aid in the identification of key brain structures.

Nissl stain of mouse brain, (A) coronal view (B) sagittal view

A **B**

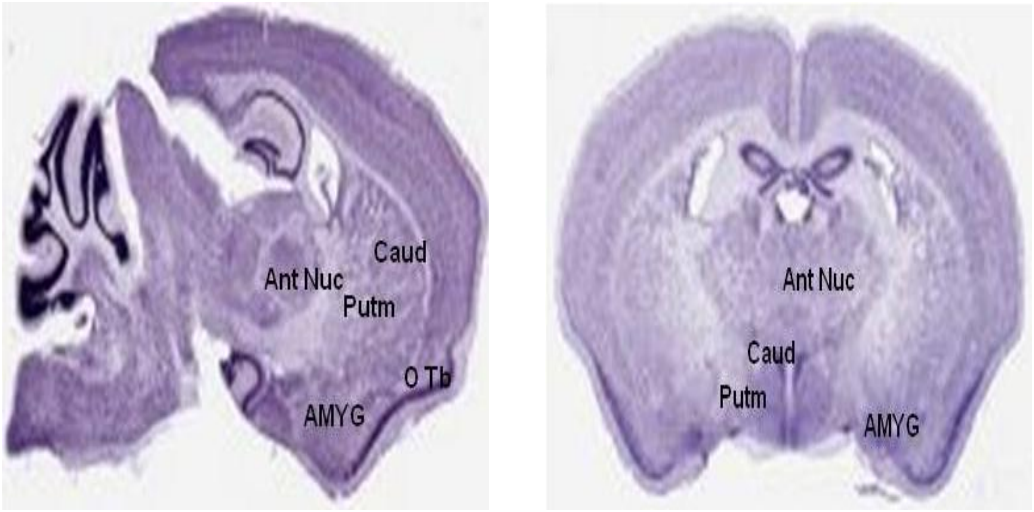

Figure 5.2: (A) Coronal and (B) sagittal sections from a mouse brain map.
Amyg = amygdala; Ant Nuc = anterior nucleus of thalamus; ant = anterior; Caud = caudate; O Tb = olfactory tubercle; Putm = putamen

5.3.7 Human case details and diagnostic criteria

All human brain tissue was obtained from Newcastle Brain Tissue Resource Bank LREC (Newcastle and Tyneside) with full ethical approval (2002/295). Frozen tissue was collected at autopsy and 1 cm coronal slices from the left hemisphere were snap frozen in liquid Arcton (ICI) and stored at -70^{o}C. The sections were then stored at -80^{o}C. Prior to sectioning, tissue slices were warmed to 15^{o}C and blocks containing the striatum were sub-dissected and

mounted onto cryostat chucks with 8% carboxymethylcellulose. Coronal sections were cryostat sectioned at a thickness of 20 µm using a Brights OTF cryostat onto Vectabond-coated glass slides, air dried for 1-2 hours and stored at -80^{o}C prior to receptor autoradiography. The right hemisphere was used for histopathological examination, following formalin fixation and paraffin embedding. Cortical and hippocampal neurofibrillary tangles were demonstrated using a modification of Palmgren's silver technique (Cross 1982) and the von Braunmühl silver impregnation technique (Bancroft et al., 1990) was used to identify senile plaques in 25 µm thick frozen sections cut from tissue blocks adjacent to those taken for paraffin processing. Counts of NFTs and neuritic plaque number were made from fields across the entire cortical ribbon, as described in Perry et al., (1990). Lewy-bodies in the substantia nigra were visualised by the use of haematoxylin and eosin staining, cortical Lewy-bodies and dystrophic neuritis were detected using ubiquitin immunohistochemistry on 5 µm thick paraffin embedded sections. Neurones in the substantia nigra were quantified following cresyl fast violet staining of 20 µm thick paraffin sections.

Control cases had no history of psychiatric or neurological disorder and had no neuropathological indications of AD, DLB or any other neurological disorder.

AD cases used in this study fulfilled NINCDS-ADRDA criteria (McKhann et al., 1984). Neuropathologically, there were NFTs and neurite plaques in the hippocampus and cortex to fulfil CERAD (Braak et al., 1991) and Reagan (The National Institute on Aging and Reagan Institute Working Group on diagnostic criteria for the neuropathological assessment of Alzheimer's

disease, 1997) criteria for pathological diagnosis of AD. DLB cases were clinically diagnosed by the presence of a progressive cognitive impairment seen in conjunction with at least two of the following symptoms: recurrent visual hallucinations; fluctuating cognition with pronounced variations in attention and alertness; spontaneous motor features of parkinsonism (McKeith et al., 1996). DLB and PD cases were distinguished from AD by the presence of brain stem and cortical Lewy-bodies, “Lewy neurites” in the CA2/3 and endplate segments of the hippocampus (McKeith et al., 1996), and by lower or moderate Alzheimer-type pathology with fewer NFT than found in AD.

5.3.9 Human cases used

The 43 cases chosen for these studies were at the level of the striatum (caudate nucleus and putamen) corresponding to coronal brain levels 9-15 using the Coronal Map of Brodmann Areas in the human Brain (Perry 1993), (Figure 5.3). Of the 43 cases, 12 were control cases, 15 AD cases and 16 DLB cases (table 5.1). For each case 5 replicates were used to measure 3 total and 2 non-specific radioligand binding values.

Summary of 43 human cases:

	n =			Age (years)			PM Delay (hours)		
	Total	Females	Males	Range	Mean	SD	Range	Mean	SD
Control	12	7	5	70-91	80.92	6.97	10-96	42	22.44
DLB	16	8	8	64-87	77.13	7.19	4-60	31.56	18.18
AD	15	9	6	74-91	83.27	4.53	4-82	33.40	21.69

Table 5.1: Summary of the 43 cases chosen for the study. (SD = standard deviation of either age or PM delay values. PM delay = post mortem delay, that is, time between death and freezing of the tissue, to allow for post-mortem examination).

Coronal Map of Brodmann Areas in the human Brain:

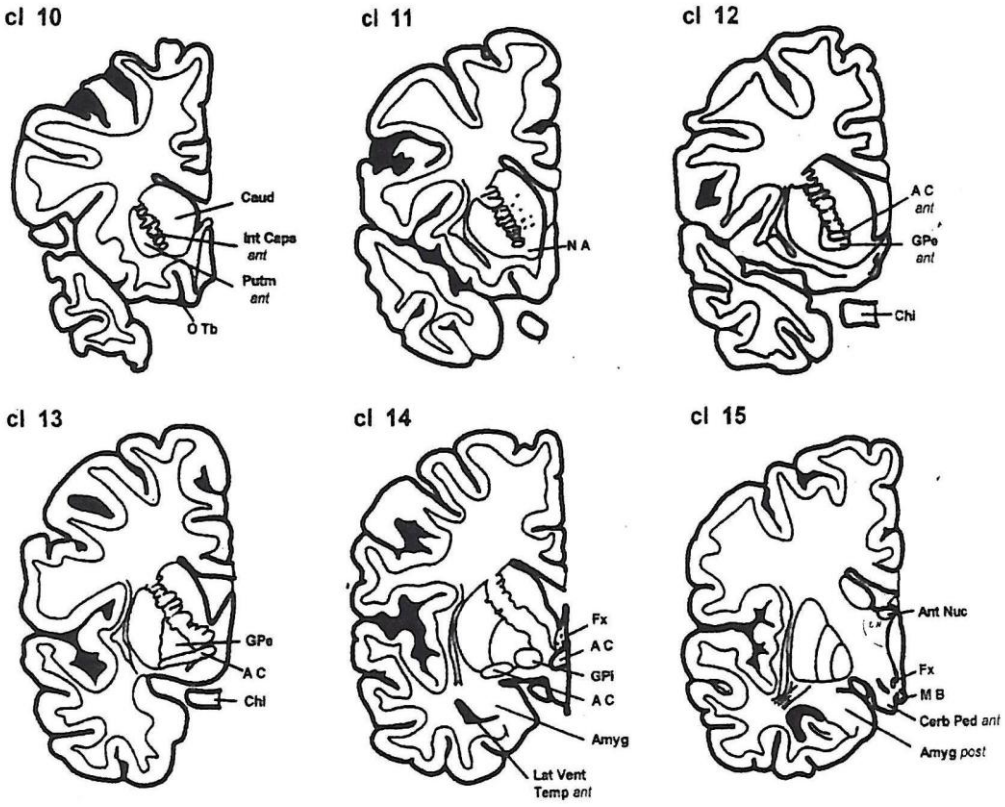

Reproduced with kind permission of IAH Newcastle-upon-Tyne

Figure 5.3: Coronal levels of striatum, 0.5 cm apart. AC = anterior commissure; Amyg = amygdala; Ant Nuc = anterior nucleus of thalamus; ant = anterior; Caud = caudate; Cerb Ped = cerebral peduncle; Chi = optic chiasma; cl = coronal level; Fx = fornix; GPe = external globus pallidus; GPi = internal globus pallidus; Int Caps = internal capsule; Lat Vent Temp = temporal horn of lateral ventricle; MB = mammillary body; NA = nucleus accumbens; O Tb = olfactory tubercle; post = posterior; Putm = putamen

5.3.10 *In vitro* Autoradiography of human brain tissue using [^{3}H] GSK189254

Human autoradiography was performed as in section 5.3.2 except the human brain tissue were incubated in (50 mM Tris, 5 mM EDTA pH 7.7) containing 2 X K_D (0.3 nM) [^{3}H] GSK189254 (specific activity = 81 Ci/mmol, stored at -20^{o}C

from Dr Medhurst (GSK, Harlow, UK) for 1 hour at RT, until equilibrium is reached.

5.3.11 The Mini Mental State Examination (MMSE)

The Mini Mental State Examination (MMSE), validated and widely used since its creation in 1975, is an effective tool for assessing cognitive mental status. The MMSE is used to detect cognitive impairment and monitor response to treatment. It is an eleven question test covering five areas of cognitive function: orientation, attention/ calculation, recall and language, and the ability to follow simple verbal and written commands. A score of 23 or below, from a possible 30 is indicative of cognitive impairment. The test is effective but does have limitations, for example, patients who are hearing and visually impaired or who have low English literacy, or with communication disorders may perform poorly even when cognitively intact (Folstein et al., 1975). The test provides a total score that places the individual on a scale of cognitive function.

5.3.11 Unified Parkinson Disease Rating Scale (UPDRS)

The UPDRS is a rating tool to follow the longitudinal course of PD. It is made up of the 1) Mentation, Behaviour and Mood, 2) Activities of Daily Living (ADL) and 3) Motor sections. These are evaluated by interview. Some sections require multiple grades assigned to each extremity. A total of 199 points are possible, where 199 represent the worst (total) disability, and 0 represents no disability.

5.4 Results

5.4.1 Autoradiography results for CD-1 and TASTPM mice

The first section of the results represents qualitative analysis of the binding data for CD-1 and TASTPM mice whilst the second section of data shows quantitative analysis of the binding levels in each tissue.

Figures 5.4 and 5.5 show digital photographic examples of [^{3}H] GSK189254 binding in CD-1 and TASTPM mice brain at each time point. In each of the examples shown, ligand binding was detected in the striatum, cortex and cingulate cortex regions.

Autoradiography showing H_3R labelling in CD-1 mice brain at 3, 9 & 12 months:

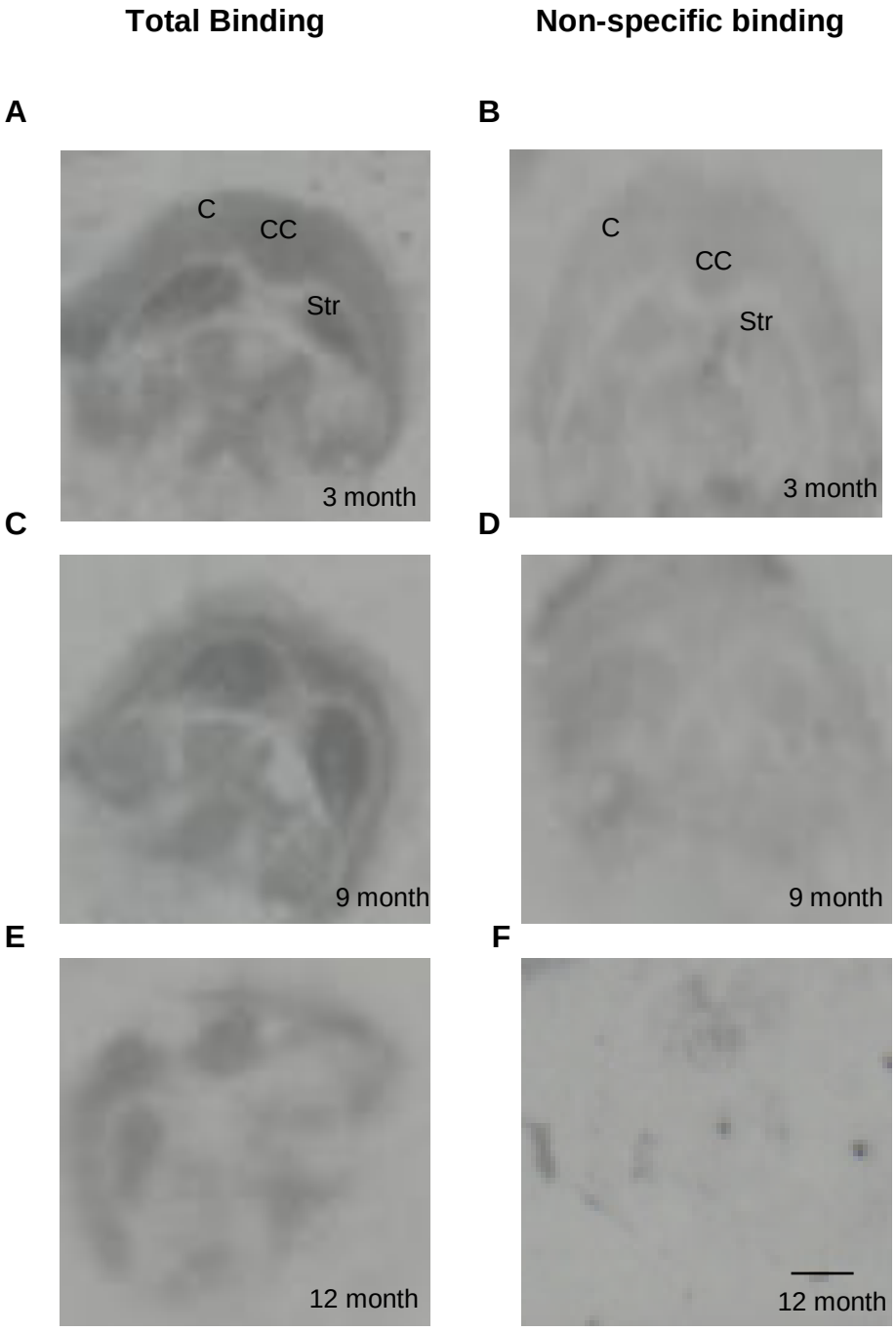

Figure 5.4: (A) Autoradiography of CD-1 mouse brain sections. Panels (A, C & E) represent total binding. Panels (B, D & F) represent non-specific binding defined by 10 µM R-α-methylhistamine. Age timeline panels (A &B) represent 3 months, panels (C & D) represent 9 months and panels (E & F) represents 12 months. C – Caudate, CC cingulate cortex and Str – Striatum. Scale bar = 250 µm and represents all images shown.

Autoradiography showing H_3R labelling in TASTPM mice brain at 3, 7 & 13 months:

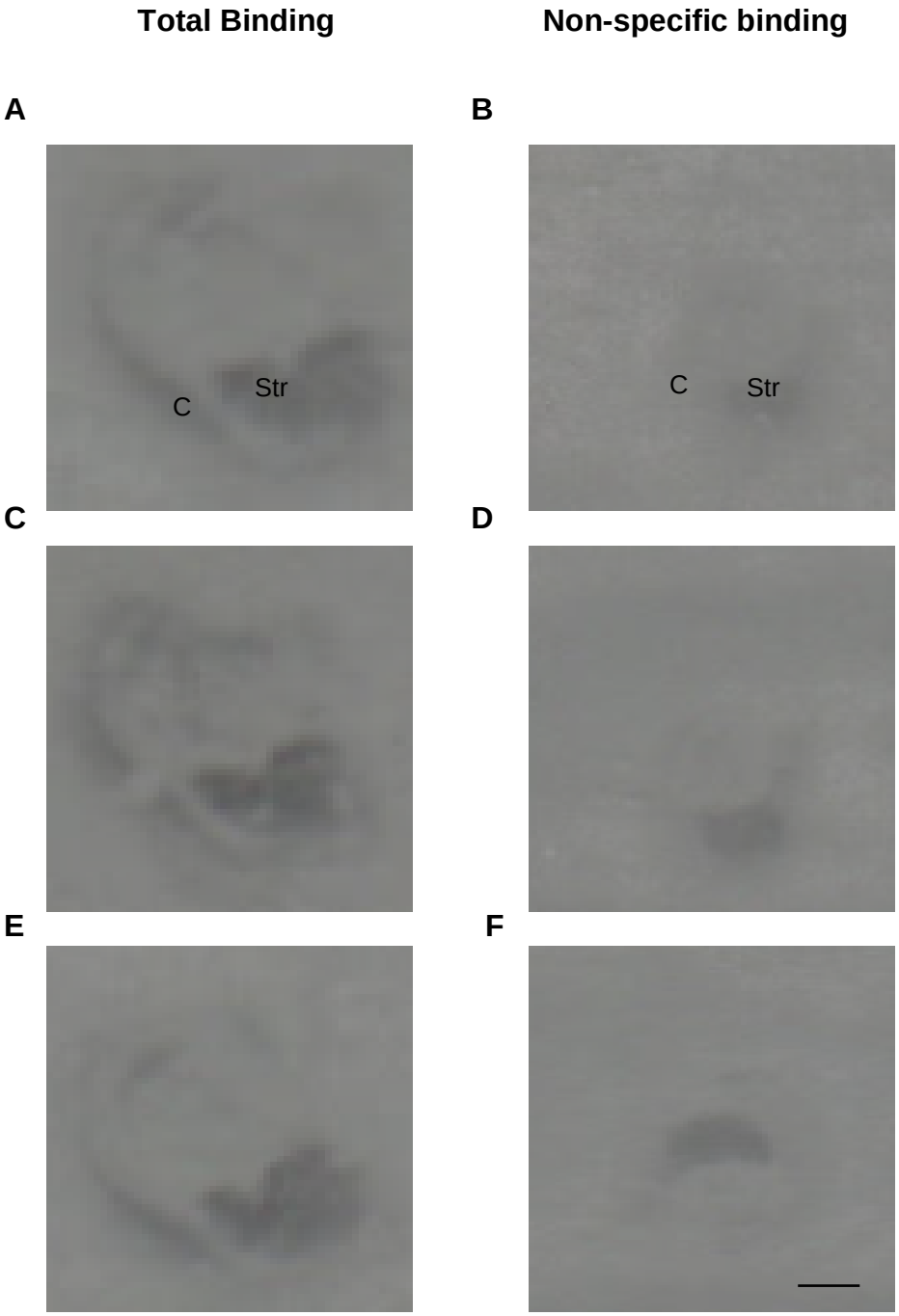

Figure 5.5: (A) Autoradiography of TASTPM mouse brain section. Panels (A, C & E) represent total binding. Panels (B, D & F) represent non-specific binding defined by 10 µM R-α-methylhistamine. Age timeline panels (A &B) represent 3 months, panels (C & D) represent 7 months and panels (E & F) represents 13 months. C – Caudate and Str – Striatum. Scale bar = 250 µm and represents all images shown.

5.4.2. Quantitative analysis of CD-1 and TASTPM mice

The data for each group were analysed to show the mean average specific binding cpm/mm^2 ± SD of [^{3}H] GSK189254 with n=3 in specific brain regions defined. Statistical analysis was performed using a one-way ANOVA test, indicated with the use of GraphPad Prism (version 4) to analyse between age time points in individual regions of the brain. Statistical significance was set at $p<0.05$ level for the one-way ANOVA analysis.

Statistical analysis of H_3R binding in regions of the CD-1 mouse brain:

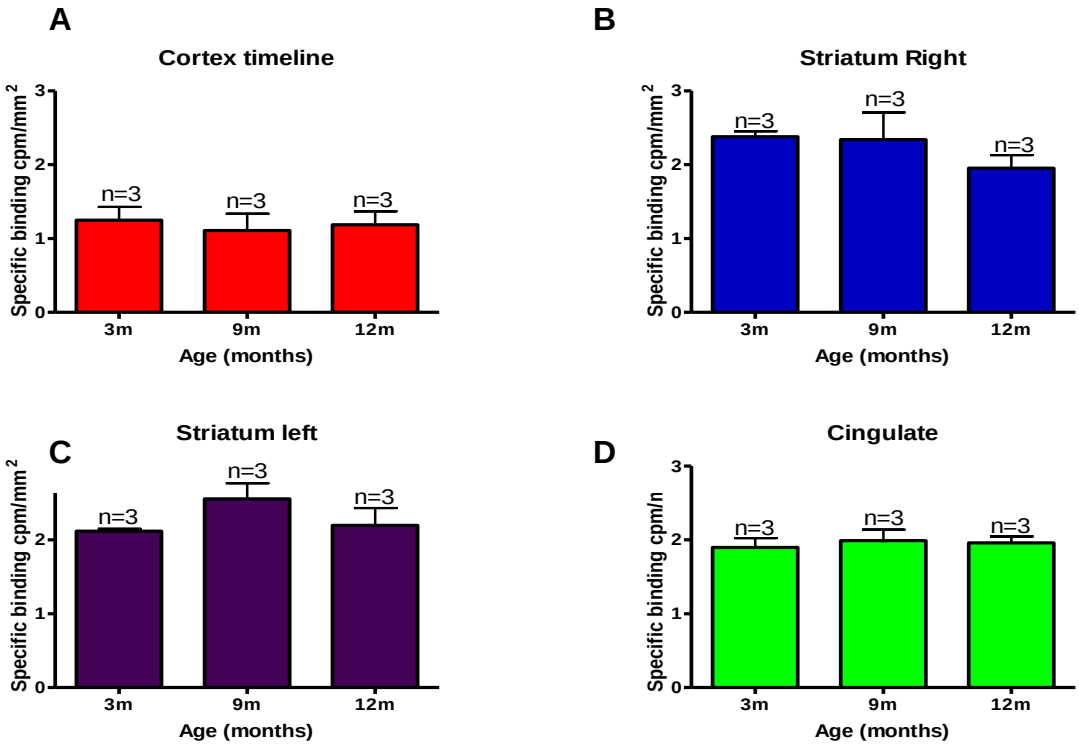

Figure 5.6: Graphs showing mean [^{3}H] GSK189254 specific binding (cpm/mm^2) densities (mean ± SEM for n determinations) for CD-1 mice at three time points 3, 9 and 12 months in (A) Cortex, (B) Striatum right hemisphere, (C) Striatum left hemisphere, (D) Cingulate cortex.

Figure 5.6 shows there were no significant differences in the mean binding densities of [^{3}H] GSK189254 in all brain regions analysed when comparing between the three age time points; 3, 9 and 12 months. Binding of the

radioligand showed higher levels of H_3R binding in the striatum and cingulate cortex with lower levels detected in the cortex.

Statistical analysis of H_3R binding in regions of the TASTPM mouse brain:

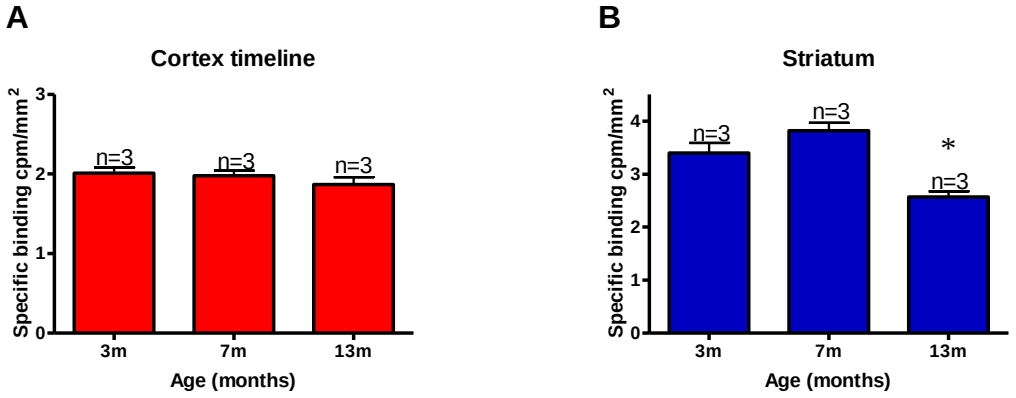

Figure 5.7: Graphs showing mean [^{3}H] GSK189254 specific binding (cpm/mm^2) densities (mean ± SEM for n determinations) for TASTPM mice at three time points 3, 7 and 13 months in (A) Cortex, (B) Striatum.

Figure 5.7 shows there were no significant differences in the binding densities of [^{3}H] GSK189254 in the cortex when comparing between the three age time points; 3, 7 and 13 months. However in the striatum there were significantly lower binding in the striatum of 13 month old TASTPM mice compared with 3 month ($p \leq 0.05$) and 7 month old ($p \leq 0.001$) TASTPM mice.

H_3R binding has been analysed in rodent brain and the next part will determine H_3R binding in human brain in normal aging and in age related dementias.

5.4.3 Human autoradiography results

The first section of the results shows typical human H_3R labelling obtained using [^{3}H] GSK189254. The second section of data shows quantitative analysis of the binding levels in each tissue. Figure 5.8 is an example showing the typical pattern of [^{3}H] GSK189254 labelling seen in many of the brain sections analysed. The section is cut at coronal level 10 (see Figure 5.3) where the striatal caudate and putamen areas are beginning to separate and the nucleus accumbens is visible. The insular cortex is also well labelled. The anterior cingulate cortex shows strong labelling and is located on the same side of the striatum as the caudate.

Autoradiography showing H_3R labelling in human brain using [^{3}H] GSK 189254

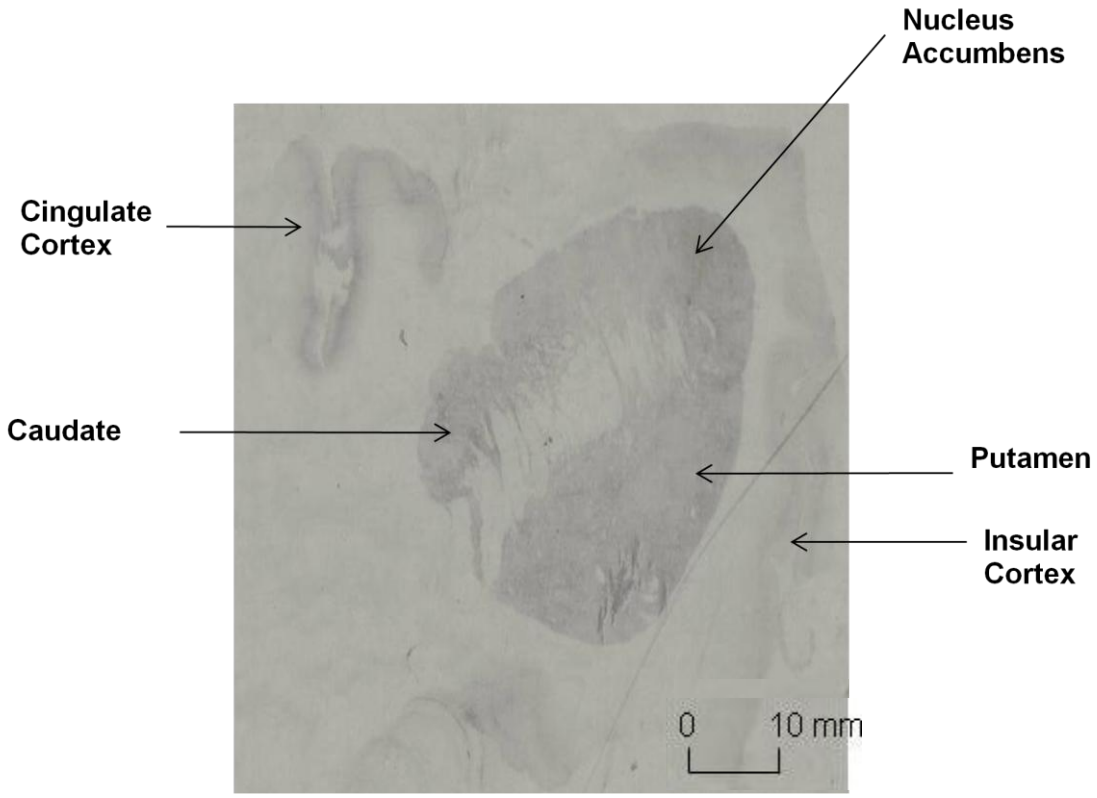

Figure 5.8: Representative image of a human brain section (80 years, female). Total H_3R labelling detected using [^{3}H] GSK189254.

Figures 5.9 below, shows digital photographic examples of [^{3}H] GSK189254 binding. Figure A represents total binding of the radioligand and figure B represents non-specific binding, defined by 10 µM RαMHA. As described in section 5.3.4., the specific binding was determined by subtracting the mean non-specific binding from the mean total binding. In each of the examples shown, ligand binding was detected in the caudate, putamen, nucleus accumbens, insular cortex, cingulate cortex regions and globus pallidus.

Autoradiography showing total and non-specific H_3R binding in human brain using [^{3}H] GSK 189254

A Total binding B Non-specific binding

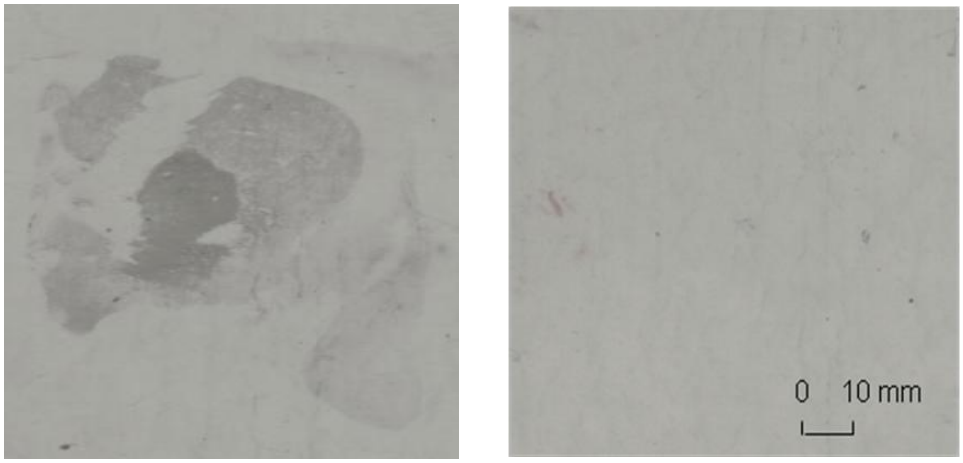

Figure 5.9: Autoradiography of human brain slices 87 years, female. (A) Total binding [^{3}H] GSK189254, (B) Non-specific binding [^{3}H] GSK189254. Non-specific binding was defined using 10 µM R-α-methylhistamine.

5.4.4 Quantitative analysis of human data - Effect of aging on H_3R binding in each group individually analysed

Brain tissue samples from 43 cases: 12 controls, 16 DLB and 15 AD cases described in section 5.3.4 and summarised in table 5.1 were assayed for radiolabelled GSK189254 binding by autoradiography. The data were analysed to show specific binding levels of [^{3}H] GSK189254 in various brain regions, correlating cpm/mm^2 with age at death of subject (in years). Estimated lines of best fit were produced using GraphPad Prism and are represented on each graph, indicating any age-dependant changes in binding levels in each tissue. The significance of the regression was determined from the generated p value, where $p \leq 0.05$ was considered to show a significant linear relationship between age and binding level. The generated correlation coefficient (r value) shows how well the data fits the regression line, where r = 1 shows strong correlation and r = 0 shows little or no correlation.

Statistical analysis of H_3R binding with age in regions of the human brain for control cases:

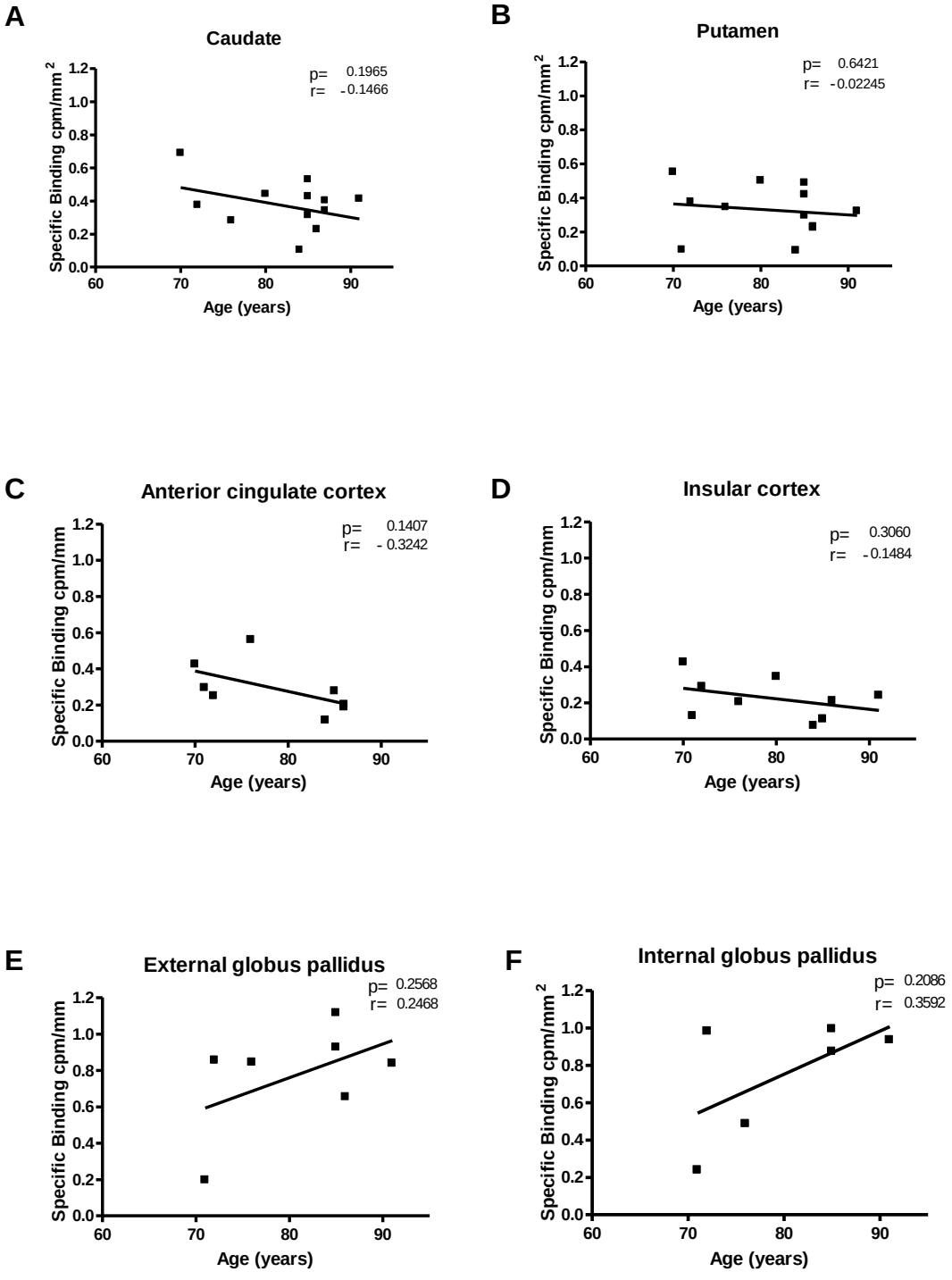

Figure 5.10 (A – F): Age-dependant absolute specific binding of [^{3}H] GSK189254 in control cases (n=12) in (A) Caudate, (B) Putamen, (C) Cingulate cortex, (D) Insular cortex, (E) External globus pallidus, (F) Internal globus pallidus. Significance of regression was determined from the generated p value, where $p \leq 0.05$ was considered to show a significant linear relationship between age and binding level.

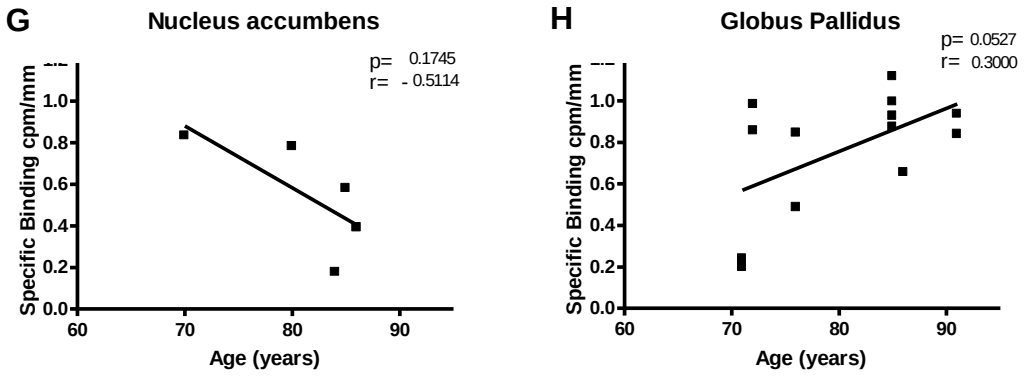

Figure 5.10 (G - H): Age-dependant absolute specific binding of [^{3}H] GSK189254 in control cases (n=12) in (G) Nucleus accumbens and (H) Combined globus pallidus. Significance of regression was determined from the generated p value, where $p \leq 0.05$ was considered to show a significant linear relationship between age and binding level.

Figure 5.10 shows specific binding levels in control cases examined for [^{3}H] GSK189254 in various brain regions against age. There were no significant age-dependant changes in all brain regions analysed ($p \geq 0.053$ in all areas). The r values ranged from -0.511 (nucleus accumbens) to 0.359 (internal globus pallidus). There appears to be a general trend showing lower ligand binding with increasing age in all brain regions except the globus pallidus.

H_3R binding does not appear to be altered in normal aging supporting previously published data of H_3R preservation. H_3R binding will next be determined in aged related dementias to see if disease state alters GSK189254 binding.

Statistical analysis of H_3R binding with age in regions of the human brain for DLB cases:

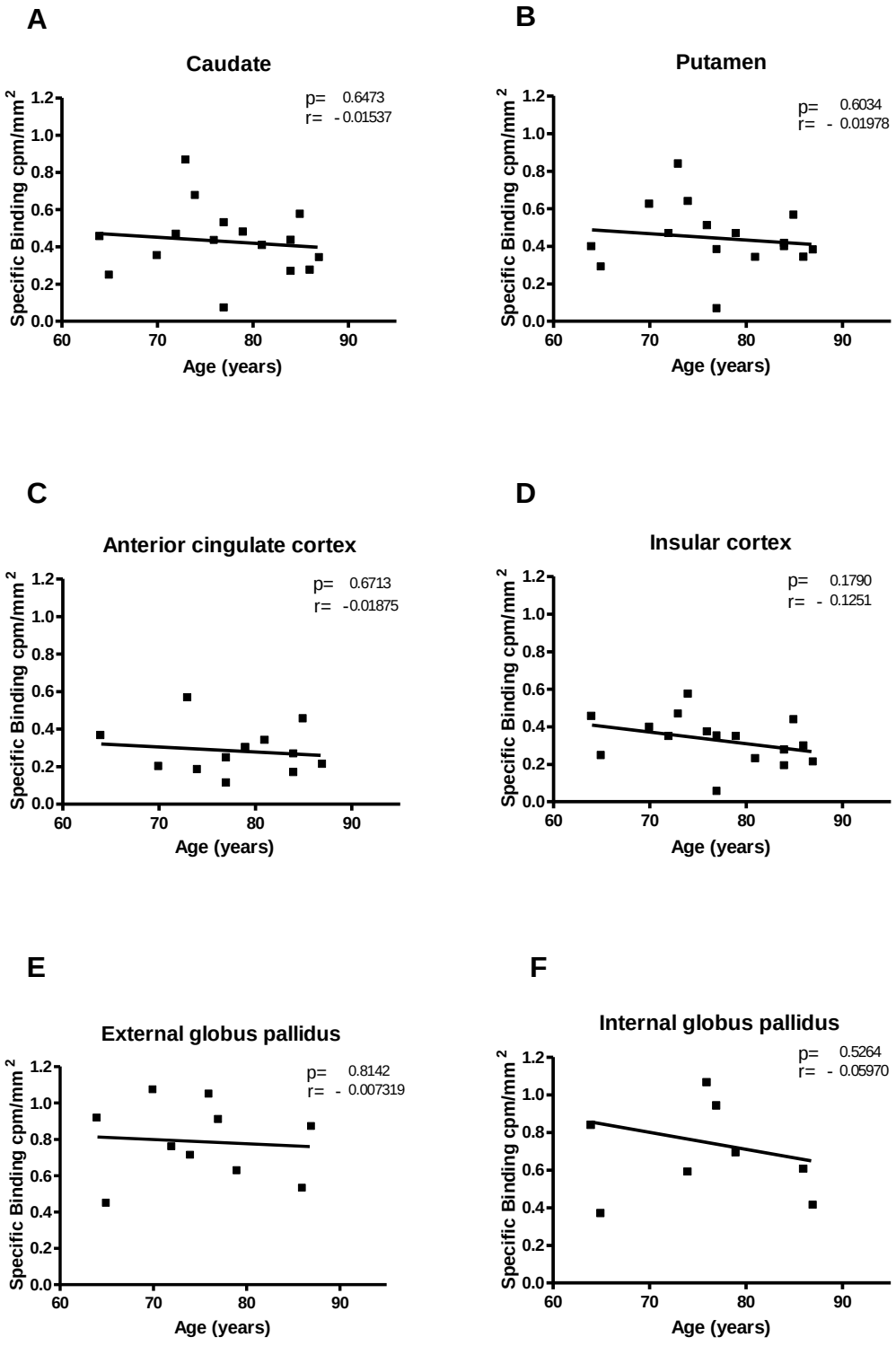

Figure 5.11 (A – F): Age-dependant absolute specific binding of [^{3}H] GSK189254 in DLB cases (n=16) in (A) Caudate, (B) Putamen, (C) Cingulate cortex, (D) Insular cortex, (E) External globus pallidus, (F) Internal globus pallidus. Significance of regression was

determined from the generated p value, where $p \leq 0.05$ was considered to show a significant linear relationship between age and binding level. .

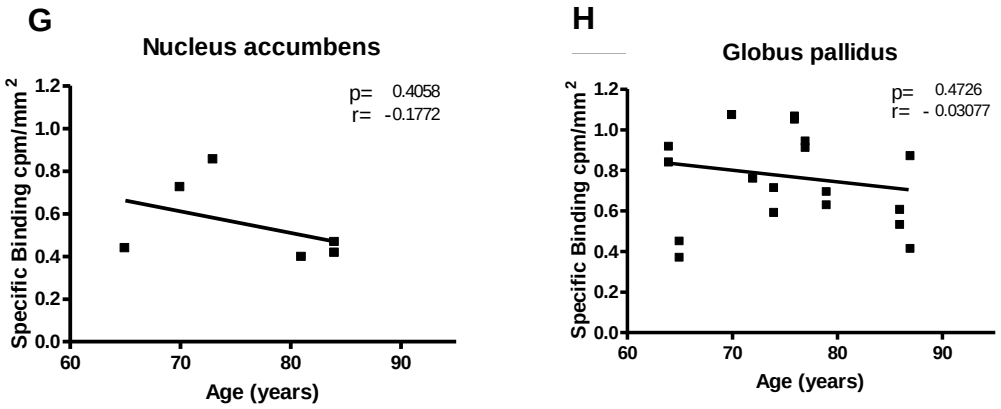

Figure 5.11 (G - H): Age-dependant absolute specific binding of [^{3}H] GSK189254 in DLB cases (n=16) in (G) Nucleus accumbens and (H) Combined globus pallidus. Significance of regression was determined from the generated p value, where $p \leq 0.05$ was considered to show a significant linear relationship between age and binding level.

Figure 5.11 shows specific binding levels in DLB cases examined for [^{3}H] GSK189254 in various brain regions against age. There were no significant age-dependant changes in all brain regions analysed ($p \geq 0.179$ in all areas). The r values ranged from -0.117 (nucleus accumbens) to -0.007 (external globus pallidus). There appears to be a general trend showing lower ligand binding with increasing age in all brain regions defined.

Statistical analysis of H_3R binding with age in regions of the human brain for AD cases:

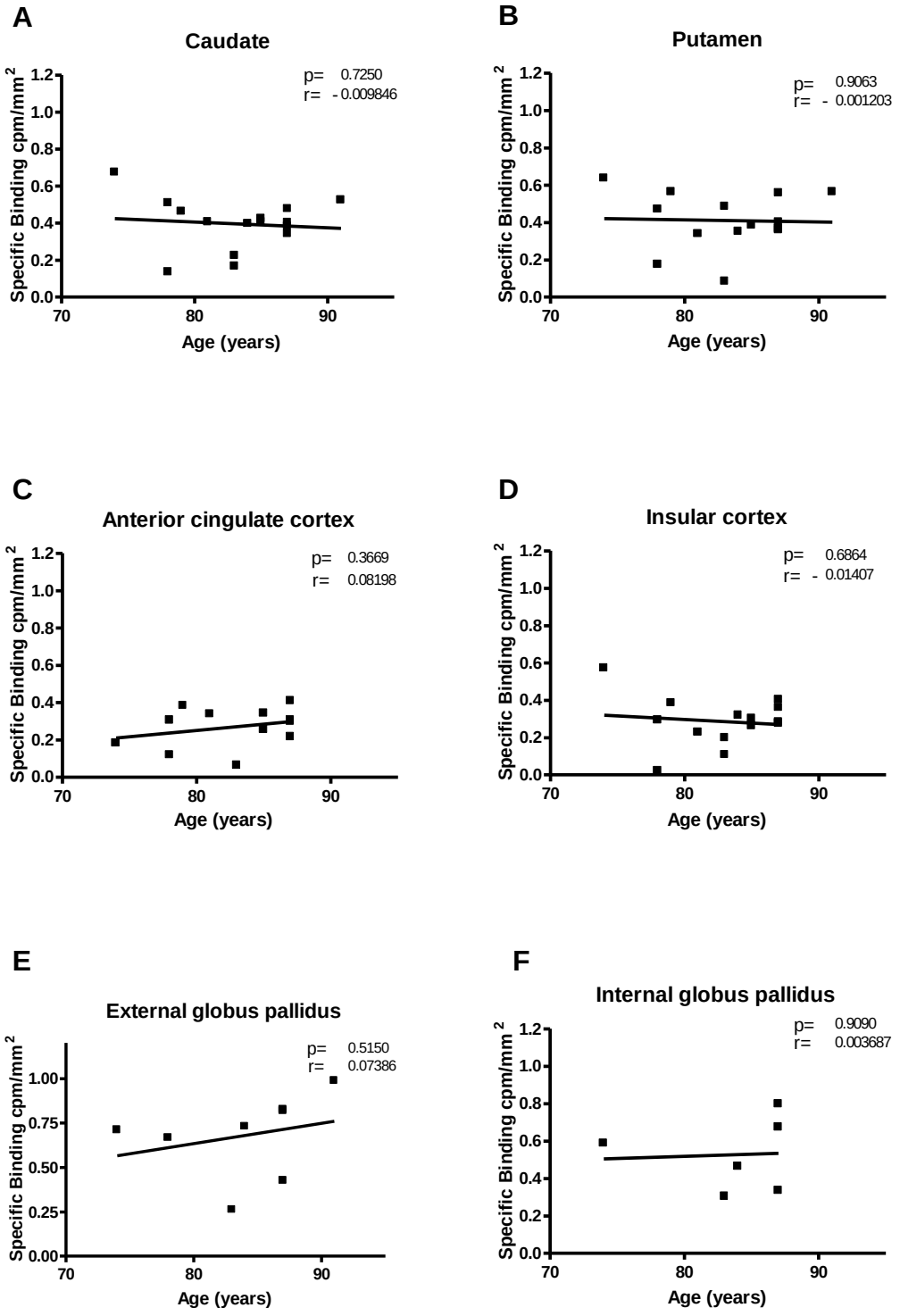

Figure 5.12 (A – F): Age-dependant absolute specific binding of [^{3}H] GSK189254 in AD cases (n=15) in (A) Caudate, (B) Putamen, (C) Cingulate cortex, (D) Insular cortex, (E) External globus pallidus, (F) Internal globus pallidus. Significance of regression was determined from the generated p value, where $p \leq 0.05$ was considered to show a significant linear relationship between age and binding level.

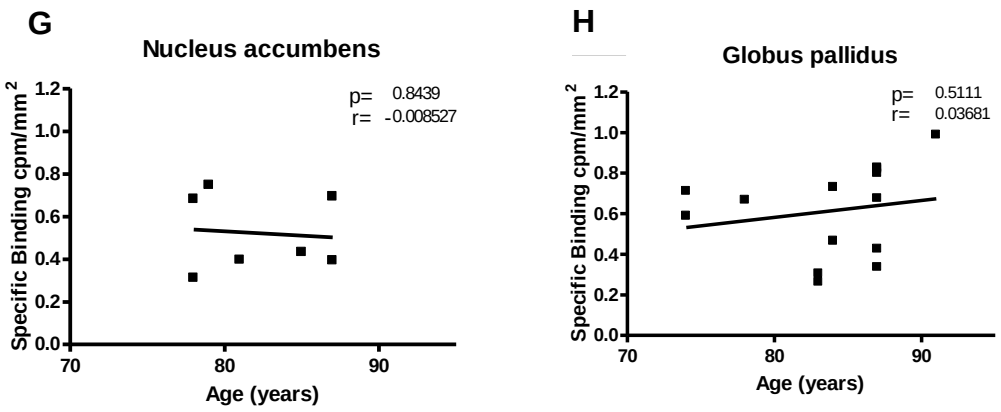

Figure 5.12 (G - H): Age-dependant absolute specific binding of [^{3}H] GSK189254 in AD cases (n=15) in (G) Nucleus accumbens and (H) Combined globus pallidus. Significance of regression was determined from the generated p value, where $p \leq 0.05$ was considered to show a significant linear relationship between age and binding level.

Figure 5.12 shows specific binding levels in AD cases examined for [^{3}H] GSK189254 in various brain regions against age. There were no significant age-dependant changes in all brain regions analysed ($p \geq 0.336$ in all areas). The r values ranged from -0.014 (insular cortex) to 0.082 (cingulate cortex).

H_3R binding is not significantly altered in ageing in both normal aging and in two common age related dementias (DLB and AD). The next parameter is to compare whether there are any age related changes in H_3R binding between control cases and disease state.

5.4.5 Quantitative analysis of human data – Comparison of H_3R binding with age between control and disease group

The same data as previously described and summarised in table 5.1 were further analysed to compare age-dependant specific binding of [^{3}H] GSK189254 between control and disease state cases. The cases were analysed by correlating cpm/mm^2 binding with age at death of the subject (in years), in each brain region defined. Estimated lines of best fit were produced using GraphPad Prism and are represented on each graph, indicating any age-dependant changes in binding levels in each tissue. The significance of the regression was determined from the generated p value, where $p \leq 0.05$ was considered to show a significant linear relationship between age and binding level. The generated correlation coefficient (r value) shows how well the data fits the regression line, where r = 1 shows strong correlation and r = 0 shows little or no correlation.

Statistical analysis of H_3R binding with age in various regions of the human brain comparing control with DLB cases:

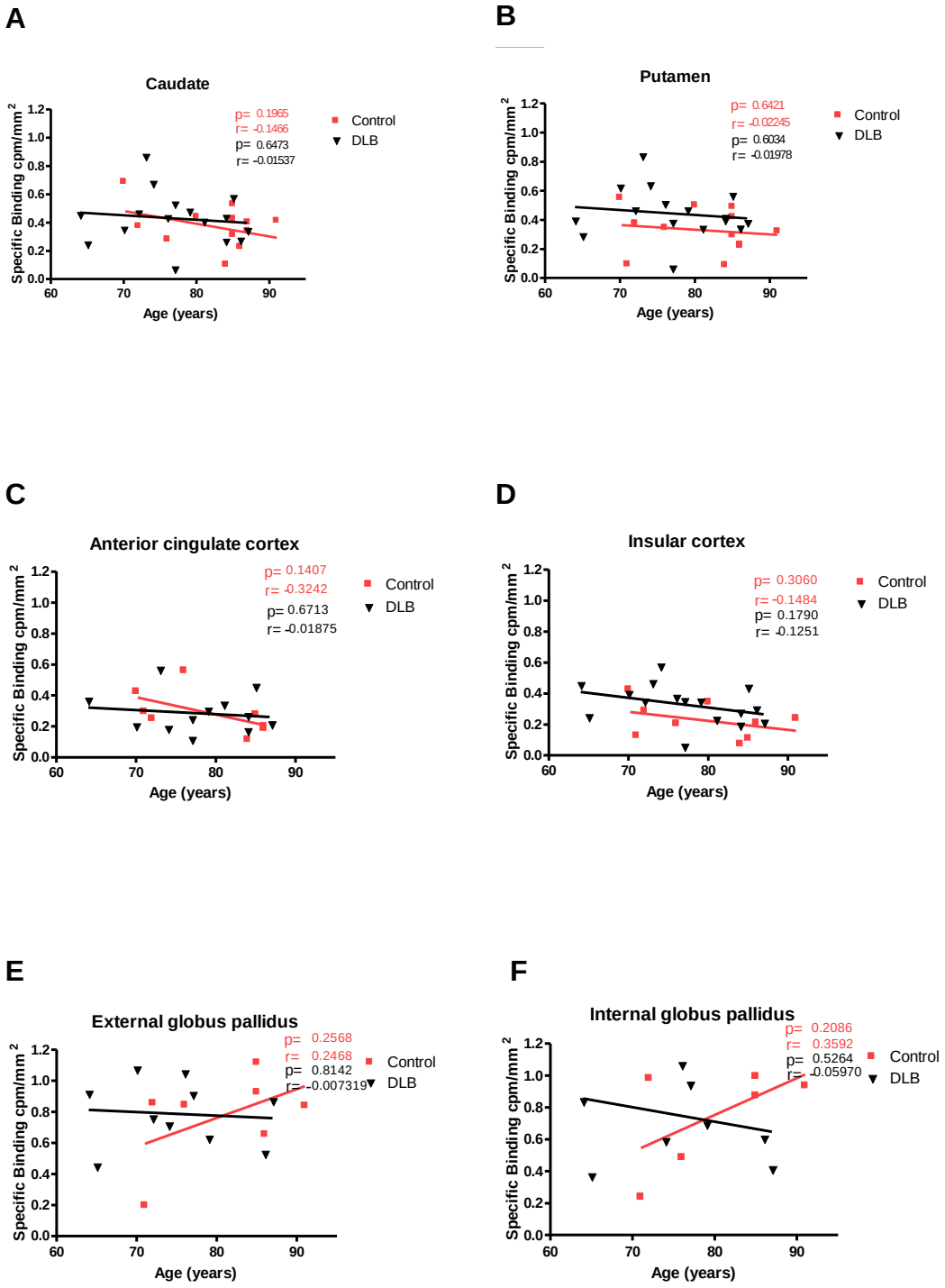

Figure 5.13 (A – F): Age-dependant absolute specific binding of [^{3}H] GSK189254 comparing control (n=12) with DLB cases (n=16) in (A) Caudate, (B) Putamen, (C) Cingulate cortex, (D) Insular cortex, (E) External globus pallidus, (F) Internal globus pallidus. Significance of regression was determined from the generated p value, where $p \leq 0.05$ was considered to show a significant linear relationship between age and binding level.

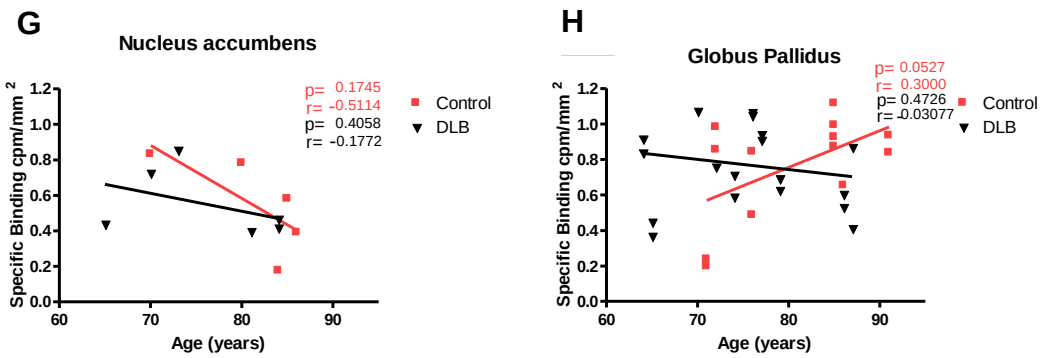

Figure 5.13 (G - H): Age-dependant absolute specific binding of [^{3}H] GSK189254 comparing control (n=12) with DLB cases (n=16) in (G) Nucleus accumbens and (H) Combined globus pallidus. Significance of regression was determined from the generated p value, where $p \leq 0.05$ was considered to show a significant linear relationship between age and binding level.

Figure 5.13 compares specific binding levels in control (n=12) and DLB (n=16) cases for [^{3}H] GSK189254 with age, ranging from 64 – 91 years in various brain regions. There were no significant difference age-dependant changes in all brain regions analysed in control and disease state cases ($p \geq 0.053$ in all cases). The combined globus pallidus control data showed borderline significance where p=0.053. The regression lines on each graph were very similar for both control and DLB data sets, showing a slight general decrease in binding levels in the caudate, putamen, anterior cingulate cortex, insular cortex and nucleus accumbens. In contrast the globus pallidus (graphs E, F and H), displayed increased binding with age in the control data set, whilst DLB cases showed decreased binding with age.

Statistical analysis of H_3R binding with age in various regions of the human brain comparing control with AD cases:

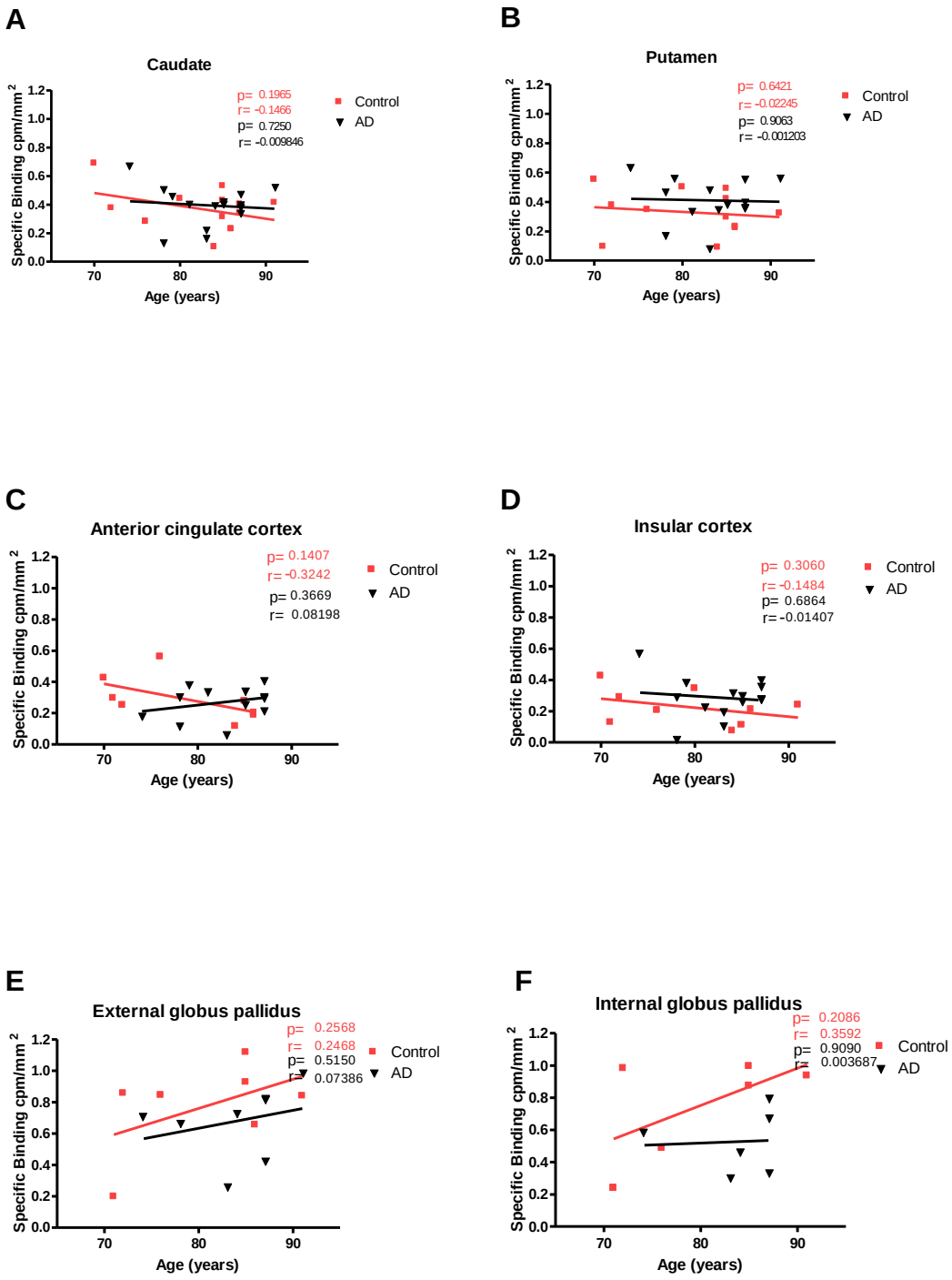

Figure 5.14 (A – F): Age-dependant absolute specific binding of [^{3}H] GSK189254 comparing control (n=12) with AD cases (n=15) in (A) Caudate, (B) Putamen, (C) Cingulate cortex, (D) Insular cortex, (E) External globus pallidus, (F) Internal globus pallidus. Significance of regression was determined from the generated p value, where $p \leq 0.05$ was considered to show a significant linear relationship between age and binding level.

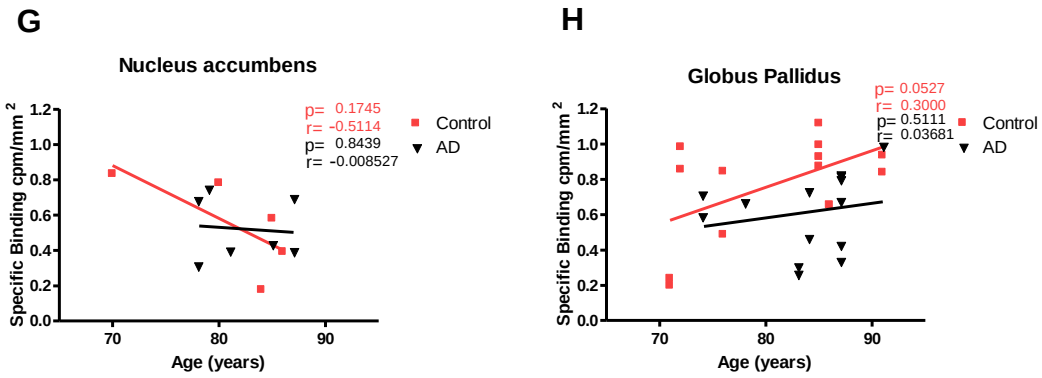

Figure 5.14 (G - H): Age-dependant absolute specific binding of [^{3}H] GSK189254 comparing control (n=12) with AD cases (n=15) in (G) Nucleus accumbens and (H) Combined globus pallidus. Significance of regression was determined from the generated p value, where $p \leq 0.05$ was considered to show a significant linear relationship between age and binding level.

Figure 5.14 compares specific binding levels in control (n=12) and AD (n=15) cases for [^{3}H] GSK189254 with age, ranging from 70 – 91 years in various brain regions. There were no significant difference age-dependant changes in all brain regions analysed in control and disease state cases ($p \geq 0.053$ in all cases). The regression lines on each graph were very similar for both control and AD data sets, showing a slight general decrease in binding levels in the caudate, putamen, insular cortex and nucleus accumbens. In contrast the globus pallidus (graphs E, F and H), displayed increased binding with age in both control and AD cases.

On comparison of H_3R binding of control data with the binding in the two disease states, there are clear differences seen in the globus pallidus between the two disease states. These differences are likely to be a result of the difference in disease pathology.

The next parameter is to compare whether there are any difference in H_3R binding between the three groups.

5.4.6 Quantitative analysis of human data – Comparison of mean H_3R binding between control and disease groups

The data for each group were further analysed to show the mean specific binding cpm/mm^2 $\pm$ SD of [^{3}H] GSK189254 for all groups for n determinations in all brain regions defined.

Statistical analysis was performed using a one-way ANOVA test, indicated with the use of Graph Pad Prism (version 4) to analyse between the groups in each of the brain regions defined. Statistical significance was set at $p<0.05$ level for the one-way ANOVA analysis.

Statistical analysis of mean specific H_3R binding between all groups in various regions of the human brain:

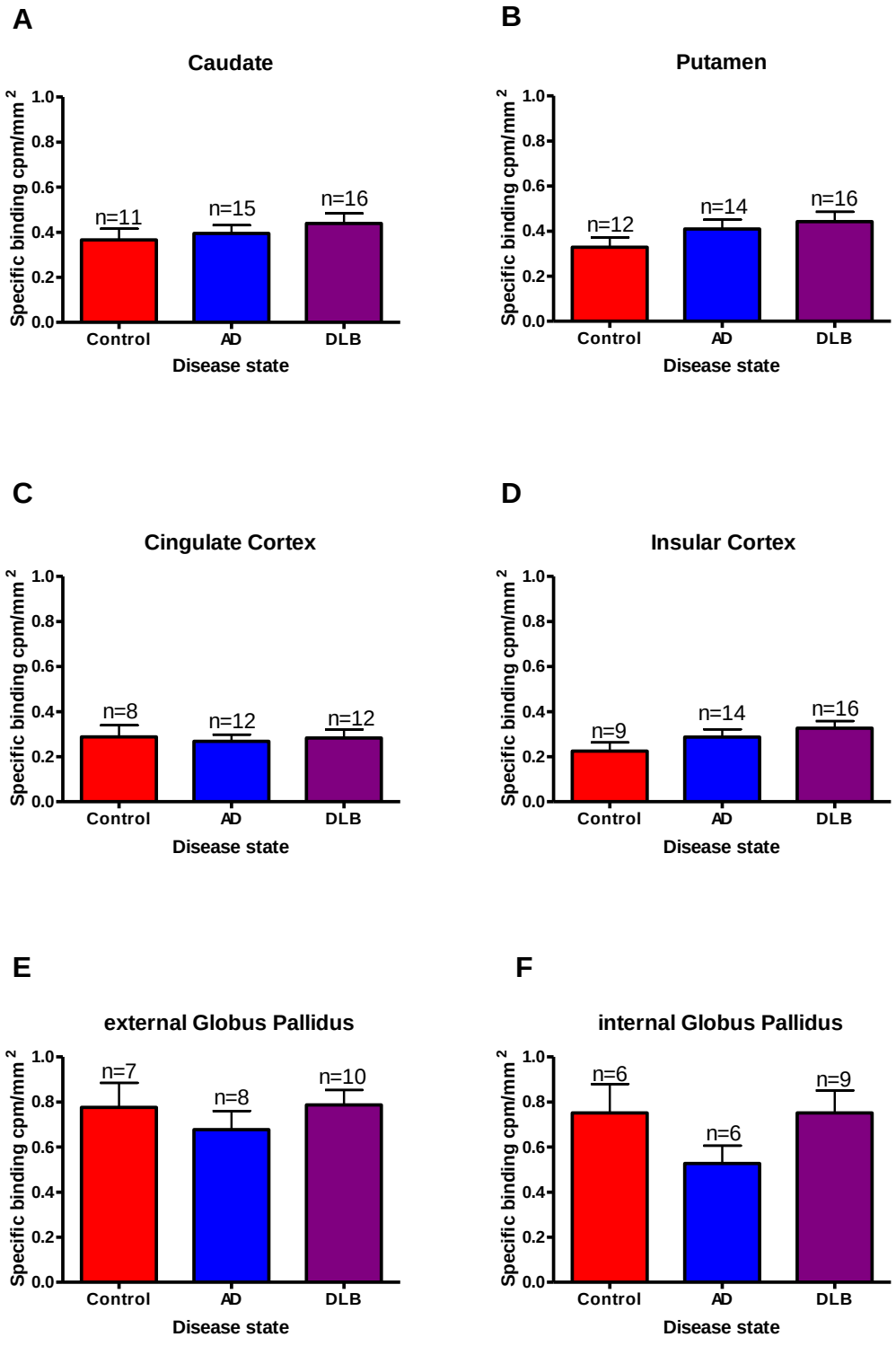

Figure 5.15 (A – F): Mean specific [^{3}H] GSK189254 binding densities (cpm/mm^2), (mean $\pm$ SEM for n determinations) between control, DLB and AD cases in (A) Caudate, (B) Putamen, (C) Cingulate cortex, (D) Insular cortex, (E) External globus pallidus, (F) Internal globus pallidus. Statistical significance was set at $p<0.05$ level for the one-way ANOVA analysis.

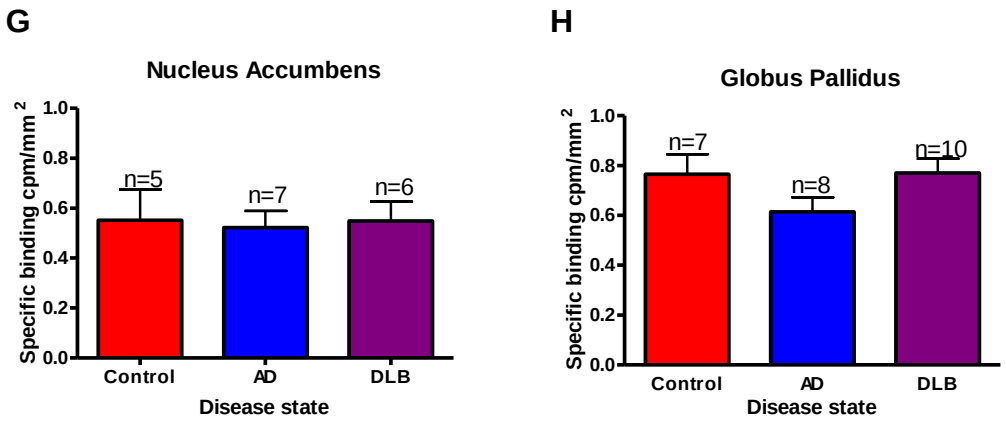

Figure 5.15 (G – H): Mean specific [^{3}H] GSK189254 binding densities (cpm/mm^2), (mean ± SEM for n determinations) between control, DLB and AD cases in G) Nucleus accumbens and (H) Combined globus pallidus. Statistical significance was set at $p<0.05$ level for the one-way ANOVA analysis.

Figure 5.15 shows no significant differences in the mean binding densities of [^{3}H] GSK189254 in all brain regions analysed when comparing between control and disease states. On first glance there appears to be a trend for binding to be lower in the globus pallidus in AD cases, although this is not statistically significant.

The data in Fig. 5.15 were further analysed for gender differences (data not shown), similar levels of binding was seen in both female and male cohorts in all brain regions defined indicating no evidence for gender bias.

5.4.7 Quantitative analysis of human data – Correlation between clinical symptoms and H_3R binding densities

The clinical data corresponding to DLB and AD cases summarised in tables 5.1 showing the relevant scores for the MMSE (mini mental state examination, see section 5.3.10) and UPDRS scores (Unified Parkinson disease rating scale, see section 5.3.11). Data relating to depression, delusions, dementia and visual hallucinations experienced by each subject were also studied. The severity of the symptoms experienced were measured on the following scale, 0 = none, 1 = mild, 2 = severe, and are indicative of the last assessment before death of the subject. In each case and in each tissue looked at, the specific binding levels of [^{3}H] GSK189254 data were shown against the relevant clinical data score. In the case of MMSE and UPDRS data, the score could be any value in a given range; therefore each case is represented on the graph. The depression, delusion and visual hallucination data has been shown for each of the score 0 no symptoms and 1+ showing symptoms, giving the mean score $\pm$ SD against binding levels in cpm/mm^2. Although in the majority of cases studied clinical data was available, unfortunately not all cases had the relevant data, and therefore only those with the data present are shown.

Estimated lines of best fit were produced using GraphPad Prism and are represented on each graph, indicating any changes in binding levels in each tissue with increasing clinical score. The significance of the regression was determined from the generated p value, where $p \leq 0.05$ was considered to show a significant linear relationship between clinical score and binding level.

Statistical analysis of MMSE score versus H_3R binding in DLB cases:

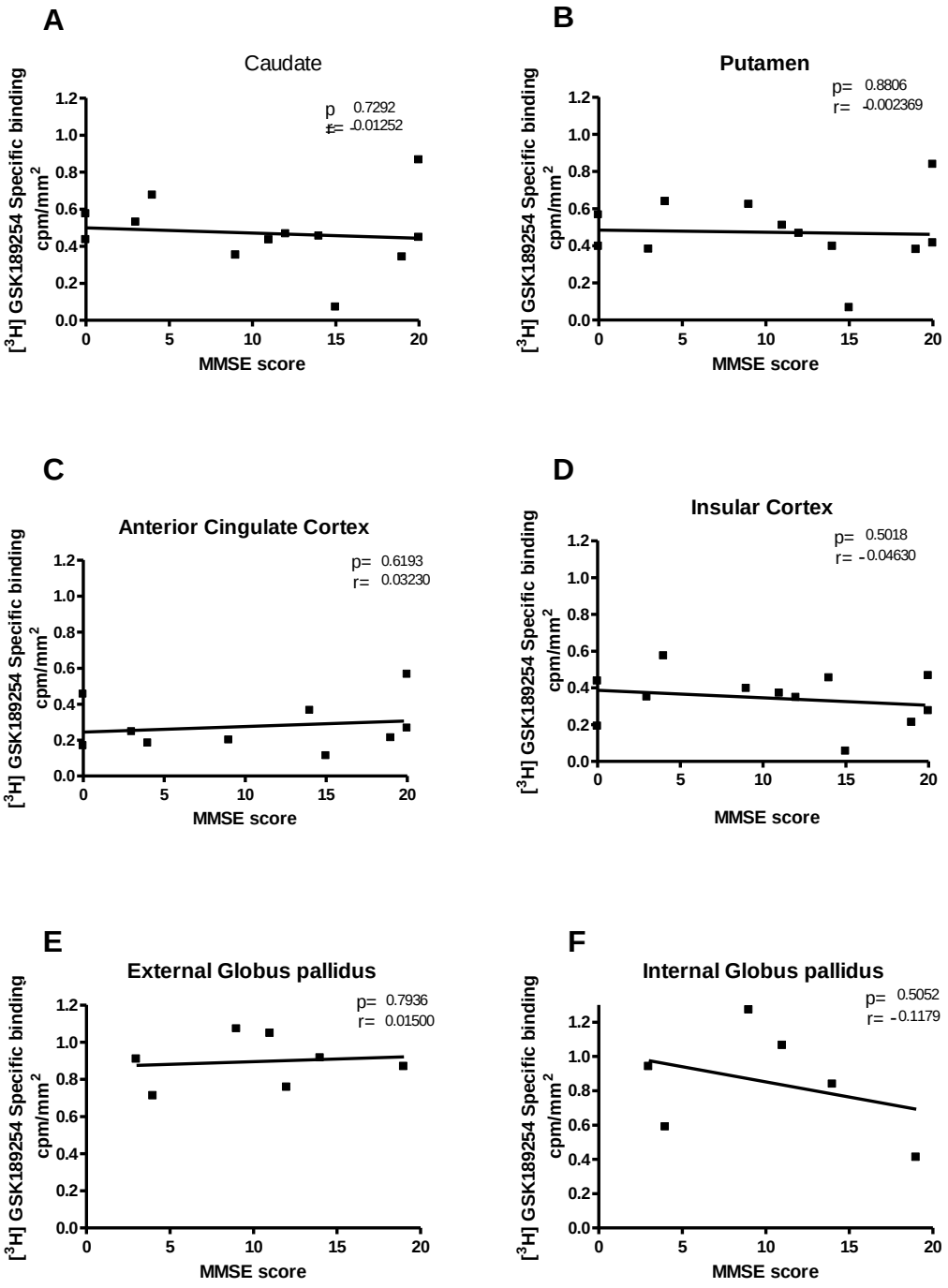

Figure 5.16 (A – F): Mini mental state examination score against specific binding cpm/mm^2 of [^{3}H] GSK189254 in DLB cases in (A) Caudate, (B) Putamen, (C) Cingulate cortex, (D) Insular cortex, (E) External globus pallidus, (F) Internal globus pallidus. Statistical significance was determined from the generated p value, where $p \leq 0.05$ was considered to show a significant linear relationship between clinical score and binding level.

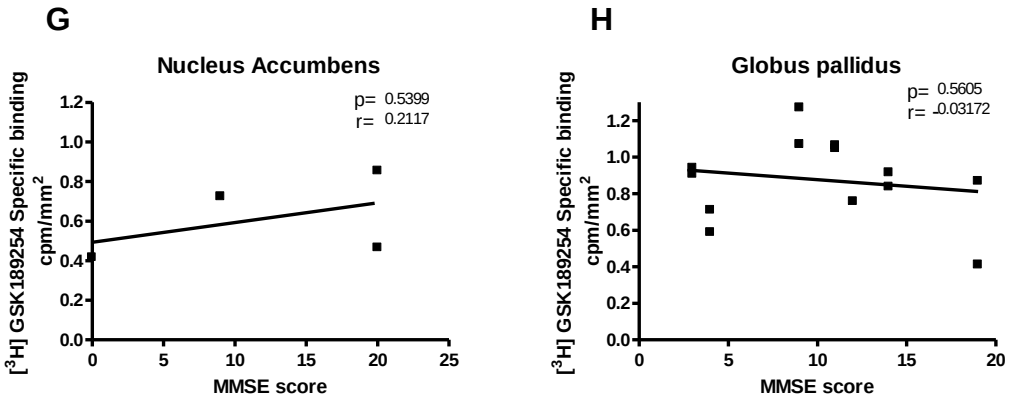

Figure 5.16 (G – H): Mini mental state examination score against specific binding cpm/mm^2 of [^{3}H] GSK189254 in DLB cases in (G) Nucleus Accumbens, (H) combined Globus Pallidus. Statistical significance was determined from the generated p value, where $p \leq 0.05$ was considered to show a significant linear relationship between clinical score and binding level.

Figure 5.16 shows the specific binding levels in DLB cases (n=16) for [^{3}H] GSK189254 against MMSE score in the brain regions defined. There were no significant differences in the binding densities of [^{3}H] GSK189254 with increased MMSE score ($p \geq 0.502$ in all areas). The general trend in all the graphs showed relatively little change in binding with increased MMSE score, except in the internal globus pallidus where there was a decrease in binding with increased MMSE score. The r values ranged from -0.118 (internal globus pallidus) to 0.212 (nucleus accumbens).

Statistical analysis of MMSE score versus H_3R binding in AD cases:

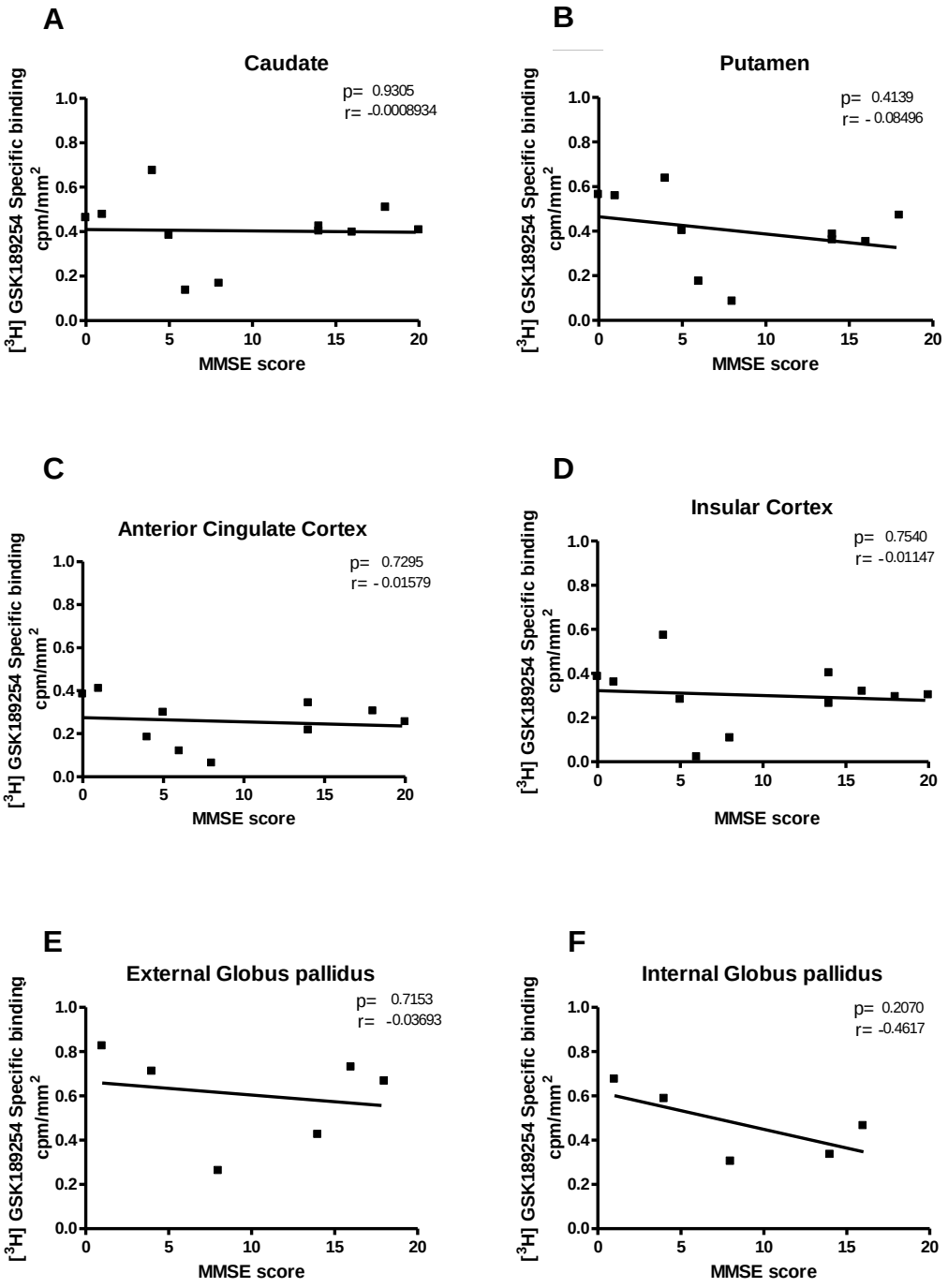

Figure 5.17 (A – F): Mini mental state examination score against specific binding cpm/mm^2 of [^{3}H] GSK189254 in AD cases in (A) Caudate, (B) Putamen, (C) Cingulate cortex, (D) Insular cortex, (E) External globus pallidus, (F) Internal globus pallidus. Statistical significance was determined from the generated p value, where $p \leq 0.05$ was considered to show a significant linear relationship between clinical score and binding level.

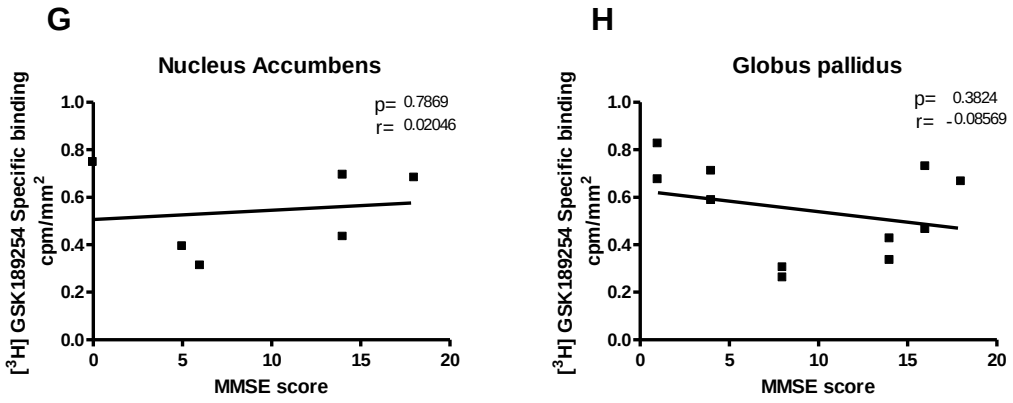

Figure 5.17 (G – H): Mini mental state examination score against specific binding cpm/mm^2 of [^{3}H] GSK189254 in AD cases in (G) Nucleus Accumbens, (H) combined Globus Pallidus. Statistical significance was determined from the generated p value, where $p \leq 0.05$ was considered to show a significant linear relationship between clinical score and binding level.

Figure 5.17 shows the specific binding levels in AD cases (n=15) for [^{3}H] GSK189254 against MMSE score in the brain regions defined. There were no significant differences in the binding densities of [^{3}H] GSK189254 with increased MMSE score ($p \geq 0.207$ in all areas). The general trend in all the graphs showed relatively little change in binding with increased MMSE score, except in the internal and external globus pallidus and the putamen where increased binding is associated with an increase in MMSE score. The r values ranged from -0.462 (internal globus pallidus) to 0.020 (nucleus accumbens).

Statistical analysis of UPDRS score versus H_3R binding in DLB cases:

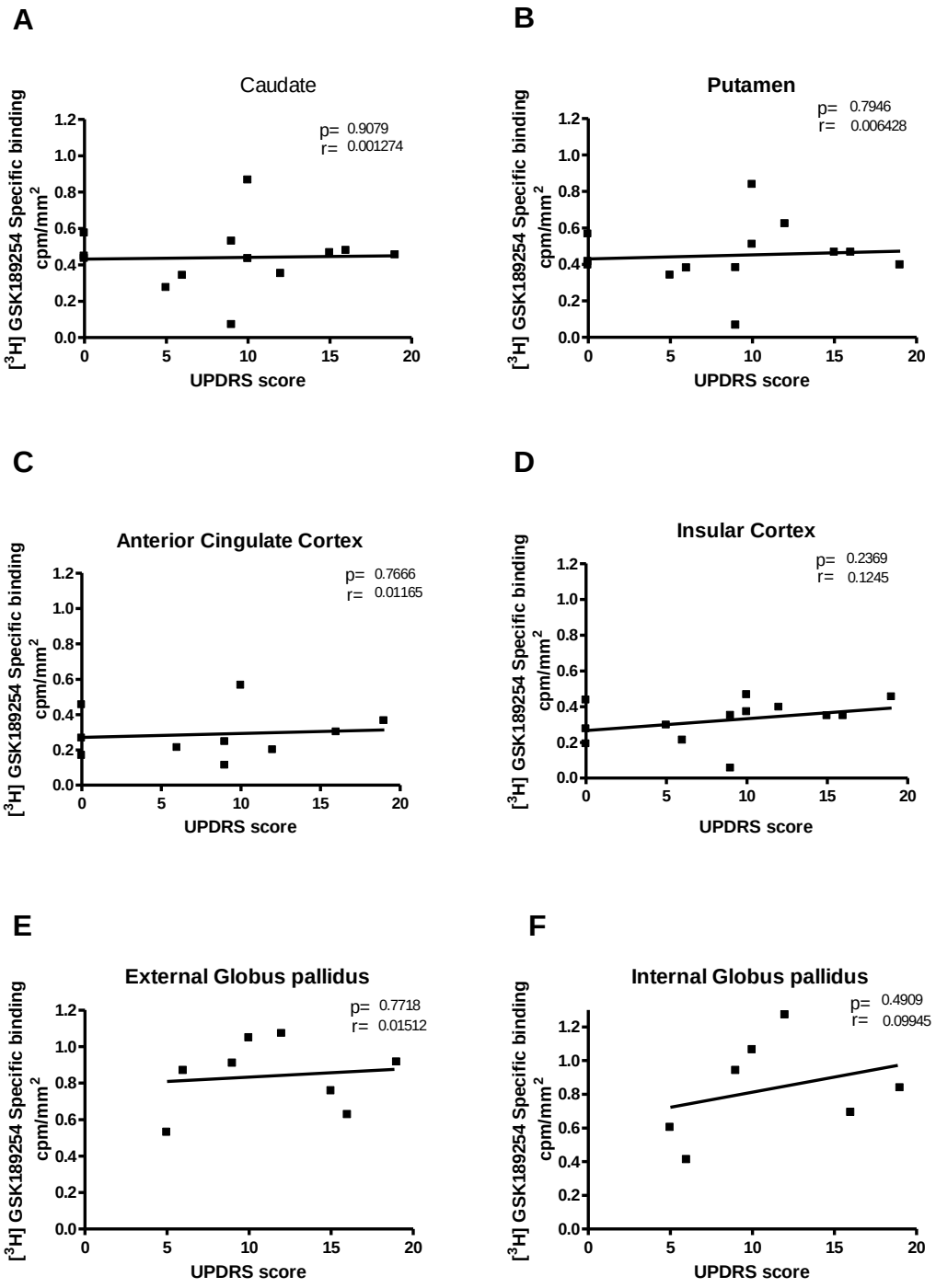

Figure 5.18 (A – F): Unified Parkinson Disease Rating Scale against specific binding cpm/mm^2 of [^{3}H] GSK189254 in DLB cases in (A) Caudate, (B) Putamen, (C) Cingulate cortex, (D) Insular cortex, (E) External globus pallidus, (F) Internal globus pallidus. Statistical significance was determined from the generated p value, where $p \leq 0.05$ was considered to show a significant linear relationship between clinical score and binding level.

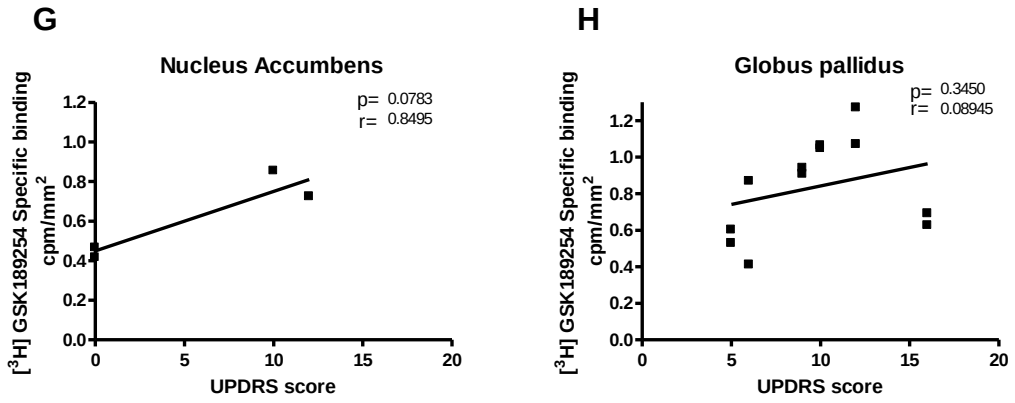

Figure 5.18 (G – H): Unified Parkinson Disease Rating Scale against specific binding cpm/mm^2 of [^{3}H] GSK189254 in DLB cases in (G) Nucleus Accumbens, (H) combined Globus Pallidus. Statistical significance was determined from the generated p value, where $p \leq 0.05$ was considered to show a significant linear relationship between clinical score and binding level.

Figure 5.18 shows the specific binding levels in DLB cases (n=16) for [^{3}H] GSK189254 against UPDRS score in the brain regions defined. There were no significant differences in the binding densities of [^{3}H] GSK189254 with increased UPDRS score ($p \geq 0.078$ in all areas). The general trend in all the graphs showed a slight increase in binding with increased UPDRS score. The r values ranged from 0.001 (caudate) to 0.850 (nucleus accumbens).

Statistical analysis of UPDRS score versus H_3R binding in AD cases:

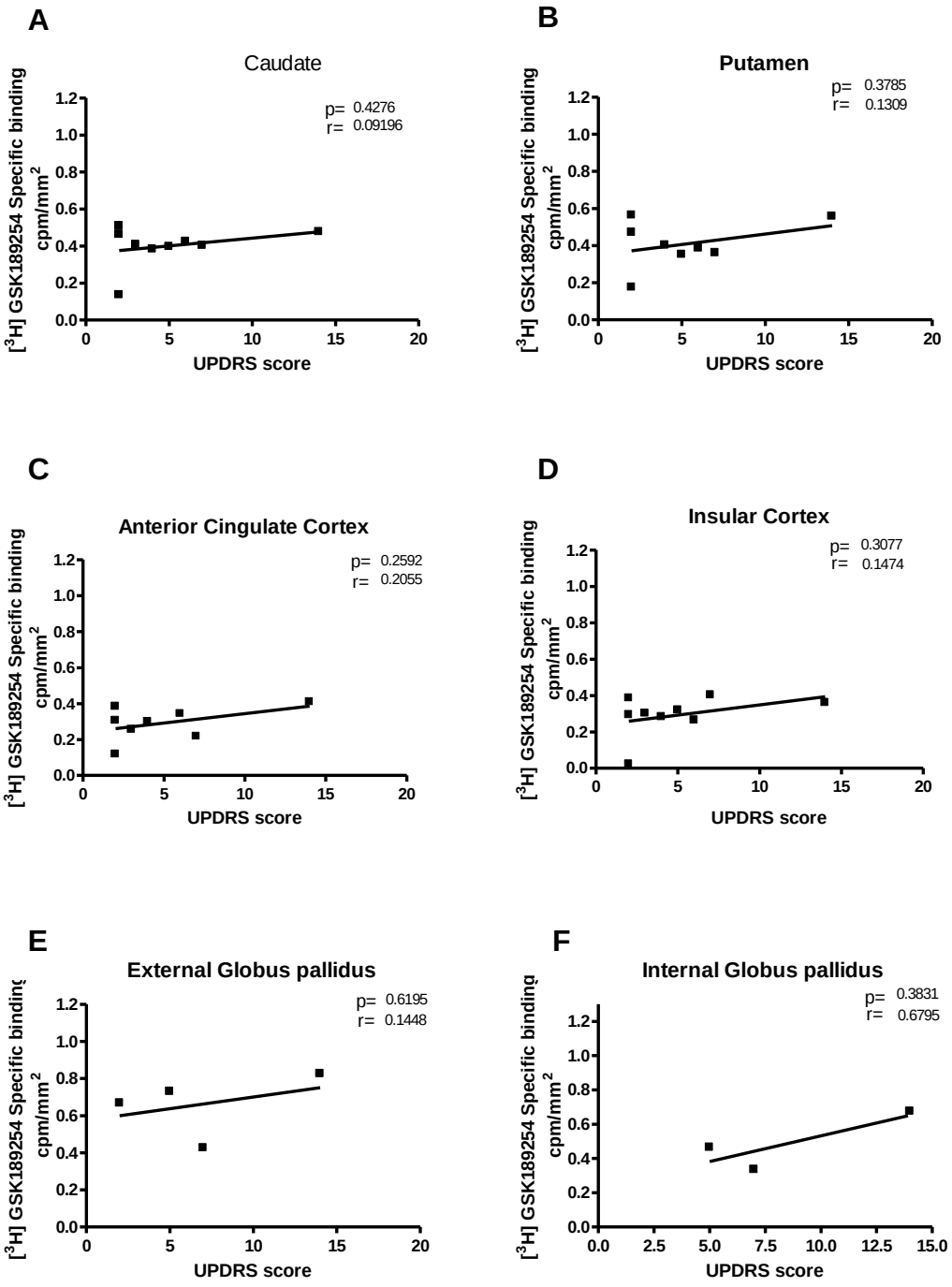

Figure 5.19 (A – F): Unified Parkinson Disease Rating Scale against specific binding cpm/mm^2 of [^{3}H] GSK189254 in AD cases in (A) Caudate, (B) Putamen, (C) Cingulate cortex, (D) Insular cortex, (E) External globus pallidus, (F) Internal globus pallidus. Statistical significance was determined from the generated p value, where $p \leq 0.05$ was considered to show a significant linear relationship between clinical score and binding level.

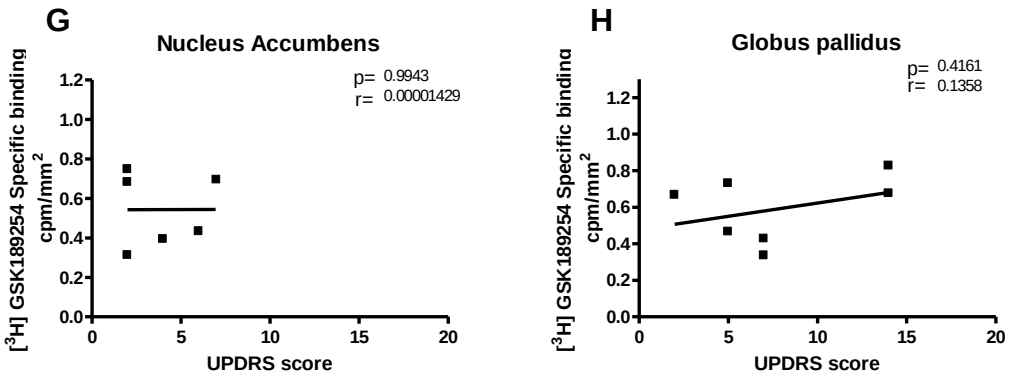

Figure 5.19 (G – H): Unified Parkinson Disease Rating Scale against specific binding cpm/mm^2 of [^{3}H] GSK189254 in AD cases in (G) Nucleus Accumbens, (H) combined Globus Pallidus. Statistical significance was determined from the generated p value, where $p \leq 0.05$ was considered to show a significant linear relationship between clinical score and binding level.

Figure 5.19 shows the specific binding levels in AD cases (n=15) for [^{3}H] GSK189254 against UPDRS score in the brain regions defined. There were no significant differences in the binding densities of [^{3}H] GSK189254 with increased UPDRS score ($p \geq 0.259$ in all areas). The general trend in all the graphs showed a slight increase in binding with increased UPDRS score. The r values ranged from 0.000 (nucleus accumbens) to 0.680 (nucleus accumbens).

Statistical analysis of depression score and H_3R binding density in DLB cases:

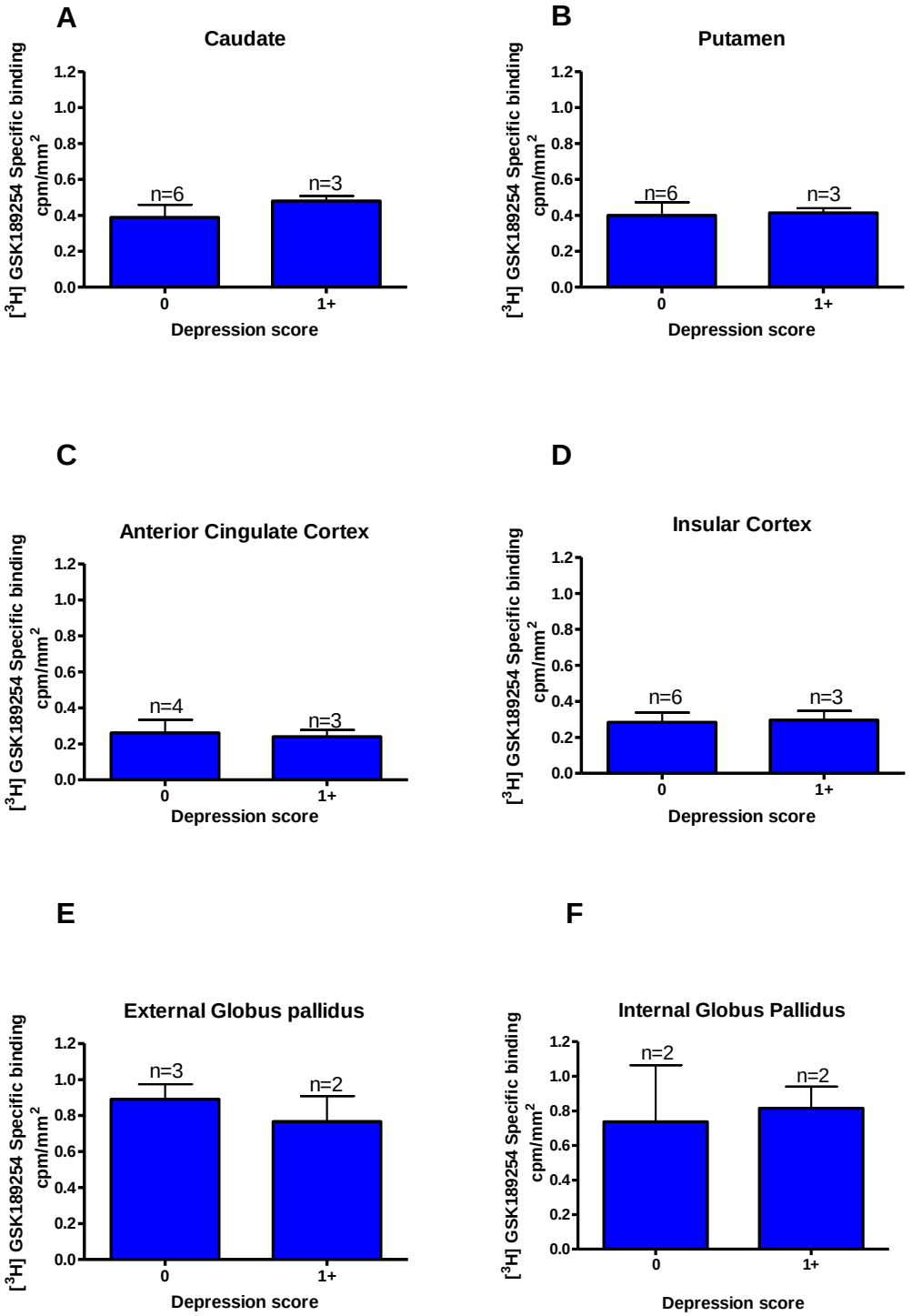

Figure 5.20 (A – F): Depression score against specific binding cpm/mm^2 of [^{3}H] GSK189254 in DLB cases in (A) Caudate, (B) Putamen, (C) Cingulate cortex, (D) Insular cortex, (E) External globus pallidus, (F) Internal globus pallidus. Statistical significance was determined

from the generated p value, where p≤0.05 was considered to show a significant linear relati[illegible] etween clinical score and binding leve[illegible]

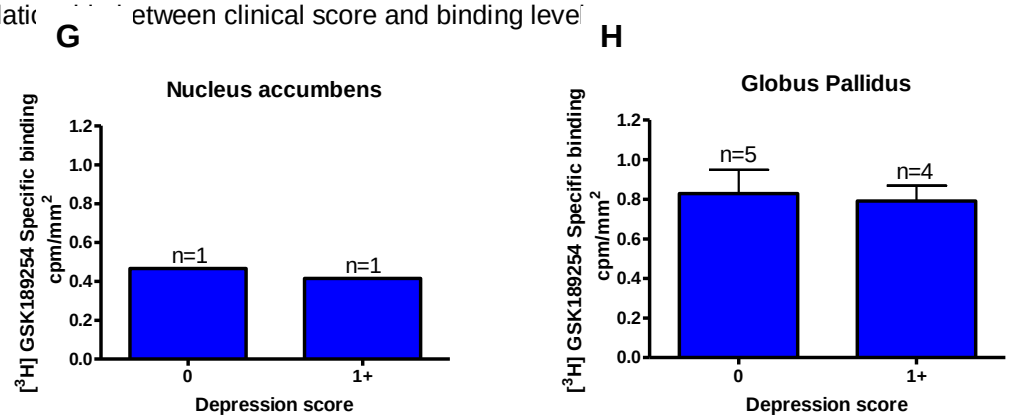

Figure 5.20 (G – H): Depression score against specific binding cpm/mm^2 of [^{3}H] GSK189254 in DLB cases in (G) Nucleus Accumbens, (H) combined Globus Pallidus. Statistical significance was determined from the generated p value, where p≤0.05 was considered to show a significant linear relationship between clinical score and binding level.

Figure 5.20 shows specific H_3R binding levels ± SD cpm/mm^2 in DLB cases (n=16) against depression score. There were no significant differences between the H_3R binding densities and severity of depression.

Statistical analysis of depression score and H_3R binding density in AD cases:

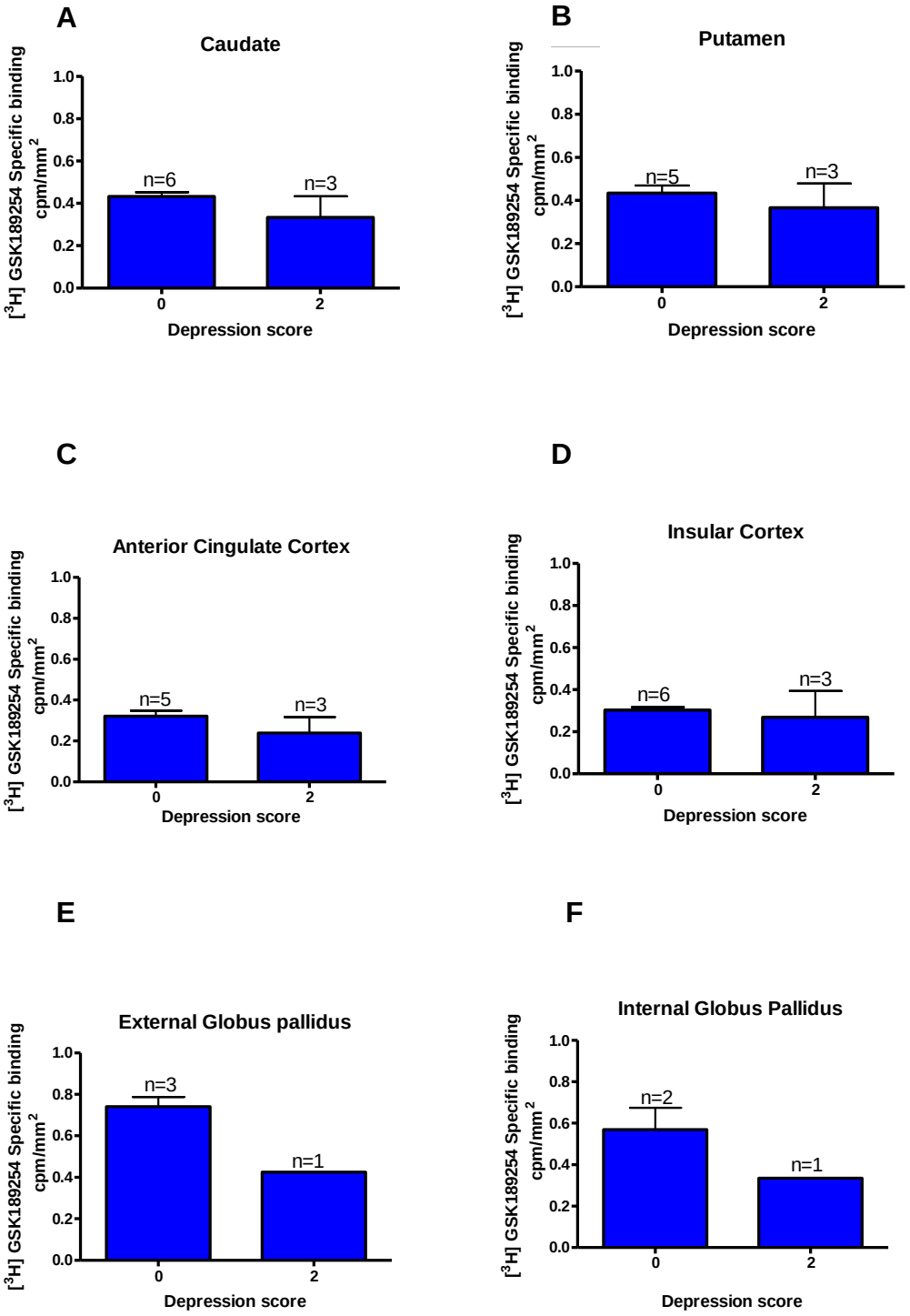

Figure 5.21 (A – F): Depression score against specific binding cpm/mm^2 of [^{3}H] GSK189254 in AD cases in (A) Caudate, (B) Putamen, (C) Cingulate cortex, (D) Insular cortex, (E)

External globus pallidus, (F) Internal globus pallidus. Statistical significance was determined from the generated p value, where p≤0.05 was considered to show a significant linear relation[illegible]tween clinical score and binding level.

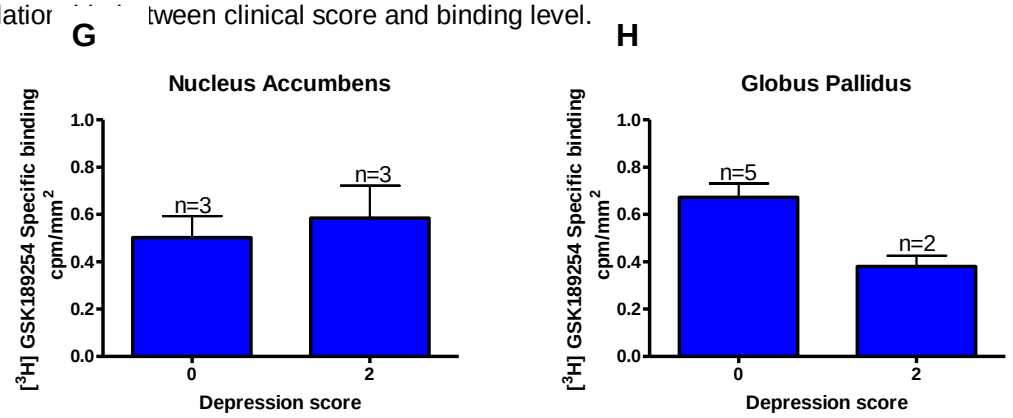

Figure 5.21 (G – H): Depression score against specific binding cpm/mm^2 of [^{3}H] GSK189254 in AD cases in (G) Nucleus Accumbens, (H) combined Globus Pallidus. Statistical significance was determined from the generated p value, where p≤0.05 was considered to show a significant linear relationship between clinical score and binding level.

Figure 5.21 shows specific H_3R binding levels ± SD cpm/mm^2 in AD cases (n=15) against depression score. There were no significant differences between the H_3R binding densities and severity of depression except in the combined globus pallidus where a decrease in H_3R binding is correlated with increase severity of depression (p=0.035).

Statistical analysis of delusion score and H_3R binding density in DLB cases:

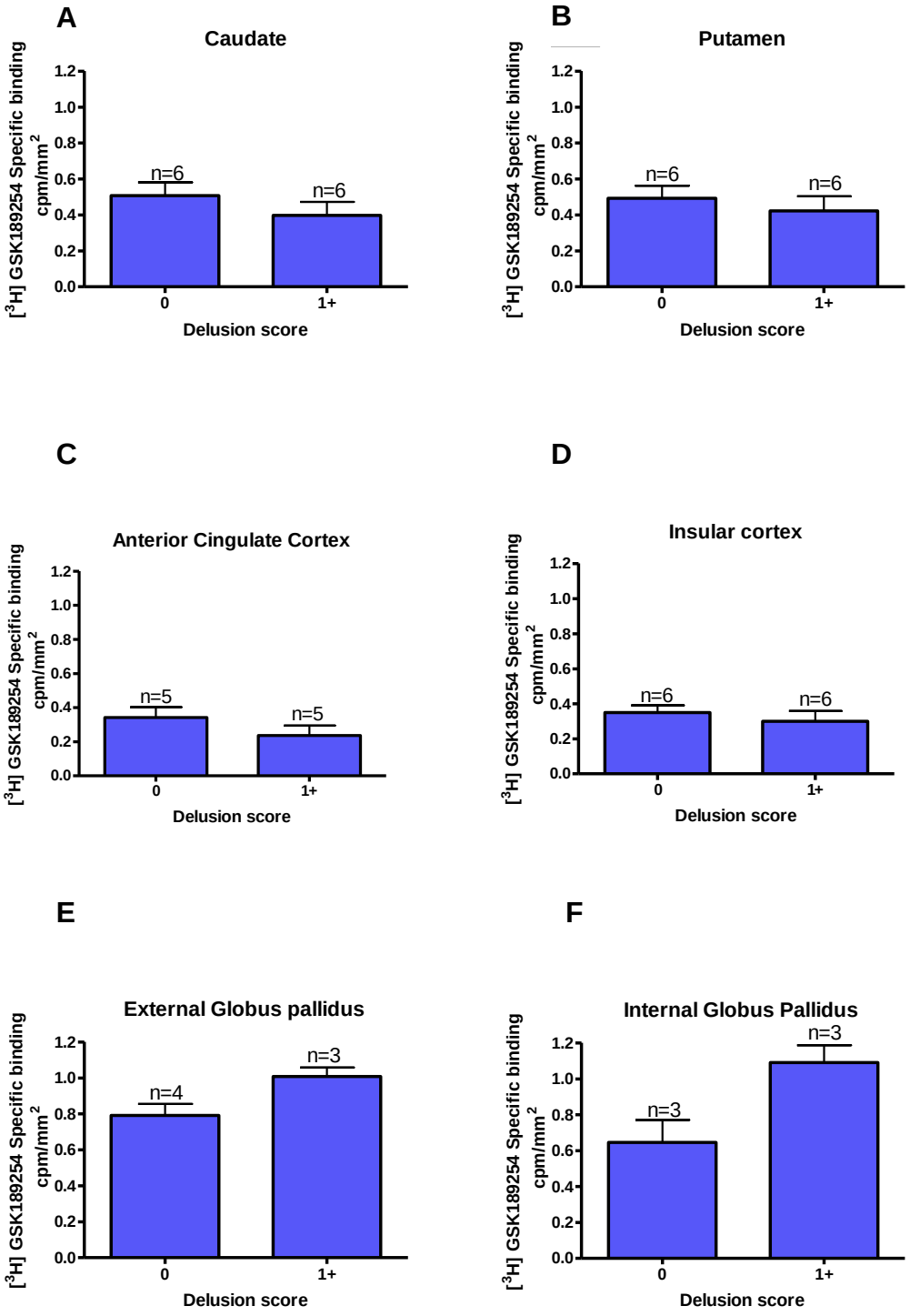

Figure 5.22 (A – F): Delusion score against specific binding cpm/mm^2 of [^{3}H] GSK189254 in DLB cases in (A) Caudate, (B) Putamen, (C) Cingulate cortex, (D) Insular cortex, (E) External globus pallidus, (F) Internal globus pallidus. Statistical significance was determined from the

generated p value, where p≤0.05 was considered to show a significant linear relationship between clinical score and binding level.

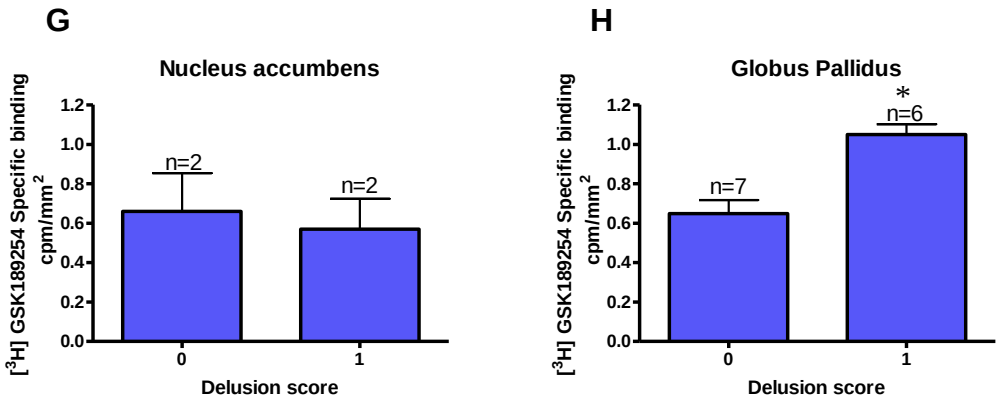

Figure 5.22 (G – H): Delusion score against specific binding cpm/mm^2 of [^{3}H] GSK189254 in DLB cases in (G) Nucleus Accumbens, (H) combined Globus Pallidus. Statistical significance was determined from the generated p value, where p≤0.05 was considered to show a significant linear relationship between clinical score and binding level.

Figure 5.22 shows specific H_3R binding levels ± SD cpm/mm^2 in DLB cases (n=16) against delusion score. There were no significant differences between the H_3R binding densities and severity of delusion except in the internal globus pallidus and combined globus pallidus where an increase in H_3R binding is correlated with increase severity of delusion (p=0.048 and p=0.009).

Statistical analysis of delusion score and H_3R binding density in AD cases:

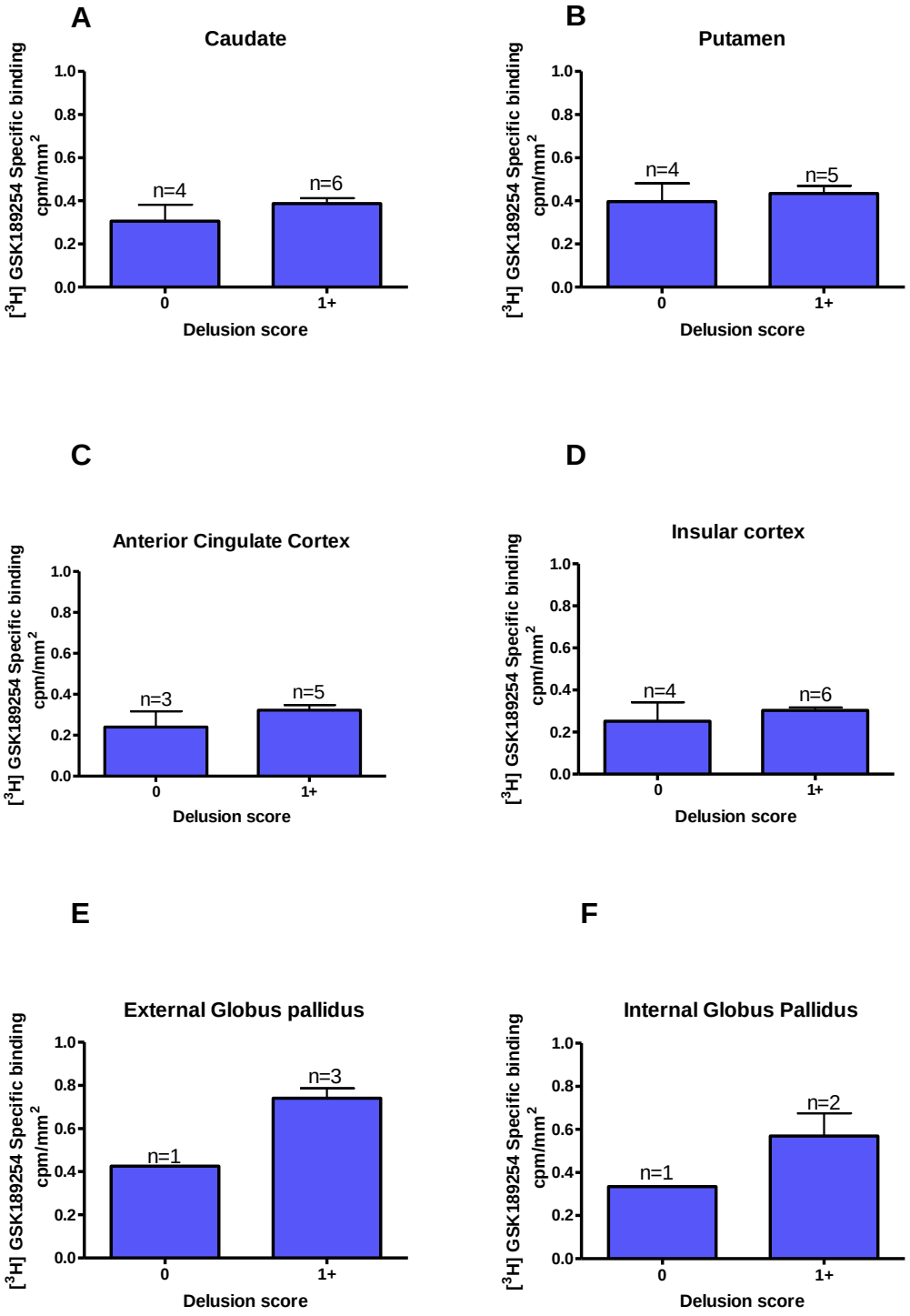

Figure 5.23 (A – F): Delusion score against specific binding cpm/mm^2 of [^{3}H] GSK189254 in AD cases in (A) Caudate, (B) Putamen, (C) Cingulate cortex, (D) Insular cortex, (E) External globus pallidus, (F) Internal globus pallidus. Statistical significance was determined from the

generated p value, where $p \leq 0.05$ was considered to show a significant linear relationship between clinical score and binding level.

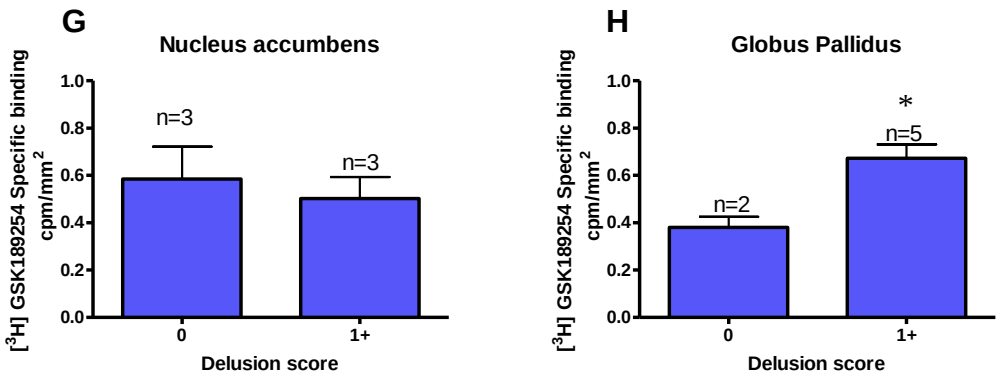

Figure 5.23 (G – H): Delusion score against specific binding cpm/mm^2 of [^{3}H] GSK189254 in AD cases in (G) Nucleus Accumbens, (H) combined Globus Pallidus. Statistical significance was determined from the generated p value, where $p \leq 0.05$ was considered to show a significant linear relationship between clinical score and binding level.

Figure 5.23 shows specific H_3R binding levels $\pm$ SD cpm/mm^2 in AD cases (n=15) against delusion score. There were no significant differences between the H_3R binding densities and severity of delusion except in the internal combined globus pallidus where an increase in H_3R binding is correlated with increase severity of delusion (p=0.035).

Statistical analysis of visual hallucination score and H_3R binding density in DLB cases:

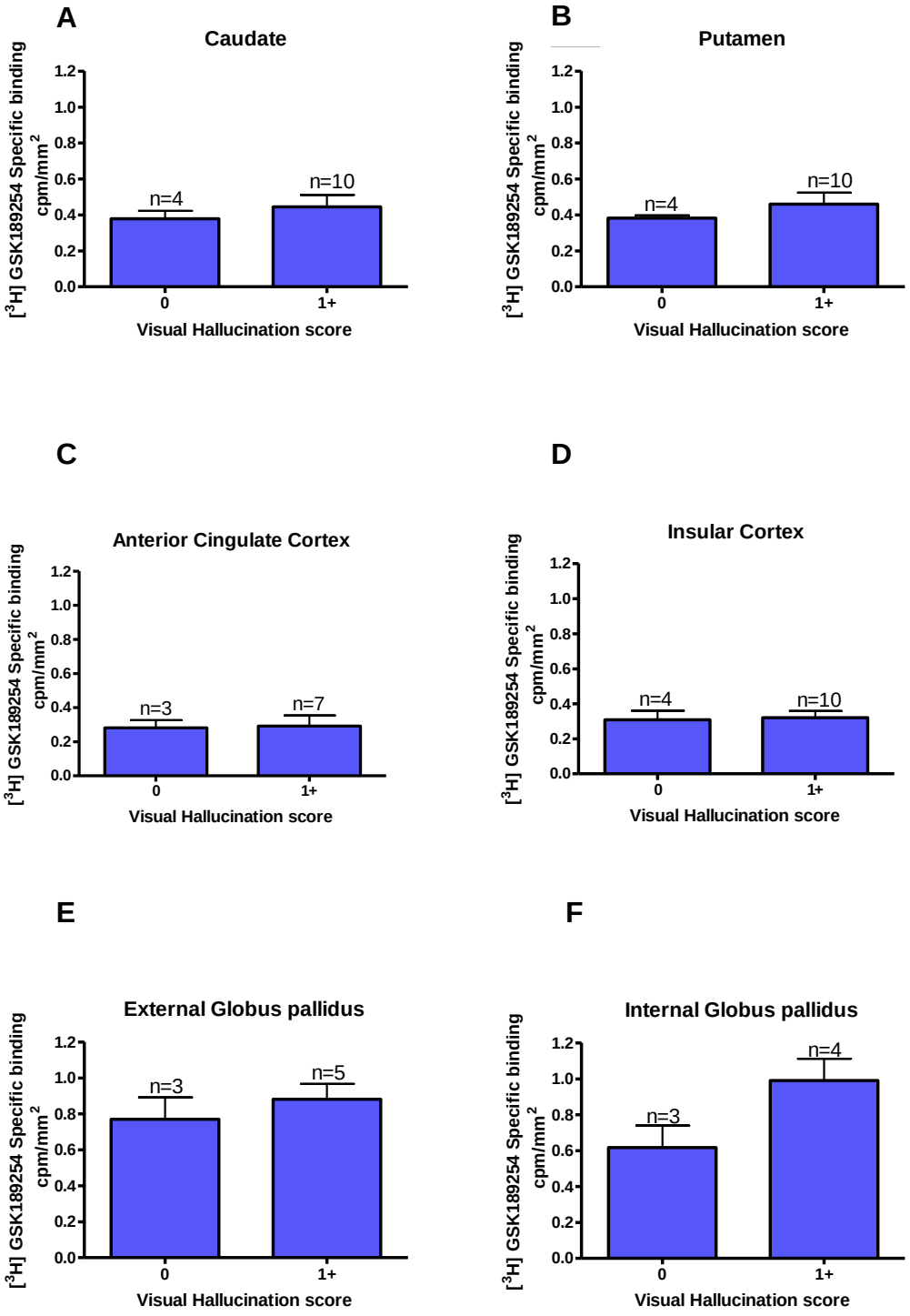

Figure 5.24 (A – F): Visual hallucination score against specific binding cpm/mm^2 of [^{3}H] GSK189254 in DLB cases in (A) Caudate, (B) Putamen, (C) Cingulate cortex, (D) Insular

cortex, (E) External globus pallidus, (F) Internal globus pallidus. Statistical significance was determined from the generated p value, where $p \leq 0.05$ was considered to show a significant linear relationship between clinical score and binding level.

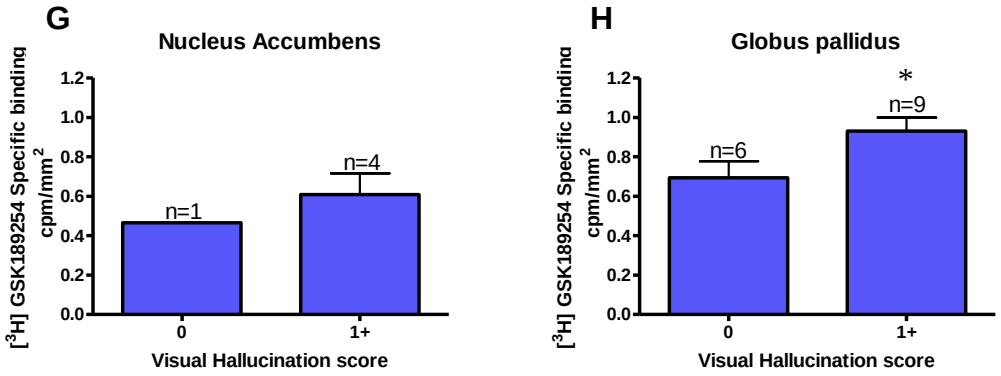

Figure 5.24 (G – H): Visual hallucination score against specific binding cpm/mm^2 of [^{3}H] GSK189254 in DLB cases in (G) Nucleus Accumbens, (H) combined Globus Pallidus. Statistical significance was determined from the generated p value, where $p \leq 0.05$ was considered to show a significant linear relationship between clinical score and binding level.

Figure 5.24 shows specific H_3R binding levels $\pm$ SD cpm/mm^2 in DLB cases (n=16) against visual hallucination score. There were no significant differences between the H_3R binding densities and severity of visual hallucinations except in the combined globus pallidus where an increase in H_3R binding is correlated with increase severity of delusion (p=0.040).

Statistical analysis of visual hallucination score and H_3R binding density in AD cases:

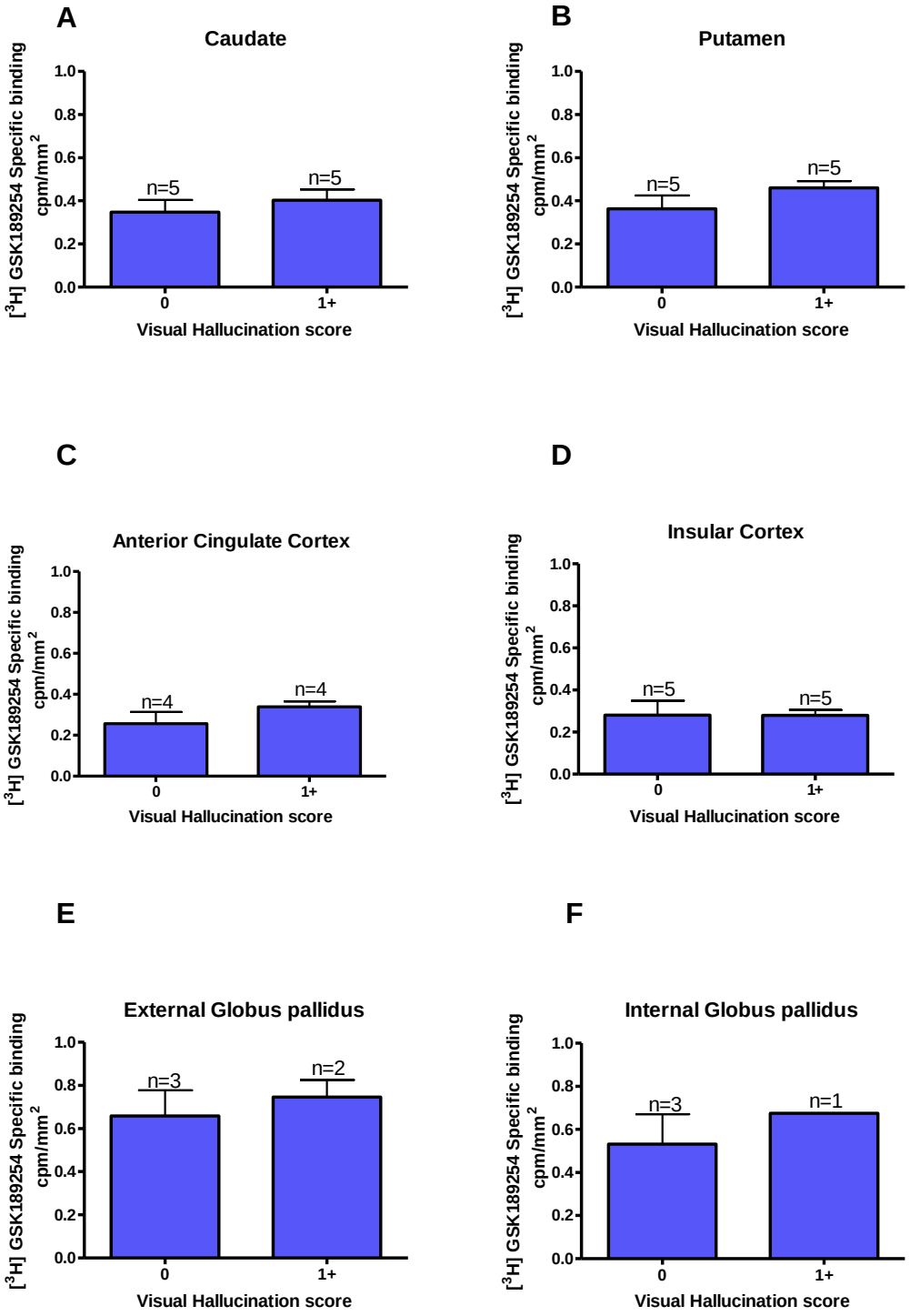

Figure 5.25 (A – F): Visual hallucination score against specific binding cpm/mm^2 of [^{3}H] GSK189254 in AD cases in (A) Caudate, (B) Putamen, (C) Cingulate cortex, (D) Insular cortex, (E) External globus pallidus, (F) Internal globus pallidus. Statistical significance was

determined from the generated p value, where $p \leq 0.05$ was considered to show a significant linear relationship between clinical score and binding level.

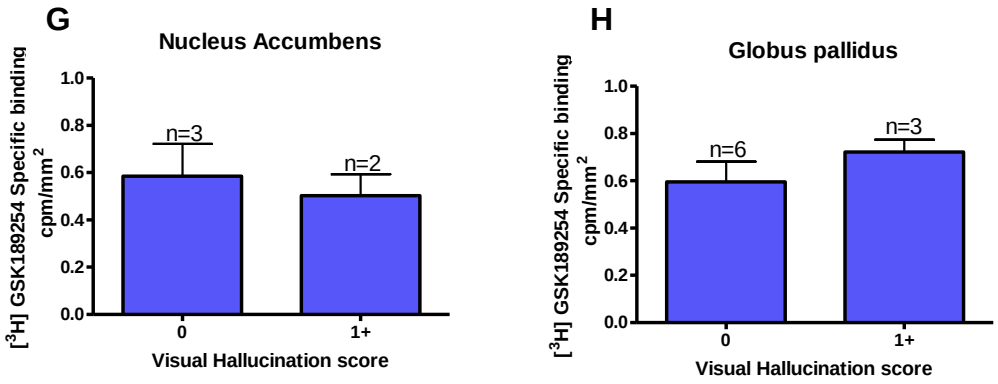

Figure 5.25 (G – H): Visual hallucination score against specific binding cpm/mm^2 of [^{3}H] GSK189254 in AD cases in (G) Nucleus Accumbens, (H) combined Globus Pallidus. Statistical significance was determined from the generated p value, where $p \leq 0.05$ was considered to show a significant linear relationship between clinical score and binding level.

Figure 5.25 shows specific H_3R binding levels $\pm$ SD cpm/mm^2 in AD cases (n=16) against visual hallucination score. There were no significant differences between the H_3R binding densities and severity of visual hallucinations.

Overall H_3R binding in both AD and DLB cases does not show any correlation with MMSE, UPDRS, depression in cortical or striatal structures in the human CNS. In contrast, increased H_3R binding positively correlated with increased severity of psychotic symptoms (delusion and visual hallucinations) in the globus pallidus in both AD and DLB patients.

5.5 Discussion

The autoradiography assays performed in this chapter have employed a highly potent and selective H_3R inverse agonist [^{3}H] GSK189254, to visualise and allow quantification of the human H_3R. A range of brain structures implicated in the characteristic symptoms of DLB and AD were investigated. For example the striatum which consists of the putamen and caudate nucleus, is known for its role in planning and modulation of movement pathways, but is also involved in a variety of other cognitive processes involving executive function. The cerebral cortex is involved in many complex brain functions including memory, attention, perceptual awareness, language and consciousness. More specifically, the anterior cingulate cortex is thought to be the neuroanatomical interface between emotion and cognition, and the insular cortex is believed to process convergent information to produce an emotionally relevant context from sensory experience. These are some of the brain regions whose functions are affected by dementia and chronic neurodegenerative diseases where cognition steadily declines. The main focus has been to determine whether there are any changes in the H_3R in relation to age and gender in control, DLB and AD cases.

Several lines of evidence suggest that manipulation of the histamine system may alleviate some of the clinical symptoms of AD and DLB. H_3R blockade with antagonist/ inverse agonists results in the up-regulation of several neurotransmitters which have been shown to have positive affects upon cognitive deficits in several animal models of dementia (Tiligada et al., 2009).

5.5.1 H_3R binding in rodent CNS in relation to aging and dementia

The first aim of this chapter was to determine the distribution pattern of the ligand binding in the brain of two strains of mouse and whether there were any differences in binding levels with increased age in each strain. H_3R binding was detected in brain regions where binding has previously been reported, with high density in the striatum and the cortex but not in the cerebellum (Le et al., 2009 and Medhurst et al., 2009). In several other studies, binding was detected in the striatal, cortical, thalamic, hippocampal, hypothalamic areas and substantia nigra, with minimal binding in white matter areas, (Pollard et al., 1993, Barbier et al., 2004 and Medhurst et al., 2009).

The next stage was to determine whether the levels of H_3R binding were altered in cortical and striatal regions associated with dementia, the cortex, cingulate cortex and striatum. The mean H_3R binding density in both cortical and striatal regions in CD-1 mice CNS show no significant difference in ligand binding over the age range of 3 - 12 months when learning deficits have been shown to occur (Michalikova et al., 2007 and Ennaceur et al., 2008). These data support the preservation of H_3Rs previously seen in the cortex, hippocampus and hypothalamus of wild type and TASTPM mice (Medhurst et al., 2009 & Chapter 4). mRNA levels for the H_3R in C57BL/6 mice at 4 time points 3, 12 ,18 and 24 months were also shown to be unchanged in all areas of the brain except the medulla, where there was a significant decrease from 18 month onwards (Terao et al., 2004).

In contrast, the mean H_3R binding density in striatal regions in mice TASTPM CNS showed a significant decrease in binding at 13 month old TASTPM mice compared with 3 month ($p \leq 0.05$) and 7 month ($p \leq 0.001$). The significant

decrease in binding seen at 13 months is interesting since the published literature suggests that the H_3R is preserved at 13 and 16 months in TASTPM mice, despite a significant amyloid load in the frontal cortex (Medhurst et al., 2009). A decrease in H_3R density in the striatum with increasing age may be important in behavioural changes seen in AD. A decrease in H_3R expression would result in decreased H_3R activation and increased neurotransmitter release, including acetylcholine and dopamine (Medhurst et al., 2009), therefore potentially acting as a compensatory mechanism for the loss of cortical-striatal innervation seen in AD that results in reduced acetylcholine in the pre-frontal cortex and hippocampus (Whitehouse et al., 1982).

The age dependant H_3R expression changes observed in this chapter in both CD-1 and TASTPM mice timeline were also confirmed using immune-specific probes (Chapter 3).

H_3R expression in cortical and striatal regions in rodent CNS appear to be largely preserved. H_3R expression was then determined in various cortical and striatal regions of the human CNS

5.5.2 H_3R binding in the human CNS in relation to aging

The next aim of the study was to determine the distribution pattern of the ligand in normal human brain and whether there were any age-dependant differences in H_3R binding. H_3R binding was detected in brain regions where binding has previously been reported, with high H_3R densities in the internal and external segments of the globus pallidus, caudate, putamen and nucleus

accumbens with moderate levels in the anterior cingulate and insular cortices (Martinez-Mir et al., 1990 and Anichtchik et al., 2001).

The next stage was to determine whether the levels of H_3R binding were altered in cortical and striatal regions associated with dementia, the caudate, putamen, anterior cingulate cortex, insular cortex, nucleus accumbens and globus pallidus. In this study, H_3R binding densities in both cortical and striatal regions in control human cases show no significant difference in ligand binding with age. Goodchild et al., (1999) also did not report any significant age-related changes in H_3R expression in the basal ganglia in normal ageing, nor did receptor density differ between male and female cases.

H_3R binding does not appear to be altered in normal aging supporting previously published data of H_3R preservation. H_3R binding was then determined in aged related dementias to see if disease state altered H_3R expression.

5.5.3 H_3R binding in the human CNS in relation to aging in two age related dementias

The purpose of this part of the study was to investigate whether the H_3R is preserved with age in human age related dementias. H_3R binding densities in both cortical and striatal regions in both DLB and AD human cases showed no significant difference in ligand binding with age, indicating that the H_3R is preserved in a range of cortical and striatal regions associated with AD and DLB.

Having looked at H_3R binding in the disease states separately, the next stage was to determine whether there were any age related changes in H_3R binding levels in DLB and AD cases compared to age matched controls.

5.5.4 H_3R binding in control human data compared with disease cases (DLB and AD)

The purpose of this part of the study was to investigate whether there are age dependant changes in H_3R levels in disease state compared to control cases.

H_3R binding densities in both cortical and striatal regions showed no significant difference in age related binding between control and DLB cases.

H_3R binding densities in the combined globus pallidus showed borderline significance with decreased binding with age in the DLB data set compared to aged matched controls.

H_3R binding densities in both cortical and striatal regions showed no significant difference in age related binding between control and AD cases.

H_3R binding densities in the combined globus pallidus showed borderline significance with increased binding with age in the AD data set compared to aged matched controls.

H_3R binding of both DLB and AD cases compared with age matched controls displays differential age related changes in the globus pallidus, with DLB cases showing a decrease in binding with age whilst an increase in binding is observed for AD cases. The differences observed are likely to be a result of the differential pathologies of the two diseases. The decrease in H_3R binding

in the globus pallidus in DLB cases may be related to the mobility problems associated with the disease that is not seen in AD.

Mean H_3R binding densities for each brain region were compared between all three groups to determine whether there were any alterations in H_3R densities between the two disease states compared with age matched controls. H_3R binding densities in both cortical and striatal regions showed no significant difference between control and disease states.

The data suggest that there is no significant change in H_3R population overall between control and disease cases, providing further evidence for H_3R preservation. Preclinical trials have already alluded to the prospect of H_3R antagonists as a treatment for cognitive impairment. Medhurst et al., 2007, demonstrated H_3R expression was preserved in late stages of AD in the pre-frontal cortex and hippocampus in human cases. We provide further evidence showing preservation of H_3Rs in many cortical and striatal brain regions, supporting the H_3R as a viable target in treating dementias.

5.5.5 Disease state symptom correlation studies.

In this section the H_3R binding levels have been correlated with scores from various clinical tests. There was no correlation between H_3R binding and MMSE or UPDRS scores in both DLB and AD cases, indicating that H_3R does not alter with severity of cognitive and motor impairment. There was an overall increase in H_3R binding with decrease in MMSE score indicative of a decrease in cognitive function. The increase in H_3R binding maybe acting as a

compensatory mechanism to counteract changes seen elsewhere in the histaminergic system in severe AD and DLB, such as a decrease in frontal cortex H_1R in AD (Higuchi et al., 2000), and reduced H_2R expression in the hippocampus in both AD and DLB (Goodchild et al., 1999). The functional consequence of increased H_3R density could be a further decrease in cognitive neurotransmitters and hence further exacerbation of cognitive deficits, and so would not be a positive compensatory effect. Alternatively, the increase in H_3R binding in brains of individuals with more severe dementia could simply be related to loss of cholinergic neurons. The data obtained support a previous report that higher frontal cortex H_3R binding correlated with more severe dementia (MMSE) in AD (Medhurst et al., 2009).

There was no correlation between H_3R binding and severity of depression in DLB and AD cases, suggesting that the H_3R does not play a role in depression associated with AD and DLB. In contrast, increased H_3R binding in the globus pallidus positively correlated with increased severity of psychotic symptoms, delusion and visual hallucinations, in both DLB and AD cases. This rise in H_3R binding was more profound in DLB cases than AD cases, which was to be expected since DLB cases have generally more pronounced psychosis than in AD. H_3R expression has been shown to be altered in patients with Schizophrenia and bipolar disorders and is thought to be involved in disease neuropathology (Jin et al., 2009). Jin et al. (2009) showed significantly higher H_3R radioligand binding in the prefrontal cortex of schizophrenic group and bipolar subjects with psychotic symptoms, and higher H_3R binding correlated with increased severity of psychotic symptoms,

as seen in this present study. H_3Rs in the human prefrontal cortex is thought to be involved in the modulation of cognition, and this is supported by findings in animals that H_3R antagonists enhance prepulse inhibition and cognition (Fox et al., 2002 & 2005 and Browman et al., 2004). Patients with bipolar disorder have altered H_3R binding in the hippocampus, a significant decrease in CA4, a non-significant trend towards decreased binding in CA1, a significant decrease in CA2 and significant increase in the dentate gyrus (Jin et al., 2009). Recently clinical trials with pitolisant, a H_3R antagonist, decreased the psychotic symptoms in schizophrenic patients (Schwartz et al., 2010 and Schwartz et al., 2011).

Overall, the level of H_3R expression in the globus pallidus displayed a range of changes in both AD and DLB cases in comparison to control cases. The psychotic symptoms assessed by delusions and visual hallucinations did not correlate for a range of cortical and basal ganglia structures, with the exception of the globus pallidus. DLB cases with moderate to high delusion and visual hallucination scores displayed approximately 40% and 22% higher H_3R binding densities (n = 6-7 individual cases), in comparison to cases lacking such psychotic symptoms. A similar trend was present in AD cases with moderate to high delusion and visual hallucination scores displayed approximately 37% and 14% higher H_3R binding densities, in comparison to cases lacking such psychotic symptoms. The volume of the human globus pallidus has been previously shown to be positively correlated with the severity of global psychotic symptoms, as measured by both the Scale for the Assessment of Negative Symptoms and Positive Symptoms (Spinks et al.,

2005). An increase in the volume of the globus pallidus may account for this apparent increase in the H_3R density.

The main key findings of this chapter were the general preservation of the H_3R in human and rodent cortical and striatal brain structures. Previous studies have shown the involvement of the H_3R in learning and memory in array of animal behavioural paradigms (Blandina et al., 1996, Giovanni et al., 1999, Fox et al., 2005, Medhurst et al., 2007, Ligneau et al., 2007 and Giannoni et al., 2009). The H_3R has also been shown to be preserved in AD and TASTPM mice cortical and temporal brain structures (Medhurst et al., 2007 & 2009). The therapeutic potential of the H_3R and its preservation in normal aging and in diseases with severe cognitive impairment makes it a good candidate for improving learning and memory in cognitive impairment. Functional receptors are therefore available as therapeutic targets for H_3R antagonist compounds, to help alleviate some of the symptoms of cognitive decline associated with AD and DLB.

To what extent [^{3}H] GSK189254 binds to the array of isoforms potentially expressed in the CNS still requires further work, as based on Chapter 4, this present study may underestimate the hH_3R levels. Additional experiments are required to assess the expression of the H_3R and its respective isoforms to determine to what extent the receptor and its isoforms are truly preserved in ageing and what part the isoforms play, if any in dementias.

CHAPTER 6:

Effect of acute GSK334429B *(In Vivo)* Treatment on Behaviour: Novel Open Space Test with Object Recognition

6.1 Objectives

To assess the behavioural effect of the highly potent and selective H_3R antagonist/ inverse agonist, GSK334429B in a novel open space test. GSK334429B is a congener of GSK189254 and displays high affinity and selectivity for the H_3R. The behavioural paradigm is able to assess anxiety, mobility, learning and memory performance of an animal within the same experimental settings and testing conditions.

6.2 Introduction

The open space behavioural test with object recognition is a modification of the previously described open space behavioural test of anxiety, where an animal's response to the novelty of an open space environment are assessed in either a single session (emotional) or multiple sessions (learning, memory) (Ennaceur et al., 2006, 2010, 2010a-c). It has been proposed that the first few exposures to the maze are likely to induce fear of novelty-induced anxiety, therefore these initial sessions were assessed for emotional responses as well as working memory, following which repeated exposures are thought to diminish anxiety as learning improves (Ennaceur et al., 2006, 2010a & 2010c). In the initial part of this study anxiety of the mice was assessed, mice were introduced to an elevated platform (Figure 6.1) with two identical objects without prior habituation, where a protected space is not available to avoid from or escape to. In these conditions, at any one time, an approach to one

place can be considered an escape to that place or avoidance of another place. The same response can be considered as an approach, an escape or an avoidance response at the same time. The drive to escape/ avoid is confounded with the drive to explore; i.e. both cannot be dissociated. It is this un-dissociable expression of approach and escape or avoidance responses that defines anxiety in both humans and animals. Balb/c mice were chosen for this study because of their high anxiety characteristic (Ennaceur et al., 2010a).

In the second part of the study, learning and memory of the mice were assessed, the mice were placed on to the elevated platform with two different objects, one of which the mouse will have seen before and the other will be a novel to the mouse. When exposed to a familiar object alongside a novel object, mice approach frequently and spend more time exploring the novel than the familiar object. This apparent 'unconditioned preference' for a novel object is considered as an indication that a representation of the familiar object exists in memory; it forms the basis of the object recognition task in the study of memory function in rodents (Ennaceur et al., 2010 & 2010b). This behavioural paradigm is able to assess the motor activity, emotional responses, learning and memory performance of an animal within the same experimental settings and testing conditions (Ennaceur et al., 2006). The mice are placed in the central platform and left to explore the open space behavioural paradigm.

Diagram showing the open space maze:

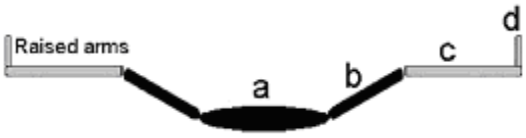

Figure 6.1: Open space test highlighting a) central platform b) mesh arm and c) elevated platform.

Previous behavioural studies have shown H_3R antagonist/ inverse agonist to have a beneficial effect in learning and memory in several behavioural paradigms. Ciproxyfan has been shown to reverse scopolamine induced amnesia (Giovannini et al., 1999). GSK189254, when orally delivered significantly improved performance of rats in a diverse range of cognition paradigms; passive avoidance, water maze, object recognition and attentional set shift (over the dose range 0.3–3mg/kg p.o.) (Medhurst et al., 2007). In cats, pitolisant markedly enhanced wakefulness at the expense of sleep states and also enhanced fast cortical rhythms of the electroencephalogram, known to be associated with improved vigilance (Ligneau et al., 2007). GT-2331 (cipralisant) and ciproxifan in a dose dependant manner significantly, enhanced cognitive performance of spontaneous hypertensive rat (SHR) pups in a repeated acquisition version of an inhibitory avoidance task, a measure of the cognitive and attention deficits often characteristic of ADHD. In contrast RαMHA, a H_3R agonist, blocked the procognitive effects seen with ciproxifan, further supporting a H_3R action (Fox et al., 2002).

Many H_3R antagonists have entered clinical trials and show promising efficacy for narcolepsy and ADHD, as well as cognitive impairment in schizophrenia and cognitive disorders. Histaminergic neurons have been shown to be largely

spared in neurodegenerative disease (Medhurst et al., 2007 & 2009 and this thesis), making H_3R targeting very attractive since modulation of this receptor results in the modulation of other neurotransmitter systems. A phase II study showed that PF-03654746 is effective in the treatment of the psychotic symptoms of adult ADHD. Pitolisant has displayed considerable promise as a vigilance-enhancing agent in PD patients experiencing excessive daytime sleepiness in a phase III study (Arnulf et al., 2009 and Schwartz et al., 2010). The role of the H_3R in anxiety remains controversial (Frisch et al., 1998, Rizk et al., 2004, Dere et al., 2004 and Acevedo et al., 2006), due to the poor validity of current behaviour tests. This study will address this issue with a new properly validated animal test of human anxiety (Ennaceur et al., 2010a, b and Michalikova et al., 2010).

The aim of this chapter was to determine the behavioural effect of a highly potent and selective H_3R antagonist/ inverse agonist, GSK334429B on mobility, anxiety, learning and memory.

6.3 Methods

6.3.1. Animals

32 male Balb/c AnNCrl mice obtained from Charles River (UK) were used in the experiments described in this study. Mice were 56-62 days old at the date of arrival and were left to acclimatize to local laboratory conditions for two weeks. Mice were housed in colony room that were held under a 12 h light/12 h dark cycle (light 0700-1900 h at 180 Lux) and at 23°C ±1°C. In order to avoid unequal light exposure, the upper shelf was occupied with plastic cages filled with clean sawdust. Mice were housed singularly and all mice had *ad libitum* access to food and water. During the period of acclimatization, mice were removed twice a week from their cages for cleaning and renewing of their food and water supply. Animal treatment and husbandry were in accordance with approved use of animals in scientific procedures regulated by the Animals (Scientific Procedures) Act 1986, UK.

6.3.2 Drugs and treatments

GSK334429B was provided by GSK (Harlow, UK). The drug was dissolved in physiological saline and prepared freshly on the days of the test and administered i.p. 1ml/kg body weight, 30 min before the start of a session. Animals were treated once a day in 5 successive days. The mice were divided into 4 groups; one group treated with saline (n=8) and separate groups treated with GSK334429B at 0.1 mg/kg (n=8), 0.3 mg/kg (n=8), 1 mg/kg (n=8).

6.3.3 Apparatus and testing procedures

The behavioural paradigm consists of a platform 80 cm x 80 cm wide, elevated 75 cm from the ground. Steep upward inclined panels (width: 80 cm x 25 cm, slope angles 103°) made of rigid wire mesh that are attached on two opposite sides of the platform (see Figure 6.2). The slopes end on a step stand (80 cm x 25 cm) that mice need to climb onto. The rationale for these stands is that we expected that all mice would climb easily onto the slopes as they usually do when housed in mesh-wire cages. Therefore, it was necessary to add a stand at the end of a slope which enables us to discriminate between strains of mice which do cross and those who do not cross onto the stands. The platform was divided into a central area covered with a white tile (16 x 16 cm wide and 0.4 cm thick), an inner area surrounding the central area (16 cm wide and 2048 cm^2), and an outer area (16 cm wide and 4096 cm^2). The outer area was further divided into areas adjacent to the slopes (2048 cm^2) and areas adjacent to void space (2048 cm^2). The surface of the platform was cleaned to minimize the effects of lingering olfactory cues. Any faeces and urine were removed with paper towels, then cleaned with antibacterial solution followed by 90% ethanol and left to dry before the introduction of the next mouse. The illumination on the surface of the elevated platform was 40 Lux.

Mice were exposed to the test apparatus in 5 sessions, one session a day for 9 min per session. In the first 3 sessions animals were released from the step stands, unfortunately only a few animals did cross onto the slopes and did not return back. In sessions 4 and 5, animals were released in the central area of the platform and the results from these two sessions are presented in this

report. The mice were weighed in a small bucket and poured gently onto the central platform at the start of a session and left to explore the apparatus.

Open space test:

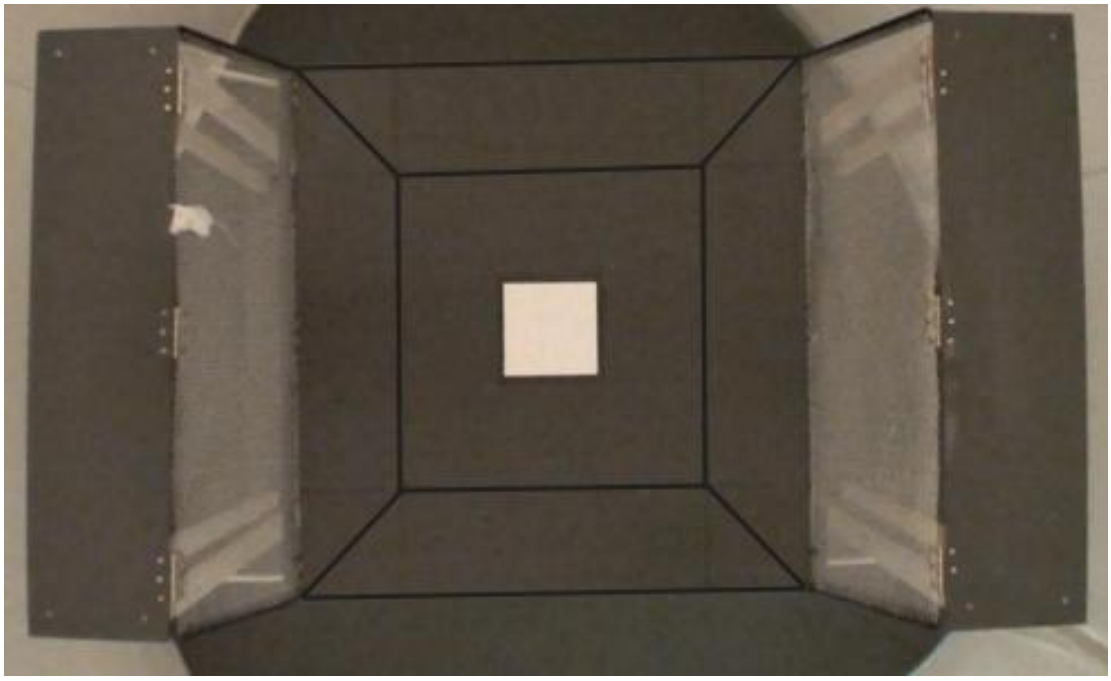

Figure. 6.2: Open space test showing central platform, mesh arms and elevated platform (top and frontal views). The recorded behavioural data consist of measures of the number of entries and duration of entries into the central area, the inner area, the outer area, the slopes and step-stands in addition to latency of first entry into each of these areas. The record of outer area was further divided into measures related to areas adjacent to the slopes and areas adjacent to void space. Note, this test has been validated by our group (in parallel studies) in terms of strain-dependent anxiety differences and sensitivity to a benzodiazepine anxiolytic drug, diazepam (eg. Ennaceur et al., 2010, Ennaceur et al., unpublished).

6.3.4 Measurement and statistical analysis

The recording of the behaviour of mice was based on entries into defined areas of the apparatus. An entry was recorded whenever a mouse crossed with all its four paws into an area. In the case of step stand entries, it is possible for a mouse to cross onto a stand and remain there for the remaining duration of a test session. An animal that is unable to return to the slope after its first entry onto a stand should be considered as anxious as the one that did

not enter the stand. In this case, the first entry is recorded only when the mouse returns back to the slope. Any subsequent re-entry is normally recorded. All sessions were video recorded and the behaviour of mice was analyzed with an in-house computer program, EventLog.

All data are expressed as mean ± s.e.m. Differences among group means values for each of the above measurements are tested for significance with one-way ANOVA repeated measures followed up with Newman–Keuls post-hoc comparisons (Statistical for Windows, version 5.5). Results are considered significant when $p \leq 0.05$. When $p \leq 0.10$, p is rounded up to the nearest value and reported as non significant.

6.4 Results

6.4.1. Total number of crossings on the surface of the platform:

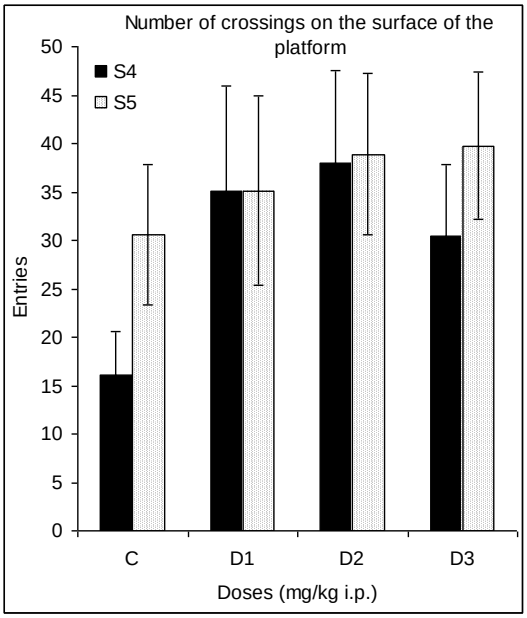

Figure 6.3: Total number of crossings on the surface of the platform. S – session number, C – control, D1 – Drug concentration 0.1 mg/ml, D2 – Drug concentration 0.3 mg/ml and D3 – Drug concentration 1.0 mg/ml.

Figure 6.3 shows there was no significant differences between groups, between sessions, and no significant interactions between groups and sessions. In saline treated mice, the number of crossings was significantly increased in session 2 (S2) compared to session 1 (S1), ($t7=2.07$, $p<0.04$).

6.4.2. Latency of first entry onto the stands (Figure. A):

6.4.3 Number of crossings onto the stands (Figure. B):

6.4.4 Duration of entries onto the stands (Figure. C):

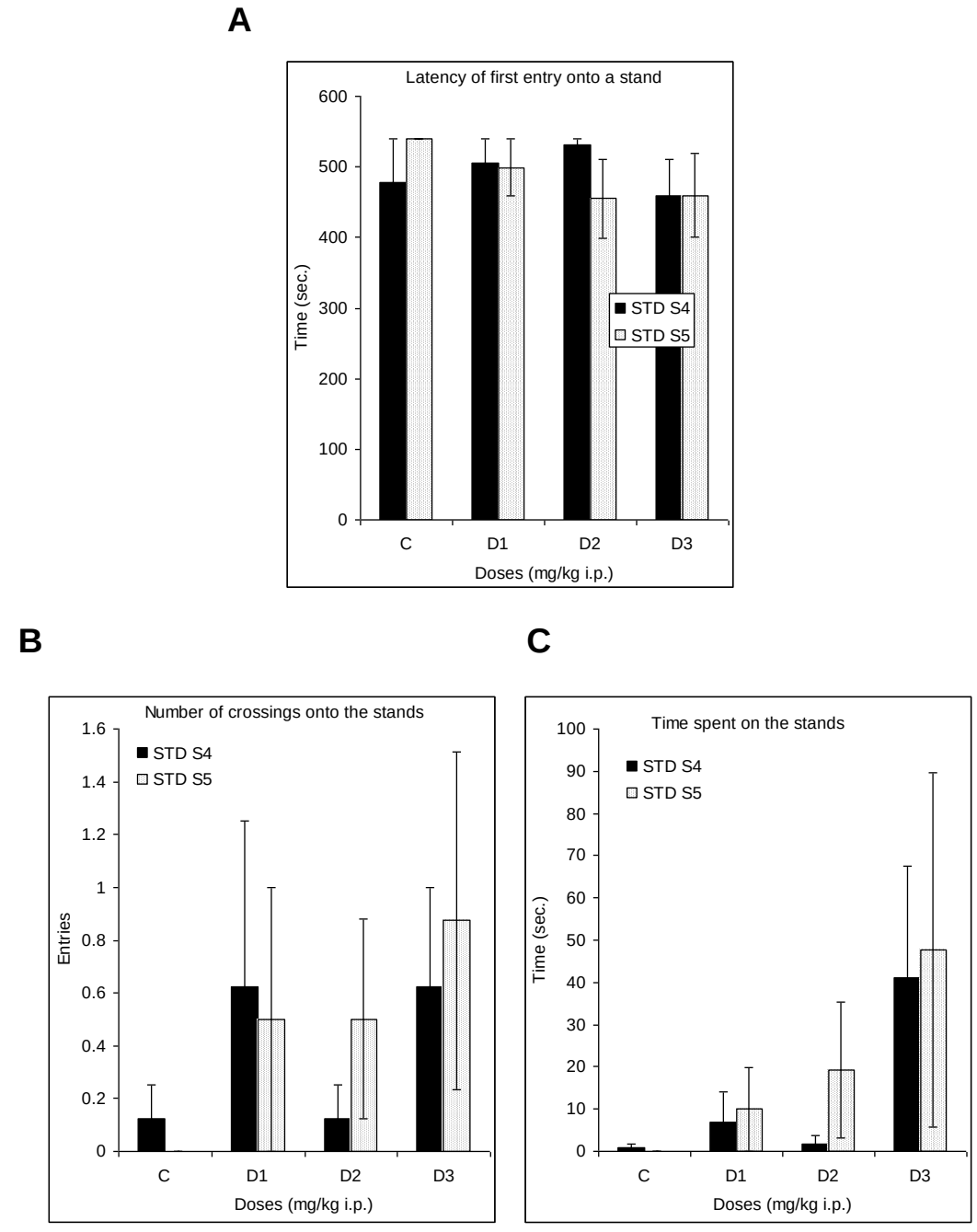

Figure. 6.4: Latency of first entry, number of entries and duration of entries onto the stands. S – session number, STD – stands, C – control, D1 – Drug concentration 0.1 mg/ml, D2 – Drug concentration 0.3 mg/ml and D3 – Drug concentration 1.0 mg/ml.

Figure 6.4 shows there was no significant differences between groups, between sessions and no significant interactions between groups and sessions.

6.4.5 Number of entries onto the slopes (Figure A):

6.4.6 Latency of first entries onto the slopes (Figure B):

A **B**

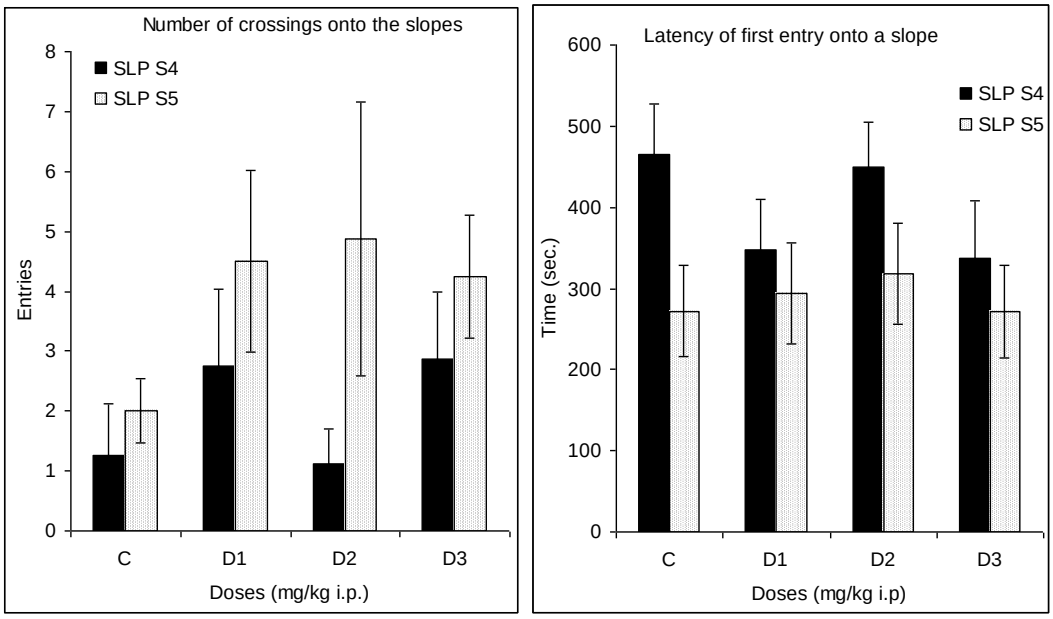

Figure. 6.5: (A) Number of entries onto the slopes. (B) Latency of first entry onto the slopes. S – session number, SLP – slope, C – control, D1 – Drug concentration 0.1 mg/ml, D2 – Drug concentration 0.3 mg/ml and D3 – Drug concentration 1.0 mg/ml.

Figure 6.5 (A) shows there were no significant differences in the number of crossings onto the slopes between groups, between sessions and no significant interactions between groups and sessions.

Figure 6.5: (B) shows there were no significant differences in the latency of first entry onto a slope between groups and no significant interactions between groups and sessions. There were however significant differences

between sessions in the number of entries ($p<0.007$) and latency of first entry ($p<0.0008$). In mice treated with 0.3 mg/kg, the number of crossings was significantly increased ($t7=1.79$ and 1.95, $p<0.05$, respectively) and the latency of entry was significantly reduced ($t7=2.12$, $p<0.04$) in session 2 compared to session 1. The latency of first entry was also significantly reduced in saline treated mice in the second session compared to the first ($t7=3.06$, $p<0.01$).

6.4.7. Number of entries onto areas adjacent to the slopes:

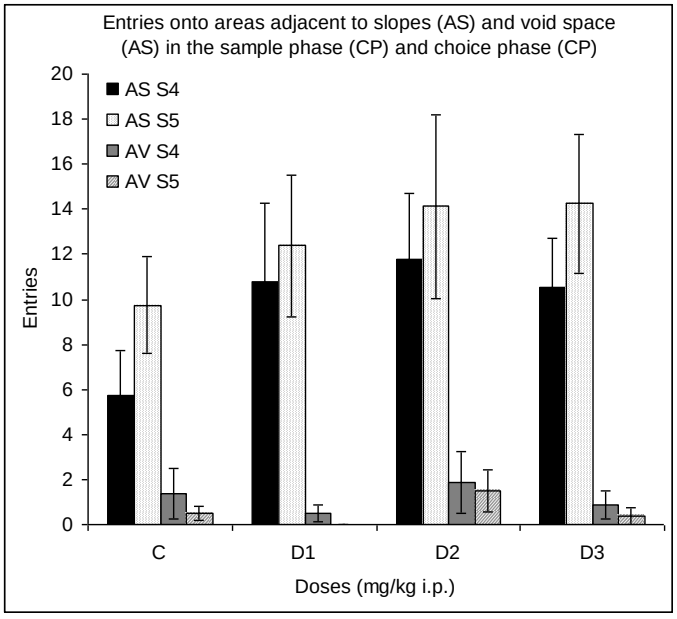

Figure. 6.6: Number of entries onto areas adjacent to the slopes. S – session number, AV – adjacent slope, C – control, D1 – Drug concentration 0.1 mg/ml, D2 – Drug concentration 0.3 mg/ml and D3 – Drug concentration 1.0 mg/ml.

Figure 6.6 shows there were no significant differences between groups and no significant interactions between groups and sessions. There were significant differences between sessions in the number of entries ($p<0.03$) but not in latency and duration. In saline treated mice, the number of crossings was significantly increased in session 5 compared to session 4 ($p<0.03$).

6.4.8 Latency of first entry, number of entries and duration of entries onto areas adjacent to the void space: There were no significant differences between groups, between sessions and no significant interactions between groups and sessions in all 3 measurements.

6.4.9 Number of entries and duration of entries onto the inner area: There were no significant differences between groups, between sessions and no significant interactions between groups and sessions in both measurements.

6.4.10 Number of entries and duration of entries onto the central area:

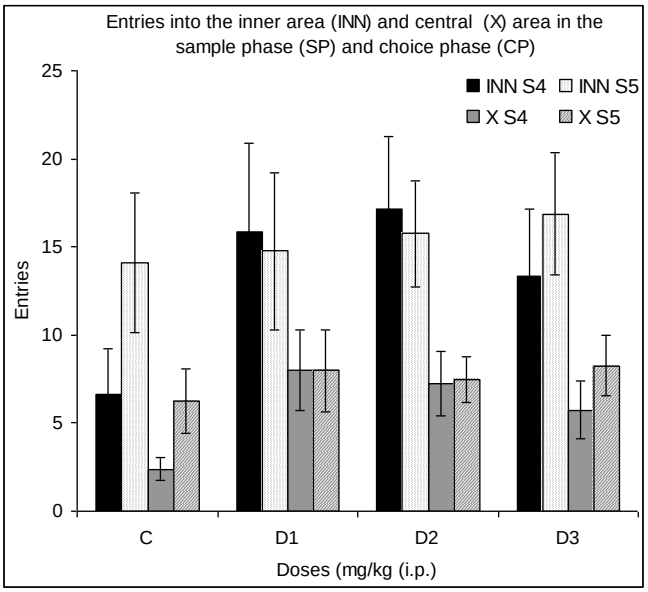

Figure. 6.7: Number of entries and duration of entries onto the central area. S – session number, X – central, INN – inner area C – control, D1 – Drug concentration 0.1 mg/ml, D2 – Drug concentration 0.3 mg/ml and D3 – Drug concentration 1.0 mg/ml.

There were no significant differences between groups, and no significant interactions between groups and sessions. There were however significant differences between sessions in the number of entries ($p<0.05$) but not in the

duration of entries. Saline treated mice crossed more frequently into the central area in session 5 than in session 4 ($p<0.04$)

6.4.11 Latency of first approach, number of approaches and duration of approaches of objects: There were no significant differences between groups, between sessions and no significant interactions between groups and sessions.

6.5 Discussion

In the present study, 2 month old Balb/c mice were divided into four groups and received either saline or a H_3R inverse agonist GSK334429B at 0.1 mg/kg, 0.3 mg/kg or 1 mg/kg i.p. (recommended doses, Dr A Medhurst, GSK) and then exposed to an open space test (Figure 6.2). This behavioural paradigm examined emotional responses to novelty and open spaces, and motor activity in initial exposures to the test, in addition to learning and memory performance in the latter phase of the test.

The emotional response or anxiety measures for an animal on the open space behavioural paradigm consisted of the number of crossings in the surface of the platform, the latency of the first entry, number of entries and duration of entries onto the stands. An increase in number of crossings onto the stands and slopes, and a reduction in the latency of first entry to the stand would suggest a decrease in anxiety and an increase in exploration, respectively. There were no significant differences in the total number of crossings onto the surface of the platform between saline and drug treated groups. There does however appear to be a trend for an increased number of crossings in session 4 in the drug treated groups compared with the saline group reflecting an increase in motor activity. In the saline treated group, the number of crossings was significantly increased in session 2 compared to session 1 indicating that the mice were more active in session 2, reflecting a reduction in the level of anxiety.

The majority of results were statistically insignificant between the 4 groups indicating that H_3R antagonists, in particular GSK334429B at a concentration of 0.1-1mg/kg are not anxiolytic or anxiogenic. However, there was

significance between sessions but this was to be expected, as the more exposed the mice are to the test they would begin to overcome the anxiety of the novelty and open space environment and increase exploration would allow for learning to commence.

Notably, the level of anxiety displayed by the mice in all groups was excessively high throughout the 5 sessions (very limited habituation), which greatly limited the learning performance of the mice (not shown). Therefore, the effects of the drug could not be assessed upon learning performance. To overcome this in future experiments mice would need to be exposed to the maze for a longer period of time or longer habituation period or alternatively a less anxious strain of mouse such as the C57 to suppress the influence of anxiety upon short-term memory performance.

This study provides further evidence that the H_3R may have a role to play in motor activity and strong evidence that the H_3R, while it may be involved in fear-avoidance responses (Dere et al., 2010), it does not have a role to play in anxiety responses. This concurs with other unpublished studies from our laboratory using the 3D maze open space anxiety test, together with both selective H_3R agonist and antagonist drugs (Ennaceur and Chazot, in preparation).

CHAPTER 7

GENERAL DISCUSSION

During the course of this PhD project, 3 new antibodies specific to isoforms of the human histamine H_3R have been generated and validated (Chapter 3). These novel immunological tools (first of their kind) have been used alongside previously validated H_3R antibodies to characterise the molecular pharmacology of the different human isoforms as well as looking at the expression of H_3R in relation to ageing in normal and neurodegenerative rodent and human brain. The key hypotheses addressed were:

7.1 H_3R are preserved in murine and human aging and age related dementias

Immunohistochemical analysis of the H_3R in CD-1 and TASTPM mouse brain displayed a wide expression profile in the CNS: globus pallidus, medial and lateral segments, caudate, putamen, hippocampus, external layers of the cortex. Highest expression was detected in the cerebral cortex, hippocampal formation and basal ganglia, areas all associated with cognition and motor activities, as well as the hypothalamus. Immunohistochemical and immunoblotting data based on the mouse timeline experiments would suggest that H_3R as a general population do not appear to alter between the ages or 3-10 months or 3-7months in CD-1 and TASTPM mice, respectively, the time periods where learning deficits are clearly evident in these mice. In contrast, between the ages of 12-19 months the expression of the H_3R dramatically decreases in the CD-1 mouse CNS in all areas examined. This is likely down

to increased CNS atrophy which is reflected behaviourally in the animal's general health. The $H_3R_{A/C}$ isoforms also appears to be preserved with age in both CD-1 and TASTPM mice (Chapter 3). Autoradiography data (Chapter 5) also confirms the immunological findings in chapter 3, showing general preservation of H_3R expression between 3-12 months in CD-1 and TASTPM mouse brain. However, autoradiography data along with immunological data displayed a trend for increased H_3R binding in TASTPM mice at 7 months which returns back to basal levels by 12 months of age. This increase in H_3R binding may reflect a compensatory mechanism occurring within the CNS as the disease progresses, between the ages of 3 - 7 months is when the profound learning deficits have been shown to develop as well as a significant increase in Aβ plaques in areas of the brain involved in cognition. The differences observed in H_3R expression between the CD-1 and TASTPM mice data sets may reflect in the pathology of the two dementias seen in these different mouse models.

Overall H_3Rs would appear to be preserved in a range of striatal and cortical structures in rodent CNS when probed with rodent specific immunological probes.

Autoradiographical analysis (Chapter 5) of the human H_3R in the brain displayed specific binding in the globus pallidus, caudate, putamen, hippocampus, nucleus accumbens, anterior cingulate cortex and insular cortex, areas associated with cognition, motor and emotional behavious. Radiolabelling of H_3R with a highly specific H_3R inverse agonist [^{3}H] GSK189254 demonstrated that H_3R expression appears to be largely preserved in an array of key cortical and striatal structures in normal human

aging and in the neurodegenerative disease cases investigated, namely DLB and AD.

Using immunological specific probes, for the first time human H_3R isoforms have been shown to be expressed at the protein level in the human brain. Preliminary immunoblotting data obtained for human disease cases suggest for the first time that H_3R isoform expression is altered in different disease states. The H_3R_{365} isoform appears to be largely unaltered in PD and DLB unlike the H_3R_{445} and H_3R_{329} isoforms which appear to be increased in DLB and PD, respectively. To what extent [^{3}H] GSK189254 binds to the array of isoforms potentially expressed in the CNS still requires further work. Based on the results obtained in Chapter 4, this study may underestimate H_3R expression in the human CNS.

Overall, a selection of novel anti-hH_3R isoform specific probes were generated which were selective for particular human H_3R isoform targets. The development of H_3R isoform specific ligands will allow for further analysis of the changes occurring in the expression of these receptor isoforms throughout disease progression. Future work is needed for the further development of isoform specific antibodies and detailed mapping of the isoforms in both rodent and human CNS. It would be interesting to see if expression and/or distribution pattern was influenced by environmental factors such as stress and disease.

7.2 Human H_3R homomeric isoforms and heteromeric subtypes display differential pharmacological properties

Saturation and competition binding assays using the highly specific H_3R inverse agonist [^{3}H] GSK189254 was used to determine the pharmacological properties of three of the major human H_3R isoforms: H_3R_{329}, H_3R_{365} and H_3R_{445} either expressed alone or co-expressed in HEK 293 cells. Saturation binding assays showed the ligand to display a 5-fold lower affinity for the shorter of the three isoforms, hH_3R_{329} and a 10-fold lower affinity for the heterodimeric combination: hH_3R_{329} + hH_3R_{365}. In certain experimental techniques [^{3}H] GSK189254 may underestimate the number of hH_3Rs due to the differential pharmacological profile at the different isoforms. To what extent other H_3R ligands may underestimate the numbers of H_3Rs is unknown.

Competition binding assays performed using an array of H_3R ligands (agonist, antagonist, inverse agonist and protean ligand) displayed a biphasic competition curve suggesting that the compounds are recognising a high and low affinity H_3R binding site. Competition binding assays showed significant differences in the high-affinity binding sites between ligands (thioperamide, GSK334429B, RαMHA, iodophenpropit and proxyfan) at the same isoform as well as across the isoforms, providing new information regarding the fundamental pharmacological nature of human H_3R and its respective isoforms. This establishes the potential for developing H_3R isoform specific ligands, which will allow for further detailed pharmacological analysis and give further insight into the heterogeneity of the H_3R isoforms that will eventually lead to the development of highly specific therapeutic drugs.

7.3 H_3R are involved in anxiety and memory behaviours

GSK334429B, a congener of GSK189254, a highly potent and selective H_3R antagonist/ inverse agonist was administered at a concentration of 0.1-1 mg/kg i.p. to 2 month old Balb/C mice. The open space maze paradigm is a novel validated all-in-one behavioural elevated platform test that is able to look at a variety of behaviours such as emotion, mobility, learning and memory. The role of the H_3R in anxiety remains controversial due to the poor validity of current behaviour tests. This newly validated behavioural paradigm showed that H_3R antagonists are not anxiogenic or anxiolytic. The level of anxiety displayed by the mice in all groups was excessively high throughout the 5 sessions which greatly limited the learning performance of the mice and, therefore, learning performance could not be assessed. To overcome this in future experiments mice would need to be exposed to the maze for a longer period of time or a longer habituation period or alternatively use a less anxious strain of mice such as C57 to suppress the influence of anxiety upon short-term memory performance. Furthermore, exploratory behaviour will be increased on the apparatus with a food deprivation strategy in future experiments.

This study provided new evidence that that the H_3R, while it may be involved in fear-avoidance responses (Dere et al., 2010), it is not involved in anxiety responses. This concurs with other unpublished studies from our laboratory using the 3D maze open space anxiety test, together with both selective H_3 agonist and antagonists (Ennaceur and Chazot, in preparation).

Additional experiments are required to assess the expression of the H_3R and its respective isoforms to determine to what extent the receptor and its isoforms are truly preserved in ageing and what role the isoforms play, if any, in dementias.

Understanding the biology of histamine and respective receptors is crucial for the development of novel therapies. Receptor heterogeneity has been a crucial focus for this thesis as it forms a major part of understanding of the histamine H_3R and its function. Drugs targeting the histamine H_1R and histamine H_2R have been available for many years for the treatment of allergies and gastric inflammation, respectively. Expectations for similar block buster drug status are expected for both the H_3R and H_4R. Drug development for both H_1 and H_2 receptors was not as complex as has been for the H_3 and H_4 receptors due to the lack of heterogeneity. The discovery of numerous receptor isoforms for both the H_3 and H_4 receptors and their implication have been a major obstacle in the development of drugs entering the clinical. We have developed the first panel of H_3R isoform specific antibodies which will help with investigating the role of these isoforms in relation to the full length receptor, their anatomical topologies in normal versus diseased brain and aid the development of isoform selective compounds.

The purpose of the different isoforms is a topic of great interest. Previous studies have shown pharmacological differences between the different isoforms. This thesis has shown that the human H_3R_{329} isoform displays a different pharmacological profile to the H_3R_{365} and $H_3R_{445.}$ Similarly, co-expression of the H_3R_{329} with the H_3R_{365} lowers the affinity of the H_3R_{365} isoforms. These studies were performed in a recombinant system with the

receptors being artificially expressed in HEK 293 cells. However, these isoforms are known to be co-expressed in the CNS and therefore one may hypothesize that such an interaction is possible. To what extent the isoform effects/ controls H_3R pharmacology, expression and function is still unknown. In order to assess their functional significance, compounds capable of distinguishing between these isoforms are required.

The histaminergic system, like the other aminergic systems plays a modulatory role. Histamine plays a major role in homeostasis and helping the animal to respond appropriately to its' environment. Complex information has to be continually processed and integrated, flexibility is crucial to its function. Heterogeneity may be the mechanism underlying this flexibility allowing for close, regulated control of receptor expression and function.

REFERENCES

Acevedo, S.F., Pfankuch, T., Ohtsu, H. and Raber, J. (2006). Anxiety and cognition in female histidine decarboxylase knockout HDC (-/-) mice. Behav Brain Res **168**: 92–99

Acevedo, S.F., Ohtsu, H., Benice, T.S., Rizk-Jackson, A. and Raber, J. (2006). Age-dependent measures of anxiety and cognition in male histidine decarboxylase knockout HDC-/- mice, Brain Res **1071**:113–123

Airaksinen, M., Paetau, A., Paljärvi, L., Reinikainen, K., Riekkinen, P., Suomalainen, R., and Panula, P. (1991). Histamine neurons in human hypothalamus: Anatomy in normal and Alzheimer diseased brain. Neuroscience **44**:465–481

Akhtar, M., Devi, P.U., Ali, A., Pillai, K.K. and Vohora, D. (2006). Antipsychotic-like profile of thioperamide, a selective H3 receptor antagonist in mice. Fundamental & Clinical Pharmacology **20**: 373-378

Akiyama, H., Barger, S., Barnum, S., Bradt, B., Bauer, J., Cole, G.M., Cooper, N.R., Eikelenboom, P., Emmerling, M., Fiebich, B.L., Finch, C.E., Frautschy, S., Griffin, W.S., Hampel, H., Hull, M., Landreth, G., Lue, L., Mrak, R., Mackenzie, I.R., McGeer, P.L., O'Banion, M.K., Pachter, J., Pasinetti, G., Plata-Salaman, C., Rogers, J., Rydel, R., Shen, Y., Streit, W., Strohmeyer, R., Tooyoma, I., Van Muiswinkel, F.L., Veerhuis, R., Walker, D., Webster, S., Wegrzyniak, B., Wenk, G. and Wyss-Coray,T.

(2000). Inflammation and Alzheimer's disease, Neurobiol. Aging **21**: 383–421

Alguacil, L.F. and Perez-Garcia, C. (2003). Histamine H3 receptor: a potential drug target for the treatment of central nervous system disorders, Curr Drug Targets CNS Neurol Disord **2:** 303–313

Alves-Rodrigues, A., Leurs, R., Wu, T.S., Prell, G.D., Foged, C. and Timmerman, H. (1996). [3H]-thioperamide as a radioligand for the histamine H3 receptor in rat cerebral cortex. Br J Pharmacol **118**: 2045-2052

Anichtchik, O.V., Peitsaro, N., Rinne, J.O., Kalimo, H., and Panula, P. (2001). Distribution and modulation of histamine H3 receptors in basal ganglia and frontal cortex of healthy controls and patients with Parkinson's disease. Neurobiol Dis **8:** 707–716

Arnulf, I. Results of clinical trials of tiprolisant in narcolepsy and Parkinson's disease. 22nd ECNP Congress (Sept 12-16, Istanbul): S.19.05.
A study to evaluate the efficacy and safety of two doses of PF-03654746 in adults with attention deficit hyperactivity disorder (ADHD) (NCT00531752). ClinicalTrials.gov Web site, March 11, 2010

Arrang, J.M., Garbarg, M. and Schwartz, J.C. (1983). Auto-inhibition of brain histamine- release mediated by a novel class H3 of histamine-receptors. Nature **302**: 832-837

Arrang, J.M., Garbarg, M., Lancelot, J.C., Lecomte, J.M., Pollard, H., Robba, M., Schunack, W. and Schwartz, J.C. (1987). Highly potent and selective ligands for histamine Ha-receptors. Nature, **327**: 117-123

Arrang, J.M., Garbarg, M., Lancelot, J.C., Lecomte, J.M., Pollard, H. and Robba, M., *et al.*, (1988). Potential interest in powerful and specific ligands for the histamine H3 receptor, Allerg Immunol **20**: 327–329

Arrang, J.M., Schwartz, J.C., Trafford, E., Tardivel-Lacombe, J., Leurs, R. and Ruat, M. (2000). Histamine receptor subtypes: molecular pharmacology. Neuropsychopharmacology. **3**: 174-176

Arrang, J.M., Druetl, G., Schwartz, J.C. (1995). Characterisation of histamine H3 receptors regulating acetylcholine release in the rat entorhinal cortex. Br J Pharmacol **114**: 1518-1522

Ash, A.S.F. and Schild, H.O. (1966) Receptors mediating some actions of histamine. Br J Pharmacol **27:** 427-439

Bakker, R.A., Lozada, A.F., van Marle, A., Shenton, F.C., Drutel, G., Karlstedt, K., Hoffmann, M., Lintunen, M., Yamamoto, Y., van Rijn, R.M.,

Chazot, P.L., Panula, P. and Leurs, R. (2006). Discovery of Naturally Occurring Splice Variants of the Rat Histamine H3 Receptor That Act as Dominant-Negative Isoforms. Mol Pharmacology **69**: 1194-1206

Ballmaier, M., O'Brien, J.T., Burton, E.J., Thompson, P.M., Rex, D.E., Narr, K.L., McKeith, I.G., DeLuca, H. and Toga, A.W. (2004). Comparing gray matter loss profiles between dementia with Lewy bodies and Alzheimer's disease using cortical pattern matching: diagnosis and gender effects. NeuroImage, **23**: 325-335

Bancroft, J.D. and Stevens, A. (1990). Theory and practice of histological techniques, 3rd edition. Churchill Livingstone, Edinburgh.

Barbier, A.J., Berridge, C., Dugovic, C., Laposky, A.D., Wilson, S.J., Boggs, J., Aluisio, L., Lord, B., Mazur, C. and Pudiak, C.M. (2004). Acute wake-promoting actions of JNJ-5207852, a novel, diamine-based H3 antagonist. Br J Pharmacol **143:** 649–661

Baudry, M., Martres, M.P. and Schwartz, J.C. (1975). H_1 and H_2 receptors in the histamine-induced accumulation of cyclic AMP in guinea pig brain slices. Nature **253:** 362-363

Bauer, J., Strauss, S., Schreiter-Gasser, U., Ganter, U., Schlegel, P., Witt, I., Yolk, B. and Berger, M. (1991). Interleukin-6 and alpha-2-macroglobulin

indicate an acute-phase state in Alzheimer's disease cortices, FEBS Lett. **285**: 111–114

Best, C.H., Dale, H., Dudley, H.W., Thorpe, W.V (1927). The nature of the vaso-dilator constituents of certain tissues. J Physiol. **62**: 397-417

Best, C.H. and McHenry, E.W. (1931). HISTAMINE. Physiol. Rev. **11**: 371-477

Bacciottini, L., Passani, M.B., Giovannelli, L., Cangioli, I., Mannaioni, P.F., Schunack, W. and Blandina, P. (2002). Endogenous histamine in the medial septum-diagonal band complex increases the release of acetylcholine from the hippocampus: a dual-probe microdialysis study in the freely moving rat. European Journal of Neuroscience **15**: 1669-1680

Barber, R., Panikkar, A., McKeith, I.G. (2001). Dementia with Lewy Bodies: diagnosis and management. Int J Geriatr Psychiatry. **16**: S12-18

Black, J.W., Duncan, W.A.M., Durant, C.J., Ganellin, C.R. and Parsons, E.M. (1972). Definition and antagonism of histamine H2-receptors. Nature **236:** 385-390

Bladina, P., Giorgetti, M., Bartolini, L., Cecchi, M., Timmerman, H., Leurs, R., Pepeu, G. and Giovannini, M.G. (1996). Inhibition of cortical

acetylcholine release and cognitive performance by histamine H3 receptor activation in rats. Br J Pharmacol **119**: 1656-1664

Blandina, P., Passani, M.B., Nosi, D., Chazot, P.L., Shenton, F.C., Medhurst, A.D. and Munari, L. (2009). Heterogeneity of histaminergic neurons in the tuberomammillary nucleus of the rat. European Journal of Neuroscience **29**: 2363-2374

Bonaventure, P., Letavic, M., Dugovic, C., Wilson, S., Aluisio, L., Pudiak, C., Lord, B., Mazur, C., Kamme, F., Nishino, S., Carruthers, N. and Lovenberg, T. (2007). Histamine H3 receptor antagonists: from target identification to drug leads. Biochem Pharmacol.**73**:1084–1096

Bongers, G., Bakker, R. and Leurs, R. (2007). Molecular aspects of the histamine H3 receptor. Biochem Pharmacol **73**:1195-1204

Braak, H. and Braak, E. (1991). Neuropathological staging of Alzheimer's related changes. Acta Neuropathology **82**: 239-259

Braak, H and Del Tredici, K. (2009). Neuroanatomy and pathology of sporadic Parkinson's disease. Adv Anat Embryol Cell Biol. **201**:1-119

Brazil, D.P., Yang, Z.Z. and Hemmings, B.A. (2004) Advances in protein kinase B signalling: AKTion on multiple fronts. Trends Biochem Sci **29**: 233–242

Bristow L.J and Bennett G.W (1988). Biphasic effects of intra accumbens histamine administration on spontaneous motor activity in the rat: a role for central histamine receptors. British Journal of Pharmacology. **95**: 1292-1302

Browman, K.E., Komater, V.A., Curzon, P., Rueter, L.E., Hancock, A.A., and Decker, M.W. (2004). Enhancement of prepulse inhibition of startle in mice by the H3 receptor antagonists thioperamide and ciproxifan. Behave Brain Res **153**: 69–76

Brown, R.E., Stevens, D.R. and Haas, H.L. (2001). The physiology of brain histamine. Progress in Neurobiology **63**: 637-672

Burroughs, S.L. (2010). Thesis entitled “Photobiomodulation with IR1072nm in the murine CNS: *in vitro* and *in vivo* studies”. Durham University

Cacabelos, R., Yamatodani, A., Niigawa, H., Hariguchi, S., Tada, K., Nishimura, T., Wada, H., Brandeis, L. and Pearson, J. (1989). Brain histamine in Alzheimer’s disease. Methods Find Exp Clin Pharmacol **11**: 353–360

Cannon, K.E. and Hough, L.B. (2005). Inhibition of chemical and low-intensity mechanical nociception by activation of histamine H3 receptors, J Pain **6:** 193–200

Cannon, K.E., Chazot, P.L., Hann, V., Shenton, F., Hough, L.B. and Rice, F.L. (2007). Immunohistochemical localization of histamine H3 receptors in rodent skin, dorsal root ganglia, superior cervical ganglia and spinal cord: potential antinociceptive targets. Pain **129**: 76–92

Chazot, P.L., Hann, V., Wilson, C., Lees, G., Thompson, C.L. (2001). Immunological identification of the mammalian H3 histamine receptor in the mouse brain. Neuroreport. **12**: 259-262

Chazot, P.L., Hann, V. and Shenton, F.C. (2005). Evidence for native and cloned H3 Histamine receptor higher oligomers. Inflammation research **54**: S48-S49

Chazot, P.L. and Shenton, F.C. (2006). Probing the importance of N-glycosylation for [^{3}H] clobenpropit binding to human H_3 receptors expressed in HEK 293 cells. Inflammation research **55**: S40-S41

Chazot, P.L. (2010). Therapeutic potential of histamine H3 receptor antagonists in dementia. Drug News & Perspectives **23**: 99-103 & Perspectives **2010, 23(2): 99-103**

Clapham, J. and Kilpatrick, G.J. (1992). Histamine H_3 receptors modulate the release of [3H]-acetylcholine from slices of rat enthorinal cortex: evidence for the possible existence of H3 receptor subtypes. Br J Pharmacol. **107**: 919-923

Clark, E.A. and Hill, S.J. (1996). Sensitivity of histamine H3 receptor agonist-stimulated [35S]GTPγS binding to pertussis toxin. Eur. J. Pharmacol **296**: 223–225

Coge, F., Guenin, S.P., Audinot, V., Renouard-Try, A., Beauverger, P., Macia, C., Ouvry, C., Nagel, N., Rique, H., Boutin, J.A. and Galizzi, J.P. (2001). Genomic organization and characterisation of splice variants of the human histamine H_3 receptor. Biochemical Journal **355**: 279-288

Cohen, S.N., Chang, A.C.Y. and Hsu, L. (1972). Nonchromosomal antibiotic resistance in bacteria: genetic transformation of Escherichia coli by R-factor DNA. Proc. Nat. Acad. Sci. **69**: 2110-2114

Connelly, W.M., Shenton, F.C., Lethbridge, N., Leurs, R., Waldvogel, H.J., Faull, R.L., Lees, G., Chazot, P.L. (2009). The histamine H4 receptor is functionally expressed on neurons in the mammalian CNS. Br J Pharmacol. **157**: 55-63

Cowart, M., Faghih, R., Curtis, M.P., Gfesser, G.A., Bennani, Y.L., Black, L.A., Pan, L., Marsh, K.C., Sullivan, J.P., Esbenshade, T.A., Fox, G.B.,

Hancock, A.A. 2005. 4-(2-[2-(2(R)-methylpyrrolidin-1-yl)ethyl]benzofuran-5-yl)benzonitrile and related 2-aminoethylbenzofuran H3 receptor antagonists potently enhance cognition and attention. J Med Chem. **48**: 38-55

Cross, R.B. (1982). Demonstration of neurofibrillary tangles in paraffin sections: A quick and simple method using a modification of Palmgren's method. Medical Laboratory Science **39**: 299-301

Dai, H.M., Kaneko, K., Kato, H., Fujii, S., Jing, Y.H., Xu, A.J., Sakuria, E., Kato, M., Okamura, N., Kuramasu, A. and Yanai, K. (2007). Selective cognitive dysfunction in mice lacking histamine H1 and H2 receptors. Neuroscience Research **57**: 306-313

Dale, H., Laidlaw, P. (1910). The physiological actions of *β*-iminazolethylamine. J. Physiol. **41**:318–344

Dale, H. and Laidlaw P.P. (1919). Histamine shock. J. Physiol. **52**: 355–390

De Esch, I.J.P., Thurmond, R.L. Jongejan, A. and Leurs, R. (2005). The Histamine H4 Receptor as a New Therapeutic Target for Inflammation. TRENDS in Pharmacology Sciences **26**: 462-469

Delacourte, A., David, J.P., Sergeant, N., Buee, L., Wattez, A., Vermersch, P., Ghozali, F., Fallet-Bianco, C., Pasquier, F., Lebert, F., Petit, H. and Di Menza, C. (1999). The biochemical pathway of neurofibrillary degeneration in aging and Alzheimer's disease, Neurology **52**: 1158–1165

Dere, E., De Souza-Silva, M.A., Spieler, R.E., Lin, J.S., Ohtsu, H. and Haas, H.L. (2004). Changes in motoric, exploratory and emotional behaviours and neuronal acetylcholine content and 5-HT turnover in histidine decarboxylase-KO mice, Eur J Neurosci **20**: 1051–1058

Dere, E., Zlomuzica, A., De Souza Silva, M.A., Ruocco, L.A., Sadile, A.G. and Huston J.P. (2010). Neuronal histamine and the interplay of memory, reinforcement and emotions. Behavioural Brain Research, **215**: 209-220

Dismukes, R.K. and Snyder, S.H. (1974). Dynamics of brain histamine. In Advances in Neurology (McDowell, F. and Barbeau, A., eds.). New York: Raven Press. 5:101

Drutel, G., Peitsaro, N., Karlstedt, K., Wieland, K., Smit, M.J., Timmerman, H., Panula, P. and Leurs, R. (2001). Identification of the rat H3 receptor isoforms with different brain expression and signalling properties. Molecular Pharmacology **59**: 1-8

Duggan, M.J., Pollard, S., Stephenson, F.A. (1991). "Immunoaffinity purification of GABAA receptor alpha-subunit iso-oligomers.

Demonstration of receptor populations containing alpha 1 alpha 2, alpha 1 alpha 3, and alpha 2 alpha 3 subunit pairs." J. Biol. Chem. **266**: 24778-24784

Emamian, E.S., Hall, D., Birnbaum, M.J., Karayiorgou, M., Gogos, J.A. (2004). Convergent evidence for impaired AKT1-GSK3beta signalling in schizophrenia. Nat Genet **36**:131–7

Ennaceur A., Michalikova S., van Rensburg R. and Chazot P.L. (2008). Detailed analysis of the behaviour and memory performance of middle-aged male and female CD-1 mice in a 3D maze Behavioural Brain Research, **187**: 312-326

Ennaceur, A. (2010). One-trial object recognition in rats and mice: Methodological and theoretical issues. Behavioural Brain Research. **In press**

Ennaceur, A., Michalikova, S., van Rensburg, R. and Chazot, P.L. (2010a). Anxiety responses in Balb/c, c57 and CD-1 mice exposed to a novel open space test. Behavioural Brain Research. **207**: 402-417

Ennaceur, A., Michalikova, S., van Rensburg, R. and Chazot, P.L. (2010b). Distinguishing anxiolysis and hyperactivity in an open space behavioural test. Behavioural Brain Research. **207**: 84-98

Ennaceur, A., Michalikova, S., van Rensburg, R. and Chazot, P.L. (2010c). Tolerance, sensitization and dependence to diazepam in Balb/c mice exposed to a novel open space anxiety test. Behavioural Brain Research. **209**: 154-164

Engelhardt, J.A., Gries, C.L. and Long, G.G. (1993). Incidence of spontaneous neoplastic and non-neoplastic lesions in Charles River CD-1 mice varies with breeding origin. Toxicol Pathol **21**: 538–541

Ericson, H, Blomqvist, A and Kohler, C (1991). Origin of neuronal inputs to the region of the tuberomammillary nucleus of the rat-brain. Journal of Comparative Neurology **311**: 45-64

Esbenshade, T.A., Fox, G.B. Krueger, K.M., Miller, T.R., Kang, C.H., Denny, L.I., Witte, D.G., Yao, B.B., Pan, L., Wetter, J., Marsh, K., Bennani, Y.L., Cowart, M.D., Sullivan, J.P. and Hancock, A.A. (2005). Pharmacological properties of ABT-239[4-(2-{2-[(2R)-2-methylpyrrolidinyl] ethyl}- benzofuran-5-yl)benzonitrile]: I. Potent and selective histamine H3 receptor antagonist with drug-like properties. J. Pharmacol. Exp. Ther., **313**: 165–175

Esbenshade, T. A., Fox, G.B., Cowart, M.D. (2006). Histamine H3 receptor antagonists: preclinical promise for treating obesity and cognitive disorders. Mol Interv: **6**: 77–88

Esbenshade, T.A., Browman, K.E., Bitner, R.S., Strakhova, M., Cowart, M.D., Brioni, J. D. (2008). The histamine H3 receptor: an attractive target for the treatment of cognitive disorders. Br J Pharmacol. **154**: 1166–1181

Farooqui, A.A., Horrocks, L.A. (2006). Phospholipase A2-generated lipid mediators in the brain: the good, the bad, and the ugly. Neuroscientist **12**: 245–260

Farzin, D., Asghari, L. and Nowrouzi, M. (2002). Rodent antinociception following acute treatment with different histamine receptor agonists and antagonists. Pharmacol Biochem Behav **72**: 751–760

Folstein, M.F., Folstein, S., McHugh, P. (1975). Mini mental state. A practical method for grading the cognitive state of patients for the clinician. Journal of Psychiatric Research **12**: 189-198

Fox, G.B., Pan, J.B., Esbenshade, T.A., Bennani, Y.L., Black, L.A., Faghih, R. (2002). Effects of histamine H3 receptor ligands GT-2331 and ciproxifan in a repeated acquisition avoidance response in the spontaneously hypertensive rat pup. Behav Brain Res **131**: 151–161

Fox, G.B., Esbenshade, T.A., Pan, J.B. (2005). Pharmacological properties of ABT-239[4-(2-{2-[(2R)-2-Methylpyrrolidinyl]ethyl}-benzofuran5yl)benzonitrile]: II. Neurophysiological characterization and broad preclinical efficacy in cognition and schizophrenia of a potent and

selective histamine H3 receptor antagonist. J Pharmacol Exp Ther **313**:176-190

Frisch, C., Hasenöhrl, R.U., Krauth, J. and Huston, J.P (1998). Anxiolytic-like behaviour after lesion of the tuberomammillary nucleus E2-region, Exp Brain Res **119**: 260–264

Frith, C.H. and Chandra, M. (1991). Incidence, distribution, and morphology of amyloidosis in Charles Rivers CD-1 mice. Toxicol Pathol **19**:123–127

Gantz, I., Scchaffer, M., Delvalle, J., Logsdon, C., Campbell, V., Uhler, M. and Yamada, T. (1991). Molecular-cloning of a gene encoding the histamine-H2-receptor. Proceedings of the National Academy of Sciences of the United States of America **88**: 429-443

Garbarg, M., Barbin, G., Feger, J. and Schwartz, J.C. (1974). Histaminergic pathway in rat-brain evidenced by lesions of medial forebrain-bundle. Science **186**: 833-835

Garbarg, M., Barbin, G., Bischoff, S., Pollard, H. and Schwartz, J.C. (1976). Dual localization of histamine in an ascending neuronal pathway and in non-neuronal cells evidenced by lesions in the lateral hypothalamic area. Brain Res. **106**: 333–348

Garduno-Torres, B., Trevino, M., Gutierrez, R. and Arias-Montano, J.A. (2007). Pre-synaptic histamine H_3 receptors regulate glutamate, but not GABA release in rat thalamus. Neuropharmacology **52**: 527–535

Gbahou, F., Vincent, L., Humbert-Claude, M., Tardivel-Lacombe, J., Chabret, C. and Arrang, J.M. (2006). Compared pharmacology of human histamine H3 and H4 receptors: structure–activity relationships of histamine derivatives, Br J Pharmacol **147**: 744–754

Gemkow, M.J., Davenport, A.J., Harich, S., Ellenbroek, B.A., Cesura, A. and Hallet, H. (2009).The histamine H3 receptor as a therapeutic drug target for CNS disorders. Drug Discovery Today, **14**: 509-515

Giannoni, P., Medhurst, A.D., Passani, M.B., Giovannini, M.G., Ballini, C., Corte, L.D., Blandina, P. (2009). Regional differential effects of the novel histamine H3 receptor antagonist 6-[(3- cyclobutyl-2,3,4,5-tetrahydro-1H-3-benzazepin-7-yl)oxy]-N-methyl-3-pyridine carboxamide hydrochloride (GSK189254) on histamine release in the central nervous system of freely moving rats. J Pharmacol Exp Ther **332**: 164-72

Giorgetti, M., Bacciottini, L., Bianchi, L., Giovannini, M. G. and Blandina, P. (1997). GABAergic modulation of cortical acetylcholine release in vivo. Soc Neurosci Abs **22**: 1255-1263

Giovannini, M.G., Bartolini, L., Bacciottini, L., Greco, L., Blandina, P (1999). Effects of histamine H3 receptor agonists and antagonists on cognitive performance and scopolamine-induced amnesia. Behav. Brain. Res. **104**: 147-55

Giovannini, M.G. Efoudebe, M., Passani, M.B., Baldi, E., Bucherelli, C., Giachi, F., Corradetti, R., Blandina, P. (2003). Improvement in fear memory by histamine-elicited ERK2 activation in hippocampal CA3 cells. J. Neurosci. **23**: 9016–9023

Gomez-Ramirez, J., Johnston, T.H., Visanji, N.P., Fox, S.H. and Brotchie, J.M. (2006). Histamine H3 receptor agonists reduce L-dopa-induced chorea, but not dystonia, in the MPTP-lesioned nonhuman primate model of Parkinson's disease. Movement Disorders **21**: 839-846

Goodchild, R.E., Court, J.A., Hobson, I., Piggott, M.A., Perry, R.H., Ince, P., Jaros, E., Perry, E.K. (1999). Distribution of histamine H3-receptor binding in the normal human basal ganglia: comparison with Huntington's and Parkinson's disease cases. Eur J Neurosci.**11**:449-456

Grandi D., Shenton F.C., Chazot P.L., Morini G. (2007) Immunolocalization of histamine H3 receptors on endocrine cells in the rat gastrointestinal tract. Histol Histopathol. **23**:789-98.

Haas, H and Panula, P (2003). The role of histamine and the tuberomammillary nucleus in the nervous system. Nature Reviews Neuroscience **4**: 121-130

Haas, H.L., Sergeeva, O.A. and Selbach, O. (2008). Histamine in the Nervous System. Physiol Rev **88**: 1183-1241

Hancock, A.A., Esbenshade, T.A., Krueger, K.M. and Yao, B.B. (2003). Genetic and pharmacological aspects of histamine h3 receptor heterogeneity. Life Sciences **73**: 3043-3072

Hardy, J. and Selkoe, D.J. (2002). The amyloid hypothesis of Alzheimer's disease: progress and problems on the road to therapeutics. Science **297**: 353–356

Hancock, A.A. (2006). The challenge of drug discovery of a GPCR target: Analysis of preclinical pharmacology of histamine H3 antagonists/ inverse agonists. Biochemical Pharmacology **78**: 1103-1113

Higuchi, M., Yanai, K., Okamura, N., Meguro, K., Arai, H., Itoh, M., Iwata, R., Ido, T., Watanabe, T., Sasaki, H. (2000). Histamine H(1) receptors in patients with Alzheimer's disease assessed by positron emission tomography. Neuroscience **99**: 721–729

Hill, S.J. 1990. Distribution, properties, and functional characteristics of three classes of histamine receptor. Pharmacol. Rev. **42**: 45–83

Hill S.J., Ganellin, C.R., Timmerman, H., Schwartz, J.C., Shankley, N.P., Young, J.M., Schunack, W., Levi, R. and Haas, H.L. (1997). International Union of Pharmacology. XIII. Classification of histamine receptors. Pharmacol. Rev. 49: 253–278

Hofstra, C.L., Desai, P.J., Thurmond, R.L. and Fung-Leung, W.P. (2003). Histamine H_4 Receptor Mediates Chemotaxis and Calcium Mobilization of Mast Cells. The Journal of Pharmacology and Experimental Therapeutics. **305:** 1212-1221

Hough, L.B. (1988). Cellular-localisation and possible functions for brain histamine – recent progress. Progress in Neurobiology **30**: 469-505

Hough, L.B. and Rice, F.L. (2011). H3 receptors and pain modulation: peripheral, spinal, and brain interactions. J Pharmacol Exp Ther. **336**: 30-7

Howlett, D.R., Richardson, J.C., Austin, A., Parsons, A.A., Bate, S.T., Davies D.C. and Gonzalez, M.I. (2004). Cognitive correlates of Abeta deposition in male and female mice bearing amyloid precursor protein and presenilin-1 mutant transgenes, Brain Res. **1017**: 130–136

Howlett, D.R., Bowler, K., Soden, P. Riddell, D., Richardson, J.C., Burbidge, S.A., Gonzalez, M.I., Irving E.A., Lawman A., Miglio G., Dawson, E.L., Howlett, E.R. and Hussain I. (2008). Abeta deposition and related pathology in an APP × PS1 transgenic mouse model of Alzheimer's disease. Histopathol. **23**: 67–76

Huang, L., Adachi, N., Nagaro, T., Liu, K. and Arai, T. (2007). Histaminergic involvement in neuropathic pain produced by partial ligation of the sciatic nerve in rats, Reg Anesth Pain Med **32**: 124–129

Ince, P.G., Perry, E.K. and Morris, C.M. (1998). Dementia with Lewy Bodies: A distinct non-Alzheimer dementia syndrome. Brain Pathology. **8**: 299-324

Jin, C.Y., Anichtchik, O. and Panula, P (2009). Altered histamine H_3 receptor radioligand binding in post-mortem brain samples from subjects with psychiatric diseases. Br J Pharmacol. **157**: 118–129

Jope, R.S. & Johnson, G.V (2004). The glamour and gloom of glycogen synthase kinase-3. Trends Biochem. Sci. **29**: 95–102

Karlstedt, K., Ahman, M.J., Anichtchik, O.V., Soinila, S. and Panula, P. (2003). Expression of the H_3 receptor in the developing CNS and brown fat suggests novel roles for histamine. Molecular and Cellular Neuroscience **24**: 614-622

Keith, J.M., Gomez, L.A., Wolin, R.L., Barbier, A.J., Wilson, S.J., Boggs, J.D., Mazur, C., Fraser, I.C., Lord, B., Aluisio, L., Lovenberg, T.W., Carruthers, N.I. (2007). Pyrrolidino-tetrahydroisoquinolines at potent dual H_3 receptor antagonists and serotonin transport inhibitors. Bioorg. Med. Chem. Lett. **17:** 2603 -2607

Kitbunnadaj, R., Hashimoto, T., Poli, E., Zuiderveld, O.P., Menozzi, A., Hidaka, R., De, E., Iwan, J.P., Bakker, R.A., Menge, W.M.P.B., Yamatodani, A., Coruzzi, G., Timmerman, H. and Leurs, R (2005). N-substituted piperidinyl alkyl imidazoles: discovery of methimepip as a potent and selective histamine H3 receptor agonist. J. Med. Chem. **48**: 2100–2107

Kjaer, A., Knigge, U., Rouleau, A., Garbarg, M. and Warberg, J. (1994). Dehydration-Induced release of vasopressin involves activation of hypothalamic histaminergic neurons. Endocrinology **135**: 675-681

Knoche, A, Yokoyama, H, Ponomarenko, A, Fricsh, C, Huston, J and Haas, H.L. (2003). High-frequency oscillation in the hippocampus of the behaving rat and its modulation by the histaminergic system. Hippocampus **13**: 273-280

Koyama, M., Seyedi, N., Fung-Leung, W.I., Lovenberg, T. and Levi, R. (2003). Norepinephrine release from the ischemic heart is greatly

enhanced in mice lacking histamine H3 receptors. Mol Pharmacol **63**: 378–382

Kwiatkowski, H. (1943). Histamine in nervous tissue. J Physiol **102**: 32-41

Labella, F., Queen, G., Glavin, G., Durant, G., Stein, D. and Brandes, L. (1992). H3 receptor antagonist, thioperamide, inhibits adrenal steroidogenisis and histamine binding to adrenocortical microsomes and binds to cytochrome P450. Br. J. Pharmacol., **107**: 161–164

Lavie, L. and Weinreb, I. (1996). Age- and strain-related changes in tissue transglutaminase activity in murine macrophages: the effects of inflammation and induction by retinol. Mech Ageing Dev **90**: 129–143

Le, S., Finn, J.P., Larijani, M.E., Marino, M.J. and Schaffhauser, H. (2009) Detection of low level histamine H3 receptor occupancy by autoradiography. J Neurosci Methods **185**: 70-75

Le, S.Y., Gruner, J., Mathiasen, J.R., Marino, M.J. and Schaffhauser, H. (2008). Correlation between ex vivo receptor occupancy and wake-promoting activity of selective H-3 receptor antagonists, J. Pharmacol. Exp. Ther. **325**: 902–909

Le Coniat, M., Traiffort, E., Ruat, M., Arrang, J.M. and Berger, R. (1994). Chromosomal location of the human histamine H1-receptor gene. Hum. Genet. **94**:186–188

Lethbridge, N.L., Shenton, F.C. and Chazot, P.L. (2009). Generation and characterisation of the first anti-human H_3R445/453 isoform specific antibody probe. Inflamm Res **58**: 43-44

Leurs, R., Traiffort, E., Arrang, J.M., Tardivel Lacombe, J., Ruat, M. and Schwartz, J.C., (1994). Guinea pig histamine H1 receptor. II. Stable expression in Chinese hamster ovary cells reveals the interaction with three major signal transduction pathways. J. Neurochem. **62**: 519–527

Leurs, R., Tulp, M.T., Menge, W.M., Adolfs, M.J., Zuiderveld, O.P., and Timmerman, H. (1995). Evaluation of the receptor selectivity of the H3 receptor antagonists, iodophenpropit and thioperamide: an interaction with the 5-HT3 receptor revealed. Br. J. Pharmacol. **116**: 2315–2321

Leurs R, Hoffmann, M, Wieland, K and Timmerman, H (2000). H3 receptor gene is cloned at last. Trends in Pharmacological Sciences **21**: 11-12

Leurs, R., Celanire, C., Wijtmans, M., Talaga, P. and de Esch, I.J.P. (2005). Histamine H3 receptor antagonist reach out for the clinical. Keynote review **10**: 1613–1627

Leurs, R., *et al.,* (2008). Presentation on 'Histamine H3 receptor heterogeneity'. European Histamine Research Society. Conference Stockholm, Sweden.

Leurs, R., *et al.,* (2009). Presentation on 'Histamine H3/ H4 receptor heterogeneity'. British Pharmacological Society. Conference London, UK.

Leurs, R. *et al.,* (2009). Presentation on "Recent advances in the molecular pharmacology of the H_4 histamine receptor". British Pharmacology Society, London, UK.

Lewis, T., Grant, R.T. (1924). Vascular reactions of the skin to injury. Part 11. The liberation of histamine-like substance in the injured skin, the underlying cause of factitious urticaria and of wheals produced by burning: and observations upon the nervous control of certain skin reactions. Heart. **11**: 209–265

Levi, R. and Smith, N.C.E. (2000). Histamine H3 receptors: A new frontier in myocardial ischemia. Journal of Pharmacology and Experimental Therapeutics. **292**: 825-830

Li, X., Bijur, G.N., Jope, R.S. 2004. Glycogen synthase kinase-3beta, mood stabilizers, and neuroprotection. Bipolar Disord **4**: 137–44

Ligneau, X., Perrin, D., Landais, L. (2007). BF2.649 [1-{3-[3-(4-Chlorophenyl)propoxy]- propyl}piperidine, hydrochloride], a nonimidazole inverse agonist/antagonist at the human histamine H3 receptor: Preclinical pharmacology. J Pharmacol Exp Ther, **320**: 365-375

Lin, J.S., Dauvilliers, Y., Arnulf, I., Bastuji, H., Anaclet, C., Parmentier, H., Kocher, L., Yanagisawa, M., Lehert, P., Ligneau, X., Perrin, D., Robert, P., Roux, M., Lecomte, J.M. and Schwartz, J.C. (2008). An inverse agonist of the histamine H-3 receptor improves wakefulness in narcolepsy: studies in orexin(−/−) mice and patients, Neurobiol. Dis. **30**: 74–83

Liu, C., Ma, X., Jiang, X., Wilson, S.J., Hofstra, C.L., Blevitt, J., Pyati, J., Li, X., Chai, W., Carruthers, N. and Lovenberg, T.W. (2001a). Cloning and Pharmacological Characterization of a Fourth Histamine Receptor (H_4) Expressed in Bone Marrow'. Molecular Pharmacology. **59:** 420-426

Lovenberg, T., Roland, B., Wilson, S., Jiang, S., Pyati, J., Huvar, A., Jackson, M. and Erlander, M. (1999). Cloning and Functional Expression of the Human Histamine H(3) Receptor. The American Society for Pharmacology and Experimental Therapeutics **55**: 1101-1107

Lovenberg, T.W., Pyati, J., Chang, H., Wilson, S.J., Erlander, M.G. (2000). Cloning of rat histamine H_3 receptor reveals distinct species pharmacological profiles. J Pharmacol Exp Ther. **293**:771–778

Lozada, A., Michelsen, K.A., Karlstedt, K., Yamamoto, Y. and Panula, P. (2004). Expression of the histamine H4 receptor during rat development. European Histamine Research Society XXXIII Annual Meeting, Dusseldorf/Kohl, Germany.

Mai, J.K., Assheuer, J., Paxinos, G. (1997). Atlas of the human brain. San Diego and London

Malmberg, A.P., Lamberti, C., Ipponi, A., Hanninen, J., Ghelardini, C. and Bartolini, A., (1997). Effects of two histamine-N-methyltransferase inhibitors, SKF 91488 and BW 301 U, in rodent antinociception. Pharmacol. **355**: 354–360

Martinez-Mir, M.I., Pollard, H., Moreau, J., Arrang, J.M., Ruat, M., Traiffort, E., Schwartz, J.C. and Palacios, J.M. (1990). Three histamine receptors (H_1, H_2 and H_3) visualized in the brain of human and non human primates. Brain Resolution. **526**: 322-327

Mazurkiewicz-Kwilecki, I.M. and Nsonwah, S. (1989). Changes in the regional brain histamine and histidine levels in post-mortem brains of Alzheimer patients. J Physiol Pharmacol **67**: 75–78

McKeith, I.G., Galasko, D., Kosaka, K., Perry, E.K., Dickson, D.W., Hansen, L.A., Salmon, D.P., Lowe, J., Mirra, S.S., Byrne, E.J., Lennox, G., Quinn, N.P., Edwardson, J.A., Ince, P.J., Bergerson, C., Burns, A., Miller,

B.L., Lovestone, S., Collerton, D., Jansen, E.N.H., Ballard, C., de Vos, R. A.I., Wilcock, F.K., Jellinger, K.A. and Perry, R.H. (1996). Consensus guidelines for the clinical and pathological diagnosis of dementia with Lewy-body (DLB): Report on the consortium on DLB international workshop. Neurology **47**: 113-124

McKeith, I.G. (2002). Dementia with Lewy Bodies. Br J Psychiatry. **180**: 144-147

McKeith, I.G., Burn, D., Ballard, C., Collerton, D., Jaros, E., Morris, C., Mclaren, A., Perry, E., Perry, R., Piggot, M., O'Brien, J. (2003). Dementia with Lewy Bodies. Semin Clin Neuropsychistry. **8**: 46-57

McKhann, G., Drachmann, D., Folstein, M., Catzmann, R., Pryce, D. and Stadlan, E. (1984). Clinical Diagnosis of Alzheimer's Disease: Report of the NINCDS/ ADRDA work group. Neurology **34**: 939-944

Medhurst, A.D., Atkins, A.R., Beresford, I.J., Brackenborough, K., Briggs, M.A., Calver, A.R., Cilia, J., Cluderay, J.E., Crook, B., Davis, J.B., Davis, R.K., Davis, R.P., Dawson, L.A., Foley, A.G., Gartlon, J., Gonzalez, M.I., Heslop, T., Hirst, W.D., Jennings, C., Jones, D.N., Lacroix, L.P., Martyn, A., Ociepka, S., Ray, A., Regan, C.M., Roberts, J.C., Schogger, J., Southam, E., Stean, T.O., Trail, B.K., Upton, N., Wadsworth, G., Wald, J.A., White, T., Witherington, J., Woolley, M.L., Worby, A., Wilson, D.M. (2007a). GSK189254, a Novel H3 Receptor Antagonist That Binds to

Histamine H3 Receptors in Alzheimer's Disease Brain and Improves Cognitive Performance in Preclinical Models. The Journal of Pharmacology and Experimental Therapeutics **321**: 1032-1045

Medhurst, A.D., Briggs, M.A., Bruton, G., Calver, A.R., Chessell, I. and Crook, B. (2007b). Structurally novel histamine H3 receptor antagonists GSK207040 and GSK334429 improve scopolamine-induced memory impairment and capsaicin-induced secondary allodynia in rats, Biochem Pharmacol **73**: 1182–1194

Medhurst, A.D., Roberts, J.C., Lee, J., Chen, C.P., Brown, S.H., Roman, S., Lai, M.K. (2009). Characterization of histamine H3 receptors in Alzheimer's Disease brain and amyloid overexpressing TASTPM mice. Br J Pharmacol **157**: 130-8

Meguro, K.I., Yanai, K., Sakia, N., Sakuria, E., Maeyama, K., Sasaki, H. and Watanabe, T. (1995). Effects of thioperamide, a histamine H_3 antagonist, on the step-through passive avoidance response and histidine decarboxylase activity in senescence-accelerated mice. Pharmacology Biochemistry and Behaviour. **50**: 321-325

Michalikova, S., Ennaceur, A., van Rensburg, R. and Chazot PL (2007). Emotional responses and memory performance of middle-aged female CD1 mice in a 3D maze: effects of near infrared light. Neurobiol Learn Memory. **89**: 480-488

Michino, M., Abola, E., GPCR Dock 2008 participants., Brooks, C.L., Dixon, J.S., Moult, J., Stevens, R.C. (2009). Community-wide assessment of GPCR structure modelling and ligand docking: GPCR Dock 2008. Nat Rev Drug Discov. **8**:455-463.

Millan-Guerrero, R.O., Pineda-Lucatero, A.G., Hernandez-Benjamin, T., Tene, C.E. and Pacheco, M.F. (2003). N-alpha-methylhistamine safety and efficacy in migraine prophylaxis: Phase I and Phase II studies. Headache **43**: 389-394

Miyazaki, S., Imaizumi, M. and Onodera, K. (1995). Effects of Thioperamide, a histamine H3 receptor antagonist, on a scopolamine-induced learning deficit using an elevated plus- maze test in mice. Life Sciences. **57**: 2137-2144

Miyazaki, S., Imaizumi, M., Timmerman, H. and Onodera, K. (1997). Effects of clobenpropit (VUF-9153), a histamine H3 receptor antagonist, on learning and memory, and on cholinergic and monoaminergic systems in mice. Life Sciences. **61**: 355-361

Mizumori, S.J., Rosenzweig, M.R., Kermisch, M.G.. (1982). Failure of mice to demonstrate spatial memory in the radial maze. Behav Neural Biol. **35**: 33-45

Mochizuki, T., Yamatodani, A., Okakura, K., Horii, A., Inagaki, N. and Wada, H., 1992. Circadian rhythm of histamine release from the hypothalamus of freely moving rats. Physiol. Behav. **51**: 391–394

Mochizuki, T., Yamatodani, A., Yamatodani, Y., Horii, A., and Okakuramochizuki, K., (1994). Histaminergic modulation of hippocampal acetylcholine release in vivo. Journal of Neurochemistry. **62**: 2275-2282

Morisset, S., Rouleau, A., Ligneau, X., Gbahou, F., Tardivel-Lacombe, J., Stark, H., Schunack, W., Ganellin, C.R., Schwartz, J.C., Arrang, J.M. (2000). High constitutive activity of native H3 receptors regulates histamine neurons in brain. Nature **408**: 860–864

Morisset, S., Sasse, A., Gbahou, F., Heron, A., Ligneau, X., Tardivel-Lacombe, J., Schwartz, J. C., Arrang, J. M. (2001). The rat H3 receptor: gene organization and multiple isoforms. Biochem Biophys Res Commun. **280**:75-80

Morse, K., Behan, J., Laz, T.M., West, R.E. Jr, Greenfeder, S.A., Anthes, J.C., Umland, S., Wan, Y., Hipkin, R.W., Gonsiorek, W., Shin, N., Gustafson, E.L., Qiao, X., Wang, S., Hedrick, J.A., Greene, J., Bayne, M., Monsma, F.J. Jr. (2001). Cloning and Characterization of a Novel Human Histamine Receptor. Journal of Pharmacology. **296**: 1058-1066

Nakamura, S., Takemura, M., Ohnishi, K., Suenaga, T., Nishimura, M., Akiguchi, I., Kimura, J. and Kimura, T. (1993). Loss of large neurons and occurrence of neurofibrillary tangles in the tuberomammillary nucleus of patients with Alzheimer's disease. Neuroscience Letters **151**: 581-587

Nakamura, T., Itadani, H., Hidaka, Y., Ohta, M. and Tanaka, K. (2000). Molecular cloning and characterisation of a new human histamine receptor, hH4R. Biochemical and Biophysical Research Communications **279**: 615-620

Nguyen, T., Shapiro, D.A., George, S.R., Setola, V., Lee, D.K., Cheng, R., Rauser, L., Lee, S.P., Lynch, K.R., Roth, B.L. and O'Dowd, B.F. (2001). Discovery of a Novel Member of the Histamine Receptor Family. Molecular Pharmacology. **59:** 427-433

Oda, T. Morikawa, N. Saito, Y. Masuho, Y. and Matsumoto, S.I. (2000). Molecular Cloning and Characterization of a Novel Type of Histamine Receptor Preferentially Expressed in Leukocytes. Journal of Biological Chemistry. **275:** 36781-36786

Oluyomi, A.O. and Hart, S.L. (1991). Involvement of histamine in naloxone-resistant and naloxone-sensitive models of swim stress induced antinociception in the mouse, Neuropharmacology **30**: 1021–1027

Orsette, M., Ferretti, C., Gamalero, S.R. and Ghi, P. (2002). Histamine H3 receptor blockade in the rat nucleus basalis magnocellularis improves place recognition memory. Psychopharmacology **159**: 133-137

Owen, S.M., Sturman, G. and Freeman, P. (1994). Modulation of morphine-induced antinociception in mice by histamine H3-receptor ligands, Agents Actions **41**: C62–C63

Panula, P., Pirvola, U., Auvinen, S. and Airaksinen, M.S. (1989). Histamine-immunoreactive nerve-fibers in the rat-brain. Neuroscience **28**: 585-610

Panula, P., Rinne, J., Kuokkanen, K., Eriksson, K.S., Sallmen, T., Kalimo, H. (1998). Neuronal histamine deficit in Alzheimer's disease. Neuroscience **82**: 993–997

Parmentier, R., Ohtsu, H., Djebbara-Hannas, Z., Valatx, J.L., Watanabe, T. and Lin, J.S. (2002). Anatomical, physiological and pharmacological characteristics of histidine decarboxylase knockout mice: Evidence for the role of brain histamine in behavioural and sleep-wake control. Journal of Neuroscience. **22**: 7695-7711

Parsons, M.E. and Ganellin, C.R. (2006). Histamine and its receptors. British Journal of Pharmacology. **147**: S127-S135

Perry, R.H., Irving, D. and Blessed, G. (1990). Senile dementia of the Lewy-body type. A clinical and neuropathologically distinct form of Lewy-body dementia in the elderly. Journal of Neurological Science **95**:119-139

Perry, R.H. (1993). A guide to the cortical regions. In G.W. Roberts, P.N. Leigh and D.R. Weinberger, Editors, Neuropsychiatric Disorders, Wolfe, London

Petrianou, G., Arafat, K., Sasse, B.C., Stark, H. (2006). Multiple enzyme inhibitions of histamine H_3 receptor antagonists as potential precognitive agents. Pharmacy **61:** 179-182

Philippu, A. and Prast, H. (1991). Patterns of histamine release in the brain. Agents Actions **33**: 124–125

Pollard, H., Moreau, J., Arrang, S. and Airaksinen, M.S. (1993). A detailed autoradiographic mapping of histamine H3 receptors in rat brain areas, Neuroscience **52**: 169–189

Prast, H., Argyriou, A. and Philippu, A. (1996). Histaminergic neurons facilitate social memory in rats. Brain research **734**: 169-189

Prell, G.D., Khandelwal, J.K. Burns, R.S., Lewitt, P.A. and Green, J.P. (1991). Influence of age and gender on the levels of histamine metabolites

and pris-methylimidazoleacetic acid in human cerebrospinal-fluid. Archives of Gerontology and Geriatrics **12**: 1-12

Richelson, E. (1978). Histamine H1 receptor-mediated guanosine 3′,5′-monophosphate formation by cultured mouse neuroblastoma cells. Science **201**: 69–71

Rickle, A., Bogdanovic, N., Volkman, I., Winblad, B., Ravid, R., Cowburn, R.F. (2004). Akt activity in Alzheimer's disease and other neurodegenerative disorders. Neuroreport **15**: 955–959

Rinne, J.O., Anichtchik, O.V., Eriksson, K.S., Kaslin, J., Tuomisto, L., Kalimo, H., Roytta, M., Panula, P. (2002). Increased brain histamine levels in Parkinson's disease but not in multiple system atrophy. J Neurochem **81**: 954–960

Rizk, A., Curley, J., Robertson, J. and Raber, J. (2004). Anxiety and cognition in histamine H3 receptor-/- mice, Eur J Neurosci **19**: 1992–1996

Rogers, J., Webster, S., Lue, L.F., Brachova, L., Civin, W.H., Emmerling, M., Shivers, B., Walker, D. and McGeer, P. (1996). Inflammation and Alzheimer's disease pathogenesis, Neurobiol. Aging **17:** 681–686

Rouleau, A., Heron, A., Cochois, V., Pillot, C., Schwartz, J.C., Arrang, J.M. (2004). "Cloning and expression of the mouse histamine H3 receptor: evidence for multiple isoforms." Journal of Neurochemistry **90**: 1331-1338

Sakia, K.M., El Mansari, J.S., Lin, Z.G., Zhang, G. and Vanni-Mercier (1990). The diencephalon and sleep. New York, Raven Press.

Sallmen, T., Lozada1, A.F., Anichtchik, O.V., Beckman, A.L. and Panula, P. (2003). Increased brain histamine H3 receptor expression during hibernation in golden-mantled ground squirrels. BMC Neuroscience **4**: 24

Schwartz, J.C., Arrang, J.M., Garbarg, M., Pollard, H. and Ruat, M. (1991). Histaminergic transmission in the mammalian brain. Physiol. Rev. **71**: 1–51

Schwartz, J.C., Bassetti, C.L., Baumann, C.R., Dauvilliers, Y., Croyal, M. and Robert, P. (2010). Cerebrospinal fluid histamine levels are decreased in patients with narcolepsy and excessive daytime sleepiness of other origin. J. Sleep Res. **19**: 620-623

Schwartz, J.C., Labeeuw, O.L., Capet, M., Dauvilliers, Y., Croyal, M. and Robert, P. (2011). Histamine and tele-methylhistamine quantification in cerebrospinal fluid from narcoleptic subjects by liquid chromatography tandem mass spectrometry with precolumn derivatization. Anal Biochem. **409**: 28-36

Selbach, O., Brown, S.M. and Hill, S.J. (1997). Long term increase of hippocampal excitability by histamine and cyclic AMP. Neuropharmacology **36**: 1539-1548

Shenton, F.C., Hann, V., Chazot, P.L. (2005). “Evidence for Native and Cloned H3 Histamine Receptor Higher Oligomers”. Inflammation research **54**: S48 – 49.

Shenton, F.C. (2007) Thesis entitled “Molecular heterogeneity of rodent and human histamine H_3 and H_4 receptors”. Durham University

Silver, R.B., Mackins, C.J., Smith, N.C.E., Koritchneva, I.L., Lefkowitz, K., Lovenberg, T.W. and Levi, R. (2001). Coupling of histamine H_3 receptors to neuronal Na+/H+ exchange: A novel protective mechanism in myocardial ischemia. Proceedings of the National Academy of Sciences of the United States of America **98**: 2855-2859

Sogawa, N., Sogawa, C., Pohjanvirta, R., Tuomisto, J., Tuomisto, L., Onodera, K. and Kitayama, S. (2004). mRNA expression for histamine H3 receptor isoforms in rat brain. Journal of Pharmacological Sciences **94**: 234-234

Strakhova, M.I., Nikkel, A.L., Manelli, A.M., Hsieh, G., Esbenshade, T.A., Brioni, J.D. and Bitner, R.S. (2009). Localization of Histamine H4

Receptors in the Central Nervous System of Human and Rat. Brain Research. **23**: 41-48

Sun, W. (2002). Glycogen synthase kinase-3β is complex with tau protein in brain microtubules. J. Biol. Chem. **277**: 11933–11940

Takahashi, K., Suwa, H., Ishikawa, T. and Kotani, H. (2002). Targeted distribution of H3 receptors results in changes in brain histamine tone leading to obese phenotype. Journal of Clinical Investigation. **110**: 1791-1799

Takeshita, Y., Watanabe, T., Sakata, T., Munakata, M., Ishibashi, H. and Akaike, N. (1998). Histamine modulates high-voltage-activated calcium channels in neurons dissociated from the rat tuberomammillary nucleus. Neuroscience **87**:797–805.

Tardivel-Lacombe, J., Morisset, S., Gbahou, F., Schwartz, J.C. and Arrang, J.M. (2001). Chromosomal mapping and organization of the human histamine H3 receptor gene. Neuroreport **12**: 321-324

Terao, A., Steininger, T.L., Morairty, S.R. and Kilduff, T.S. (2004). Age-related changes in histamine receptor mRNA levels in the mouse brain. Neuroscience Letters **355**: 81–84

Thiels, E., Klann, E. (2001). Extracellular signal-regulated kinase, synaptic plasticity, and memory. Rev Neurosci **12**: 327–45

Thoburn, K.K., Hough, L.B., Nalwalk, J.W. and Mischler, S.A., (1994). Histamine-induced modulation of nociceptive responses. Pain **58**: 29–37

Thomas, G.M., Huganir, R.L. (2004). MAPK cascade signalling and synaptic plasticity. Nat Rev Neurosci **5**: 173–183

Tiligada, E., Zampeli, E., Sander, K. and Stark, H. (2009). Histamine H3 and H4 receptors as novel drug targets. Expert Opin. Investig Drugs **18**:1519-1531

Toyota, H., Dugovic, C., Koehl, M., Laposky, A.D., Weber, C., Ngo, K., Wu, Y., Lee, D.H., Yanai, K., Sakurai, E., Watanabe, T., Liu, C.L., Chen, J.C., Barbier, A.J., Turek, F.W., Fung-Leung, W.P. and Lovenberg, T.W. (2002). Behavioural characterisation of mice lacking histamine H_3 receptors. Molecular Pharmacology **62**: 389-397

Van Der Goot. and Timmerman, H (2000). Selective ligands as tools to study histamine receptors. European journal of medicinal chemistry **35**: 5–20

van Rijn, R.M., Chazot, P.L., Shenton, F.C., Sansuk, K., Bakker, R.A., Leurs, R. (2006). Oligomerization of Recombinant and Endogenously

Expressed Human Histamine H4 Receptors. Mol Pharmacology **70**: 604-615

van Rijn, R.M., van Marle, A., Chazot, P.L., Langemeijer, E., Qin, Y., Shenton, F.C., Lim, H.D., Zuiderveld, O.P., Sansuk, K., Dy, M., Smit, M.J., Tensen, C.P., Bakker, R.A., Leurs, R. (2008). Cloning and characterization of dominant negative splice variants of the human histamine H4 receptor. Biochem J. **414**:121-131

Villemagne, V.L., Dannals, R.F., Sanchezroa, P.M., Ravert, H.T., Vazquez, S., Wilson, A.A., Natarajan, T.K., Wong, D.F., Yanai, K. and Wagner, H.N. (1991). Imaging histamine H1 receptors in the living human brain with carbon-11-pyrilamine. Journal of Nuclear Medicine **32**: 308-311

Wada, H., Inagaki, N., Yamatodani, A. and Watanabe, T. (1991). Is the histaminergic neuron system a regulatory center for whole-brain activity? Trends Neurosci. **14**: 415–418

Watanabe, T., Taguchi, Y., Hayashi, H., Tanaka, J., Shiosaka, S., Tohyama, M., Kubota, H., Terano, Y., Wada, H. (1984). Distribution of the histaminergic neuron system in the central nervous system of rats; a flourescent immunohistochemical analysis with histamine decarboxylase as a marker. Brain Res **295**: 13-25

Wellendorph, P., Goodman, M,W., Burstein, E.S., Nash, N.R., Brann, M.R., Weiner, D.M. (2002). Molecular cloning and pharmacology of functionally distinct isoforms of the human histamine H3 receptor. Neuropharmacology **42**: 929-940

West, R.E., Zweig, A., Shih, N.Y., Siegal, M.I., Egan, R.W. and Clark, M.A. (1990). Identificastion of 2-H-3-Histamine Receptor subtypes. Molecular Pharmacology **38**: 610-613

Whitehouse, P.J., Price, D.L., Struble, R.G., Clark, A.W., Coyle, J.T., Delon, M.R. (1982). Alzheimer's disease and senile dementia: loss of neurons in the basal forebrain. Science **215**: 1237–1239

Wiedemann, P., Bonisch, H., Oerters, F. and Bruss, M. (2002). Structure of the human histamine H3 receptor gene (HRH3) and identification of naturally occurring variations. Journal of Neural Transmission **109**: 443-453

Windaus, A and Vogt, W (1907). Synthese des Imidazolyläthylamins. Chem Ber **40:** 3691-3694

Witkin, J.M. and Nelson, D.L. (2004). Selective histamine H3 receptor antagnists for treatment of cognitive deficiencies and other disorders of the central nervous system. Pharmacology & therapeutics **103**: 1-20

Witte, D.G., Yao, B.B., Miller, T.R., Carr, T.L., Cassar, S., Sharma, R., Faghih, R., Surber, B.W., Esbenshade, T.A., Hancock, A.A. and Krueger, K.M. (2009). Detection of multiple H_3 receptor affinity states utilizing [^{3}H]A-349821, a novel, selective, non-imidazole histamine H_3 receptor inverse agonist radioligand. Br. J. Pharmacology. **148**: 657-670

Wyss-Coray, T. and Mucke, L. (2002). Inflammation in neurodegenerative disease a double-edged sword. Neuron **35**: 419–432

Yamashita, M, Fukui, H, Sugama, K, Horio, Y, Ito, S, Mizuguchi, H and Wada, H (1991). Expression cloning of a Cdna-encoding the bovine histamine-H1 receptor. Proceedings of the National Academy of Sciences of the United States of America **88**: 11515-11519

Yanai, K, Watanabe, T, Yokoyama, H, Hatazawa, J, Iwata, R, Ishiwata, K, Meguro, K, Itoh, M, Takahashi T, Ido, T and Matsuzawa, T. (1992). Mapping of histamine H1 receptors in the human brain using [C-11] pyrilamine and positron emission tomography. Journal of Neurochemistry **59**: 128-136

Yang, R., Hey, J.A., Aslanian, R. and Rizzo, C.A. (2002). Coordination of histamine H3 receptor antagonists with human adrenal cytochrome P450 enzymes. Pharmacology, **66**: 128–135

Yao, B.B., Sharma, R., Cassar, S., Esbenshade, T.A., Hancock, A.A. (2003). Cloning and pharmacological characterization of the monkey histamine H_3 receptor. Eur J Pharmacol. **482**:49–60

Yücel, M., Stuart, G.W., Maruff, P., Velakoulis, D., Crowe, S.F., Savage, G. and Pantelis, C. (2001). Hemispheric and Gender-related Differences in the Gross Morphology of the Anterior C**in**gulate/Parac**in**gulate Cortex **in** Normal Volunteers: An MRI Morphometric Study. Cerebral Cortex **11**: 17-25

Zavitsanou, K. Katsifis, A. Yu, Y. Huang X.F. (2005). M2/M4 muscarinic receptor binding in the anterior cingulate cortex in schizophrenia and mood disorders. Brain Research Bulletin. **65**: 397-403

PUBLICATIONS

Connelly,W.M., Shenton, F.C., Lethbridge, N., Leurs. R., Waldvogel, H.J., Faull, R.L., Lees, G. and Chazot, P.L. (2010). The H_4 Histamine Receptor is functionally expressed on Central Neurons. British Journal of Pharmacology. **157**: 55-63.

Ling, S., Bossers, K., Balesar, R., Lethbridge, N., Chazot, P.L., Bao, M.A. and Swaab, D. (2011). Alterations in the histaminergic system in the Substantia Nigra of Parkinson patients: a postmortem study. Brain Pathology. In press

Lethbridge, N. and Chazot, P.L. (2010). Immunological identification of the mouse H_4 histamine receptor on spinal cord motor neurons using a novel anti - mouse H_4R antibody. Inflammation Res **59**:S197-198.

Lethbridge, N., Shenton, F. and Chazot, P.L. (2009). Generation and characterisation of the first anti-human H_3R445/453 isoform specific antibody probe. Inflammation Res **58**:43-44.

MEETING REPORTS

Lethbridge, N. and Chazot, P.L. (2009). The XXXVIII Annual Meeting of the European Histamine Research Society 13-16th May 2009, Fulda, Germany.

Lethbridge, N. (2009). Histamine H_4 Receptor Pharmacology. British Pharmacology Society Winter meeting 15-17th December 2009*:* UK

Lethbridge, N. and Chazot, P.L. (2008). The XXXVII Annual Meeting of the European Histamine Research Society 7-10th May 2008, Stockholm, Sweden.

Lethbridge, N., Burroughs, S.and Chazot, P.L. (2008). Neuropharmacology.
BPS Winter meeting 15-17th December 2008: UK

ABSTRACTS

Lethbridge, N. and Chazot, P.L. (2010). Major Histamine H_3 receptors show differences in pharmacology. European Histamine Research Society. UK

Lethbridge, N., Chazot, P.L., Shenton, F. and Hann, V. (2010). Immunological Probes for Human H_3 Histamine Receptor Isoforms. (Anti-human H_3R_{329} specific antibody, Anti- human $H_3R_{365/445}$ specific antibody, Anti- human H_3R_{445} specific antibody Anti- H_3R pan specific antibody). European Histamine Research Society. UK

Lethbridge, N., Chazot, P.L., Shenton, F. and Katebe, M. (2010). Species-directed immunological probes for the histamine H_4 receptor: evidence of multiple roles for the H_4R. Anti- human H_4R antibody, Anti- mouse

H_4R antibody and Anti- rat H_4R antibody. European Histamine Research Society. UK

Shan, L., Liu, C.Q., Bossers, K., Balesar, R., Van Heerikhuize, J.J., Wu, J.L., Lethbridge, N.L., Chazot, P.L., Bao, A.M. and Swaab, D.F. (2010). The Histaminergic system in Parkinson's Disease European Histamine Research Society. UK

Lethbridge, N. and Chazot, P.L. (2009).. A 116-Amino Acid Deletion in the Third Intracellular Loop of a Naturally Occurring Human Histamine H_3 receptor Isoform Confers inverse agonist Pharmacological Differences. British Pharmacology Society Winter Meeting. 15-17th December 2009*:* UK

Lethbridge, N., Chazot, P.L. and Medhurst, A.D. (2009). Histamine H_3 receptors in major human dementias: an autoradiographical study with [^{3}H] GSK189254. European Histamine Research Society. Germany

Lethbridge, N., Chazot, P.L., Shenton, F.. Connelly, W., Van Rensburg, R. and Lees, G. (2008). Further Evidence for H_4 Histamine Receptor Expression on Central Neurons. Neuroscience North East and Biochemical Society The First Panel of Immunological Probes for Human H_3 Histamine Receptor Isoforms – Anti- human H_3R 200 specific antibody. European Histamine Research Society. Sweden